EARTHQUAKE ANALYSIS AND RESPONSE OF CONCRETE ARCH DAMS

by

Hanchen Tan

Anil K. Chopra

A Report on Research Conducted
Under Grant BCS-9121943 from
the National Science Foundation

Report No. UCB/EERC-95/07
Earthquake Engineering Research Center
University of California
Berkeley, California

July 1995

ABSTRACT

Reliable analytical procedures to predict the earthquake response of arch dams are essential to design dams to be earthquake resistant or to evaluate the earthquake safety of existing dams. The objectives of this study are: (a) to develop an effective procedure for analyzing the response of concrete arch dams to earthquake ground motion, including the effects of dam-foundation rock interaction with inertia and damping of the foundation rock considered, dam-water interaction, and reservoir boundary absorption; (b) to identify the limitations of the "standard" analysis procedure which considers the flexibility of the foundation rock but ignores its inertia and damping — material and radiation — effects; and (c) to study the effects of dam-foundation rock interaction in the presence of dam-water interaction and reservoir boundary absorption on the response of the dam, leading to better understanding of these effects. This investigation emphasizes the effects of dam-foundation rock interaction compared to dam-water interaction which have already been studied extensively.

The available substructure method and computer program for the earthquake response analysis of arch dams, including the effects of dam-water interaction, reservoir boundary absorption, and foundation rock flexibility, is extended to include the effects of dam-foundation rock interaction with inertia and damping of the foundation rock considered. Efficient techniques are developed for evaluating the foundation impedance terms, computationally the most demanding part of the procedure.

Utilizing the resulting analytical procedure, the frequency response of Morrow Point Dam to harmonic ground motions is computed and studied for a wide range of the important parameters characterizing the properties of the dam, foundation rock, impounded water and reservoir boundary materials. It is shown that: (a) dam-foundation rock interaction reduces the fundamental resonant frequency of the dam and generally reduces the fundamental resonant response because the frequency bandwidth at the fundamental resonance is widened by the interaction; dam-foundation rock

interaction also reduces the amplitude of higher resonant peaks and their resonant frequencies; (b) dam-foundation rock interaction affects the response of the dam in its symmetric vibration modes, excited by upstream and vertical ground motions, more than its antisymmetric vibration modes, excited by cross-stream ground motion; (c) the commonly used "standard" analysis, which considers only the flexibility of the foundation rock, ignores important effects of dam-foundation rock interaction and overestimates the response amplitudes at the fundamental and higher resonant frequencies; (d) dam-foundation rock interaction has little effect on the percentage reduction in the fundamental resonant frequency due to dam-water interaction, especially if the reservoir is close to full; and (e) the radiation damping due to reservoir boundary absorption is more effective in reducing the response of the dam if the foundation rock is rigid, and the damping — material and radiation — due to dam-foundation rock interaction is more effective in reducing the response of the dam if the reservoir boundary is less absorptive.

Utilizing the new analytical procedure, the earthquake response of Morrow Point Dam due to Taft ground motion is also computed and studied for a wide range of the important parameters characterizing the properties of the dam, foundation rock, impounded water and reservoir boundary materials. It is shown that: (a) the "standard" procedure, which considers only the flexibility of the foundation rock but ignores other effects of dam-foundation rock interaction, significantly overestimates the earthquake-induced stresses in arch dams; (b) dam-foundation rock interaction generally increases by a small amount the maximum tensile stresses computed for the dam on rigid foundation rock, but does not significantly alter the distribution of stresses over the dam faces; (c) dam-water interaction and reservoir boundary absorption effects on the response of the dam are affected by dam-foundation rock interaction differently due to symmetric (upstream and vertical) ground motions and antisymmetric (cross-stream) ground motion; (d) for the dam with impounded water and non-absorptive reservoir boundary, the response to the vertical component of ground motion is so large that it dominates the total response; however, this dominance drastically decreases as the reservoir boundary becomes more absorptive; and (e) the small increase in stresses in an arch

dam due to dam-foundation rock interaction is in contrast to gravity dams whose response is reduced significantly by interaction; however, dam-water interaction and reservoir boundary absorption effects have more significant influence on the earthquake response of arch dams than on the response of gravity dams.

The results presented demonstrate that foundation-rock inertia and damping, dam-water interaction, and reservoir boundary absorption may significantly affect the earthquake response of arch dams. Therefore, these effects should be included in the design of new arch dams and in the seismic safety evaluation of existing dams.

ACKNOWLEDGMENTS

This research investigation was supported by the National Science Foundation under Grant BCS-9121943. The authors are grateful for this support.

Except for editorial changes, the report is the same as Hanchen Tan's doctoral dissertation, which has been submitted to the University of California, Berkeley. The dissertation committee consisted of Professors A. K. Chopra (Chairman), E. L. Wilson and B. A. Bolt. The authors are grateful to Professors Wilson and Bolt for reviewing the manuscript and suggesting improvements.

Parts of this investigation are closely related to a companion work: "Earthquake Analysis and Response of Concrete Arch Dams" by Ka-Lun Fok and Anil K. Chopra, published in July 1985. The superb organization of the figures and tables presenting the response results and of their discussion in this companion study served as an excellent model for this report.

TABLE OF CONTENTS

1 INTRODUCTION

Reliable analytical procedures to predict the earthquake response of concrete arch dams are essential to design dams to be earthquake resistant or to evaluate the earthquake safety of existing dams. Many techniques have been developed for this purpose, and ADAP [1] was one of the earliest computer programs based on the finite element method. While foundation flexibility effects were considered in the original computer program, later an added mass approximation of hydrodynamic effects was included. [2,3] In order to develop better representation of the hydrodynamic effects, a substructure method was developed in the frequency domain [4,5]. This procedure and the implementing computer program [6] includes the effects of dam-water interaction, water compressibility and reservoir boundary absorption. Parametric response studies using this analysis procedure demonstrated that each of these effects can be significant so that they should be considered in analyzing the earthquake response of arch dams [7,8,9].

Since an arch dam carries loads in part by transmitting them through arch action to the abutments, and it is in contact with foundation rock extending over the dam height, the effects of dam-foundation rock interaction may be important in the earthquake response of arch dams. Therefore, it is necessary to develop rigorous procedures for considering dam-foundation rock interaction, which remove the untenable assumption of massless foundation rock employed in current computer programs, including EADAP [3] and EACD-3D [6]. Analyses based on this assumption ignore foundation material and radiation damping, perhaps a significant interaction effect. To overcome this limitation, a boundary element procedure has been developed for analysis of the dam-water-foundation rock system showing good results [10,11]. This method in which a large foundation rock region extending significant distances in the upstream and downstream directions is modeled by surface boundary elements apparently requires enormous computational effort.

Required in the substructure method for earthquake analysis of concrete dams is the impedance matrix (or the frequency-dependent stiffness matrix) for the foundation rock region, defined at the

nodal points on the dam-foundation rock interface [12]. Computation of this foundation impedance matrix for arch dams requires solution of a series of mixed boundary value problems governing the steady-state response of the canyon cut in a three-dimensional, semi-unbounded foundation rock region. A direct boundary element procedure has been developed to solve these boundary value problems for a canyon cut in a homogeneous viscoelastic half-space [13]. The canyon is infinitely long and may be of arbitrary but uniform cross-section. The uniform cross-section of the canyon permits analytical integration along the canyon axis of the three-dimensional boundary integral equation. Thus, the original three-dimensional problem is reduced to an infinite series of two-dimensional boundary value problems, each of which corresponds to a particular wave number and involves Fourier transforms of full-space Green's functions. Appropriate superposition of the solutions of these two-dimensional boundary problems leads to a dynamic flexibility matrix that is inverted to determine the impedance matrix, which forms the starting point of this investigation.

The objectives of this study are: (a) to develop an effective procedure for analyzing the response of concrete arch dams to earthquake ground motion, including the effects of dam-foundation rock interaction with inertia and damping of the foundation rock considered, dam-water interaction, and reservoir boundary absorption; (b) to identify the limitations of "standard" analysis which considers the flexibility of the foundation rock but ignores its inertia and damping — material and radiation — effects; and (c) to study the effects of dam-foundation rock interaction in the presence of dam-water interaction and reservoir boundary absorption on the response of the dam, leading to better understanding of these effects. This investigation emphasizes the effects of dam-foundation rock interaction compared to dam-water interaction that has already been studied extensively [7,8,9].

Discussed in Chapter 2 is the general concrete arch dam system consisting of three substructures: the dam body, the foundation rock region, and the impounded reservoir. The material and geometrical properties of each of these three substructures are stated. The input ground motion is also defined.

The Morrow Point Dam-water-foundation rock system which is the subject of this investigation is described in Chapter 3. In particular, the incompatibility between the dam body and the foundation rock caused by the uniform canyon assumption is discussed.

The earlier analytical procedure [5] is summarized in Chapter 4 and extended to include inertia and damping effects of the foundation rock by including the foundation impedance matrix in the substructure method. The properties and accuracy of the foundation impedance matrix are investigated. Efficient procedures are also presented for computation of the foundation impedance coefficients.

Utilizing the analytical procedure presented in Chapter 4, the response of Morrow Point Dam to harmonic ground motion in the upstream, vertical and cross-stream directions is determined and presented in the form of complex-valued frequency response functions for a wide range of the important parameters characterizing the properties of the dam, foundation rock, impounded water and reservoir boundary materials in Chapter 5. Based on the frequency response results, the influence of damping — material and radiation — and the inertia of the foundation rock beside its flexibility on the response of the dam is studied. We then identify the significance of dam-foundation rock interaction effects ignored in standard analyses [3,6] that consider flexibility of the foundation rock but not its inertia or damping — material and radiation — effects. Finally, the effects of dam-foundation rock interaction in the presence of dam-water interaction and reservoir boundary absorption on the response of the dam are also investigated, leading to better understanding of these effects.

Presented in Chapter 6 is the earthquake response of Morrow Point Dam to Taft ground motion, determined for a wide range of parameters characterizing the properties of the dam, foundation rock, impounded water and reservoir boundary materials, using the analytical procedure developed in Chapter 4. The response results presented are the time variations of radial displacements at the dam crest and the envelope values of the maximum tensile stresses at the upstream and downstream faces of the dam. Based on these response results, the effects of dam-foundation rock

interaction with empty reservoir are studied first. The significance of these interaction effects ignored in standard analyses that consider flexibility of the foundation rock but not its inertia or damping — material and radiation — effects are then identified. The combined effects of dam-foundation rock interaction, dam-water interaction, and reservoir boundary absorption are studied next. The relative significance of the response to the three components of ground motion are also investigated. Finally, the results of a practical earthquake analysis of the arch dam are presented to demonstrate the effectiveness of the analytical procedure.

Presented in Chapter 7 are the principal conclusions of this investigation regarding (1) the analytical procedure developed, (2) the significance of the dam-foundation rock interaction effects ignored in standard analysis procedures, and (3) the effects of dam-foundation rock interaction, dam-water interaction, and reservoir boundary absorption, on the response of arch dams to harmonic and earthquake ground motions.

2 SYSTEM AND GROUND MOTION

2.1 System Geometry and Assumptions

The system consists of a concrete arch dam supported by flexible foundation rock in a canyon and impounding a reservoir of water in the upstream direction (Figure 2.1). Although the arch dam is usually built in a narrow bank of the canyon, in this study the canyon is assumed to be infinitely long with an arbitrary but uniform cross-section cut in a homogeneous viscoelastic half-space. The cross-section is defined by the dam-foundation rock interface (Figure 2.2). The system is analyzed under the assumption of linear behavior for the concrete dam, impounded water, and foundation rock. Thus the possibility of water cavitation, concrete cracking, or opening of construction joints during vibration of the dam is not considered.

2.2 Arch Dam

The idealization of the dam-fluid-foundation rock system is shown in Figures 2.3(a)-(c). The concrete arch dam is idealized as an assemblage of finite elements [Figure 2.3(a)]. Thick-shell finite elements are normally used in the major part of the dam and transition elements along its junction with foundation rock. The transition elements are designed to connect the thick-shell finite elements in the dam to the surface boundary elements idealizing the foundation rock [Figure 2.3(b)]. The assumption of a uniform canyon may introduce incompatibility between the dam abutment and the canyon [Figure 3(d)] which requires special treatment as described in the next chapter.

The properties of each finite element are characterized by the Young's modulus E_s, Poisson's ratio ν_s, and unit weight w_s of the concrete. The vibrational energy dissipation properties of the dam are characterized by the constant hysteretic damping factor η_s.

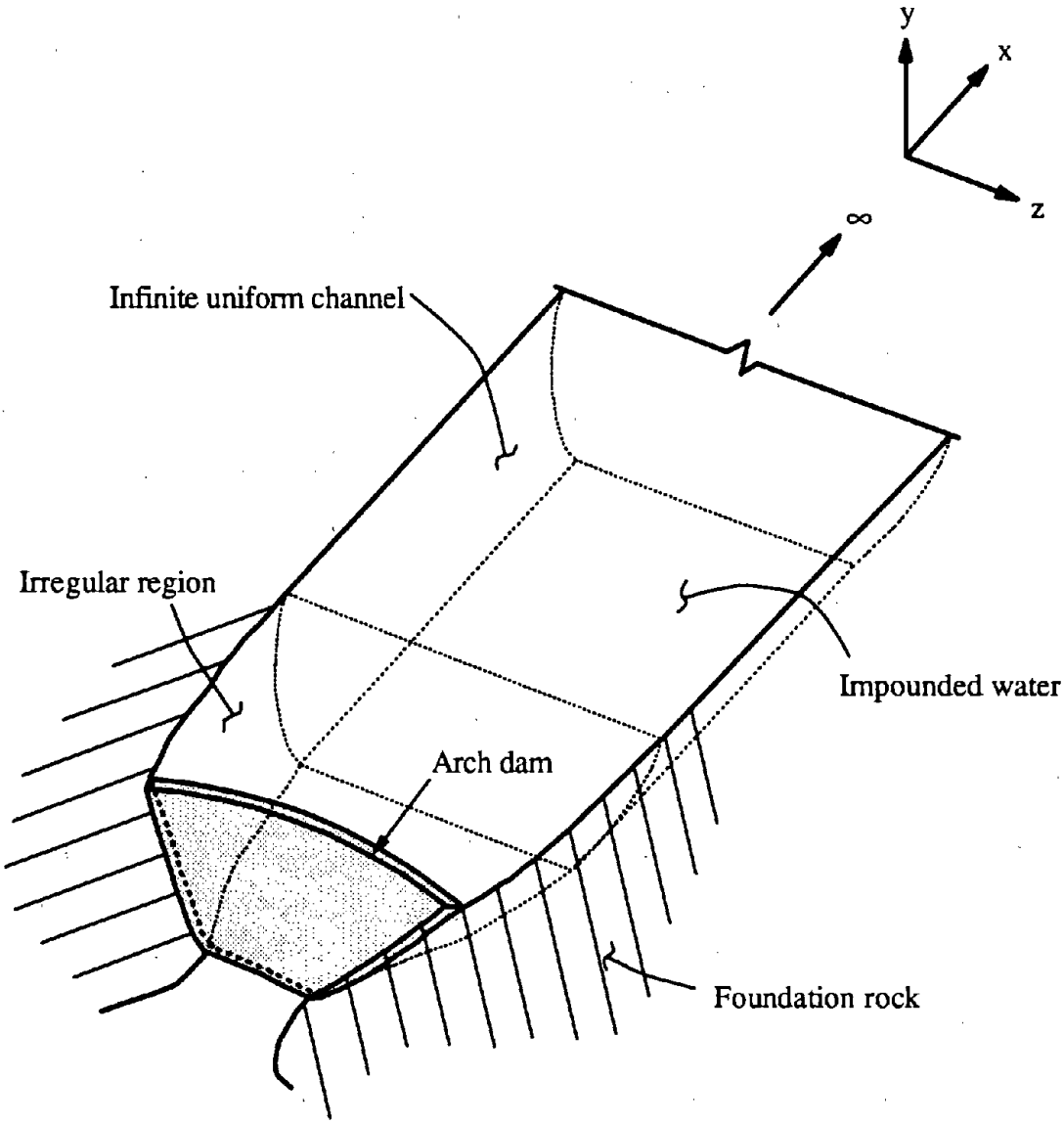

Figure 2.1 Arch dam-water-foundation rock system.

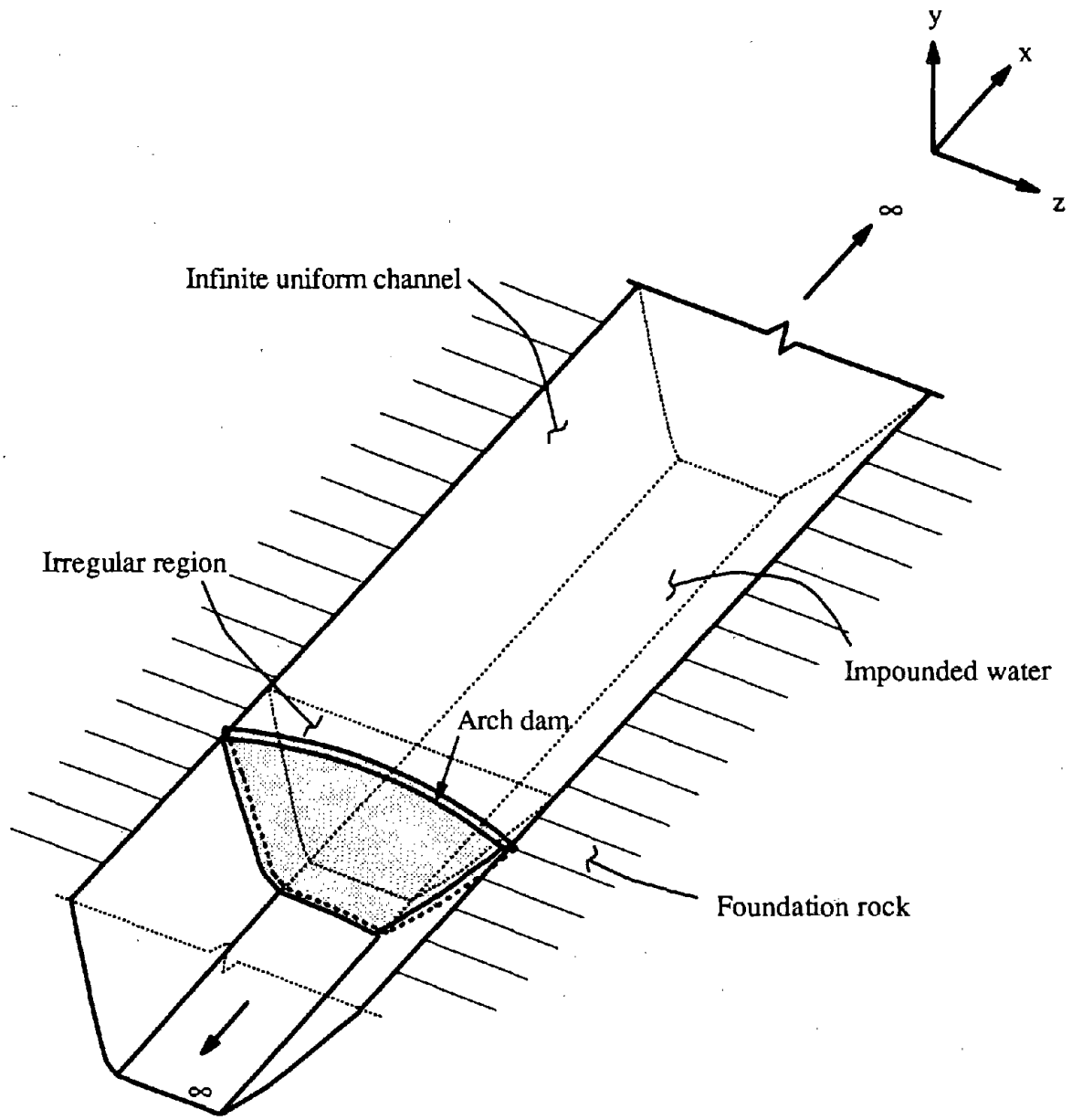

Figure 2.2 Idealized arch dam-water-foundation rock system in an infinitely-long uniform canyon.

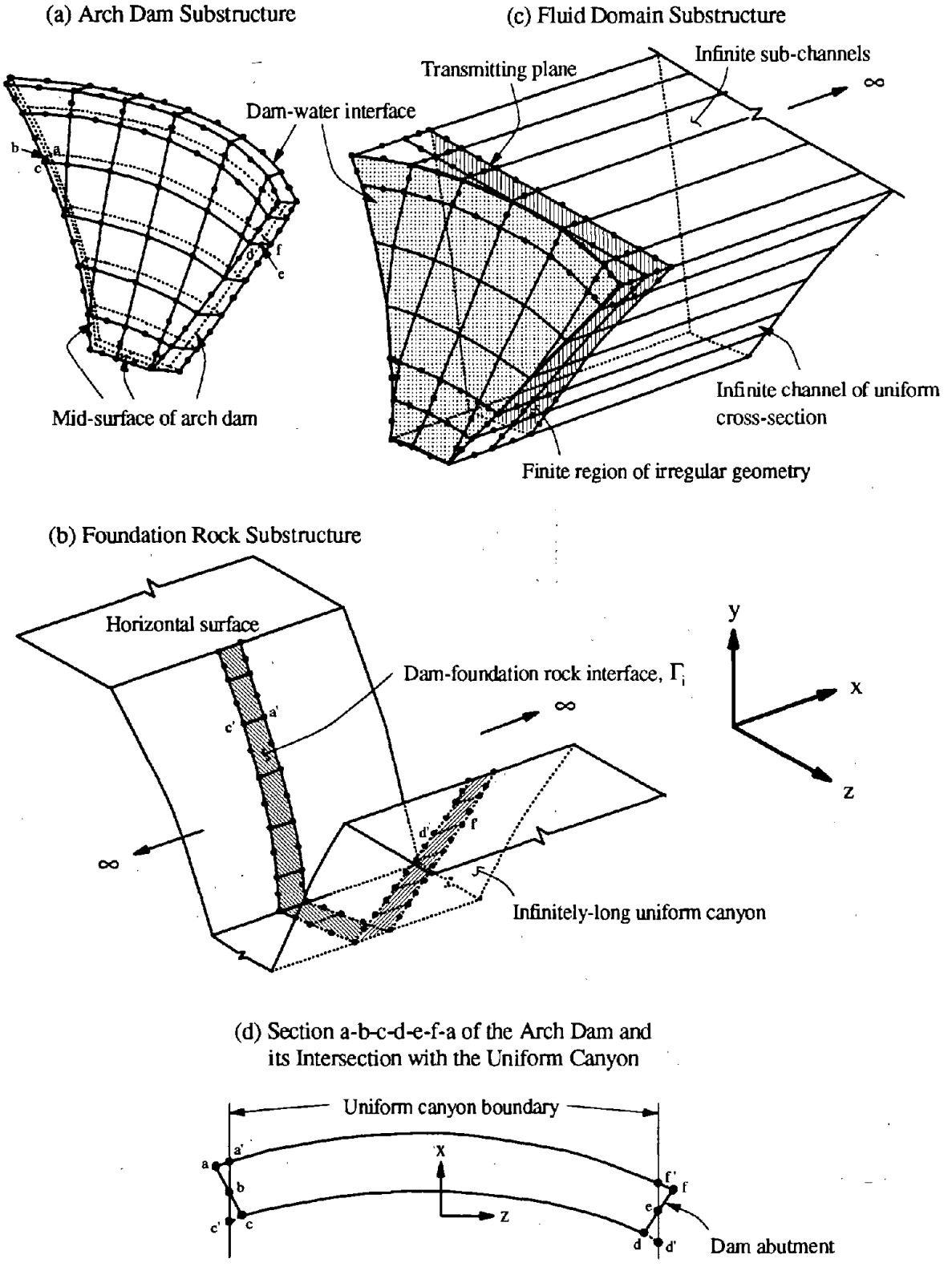

Figure 2.3 (a)-(c) Finite element models of dam and fluid domain substructures and boundary element model of foundation rock [parts (a) and (c) adapted from Reference [5]; (d) Incompatibility between the dam abutment and canyon.

2.3 Foundation Rock

Required in the substructure method for analysis of earthquake response of arch dams is the frequency-dependent impedance (or dynamic stiffness) matrix for the foundation rock region, defined at the nodal points on the dam-foundation rock interface. The impedance matrix, $\mathbf{S}_f(\omega)$, where ω is the excitation frequency, relates the interaction forces $\mathbf{R}_f(t)$ at the dam-foundation rock interface, Γ_i, to the corresponding displacements, $\mathbf{r}_f(t)$, relative to the earthquake-induced displacements in the absence of the dam [Figure 2.3(b)]:

$$\mathbf{S}_f(\omega)\overline{\mathbf{r}}_f(\omega) = \overline{\mathbf{R}}_f(\omega) \tag{2.1}$$

where the bar denotes a Fourier transform of the time functions. The size of the square matrix, $\mathbf{S}_f(\omega)$, is equal to the number of degrees of freedom (DOFs) in the finite element idealization of the dam at its interface with the foundation. The n^{th} column of this matrix multiplied by $e^{i\omega t}$ is the set of complex-valued forces required at the interface DOFs to maintain a unit harmonic displacement, $e^{i\omega t}$, in the n^{th} DOF with zero displacements in all other DOFs.

Evaluation of these forces requires solution of a series of mixed boundary value problems (BVP) with displacements prescribed at the interface, Γ_i, and tractions prescribed as zero outside Γ_i — on the canyon wall and the half-space surface. Instead of directly solving this mixed BVP, it is more convenient to solve a stress BVP in which non-zero tractions are specified at the interface, Γ_i, and the resulting displacements at Γ_i are determined. Assembled from these displacements, the dynamic flexibility influence matrix is inverted to determine the impedance matrix $\mathbf{S}_f(\omega)$.

A direct boundary element procedure has been developed to determine the impedance matrix [13]. The assumption of uniform cross-section of the canyon permits analytical integration along the canyon axis of the three-dimensional boundary integral equation. Thus, the original three-dimensional problem is reduced to an infinite series of two-dimensional problems, each of which corresponds to a particular wave number and involves Fourier transforms of full-space Green's functions. Appropriate superposition of the solutions of these two dimensional boundary value problems leads to a dynamic

flexibility influence matrix which is inverted to determine the impedance matrix. This procedure is shown to be more accurate and efficient than the general three-dimensional boundary element method [13].

For this direct boundary element procedure, the dam-foundation rock interface is discretized into a set of boundary elements with their nodal points matching the finite element idealization of the dam [Figure 2.3(b)]. The properties of the foundation rock are characterized by its Young's modulus E_f, Poisson's ratio ν_f, and unit weight w_f. The vibrational energy dissipation properties of the foundation rock are characterized by the constant hysteretic damping factor η_f.

2.4 Impounded Water

The reservoir behind a dam is of complicated shape, as dictated by the natural topography of the site, and extends several miles in the upstream direction. To efficiently recognize the long extent of the reservoir in the upstream direction, the fluid domain is idealized as a finite region of irregular geometry adjacent to the dam connected to an infinitely-long channel with uniform cross-section [5]. This assumption permits uncoupling of the three-dimensional boundary value problem for the infinite channel into two problems: a one-dimensional problem in the upstream direction and a two-dimensional problem over the cross-section. Typically the irregular region of the fluid domain connects the narrow canyon at the upstream face of the dam to a wider cross-section that defines the infinite uniform channel. However, this geometry of the fluid domain is not compatible with the boundary of the foundation rock.

To avoid such incompatibility, the fluid domain is defined as shown in Figure 2.3(c). The finite region of irregular geometry is idealized as an assemblage of three-dimensional finite elements [Figure 2.3(c)], with the finite element mesh compatible with that of the dam at its upstream face. For the infinite channel, a discretization of the cross-section, compatible with the discretization of the irregular region over the common cross-section [the transmitting plane in Figure 2.3(c)] combined with a continuum representation in the infinite direction provides for the proper transmission of

pressure waves. Physically, this treatment can be interpreted as a discretization of the fluid domain into subchannels of infinite length [Figure 2.3(c)]. The properties of the impounded water are characterized by the pressure wave velocity C and the unit mass ρ or unit weight w_w.

2.5 Absorptive Reservoir Boundary

The boundary of a reservoir upstream from a dam would typically consist of alluvium, silt, and other sedimentary material. This section on modeling of these materials in this study is taken from an earlier work on concrete gravity dams [12].

Over a long period of time, the sediments may deposit to a significant depth in some reservoirs. The depth of sediments can be recognized in the analytical procedure presented in this study by correspondingly reducing the depth of the fluid domain. However, the influence of the sediments on the static stresses in the dam or on the vibration properties of the dam is not considered in the analysis because it should be negligible as the sediments are very soft, highly saturated and exert lateral forces only on the lower part of the dam.

The effects of interaction between the impounded water and the foundation rock would be dominated by the overlying alluvium and sediments, possibly deposited to a significant depth. These reservoir boundary materials are highly saturated with a low shear modulus. A hydrodynamic pressure wave impinging on such materials will partially reflect back into the water and partially refract, primarily as a dilatational wave, into the layer of reservoir boundary materials. Because of the considerable energy dissipation that results from hysteretic behavior and sediment particle turbulence, the refracted wave is likely to be absorbed in the layer of soft, saturated sediments and essentially dissipated before reaching the underlying foundation rock.

The absorption of hydrodynamic waves at the reservoir boundary can be represented approximately by a one-dimensional model, normal to the boundary and independent of the location on the boundary, that does not explicitly consider the thickness of the sediment layer. For this model, the boundary condition at the reservoir boundary is developed in References [4,12,14]. The

fundamental parameter characterizing the effects of absorption of hydrodynamic pressure waves at the reservoir boundary is the admittance or damping coefficient $q = \rho/\rho_r C_r$ in which $C_r = \sqrt{E_r/\rho_r}$ where E_r is the Young's modulus and ρ_r is the unit mass of the materials at the reservoir boundary. The wave reflection coefficient α, which is the ratio of the amplitude of the reflected hydrodynamic pressure wave to the amplitude of a normally propagating pressure wave incident on the reservoir boundary, is related to the damping coefficient q by [4,14]

$$\alpha = \frac{1 - qC}{1 + qC} \tag{2.2}$$

The wave reflection coefficient α is a more physically meaningful description than q of the behavior of the absorption of hydrodynamic pressure waves at the reservoir boundary. Although the wave reflection coefficient depends on the angle of incidence of the pressure wave at the reservoir boundary, the value α for normally incident waves, as given by Equation (2.2) is used here for convenience. The wave reflection coefficient α may range within the limiting values of 1 and –1. For non-absorptive reservoir boundary materials, $C_r = \infty$ and $q = 0$, resulting in $\alpha = 1$. For very soft reservoir boundary materials, $C_r \to 0$ and $q = \infty$, resulting in $\alpha = -1$. It is believed that α values from 1 to 0 would cover the wide range of materials encountered at the boundary of actual reservoirs.

2.6 Ground Motion

In earthquake response analysis of dams by the substructure method, the earthquake input is specified as the free-field ground motion at the dam-foundation rock interface [4]. This free-field ground motion was assumed to be uniform across the base in two-dimensional analyses of concrete gravity dams [12]. For arch dam sites this free-field ground motion is expected to vary significantly over the interface [e.g. 15-17]. However, these spatial variations in ground motion are not included in this investigation which concentrates on the effects of dam-foundation rock interaction. The three components of ground motion: $a_g^x(t)$ in the upstream direction, $a_g^z(t)$ in the cross-stream direction, and $a_g^y(t)$ in the vertical direction, are assumed to be uniform along the canyon.

3 IDEALIZATION OF MORROW POINT DAM-WATER-FOUNDATION ROCK SYSTEM

3.1 Morrow Point Dam

The response results presented in this report are all for Morrow Point Dam located on the Gunnison River in Colorado. It is a 465 ft high, approximately symmetric, single centered arch dam. Detailed description of the geometry of this dam is available in References [4] and [18]. To simplify the dynamic analysis, the dam and its supporting canyon are assumed to be symmetric about the x-y plane. The fluid domain is also assumed symmetric about the x-y plane and extending to infinity in the upstream direction. With the assumption of symmetry, only one-half of the dam-fluid-foundation rock system needs to be analyzed. The response to the upstream (x) or the vertical (y) component of ground motion, which is symmetric about the x-y plane, is determined by analyzing one-half of the system with symmetric boundary conditions on the x-y plane. The response to the cross-stream (z) component of ground motion, which is antisymmetric about the x-y plane, is determined by analyzing one-half of the system with antisymmetric boundary conditions on the x-y plane.

The finite element idealization of one-half of the dam body (Figure 3.1) consists of 8 thick-shell finite elements in the main part of the dam and 8 transition elements in the part of the dam near its junction with the foundation rock, with a total of 61 nodal points at the mid-surface of the dam. The DOFs in a thick-shell element are associated with these mid-surface nodes, each of which is associated with two auxiliary "nodes" — one on the upstream face and the other on the downstream face of the dam (Figure 3.1). Each mid-surface node has five DOFs: x, y, and z translations and two rotations of the "normal" connecting the upstream and downstream auxiliary nodes [19]. The transition element is actually a thick-shell finite element with five (three translational and two rotational) DOFs for each mid-surface node that is not on the abutment of the dam. However, for a node on the abutment of the dam, the five DOFs are transformed to six translational DOFs at the two auxiliary nodes. Therefore when dam-foundation rock interaction is considered, this idealization has a

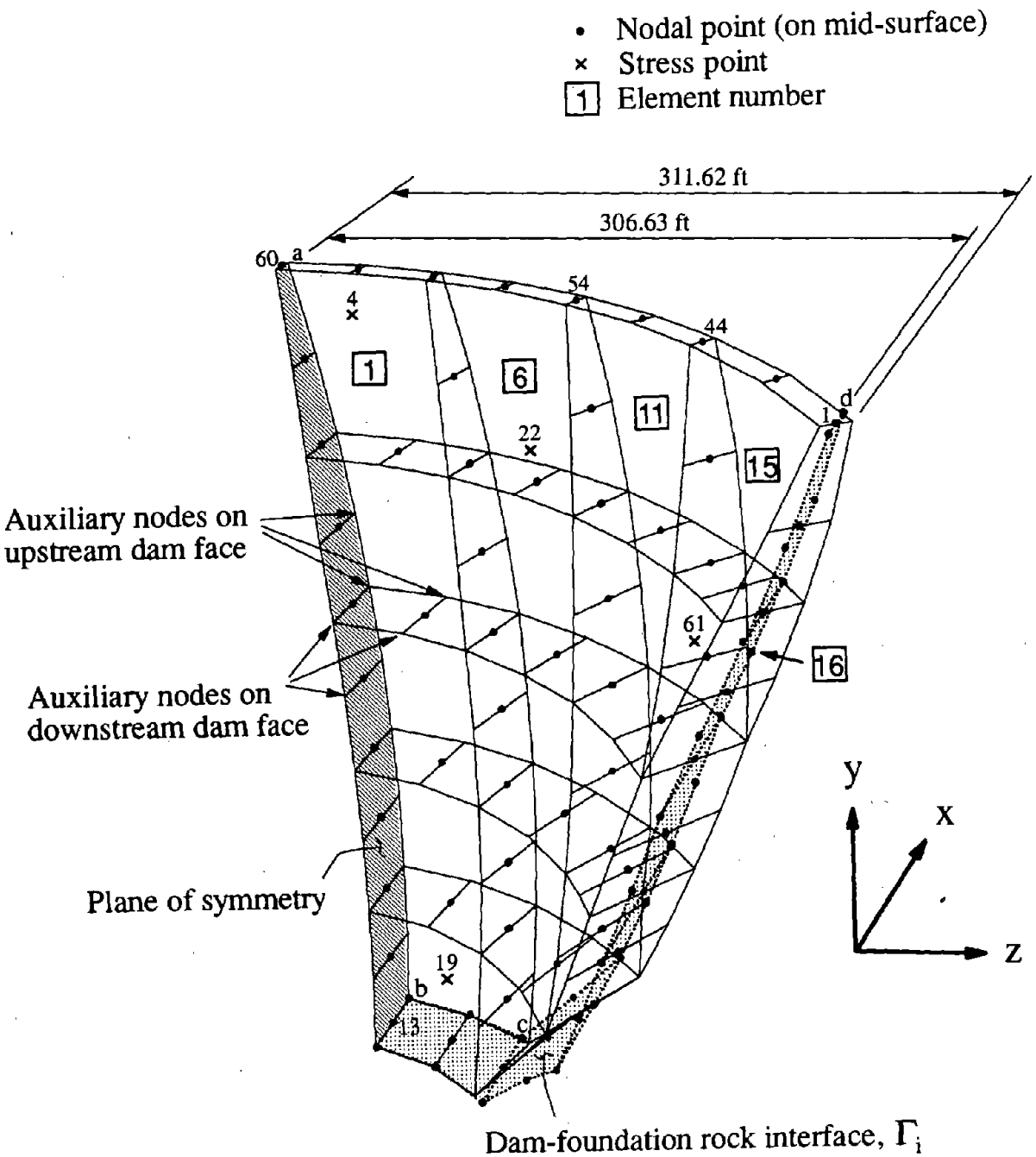

Figure 3.1 Finite element mesh of one-half of Morrow Point Dam.

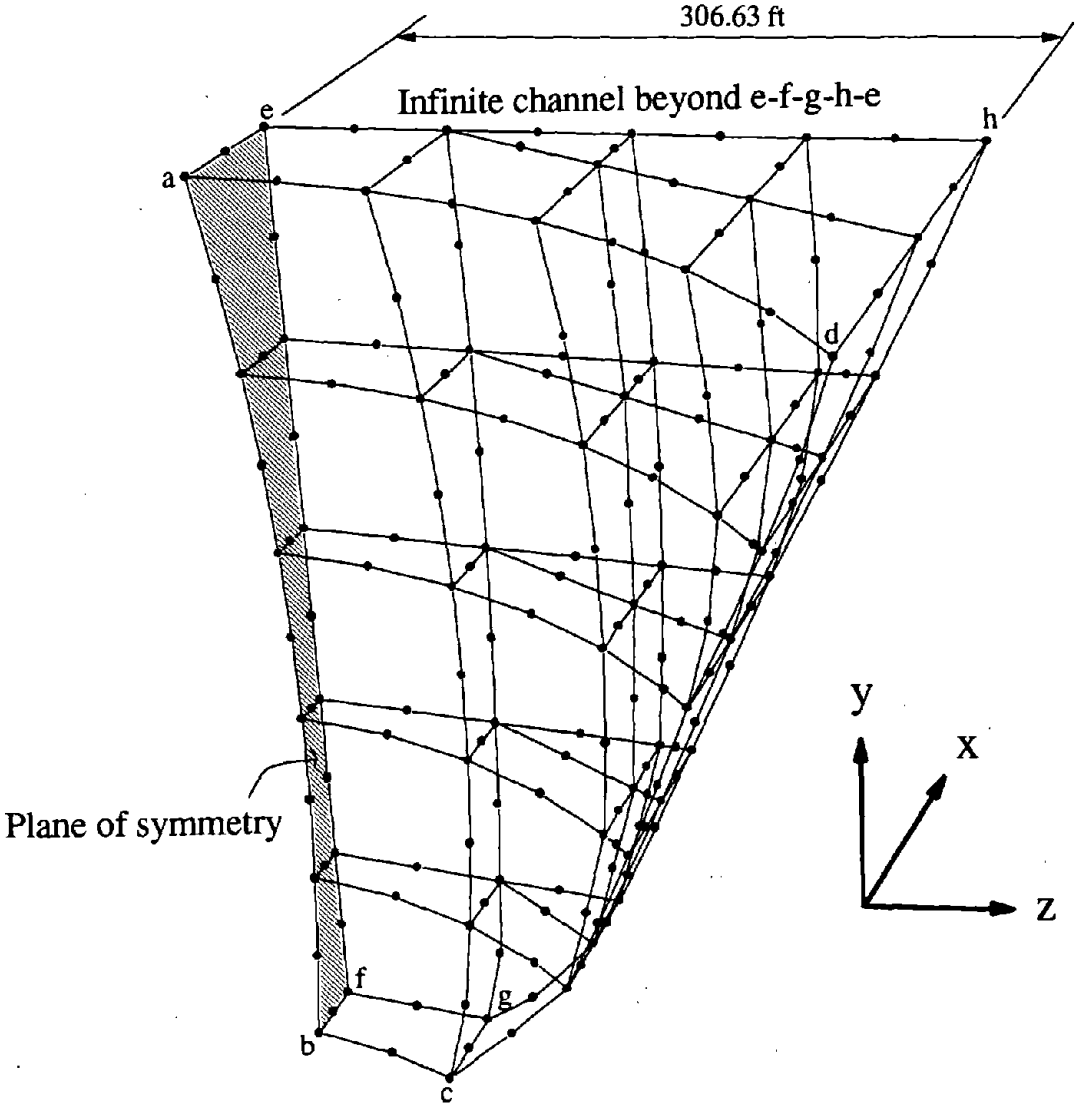

Figure 3.2 Finite element mesh of one-half of the fluid domain of Morrow Point Dam-water-foundation rock system.

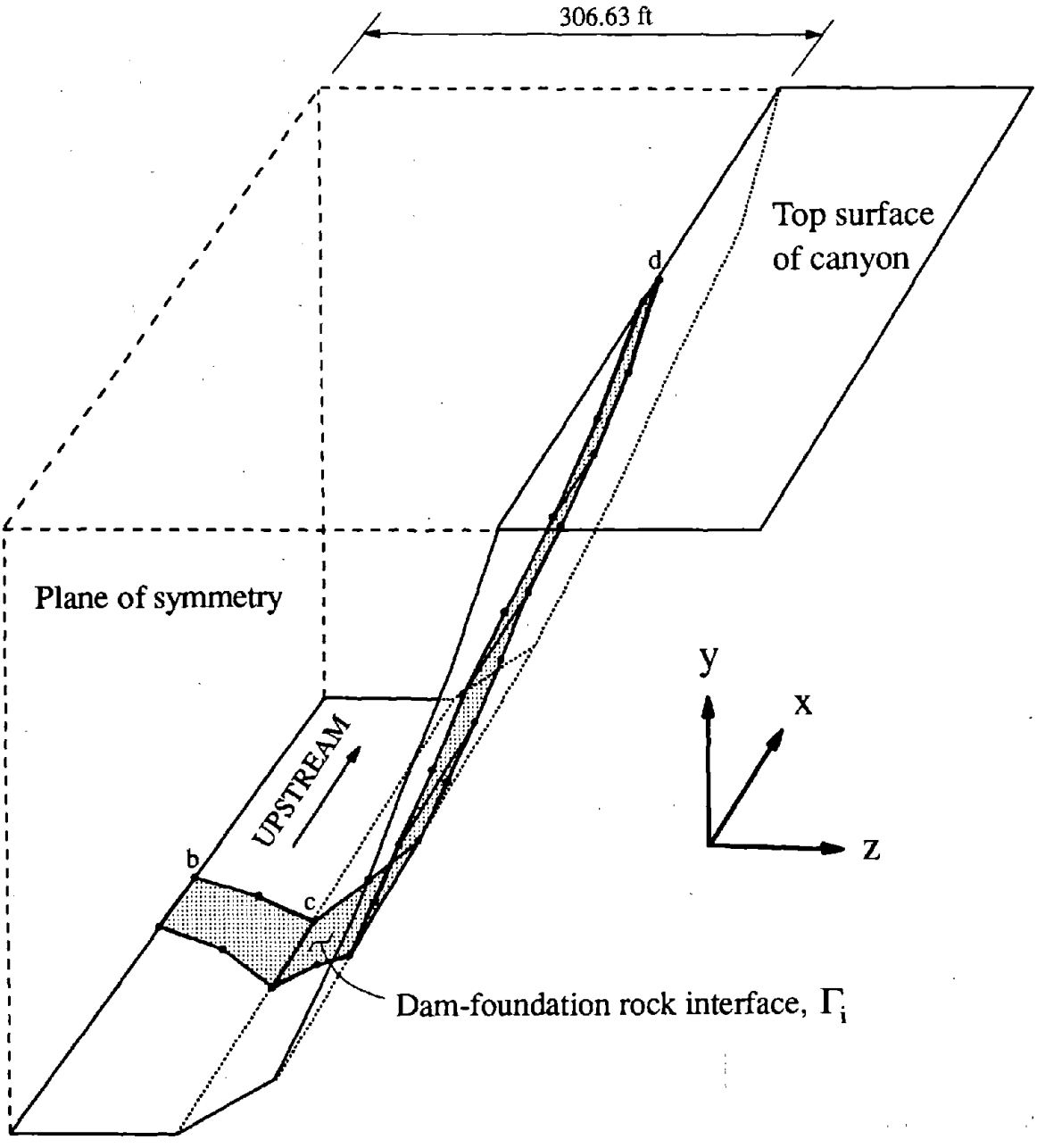

Figure 3.3 Boundary element mesh of one-half of the dam-foundation rock interface in the Morrow Point Dam-water-foundation rock system.

total of 296 DOFs for symmetric (x- and y-component) ground motion and 284 DOFs for antisymmetric (z-component) ground motion.

The mass concrete in the dam is assumed to be homogeneous, isotropic and linear elastic with the following properties: Young's modulus E_s = 4.0 million psi, unit weight w_s = 155 pcf, and Poisson's ratio ν_s = 0.2. A constant hysteretic damping factor η_s = 0.10, which corresponds to 5% viscous damping in all natural vibration modes of the dam with empty reservoir on rigid foundation rock, is selected.

3.2 Impounded Water

The response analysis can handle any water level provided the finite element mesh for the dam is defined to include nodal points at the water level. For most analyses in this investigation, however, the water level is assumed to be at the crest level (full reservoir); the exceptions are the analyses presented in Chapter 5 to study the influence of reservoir level on the fundamental period of the system. Due to the assumption of symmetry about the x-y plane, only one-half of the fluid domain is needed for analysis. The combined finite element-continuum idealization of one-half of the fluid domain with water level assumed to be at the dam crest consists of 27 three-dimensional finite elements for the irregular fluid region with 189 nodal points (Figure 3.2). This idealization contains 157 pressure DOFs for symmetric (x- and y-component) ground motion and 132 pressure DOFs for antisymmetric (z-component) ground motion. The irregular fluid region is bounded by the upstream face of the dam, the uniform canyon, and the transmitting plane e-f-g-h-e. Therefore, the surface a-b-c-d-a of the irregular fluid region (Figure 3.2) coincides with the surface a-b-c-d-a of the upstream face of the dam (Figure 3.1), and lines a-e, b-f, c-g and d-h are all parallel to x-axis. Special equilibrium and compatibility conditions are imposed on the transmitting plane to connect the irregular fluid region with the infinite channel (Figure 3.2). The following properties are assumed for the impounded water: velocity of pressure waves C = 4720 ft/sec and unit weight w_w = 62.4 pcf. There are no data available for the alluvium and sediments at the bottom and sides of the reservoir

impounded by Morrow Point Dam. The wave reflection coefficient α, used to account for the reservoir boundary absorption, is varied in this investigation: 0, 0.5, 0.75, 0.9, 0.95, and 1.0 (non-absorptive reservoir boundary).

3.3 Infinitely-long Uniform Canyon and the Dam-Foundation Rock Interface

The cross-section of the infinitely-long uniform canyon shown in Figure 3.3 is uniquely defined by the projection of the mid-surface of the Morrow Point Dam on the y-z plane. Therefore, the half-width of the canyon, 306.63 ft, is smaller than the half-width of the dam, 311.62 ft (Figure 3.1). The boundary element idealization of one-half of the dam-foundation rock interface that lies completely on the surface of the infinitely-long uniform canyon is shown in Figure 3.4; the top surface of the canyon is assumed to be horizontal. The projections of the boundary element mesh of the dam-foundation rock interface on the x-z plane (plan view) and y-z plane (vertical view) are shown as the solid lines in Figure 3.4(a) and Figure 3.4(b), respectively. The mesh consists of 6 boundary elements with 26 nodes with three translational DOFs for each node. Consequently, there are 76 DOFs for symmetric (x- and y-component) ground motion and 74 DOFs for antisymmetric (z-component) ground motion. The number of nodes and DOFs match those of the finite element mesh for the dam. Also shown in Figures 3.4(a) and 3.4(b) are the dotted lines representing the projections of the finite element mesh of the dam at its interface with the foundation rock on the x-z plane and y-z plane, respectively. The dotted lines do not coincide with the solid lines because of the difference in the geometry of the arch dam abutment and the uniform canyon.

The foundation rock is assumed to be homogeneous, isotropic, and viscoelastic with the following properties: unit weight w_f = 165 pcf, Poisson's ratio ν_f = 0.2, and the Young's modulus E_f is varied as discussed in Section 5.2.1 (for the frequency response functions presented in Chapter 5) and in Section 6.2.1 (for the earthquake response presented in Chapter 6). Energy dissipation in the flexible foundation rock is represented by a constant hysteretic damping factor η_f = 0.10, which corresponds to viscous damping ratio of 5%.

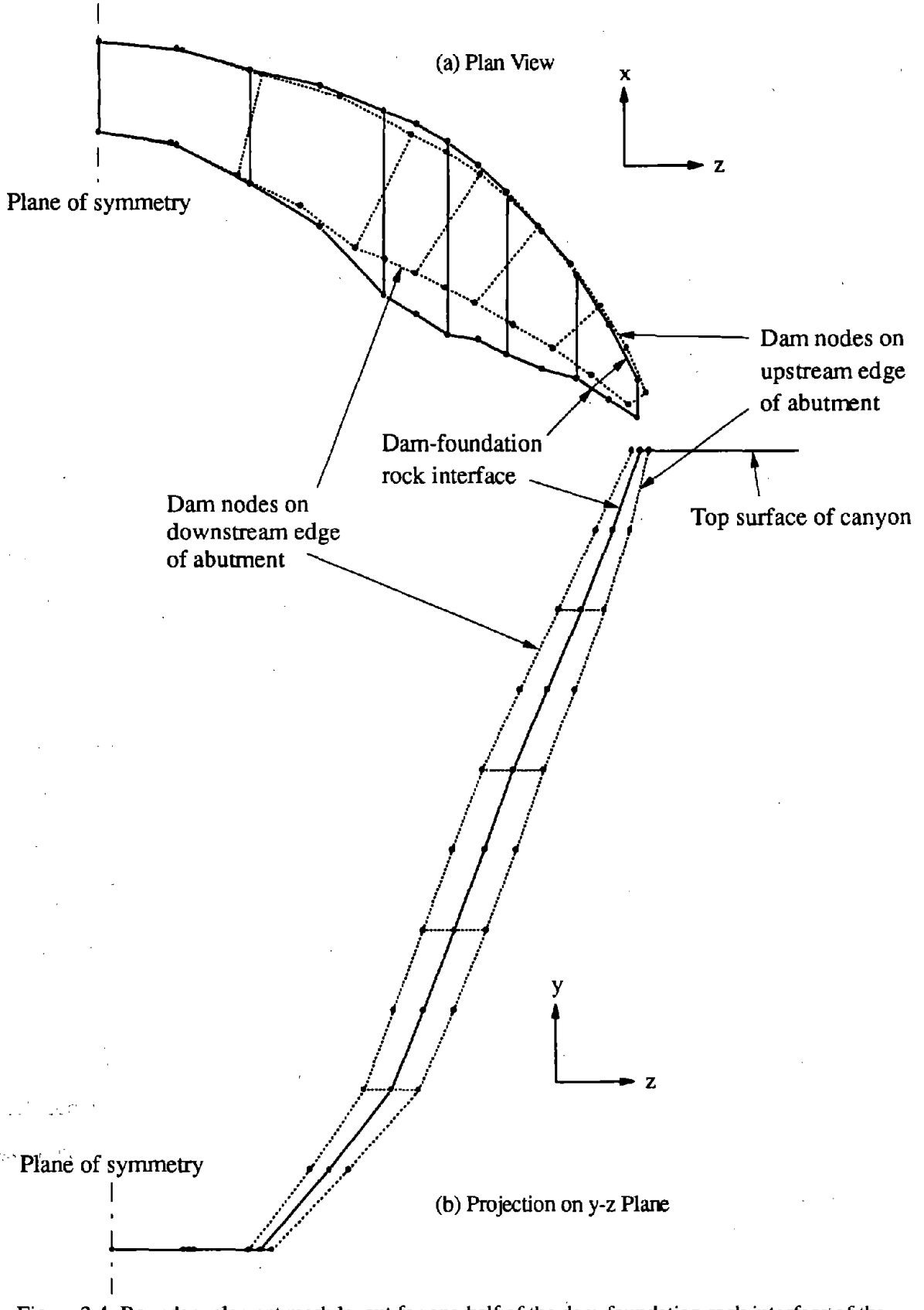

Figure 3.4 Boundary element mesh layout for one-half of the dam-foundation rock interface of the Morrow Point Dam on an infinitely-long uniform canyon.

3.4 Incompatibility between Dam and Canyon

As mentioned earlier, the assumption of a uniform canyon introduces incompatibility between the dam abutment and the canyon. Therefore the stiffness matrix of the dam with reference to the nodal points on its abutment is modified by a linear transformation to redefine it using the nodal points on the dam-foundation rock interface on the uniform canyon. This concept is explained by examining the horizontal cross-section a-b-c-d-e-f-a of the dam [Figure 2.3(d)]. The 5 DOFs (3 translational and 2 rotational) of nodal point b, the middle point of the dam abutment a-c, are linearly transformed to the 6 translational DOFs of nodal points a' and c' on the dam-foundation rock interface, Γ_i, instead of the 6 translational DOFs of nodal points a and c [Figure 2.3(d)]. Similarly, the 5 DOFs of nodal point e, the middle point of the dam abutment d-f, are linearly transformed to the translational DOFs of nodal points d' and f'. With this approximate treatment, we achieve two objectives: the dam substructure retains its original geometry, and displacement compatibility is ensured between the nodal points on the abutment of the dam and those on the dam-foundation rock interface on the uniform canyon.

We now examine the resulting error in the response of the dam. The system is analyzed for two conditions: (1) the cross-section of the canyon is uniform except at and near the dam-foundation rock interface, where it matches the true shape of the dam abutment [ac and fd in Figure 2.3(d)]; and (2) the canyon is uniform throughout [a'c' and f'd' in Figure 2.3(d)]. To enable solution of the problem for the first case, we resort to a finite-sized foundation modeled by finite elements (Figure 3.5) and only foundation flexibility is considered [5]. For consistency, the same finite-element procedure is used even when the canyon is assumed uniform. The frequency response functions for the dam with $E_f/E_s = 1$ are plotted in Figure 3.6 against the normalized excitation frequency parameter ω/ω_1 where ω_1 is the fundamental natural frequency of the dam supported on rigid foundation rock ($E_f = \infty$) with empty reservoir; $\omega_1 \equiv \omega_1^s$ of the symmetric mode for response to upstream and vertical ground motions, and $\omega_1 \equiv \omega_1^a$ of the antisymmetric mode for response to cross-stream ground motion. The two frequency response functions obtained for the two idealizations are close, thus justifying the

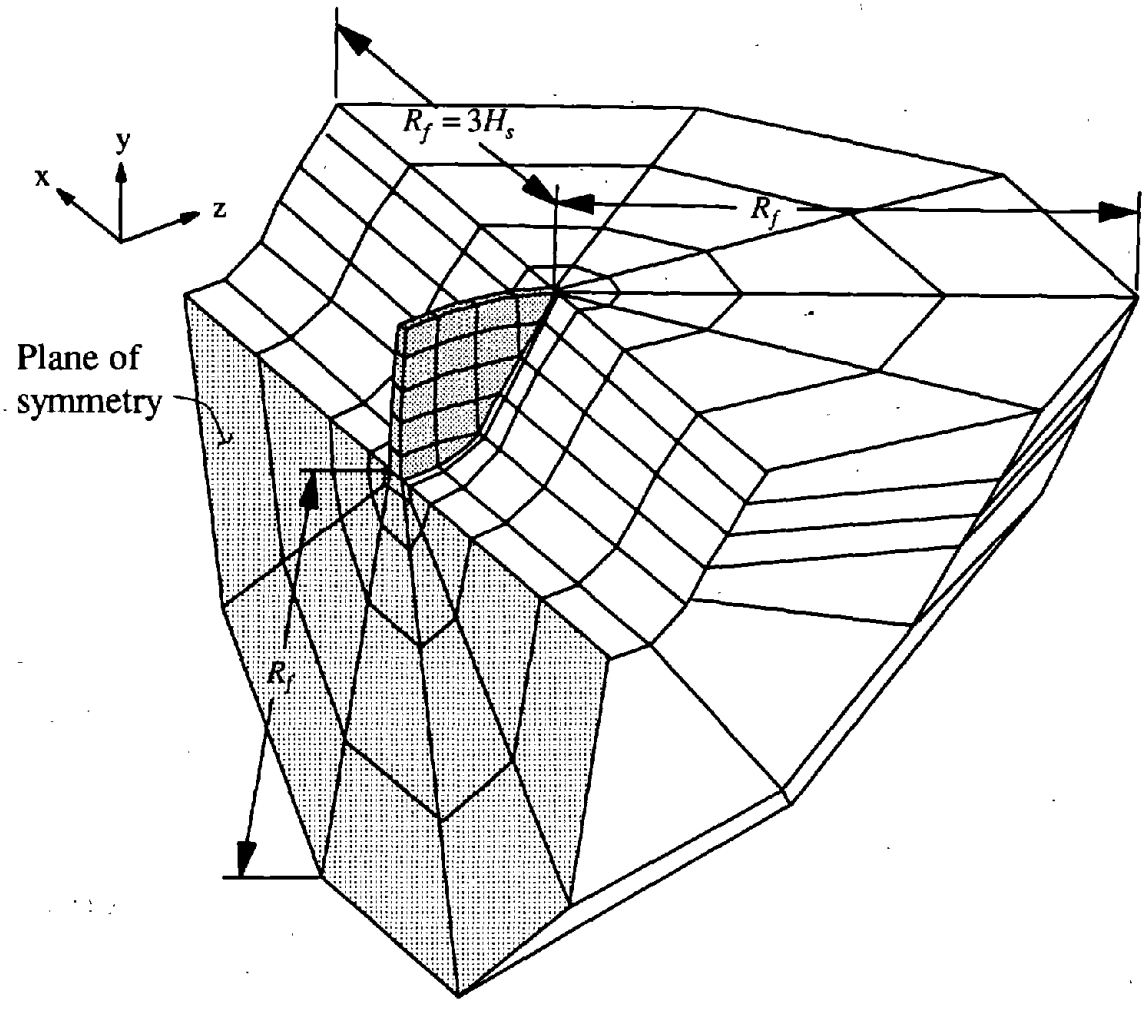

Figure 3.5 Finite element meshes of one-half of the Morrow Point Dam-foundation rock system on an infinitely-long uniform canyon (adapted from Reference [5]).

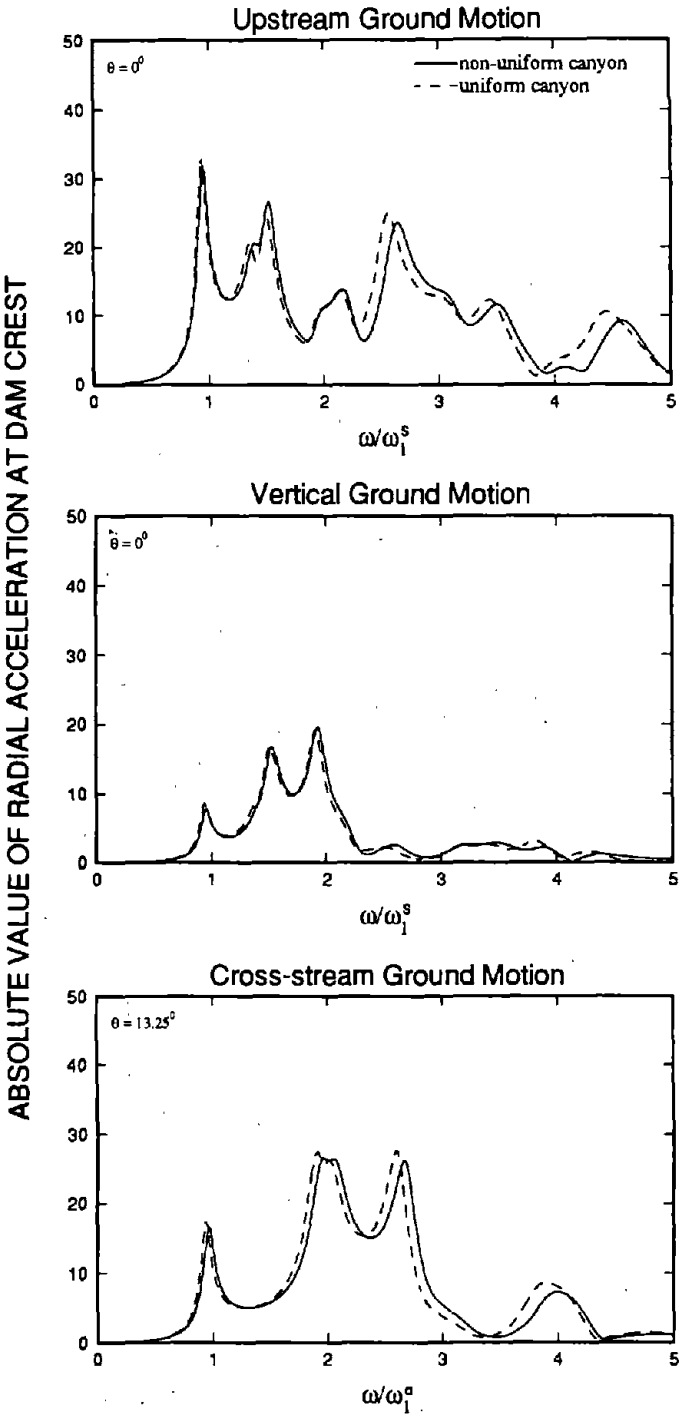

Figure 3.6 Canyon geometry effects on response of Morrow Point Dam with empty reservoir, supported on flexible foundation rock with $E_f/E_s = 1$, to harmonic ground motion. Results presented are from finite element modeling of the foundation rock region considering only foundation flexibility effects.

approximate special treatment to ensure displacement compatibility between the dam and foundation rock substructures.

4 RESPONSE ANALYSIS PROCEDURE

Based on the substructure method of analysis and frequency domain analysis concepts, a procedure is available to evaluate the earthquake response of arch dams. Developed earlier under the assumption of massless foundation rock, this analysis procedure is extended in this chapter to include the effects of dam-foundation rock interaction with the inertia and damping of the foundation rock considered. This formulation is similar to the one for two-dimensional analysis of gravity dams [12].

4.1 Frequency Domain Equations

4.1.1 Dam Substructure

The equations of motion for the dam idealized as a three-dimensional finite element system (Figure 4.1) are:

$$\mathbf{m}_c\ddot{\mathbf{r}}_c + \mathbf{c}_c\dot{\mathbf{r}}_c + \mathbf{k}_c\mathbf{r}_c = -\mathbf{m}_c\mathbf{1}_c^x a_g^x(t) - \mathbf{m}_c\mathbf{1}_c^y a_g^y(t) - \mathbf{m}_c\mathbf{1}_c^z a_g^z(t) + \mathbf{R}_b(t) + \mathbf{R}_h(t) \tag{4.1}$$

in which $\mathbf{m}_c$, $\mathbf{c}_c$, and $\mathbf{k}_c$ are the mass, damping and stiffness matrices for the finite element system; $\mathbf{r}_c$ is the vector of nodal point displacements relative to the free-field ground displacement (Figure 4.1):

$$\mathbf{r}_c = \left\langle r_1^x \quad r_1^y \quad r_1^z \quad r_2^x \quad r_2^y \quad r_2^z \quad \cdots \quad r_n^x \quad r_n^y \quad r_n^z \quad \cdots \quad r_{N+N_b}^x \quad r_{N+N_b}^y \quad r_{N+N_b}^z \right\rangle^T \tag{4.2}$$

where r_n^x, r_n^y and r_n^z are the x-, y- and z-components of displacements of nodal point n; N is the number of nodal points other than on the dam-foundation rock interface; N_b is the number of nodal points on the dam-foundation rock interface; and vectors $\mathbf{1}_c^x$, $\mathbf{1}_c^y$, and $\mathbf{1}_c^z$ contain ones in positions corresponding to the x, y, and z translational DOFs, respectively, with zeros elsewhere:

$$\begin{aligned}
\mathbf{1}_c^x &= \langle 1 \quad 0 \quad 0 \quad 1 \quad 0 \quad 0 \quad \cdots \quad 1 \quad 0 \quad 0 \quad \cdots \quad 1 \quad 0 \quad 0 \rangle^T \\
\mathbf{1}_c^y &= \langle 0 \quad 1 \quad 0 \quad 0 \quad 1 \quad 0 \quad \cdots \quad 0 \quad 1 \quad 0 \quad \cdots \quad 0 \quad 1 \quad 0 \rangle^T \\
\mathbf{1}_c^z &= \langle 0 \quad 0 \quad 1 \quad 0 \quad 0 \quad 1 \quad \cdots \quad 0 \quad 0 \quad 1 \quad \cdots \quad 0 \quad 0 \quad 1 \rangle^T
\end{aligned} \tag{4.3}$$

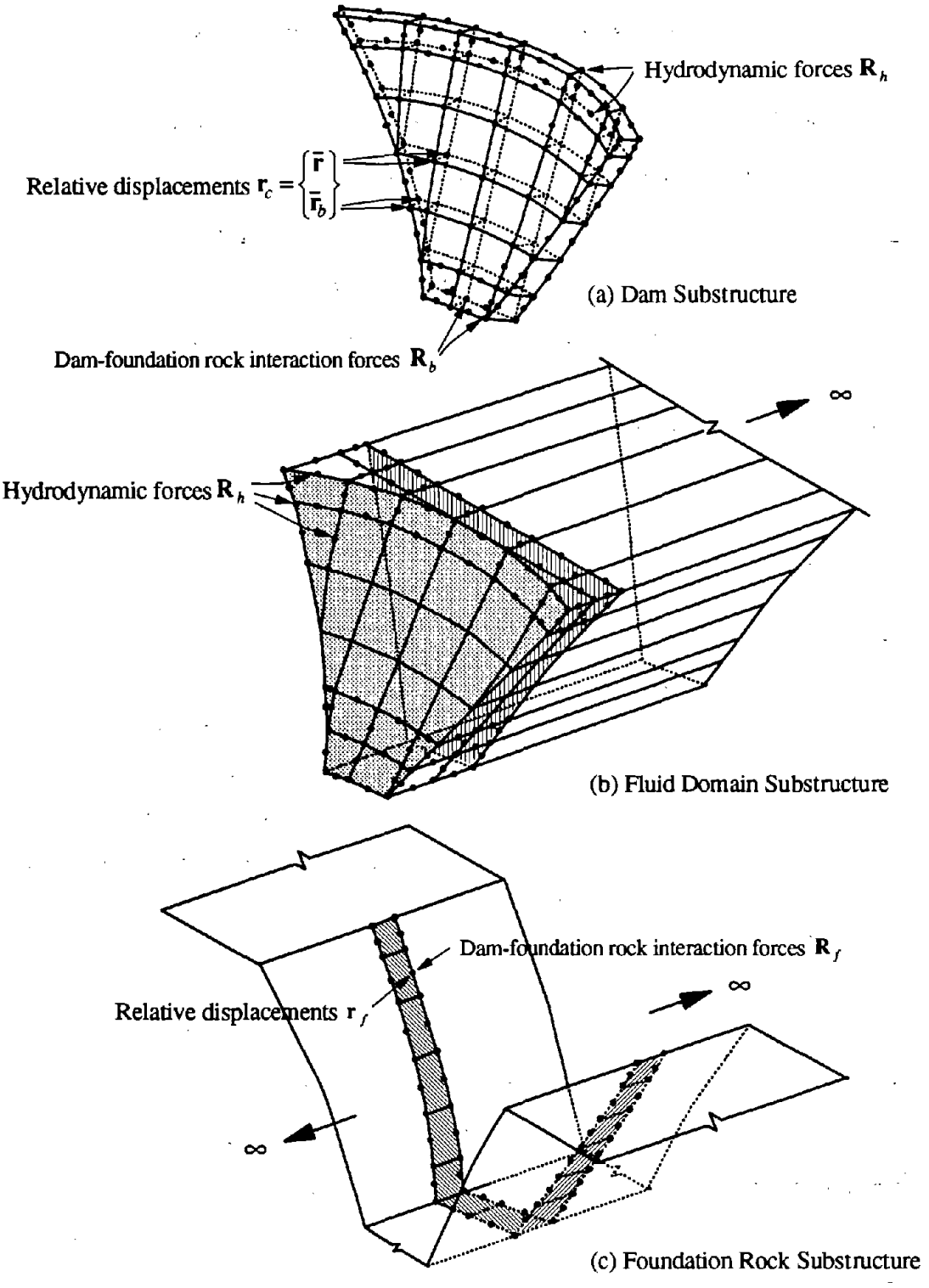

Figure 4.1 Substructure representation of the dam-water-foundation rock system.

The force vector $\mathbf{R}_b(t)$ represents the forces at the dam-foundation rock due to interaction between the dam and the foundation rock. The force vector $\mathbf{R}_h(t)$ includes the hydrodynamic forces at the upstream face of the dam.

For harmonic ground acceleration $a_g^l(t) = e^{i\omega t}$ in the $l = x$ (upstream), $l = y$ (vertical) or $l = z$ (cross-stream) direction, the displacements and forces can be expressed in terms of their complex-valued frequency response functions:

$$\begin{aligned} \mathbf{r}_c^l(t) &= \overline{\mathbf{r}}_c^l(\omega)e^{i\omega t} \\ \mathbf{R}_b^l(t) &= \overline{\mathbf{R}}_b^l(\omega)e^{i\omega t} \\ \mathbf{R}_h^l(t) &= \overline{\mathbf{R}}_h^l(\omega)e^{i\omega t} \end{aligned} \tag{4.4}$$

Partitioning $\mathbf{r}_c$ into $\mathbf{r}$ for nodal points other than on the dam-foundation rock interface, and $\mathbf{r}_b$ for nodal points on the dam-foundation rock interface, Equation (4.1) can be expressed in the frequency domain as

$$\left[-\omega^2\begin{bmatrix}\mathbf{m} & \mathbf{0}\\ \mathbf{0} & \mathbf{m}_b\end{bmatrix}+(1+i\eta_s)\begin{bmatrix}\mathbf{k} & \mathbf{k}_b\\ \mathbf{k}_b^T & \mathbf{k}_{bb}\end{bmatrix}\right]\begin{Bmatrix}\overline{\mathbf{r}}^l(\omega)\\ \overline{\mathbf{r}}_b^l(\omega)\end{Bmatrix}=-\begin{Bmatrix}\mathbf{m}\mathbf{1}^l\\ \mathbf{m}_b\mathbf{1}_b^l\end{Bmatrix}+\begin{Bmatrix}\overline{\mathbf{R}}_h^l(\omega)\\ \overline{\mathbf{R}}_b^l(\omega)\end{Bmatrix} \tag{4.5}$$

where η_s is the constant hysteretic damping factor for the dam. The hydrodynamic forces $\overline{\mathbf{R}}_h$ will be expressed later in terms of the acceleration at the upstream face of the dam by analysis of the fluid domain substructure. Also the dam-foundation rock interaction forces $\overline{\mathbf{R}}_b$ will be expressed in terms of interaction displacements at the dam-foundation rock interface.

4.1.2 Foundation Rock Substructure

The foundation rock substructure should include the dam-foundation rock interface and part of the reservoir boundary along the upstream canyon surface to account for dam-foundation rock interaction and water-foundation rock interaction effects, respectively. However, because water-foundation rock interaction effects are insignificant compared to dam-foundation rock interaction effects, the reservoir boundary part has been excluded in the dynamic analysis of gravity dams [12]

and subsequently in earlier analysis of arch dams [5]. In this study also, the water-foundation rock interaction effects are neglected.

The complex-valued impedance (dynamic stiffness) matrix for the foundation rock region, defined relating to the DOFs of the dam-foundation rock interface, relates the interaction forces and displacements relative to free-field ground motion in the l^{th} direction (Figure 4.1):

$$\mathbf{S}_f(\omega)\bar{\mathbf{r}}_f^l(\omega) = \bar{\mathbf{R}}_f^l(\omega) \tag{4.6}$$

which is similar to Equation (2.1).

4.1.3 Dam-Foundation Rock Substructure

Equilibrium of the interaction forces between the dam and the foundation rock substructures at the dam-foundation rock interface requires that:

$$\bar{\mathbf{R}}_f^l(\omega) = -\bar{\mathbf{R}}_b^l(\omega) \tag{4.7}$$

and compatibility of interaction displacements at the dam-foundation rock interface requires that:

$$\bar{\mathbf{r}}_f^l(\omega) = \bar{\mathbf{r}}_b^l(\omega) \tag{4.8}$$

Using Equations (4.7) and (4.8), Equation (4.6) becomes

$$\bar{\mathbf{R}}_b^l(\omega) = -\mathbf{S}_f(\omega)\bar{\mathbf{r}}_b^l(\omega) \tag{4.9}$$

which upon substitution in Equation (4.5) gives

$$\left[-\omega^2\begin{bmatrix}\mathbf{m} & \mathbf{0}\\ \mathbf{0} & \mathbf{m}_b\end{bmatrix} + (1+i\eta_s)\begin{bmatrix}\mathbf{k} & \mathbf{k}_b\\ \mathbf{k}_b^T & \mathbf{k}_{bb}\end{bmatrix} + \begin{bmatrix}\mathbf{0} & \mathbf{0}\\ \mathbf{0} & \mathbf{S}_f(\omega)\end{bmatrix}\right]\begin{Bmatrix}\bar{\mathbf{r}}^l(\omega)\\ \bar{\mathbf{r}}_b^l(\omega)\end{Bmatrix} = -\begin{Bmatrix}\mathbf{m}\mathbf{1}^l\\ \mathbf{m}_b\mathbf{1}_b^l\end{Bmatrix} + \begin{Bmatrix}\bar{\mathbf{R}}_h^l(\omega)\\ \mathbf{0}\end{Bmatrix} \tag{4.10}$$

The vector $\overline{\mathbf{R}}_h^l$ of frequency response functions for hydrodynamic forces contains non-zero terms only at the nodal points on the upstream face of the dam.

4.1.4 Reduction of Degrees of Freedom

Equation (4.10) represents a set of $3(N+N_b)$ frequency-dependent, complex-valued equations. Enormous computational effort would be required for repeated solution of these equations for many values of the excitation frequency. Therefore, it is important to reduce the number of DOFs. An approach based on the Ritz concept is effective in reducing the number of DOFs in analysis of two-dimensional as well as three-dimensional dam-foundation rock systems [5,12,20]. The displacements $\mathbf{r}_c$ are expressed as linear combinations of J Ritz vectors derived from an associated dam-foundation rock system:

$$\mathbf{r}_c(t)=\sum_{j=1}^{J} Z_j(t)\boldsymbol{\psi}_j \tag{4.11}$$

in which $Z_j(t)$ is the generalized coordinate that corresponds to the j^{th} Ritz vector $\boldsymbol{\psi}_j$. For harmonic ground acceleration, Equation (4.11) can be expressed in terms of the complex-valued frequency response functions for the generalized coordinates:

$$\overline{\mathbf{r}}_c^l(\omega)=\sum_{j=1}^{J} \overline{Z}_j^l(\omega)\boldsymbol{\psi}_j \tag{4.12}$$

The associated dam-foundation rock system is obtained by replacing $\mathbf{S}_f(\omega)$ by the static value $\mathbf{S}_f(0)$. The vibration frequencies λ_j and corresponding Ritz vectors $\boldsymbol{\psi}_j$ are the solutions of the following eigenvalue problem:

$$\left[\mathbf{k}_c+\tilde{\mathbf{S}}_f(0)\right]\boldsymbol{\psi}_j=\lambda_j^2\mathbf{m}_c\boldsymbol{\psi}_j \tag{4.13}$$

where

$$\tilde{\mathbf{S}}_f(\omega)=\begin{bmatrix}\mathbf{0} & \mathbf{0}\\ \mathbf{0} & \mathbf{S}_f(\omega)\end{bmatrix} \tag{4.14}$$

is the expanded version of $\mathbf{S}_f$ with zero values corresponding to all DOFs of the dam not on the dam-foundation rock interface. For convenience, the Ritz vectors are normalized such that $\psi_j^T \mathbf{m}_c \psi_j = 1$.

Introducing Equation (4.12) into Equation (4.10), premultiplying by ψ_j^T and utilizing the orthogonality properties of the eigenvectors of the associated dam-foundation rock system with respect to the stiffness and mass matrices of Equation (4.13), results in:

$$\mathbf{S}(\omega)\overline{\mathbf{Z}}^l(\omega) = \mathbf{L}^l(\omega) \tag{4.15}$$

where the elements of the matrix $\mathbf{S}(\omega)$ and the vector $\mathbf{L}^l(\omega)$ are:

$$\begin{aligned} S_{nj}(\omega) &= \left[-\omega^2 + (1+i\eta_s)\lambda_n^2\right]\delta_{nj} + (\psi_n^b)^T\left[\mathbf{S}_f(\omega) - (1+i\eta_s)\mathbf{S}_f(0)\right]\psi_j^b \\ L_n^l(\omega) &= -\psi_n^T \mathbf{m}_c \mathbf{1}_c^l + \{\psi_n^f\}^T \overline{\mathbf{R}}_h^l(\omega) \end{aligned} \tag{4.16}$$

for $n, j = 1, 2, 3, \cdots, J$; $\overline{\mathbf{Z}}^l(\omega)$ is the vector of frequency response functions $\overline{Z}_j^l(\omega)$ for the generalized coordinates; δ_{nj} is the Kroneker delta function; ψ_n^f is a subvector of ψ_n that contains only the elements corresponding to the nodal points at the dam-water interface; and ψ_n^b is a subvector of ψ_n that contains only the elements corresponding to the nodal points at the dam-foundation rock interface.

Equations (4.15) and (4.16) represents J simultaneous, complex-valued equations in the generalized coordinates for each excitation frequency ω. These equations need to be solved over a range of values of the excitation frequency to compute the frequency response functions. Accurate solutions can be obtained by including a small number of Ritz vectors, typically, less than 10 for gravity dams [12] and 18 for arch dams [5], thus greatly reducing the computational effort.

4.1.5 Fluid Domain Substructure

The unknown forces $\mathbf{R}_h(t)$ in Equation (4.1), whose frequency response functions $\overline{\mathbf{R}}_h^l(\omega)$ appear in Equation (4.16), can be expressed in terms of the accelerations at the upstream face of the

dam and at the reservoir boundary by analysis of the fluid domain. The motion of the water is governed by the three-dimensional wave equation:

$$\frac{\partial^2 p}{\partial x^2}+\frac{\partial^2 p}{\partial y^2}+\frac{\partial^2 p}{\partial z^2}=\frac{1}{C^2}\frac{\partial^2 p}{\partial t^2} \tag{4.17}$$

where $p(x,y,z,t)$ is the hydrodynamic pressure (in excess of hydrostatic pressure) and C is the velocity of pressure waves in water. For harmonic ground acceleration $a_g^l(t)=e^{i\omega t}$, the hydrodynamic pressure can be expressed as $p(x,y,z,t)=\overline{p}(x,y,z,\omega)e^{i\omega t}$, where $\overline{p}(x,y,z,\omega)$ is the complex-valued frequency response function for hydrodynamic pressure, and Equation (4.17) becomes the Helmholtz equation:

$$\frac{\partial^2 \overline{p}}{\partial x^2}+\frac{\partial^2 \overline{p}}{\partial y^2}+\frac{\partial^2 \overline{p}}{\partial z^2}+\frac{\omega^2}{C^2}\overline{p}=0 \tag{4.18}$$

The hydrodynamic pressure is generated by accelerations at the upstream face of the dam and at the reservoir boundary.

The linear form of the governing equation and the boundary conditions permits the hydrodynamic pressure to be expressed as:

$$\overline{p}^l(x,y,z,\omega)=\overline{p}_0^l(x,y,z,\omega)+\sum_{j=1}^{J}\overline{Z}_j^l(\omega)\overline{p}_j^f(x,y,z,\omega) \tag{4.19}$$

In Equation (4.19), the frequency response function $\overline{p}_0^l(x,y,z,\omega)$ is the hydrodynamic pressure due to the l^{th} component of ground acceleration of a rigid dam and reservoir boundary [Figure 4.2(a)], it is the solution of Equation (4.18) subjected to the radiation condition at $x=\infty$ and the following boundary conditions:

$$\begin{aligned}
&\frac{\partial}{\partial n}\overline{p}_0^l(s,r,\omega)=-\rho\in^l(s,r)\\
&\left[\frac{\partial}{\partial n}-i\omega q\right]\overline{p}_0^l(s,r,\omega)=-\rho\in^l(s',r')\\
&\overline{p}_0^l(x,H,z,\omega)=0
\end{aligned} \tag{4.20}$$

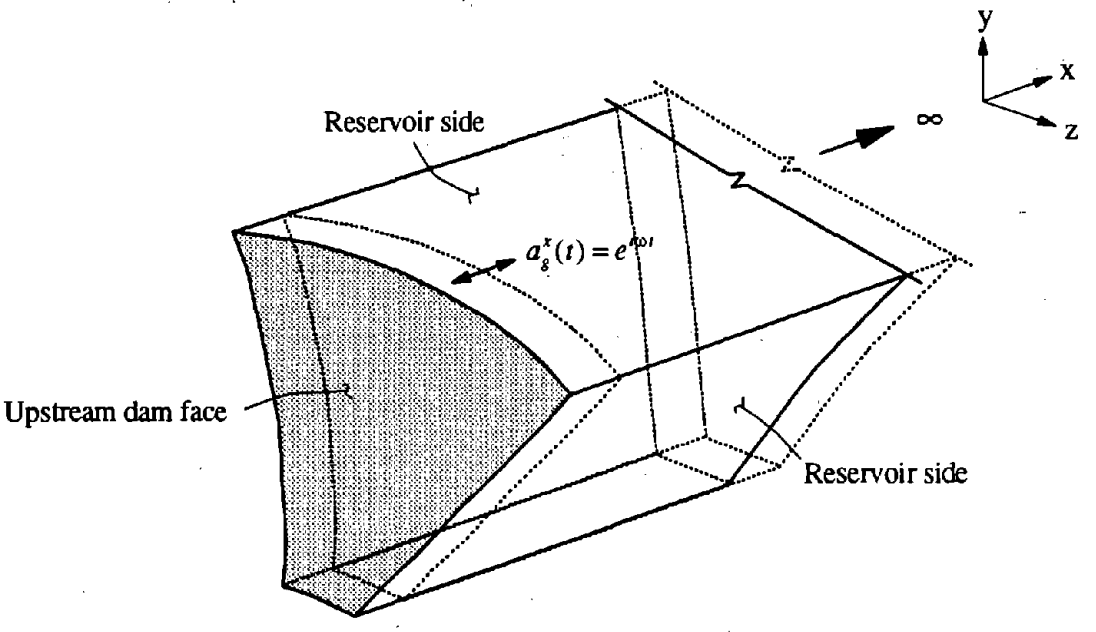

(a) Boundary Accelerations Causing $\hat{p}_0^x(s,r,\omega)$

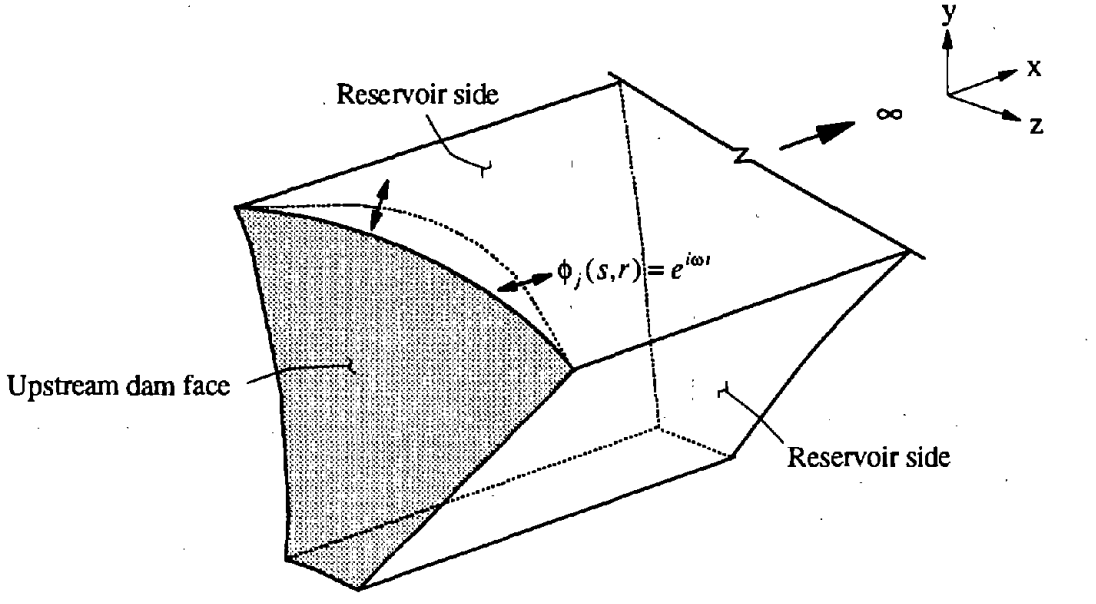

(b) Boundary Accelerations Causing $\hat{p}_j(s,r,\omega)$

Figure 4.2 Reservoir boundary accelerations causing hydrodynamic pressures on the upstream face of the dam by frequency response functions $\hat{p}_0^x(s,r,\omega)$ and $\hat{p}_j(s,r,\omega)$.

In Equation (4.20), H is the y-coordinate of the free surface of water measured from the base of the dam; ρ is the mass density of water; q is the admittance or damping coefficient (Section 2.5); s, r are the localized spatial coordinates on the upstream face of the dam; s', r' are the localized spatial coordinates on the reservoir boundary (Figure 4.3); $\epsilon^l(s,r)$ is a function defined along accelerating boundaries (s, $r = s$, r for upstream face of the dam or s, $r = s'$, r' for the reservoir boundary) which gives the length of the component of a unit vector along l (l = x, y, or z) in the direction of the inward normal n (Figure 4.3).

In Equation (4.19), the frequency response function $\bar{p}_j^f(x,y,z,\omega)$ is the amplitude of hydrodynamic pressure due to normal harmonic acceleration of dam in the j^{th} Ritz vector, without any reservoir boundary motion [Figure 4.2(b)]. It is the solution of Equation (4.18) subjected to the radiation condition at $x = \infty$ and the following boundary conditions:

$$\begin{aligned} &\frac{\partial}{\partial n}\bar{p}_j^f(s,r,\omega) = -\rho\psi_j^f(s,r) \\ &\left[\frac{\partial}{\partial n} - i\omega q\right]\bar{p}_j^f(s',r',\omega) = 0 \\ &\bar{p}_j^f(x,H,z,\omega) = 0 \end{aligned} \tag{4.21}$$

where $\psi_j^f(s,r)$ is the function representing the normal component of the j^{th} Ritz vector at the dam-water interface.

Procedures for solving these boundary value problems and evaluating $\bar{p}_0^l(x,y,z,\omega)$ and $\bar{p}_j^f(x,y,z,\omega)$ for the fluid domain idealized as in Figure 2.3(c) are available [4,5]. The frequency response functions for hydrodynamic forces $\mathbf{R}_h(t)$ associated with the hydrodynamic pressure $\bar{p}^l(x,y,z,\omega)$ are from Equation (4.19):

$$\bar{\mathbf{R}}_h^l(\omega) = \bar{\mathbf{R}}_0^l(\omega) + \sum_{j=1}^{J} \bar{\bar{Z}}_j^l(\omega)\bar{\mathbf{R}}_j^f(\omega) \tag{4.22}$$

where $\bar{\mathbf{R}}_0^l(\omega)$ and $\bar{\mathbf{R}}_j^f(\omega)$ are the nodal forces statically equivalent to the pressure functions $-\bar{p}_0^l(x,y,z,\omega)$ and $-\bar{p}_j^f(x,y,z,\omega)$, respectively.

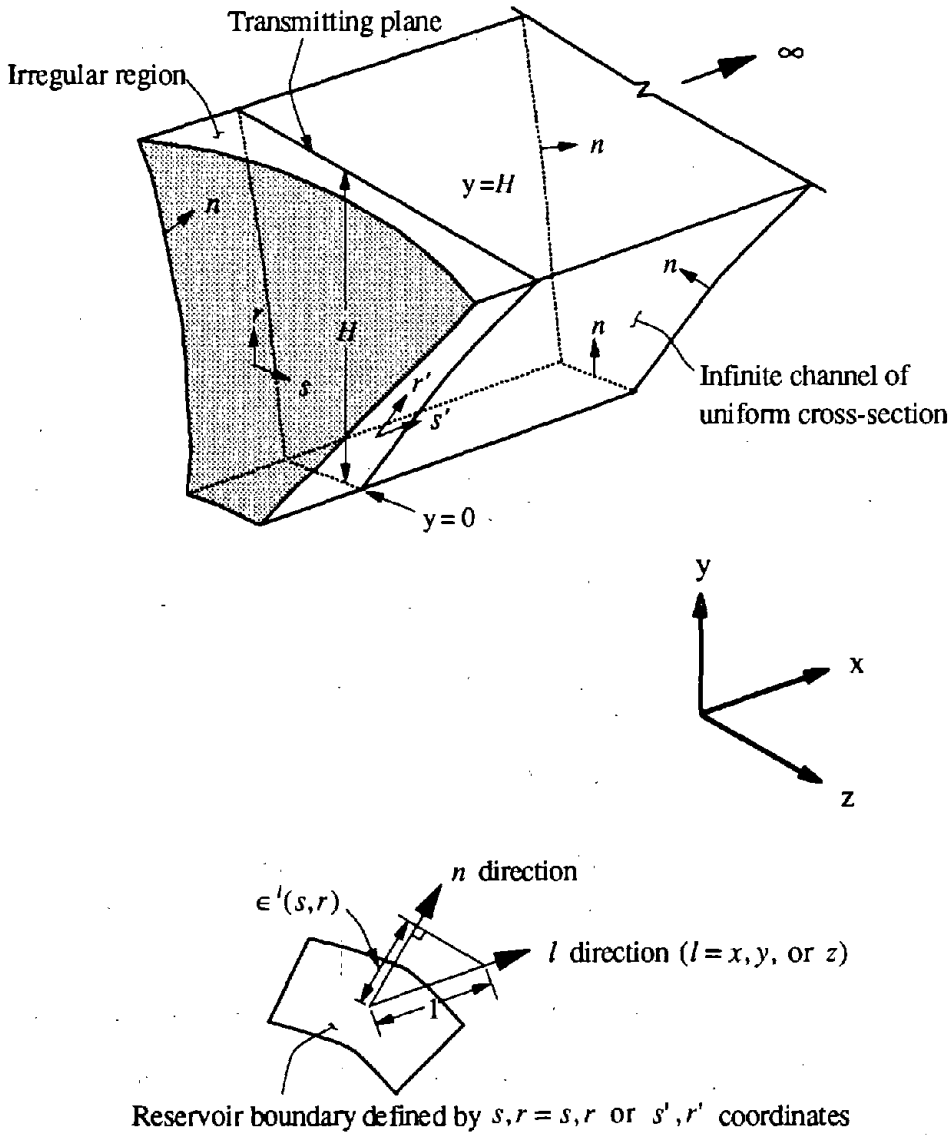

Figure 4.3 Definition of various terms associated with the fluid domain substructure.

4.1.6 Dam-Water-Foundation Rock System

Introducing Equation (4.22) with $\ddot{\overline{Z}}_j^l(\omega) = -\omega^2 \overline{Z}_j^l(\omega)$ into Equations (4.15) and (4.16) leads to:

$$\mathbf{S}(\omega)\overline{\mathbf{Z}}^l(\omega) = \mathbf{L}^l(\omega) \tag{4.23}$$

where, after rearrangement, the elements in the matrix $\mathbf{S}(\omega)$ and the vector $\mathbf{L}^l(\omega)$ are given by:

$$\begin{aligned} S_{nj}(\omega) &= \left[-\omega^2 + (1+i\eta_s)\lambda_n^2\right]\delta_{nj} + (\psi_n^b)^T\left[\mathbf{S}_f(\omega) - (1+i\eta_s)\mathbf{S}_f(0)\right]\psi_j^b \\ &\quad + \omega^2(\psi_n^f)^T\overline{\mathbf{R}}_j^f(\omega) \\ L_n^l(\omega) &= -\psi_n^T\mathbf{m}_c\mathbf{1}_c^l + (\psi_n^f)^T\overline{\mathbf{R}}_0^l(\omega) \end{aligned} \tag{4.24}$$

Equations (4.23) and (4.24) contain the effects of dam-water interaction and of dam-foundation rock interaction considering inertia, damping, and flexibility of the foundation rock. The effects of reservoir boundary absorption are contained in the hydrodynamic terms $\hat{\mathbf{R}}_0^l(\omega)$ and $\hat{\mathbf{R}}_j^f(\omega)$. However, water-foundation rock interaction effects have been excluded.

Note that if the static stiffness $\mathbf{S}_f(0)$ is used instead of $\mathbf{S}_f(\omega)$ for all frequency values, Equation (4.24) reduces to:

$$\begin{aligned} S_{nj}(\omega) &= \left[-\omega^2 + (1+i\eta_s)\lambda_n^2\right]\delta_{nj} - i\eta_s(\psi_n^b)^T\mathbf{S}_f(0)\psi_j^b + \omega^2(\psi_n^f)^T\overline{\mathbf{R}}_j^f(\omega) \\ L_n^l(\omega) &= -\psi_n^T\mathbf{m}_c\mathbf{1}_c^l + (\psi_n^f)^T\overline{\mathbf{R}}_0^l(\omega) \end{aligned} \tag{4.25}$$

These equations are used in the EACD-3D program [5,6].

4.2 Response to Arbitrary Ground Motion

Once the complex-valued frequency response functions, $\overline{Z}_j^l(\omega)$, $l = x,y,z$, $j = 1,2,\cdots,J$, for the generalized coordinates are obtained by solving Equations (4.23) and (4.24) for excitation frequencies in the range of interest, the response of the dam to arbitrary ground motion can be computed. The

generalized coordinates are given by the Fourier integral as a superposition of responses to individual harmonic components of the ground motion:

$$Z_j^l(t) = \frac{1}{2\pi}\int_{-\infty}^{\infty} \bar{Z}_j^l(\omega) A_g^l(\omega) e^{i\omega t} d\omega \tag{4.26}$$

where $A_g^l(\omega)$ is the Fourier transform of the l-component of the specified free-field ground acceleration $a_g^l(t)$:

$$A_g^l(\omega) = \int_0^d a_g^l(t) e^{-i\omega t} dt \tag{4.27}$$

in which d is the duration of the ground motion. The displacement response to the upstream, vertical and cross-stream components of ground motion, simultaneously, is obtained by transforming the generalized coordinates back to the nodal displacements according to Equation (4.12):

$$\mathbf{r}_c(t) = \sum_{j=1}^{J} [\bar{Z}_j^x(t) + \bar{Z}_j^y(t) + \bar{Z}_j^z(t)]\psi_j \tag{4.28}$$

The stresses in the dam at any instant of time can be determined from the nodal displacements. The stress vector $\boldsymbol{\sigma}_p(t)$ in finite element p of the dam is related to the nodal displacement vector $\mathbf{r}_p(t)$ for that element by

$$\boldsymbol{\sigma}_p(t) = \mathbf{T}_p \mathbf{r}_p(t) \tag{4.29}$$

where $\mathbf{T}_p$ is the stress-displacement transformation matrix for finite element p.

4.3 Summary of Analysis Procedure

The above-described procedure for analysis of the earthquake response of arch dams is summarized as a sequence of steps:

1. Formulate $\mathbf{m}_c$ and $\mathbf{k}_c$, the mass and stiffness matrices for the finite element idealization of the arch dam, respectively, with reference to the DOFs of all nodal points in the idealization including those on the dam-foundation rock interface.

2. Compute $\mathbf{S}_f(\omega)$, the complex-valued frequency-dependent foundation impedance matrix for the boundary element idealization of the foundation rock region, at selected frequencies that cover the range of interest. $\mathbf{S}_f(\omega)$ is needed with reference to the DOFs of nodal points on the dam-foundation rock interface. If the boundary element mesh for the foundation is finer than the finite element mesh for the dam, the extra DOFs should be condensed out. If the foundation impedance matrix is available for foundation rock with a particular value of Young's modulus E_f, the foundation impedance matrix for foundation rock with a different E_f but with same Poisson's ratio can be obtained readily (see next section).

3. Solve the eigenvalue problem of Equation (4.13) to obtain the first J eigenvalues λ_j and the corresponding eigenvectors ψ_j which are normalized such that $\psi_j^T \mathbf{m}_c \psi_j = 1$.

4. Evaluate the frequency response function $\overline{p}_0^l(s,r,\omega)$, $l = x,y,z$, for hydrodynamic pressure on the upstream face of the dam due to the l^{th} component of ground (includes reservoir boundary) acceleration with a rigid dam [Figure 4.2(a)].

5. Evaluate the frequency response function $\overline{p}_j(s,r,\omega)$, $j = 1,2,\cdots,J$, for hydrodynamic pressure due to normal acceleration $\psi_j^f(s,r)$ at the upstream face of the dam corresponding to the j^{th} Ritz vector, with no motion of the reservoir boundary [Figure 4.2(b)].

6. Evaluate the vectors of nodal forces $\overline{\mathbf{R}}_0^l(\omega)$ and $\overline{\mathbf{R}}_j(\omega)$ statically equivalent to $-\overline{p}_0^l(s,r,\omega)$ and $-\overline{p}_j(s,r,\omega)$, respectively, evaluated in Steps 4 and 5.

7. Formulate the J complex-valued equations in the unknown frequency response functions $\overline{Z}_j^l(\omega)$, $j = 1,2,\cdots,J$, for the J generalized coordinates corresponding to the Ritz vectors included in the analysis [Equations (4.23) and (4.24)].

8. Determine the frequency response functions $\overline{\mathbf{Z}}^j(\omega)$ for the generalized coordinates. Repeated solutions of Equations (4.23) and (4.24) for excitation frequencies covering the range over which the earthquake ground motion and structural response have significant components lead to the frequency response function $\overline{\mathbf{Z}}^j(\omega)$.

9. Determine $\mathbf{Z}^j(t)$, the response of the dam to arbitrary ground motion, from Equations (4.26) and (4.27). The Fourier integrals in these two equations are computed in their discrete form using an efficient Fast Fourier Transform (FFT) algorithm [21].

10. Determine the displacement response $\mathbf{r}_c(t)$ to the upstream (x), vertical (y) and cross-stream (z) components of ground motion simultaneously by transforming the generalized coordinates to the nodal coordinates [Equation (4.28)].

11. Determine the stresses in the dam as a function of time from the nodal displacements. At any instant of time, the vector $\boldsymbol{\sigma}_p(t)$ of stress components in finite element p is related to the nodal displacement vector $\mathbf{r}_p(t)$ for that element by Equation (4.29).

4.4 Efficient Evaluation of Foundation Impedance Terms

In this section, we discuss three issues regarding efficient evaluation of the foundation impedance matrix $\mathbf{S}_f(\omega)$ relating the interaction forces $\overline{\mathbf{R}}_f(\omega)$ to the corresponding displacements $\overline{\mathbf{r}}_f(\omega)$ [Equations (2.1) and (4.6)]: (1) selecting boundary element mesh, (2) selecting number of frequency values, and (3) utilizing existing impedance matrix.

4.4.1 Selecting Boundary Element Mesh

The accuracy of the impedance matrix depends on the fineness of the boundary element mesh. This can be demonstrated by comparing the impedance matrices computed for the dam-foundation rock interface discretized by the two different meshes shown in Figure 4.4. The mesh in Figure 4.4(a) is a "standard" mesh with nodes and DOFs matching those of the finite element mesh of the dam; it includes 26 nodes and 76 DOFs for symmetric (x- and y-component) ground motion and 74 DOFs for

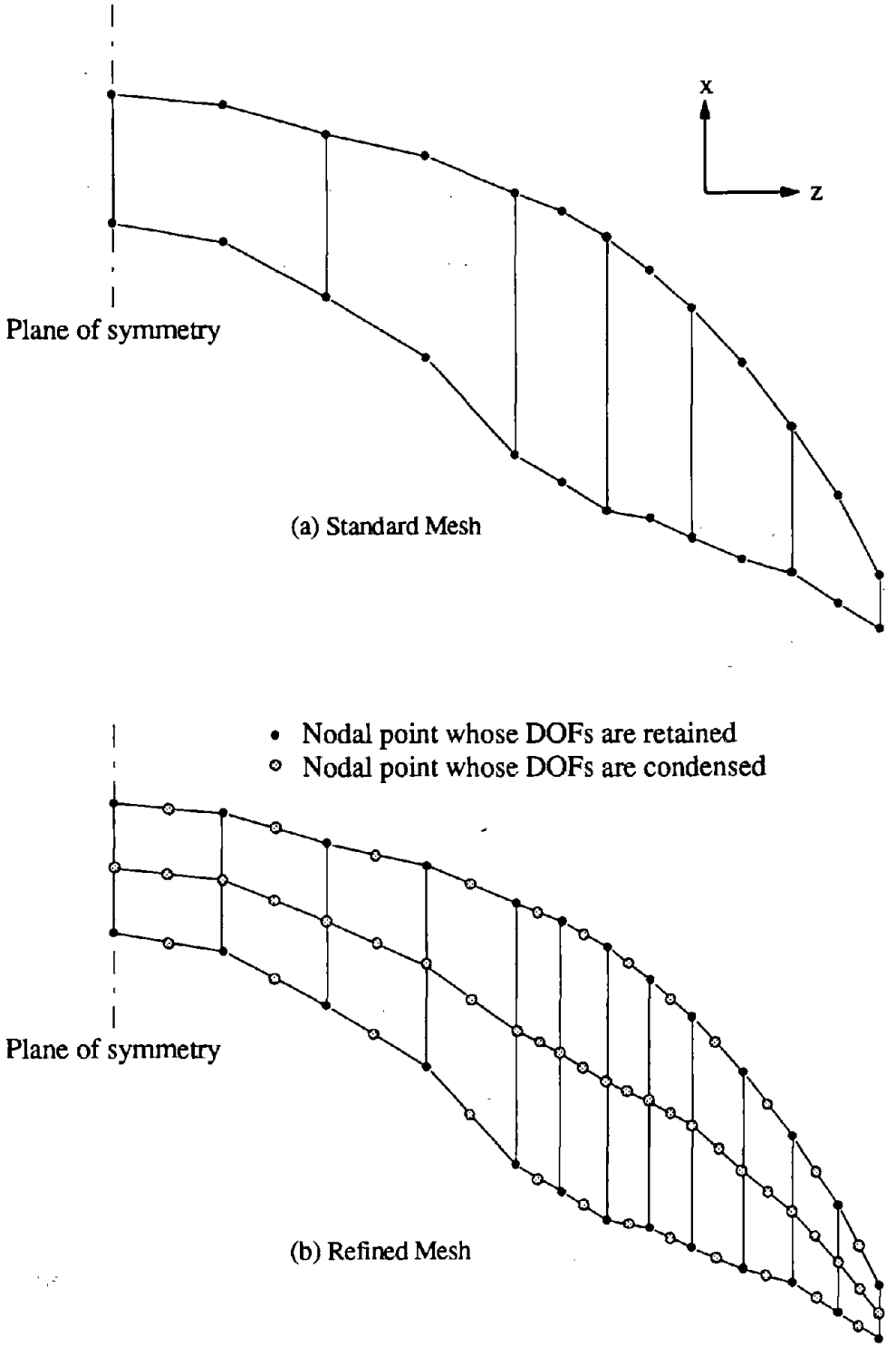

Figure 4.4 Boundary element meshes for one-half of the dam-foundation rock interface of Morrow Point Dam: (a) standard mesh matching the finite element mesh of the dam body, and (b) refined mesh with additioned nodes.

antisymmetric (z-component) ground motion. The largest element size in this mesh is about 120 ft. The mesh in Figure 4.4(b) is a refined mesh that divides each element of the standard mesh into 4 smaller elements. It includes 75 nodes and 222 DOFs for symmetric ground motion and 219 DOFs for antisymmetric ground motion. In this refined mesh the largest element size is about 60 ft.

The impedance matrices using the two meshes will be compared assuming that the dam-foundation rock interface moves as a rigid body. Consider the displacements $\bar{\mathbf{r}}_{rigid}(\omega)e^{i\omega t}$ in the six DOFs at O (Figure 4.5), where

$$\bar{\mathbf{r}}_{rigid}(\omega)=\left\langle r_x(\omega) \quad r_y(\omega) \quad r_z(\omega) \quad r_r(\omega) \quad r_t(\omega) \quad r_m(\omega)\right\rangle^T \tag{4.30}$$

and the forces $\bar{\mathbf{R}}_{rigid}(\omega)e^{i\omega t}$ in the same DOFs, where

$$\bar{\mathbf{R}}_{rigid}(\omega)=\left\langle R_x(\omega) \quad R_y(\omega) \quad R_z(\omega) \quad R_r(\omega) \quad R_t(\omega) \quad R_m(\omega)\right\rangle^T \tag{4.31}$$

The force-displacement relation is

$$\mathbf{S}_{f_{rigid}}(\omega)\,\bar{\mathbf{r}}_{rigid}(\omega)=\bar{\mathbf{R}}_{rigid}(\omega) \tag{4.32}$$

The 6×6 impedance matrix can be expressed as

$$\mathbf{S}_{f_{rigid}}(\omega)=\mu_f L\begin{bmatrix} s_{xx} & s_{xy} & 0 & 0 & 0 & Ls_{xm} \\ & s_{yy} & 0 & 0 & 0 & Ls_{ym} \\ & & s_{zz} & Ls_{zr} & Ls_{zt} & 0 \\ & & & L^2 s_{rr} & L^2 s_{rt} & 0 \\ & sym. & & & L^2 s_{tt} & 0 \\ & & & & & L^2 s_{mm} \end{bmatrix} \tag{4.33}$$

where μ_f is the shear modulus of the foundation rock and L is a reference length taken as the half-width of the canyon. The impedance coefficients s_{ij} are dimensionless, frequency-dependent and complex-valued. In particular, s_{xx}, s_{yy}, s_{zz} are the translational impedance coefficients, s_{rr} and s_{mm} are the rocking impedance coefficients, s_{tt} is the torsional impedance coefficients, and others are the coupling terms.

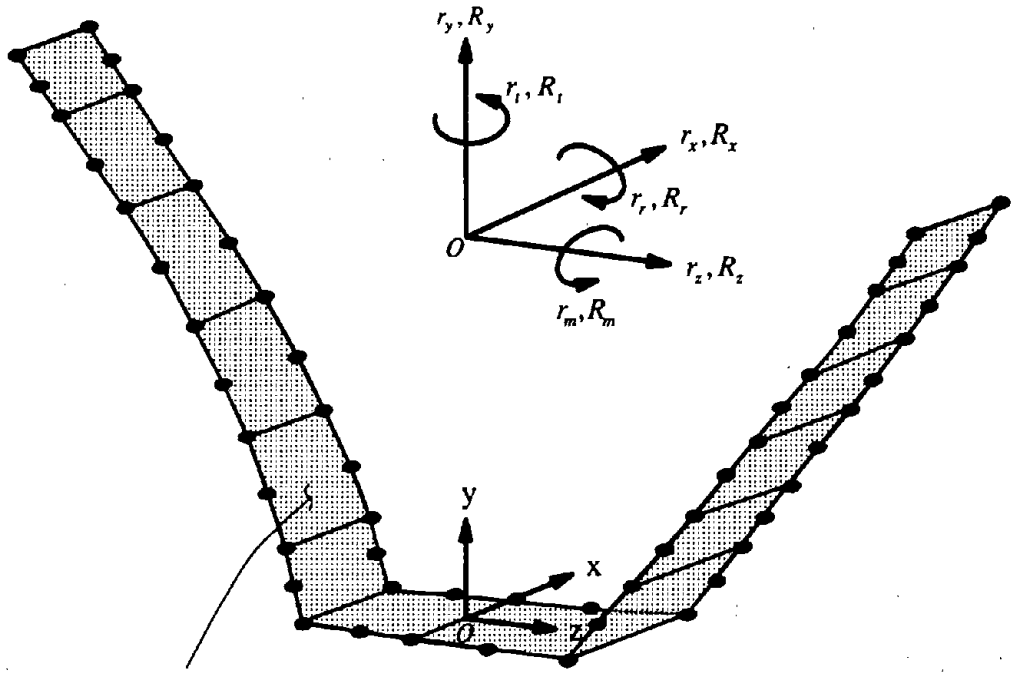

Figure 4.5 Coordinate system and rigid body degrees of freedom of the dam-foundation rock interface.

The impedance coefficients s_{ij} computed by the direct boundary element method [13] are shown in Figures 4.6 to 4.9 for the standard and refined meshes of Figure 4.4. These coefficients, corresponding to E_f = 1.0 million psi, are plotted against the excitation frequency parameter a_0, which is widely used as a non-dimensional frequency (e.g. Reference [13]), defined as

$$a_0 = \frac{\omega L}{C_s} = 2\pi L \frac{f}{C_s} \tag{4.34}$$

where C_s is the shear wave velocity of the foundation rock and L is a reference length, taken as the half-width of the canyon. The real parts of the impedance coefficients for the standard and refined meshes are close at lower frequencies and they deviate increasingly as the frequency increases. The imaginary parts of the impedance coefficients divided by a_0 from the two meshes are essentially "parallel" to each other, indicating that the coefficients depart linearly from each other as the frequency increases. Thus the boundary element mesh should be chosen to be fine enough for the frequency range over which the earthquake excitation and structural responses are significant. However, the CPU time required for the refined mesh is 10 times that required for the standard mesh. Figure 4.10 shows the CPU (central processing unit) time in seconds to compute the impedance matrices of the foundation rock region using the two boundary element meshes of Figure 4.4 on a CRAY X-MP EA/1 supercomputer. About 1000 seconds are required to compute the impedance matrix at one frequency for the refined mesh and such computations have to be repeated for the relevant range of frequencies. Clearly this is a huge computational job.

Also plotted in Figures 4.6 to 4.9 are the stiffness coefficients s_{ij} determined by static analysis of the foundation rock region using the EACD-3D computer program [6]. In this case the finite element idealization of the foundation rock region is shown in Figure 3.5 with the nodes on the outer boundary fixed. The static stiffness coefficients s_{ij} are obviously real-valued and independent of the excitation frequency because the mass and damping of the foundation rock are not considered. Note that these static values for all diagonal terms s_{ii} are larger than the real part of the corresponding s_{ii} at zero frequency computed by the direct boundary element method (Figures 4.6 and 4.8). This

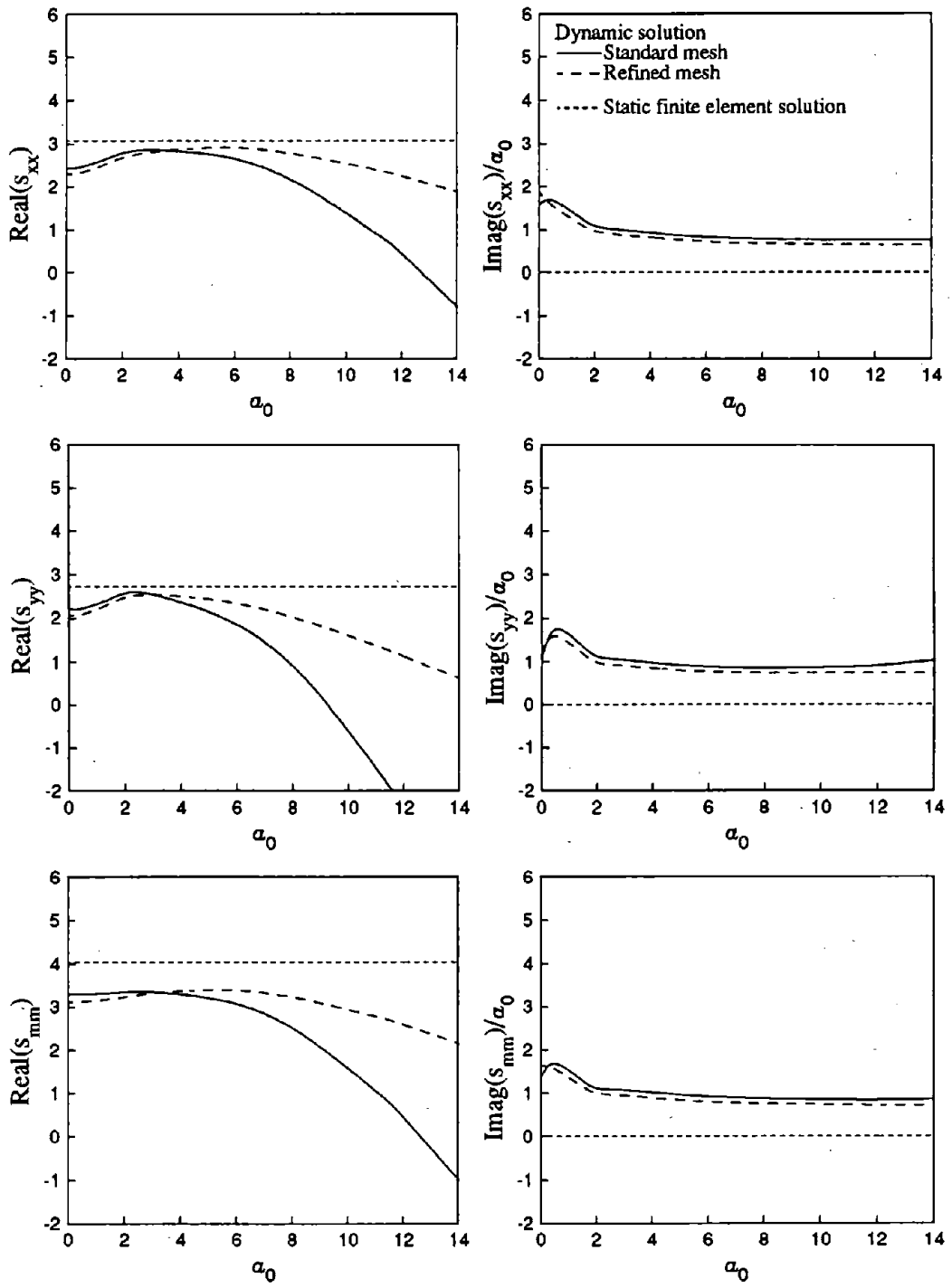

Figure 4.6 Dimensionless foundation impedance coefficients s_{xx}, s_{yy} and s_{mn} for the dam-foundation rock interface assumed to be rigid; E_f = 1 million psi.

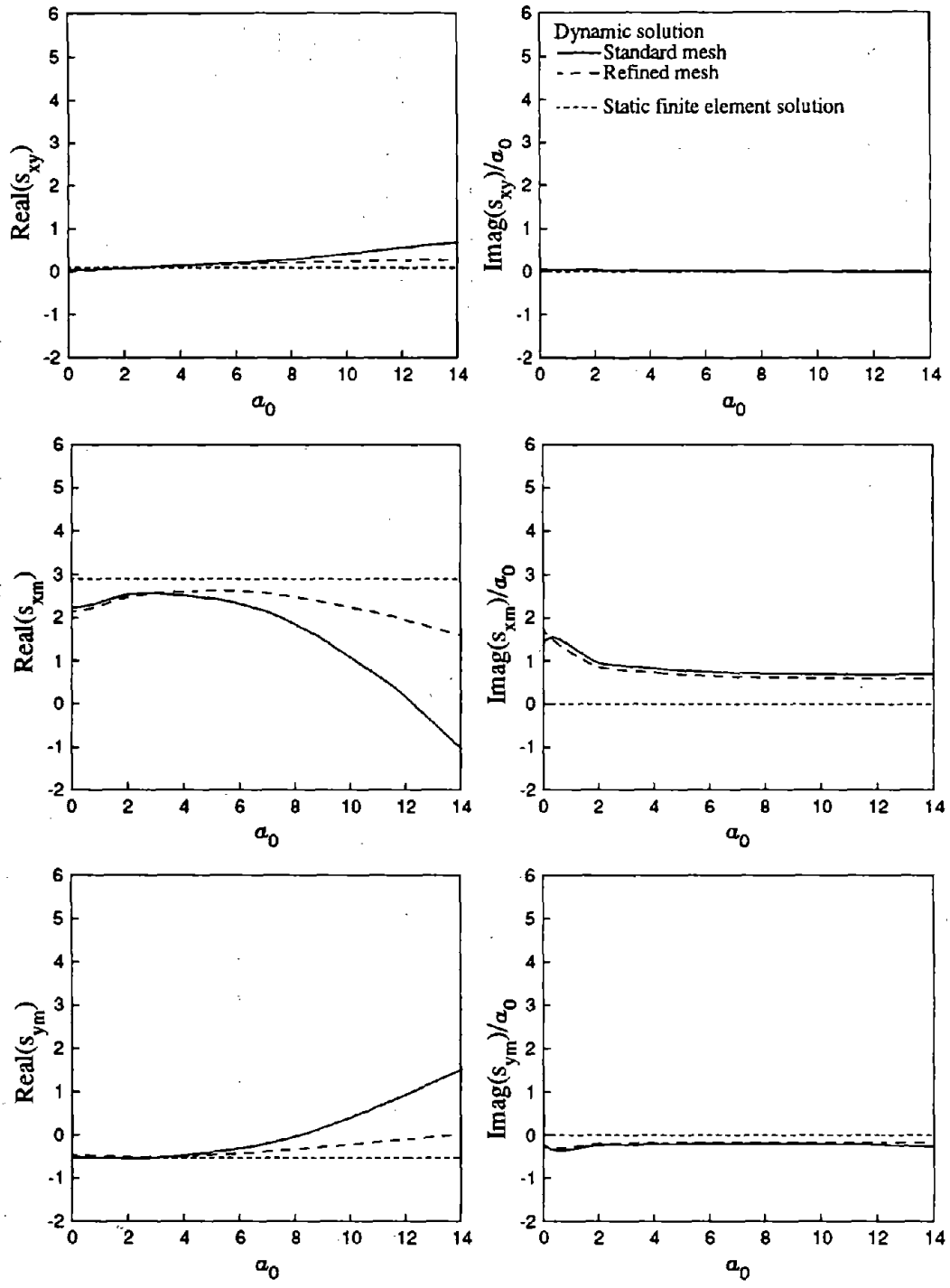

Figure 4.7 Dimensionless foundation impedance coefficients s_{xy}, s_{xm} and s_{ym} for the dam-foundation rock interface assumed to be rigid; E_f = 1 million psi.

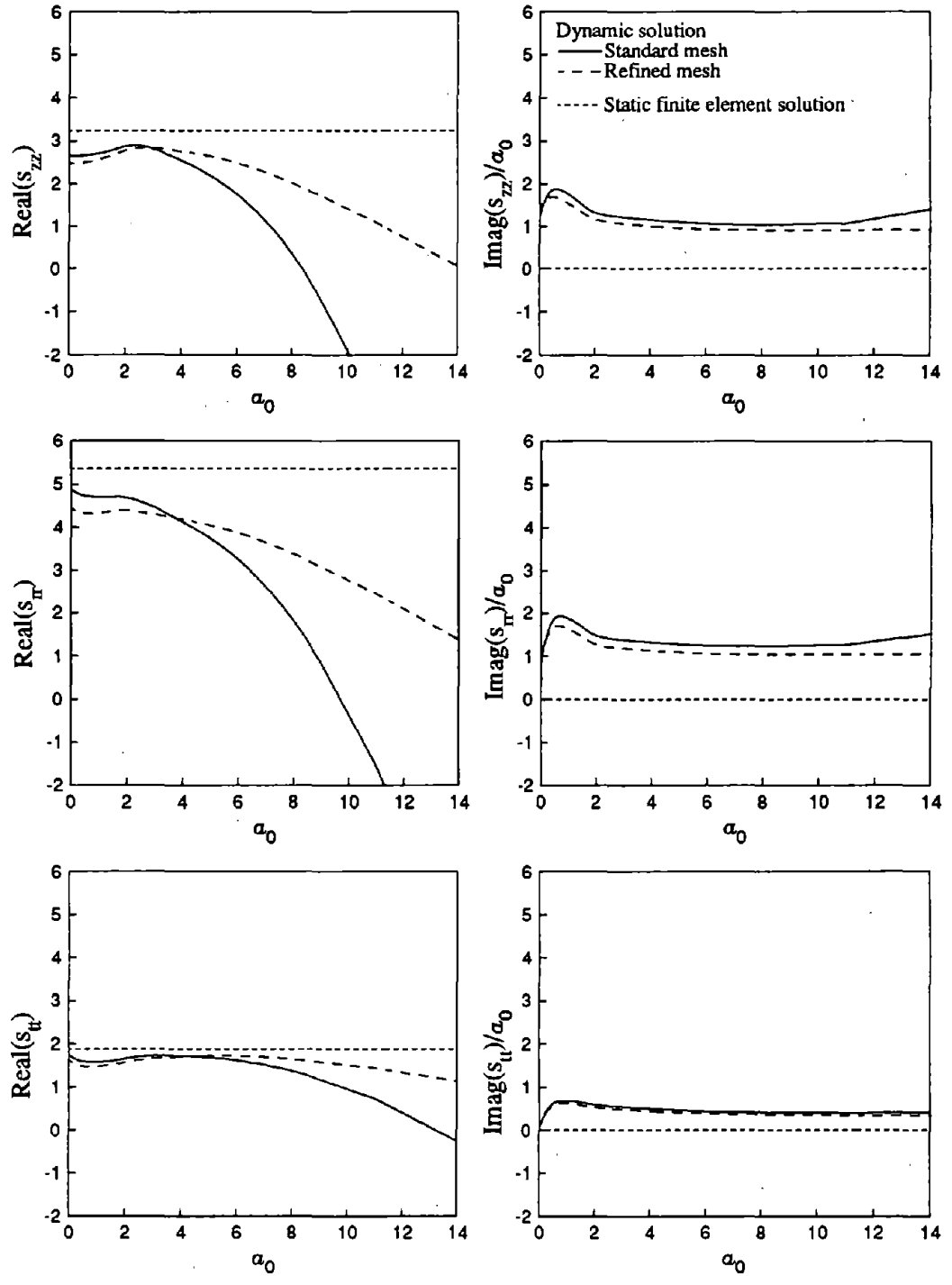

Figure 4.8 Dimensionless foundation impedance coefficients s_{zz}, s_{rr} and s_{tt} for the dam-foundation rock interface assumed to be rigid; E_f = 1 million psi.

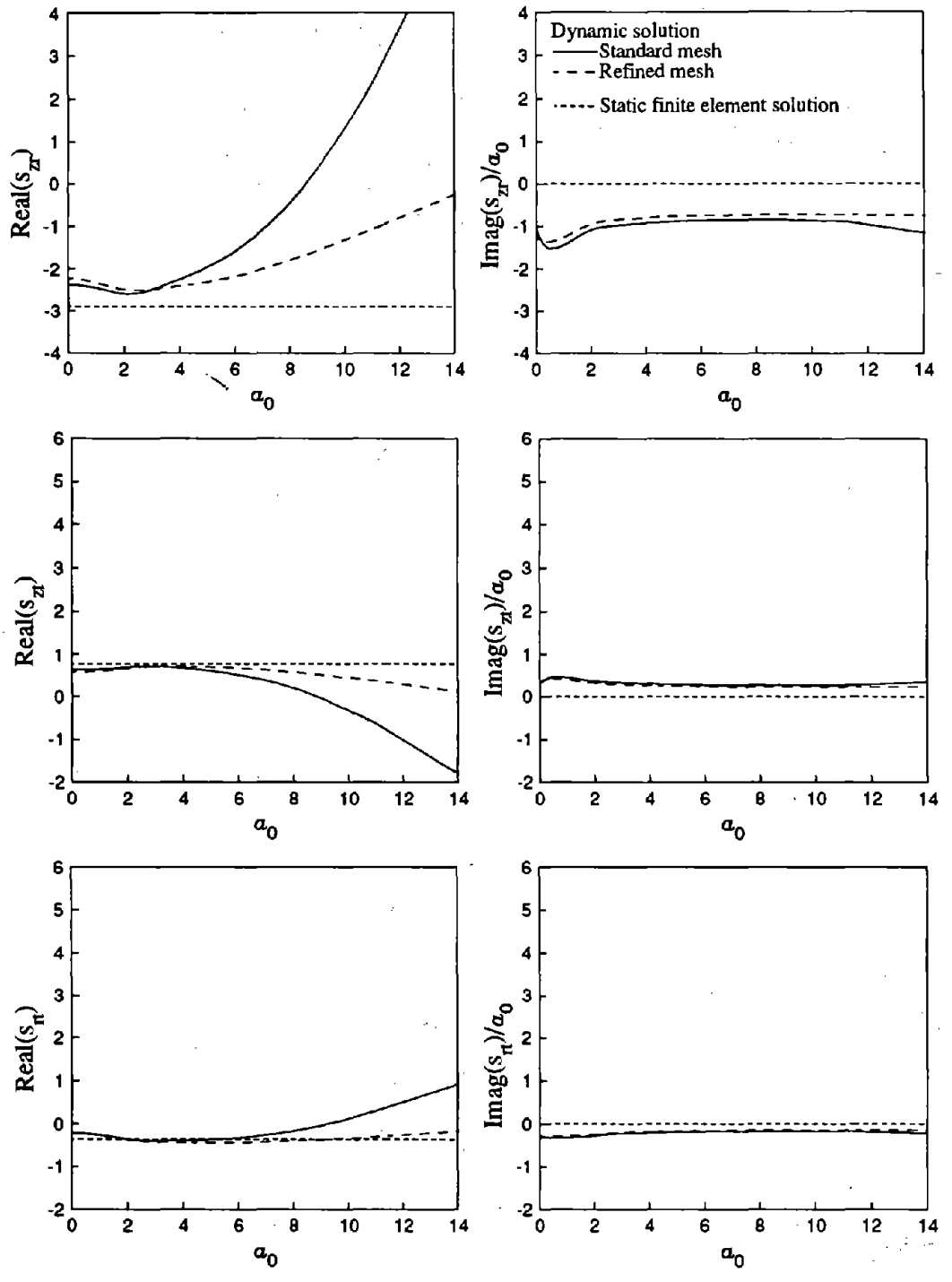

Figure 4.9 Dimensionless foundation impedance coefficients s_{zz}, s_{zr} and s_{rr} for the dam-foundation rock interface assumed to be rigid; E_f = 1 million psi.

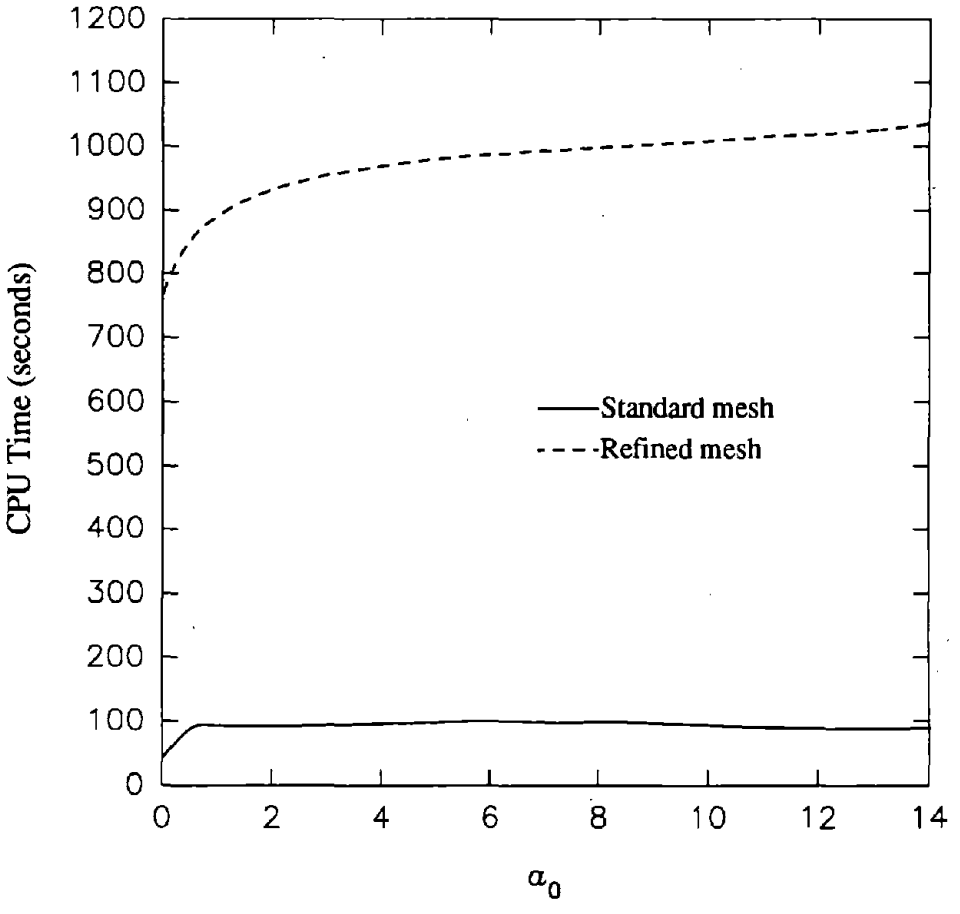

Figure 4.10 CPU time in seconds to compute the foundation impedance matrices at different excitation frequencies for Morrow Point Dam on a CRAY computer.

discrepancy implies as expected that, because of the artificial constraint on the outer boundary, the finite element system is "stiffer" than the unbounded region.

Figure 4.11 shows the frequency response functions of Morrow Point Dam with $\mathbf{S}_f(\omega)$ computed for the standard and refined boundary meshes (Figure 4.4). With the refined mesh, the static condensation procedure is used to eliminate from $\mathbf{S}_f(\omega)$ the DOFs of nodal points other than those in the standard mesh (Figure 4.4). The two frequency response functions are similar; however, the peak responses using the standard mesh are generally smaller than those from the refined mesh, especially due to upstream and cross-stream ground motions. The resulting discrepancy is small in the earthquake response of the dam (Figure 4.12), suggesting that the standard boundary element mesh is adequate for earthquake analysis of Morrow Point Dam.

4.4.2 Selecting Number of Frequency Values

In order to reduce the computational effort, we recognize that the elements of the foundation impedance matrix $\mathbf{S}_f(\omega)$ are smooth functions of the excitation frequency, and determine their numerical values by interpolating between their known values at selected frequencies. Cubic interpolation is used in which any complex-valued function $f(\omega)$ of real-valued variable ω is approximated by a polynomial with complex-valued coefficients c_0, c_1, c_2, and c_3:

$$f(\omega) = c_3\omega^3 + c_2\omega^2 + c_1\omega + c_0 \tag{4.35}$$

Thus if $f(\omega)$ is given at four frequencies in ascending order: ω_i, ω_{i+1}, ω_{i+2} and ω_{i+3} (Figure 4.13), the coefficients c_0, c_1, c_2, and c_3 can be uniquely determined by solving the following linear equations:

$$\begin{bmatrix} \omega_i^3 & \omega_i^2 & \omega_i & 1 \\ \omega_{i+1}^3 & \omega_{i+1}^2 & \omega_{i+1} & 1 \\ \omega_{i+2}^3 & \omega_{i+2}^2 & \omega_{i+2} & 1 \\ \omega_{i+3}^3 & \omega_{i+3}^2 & \omega_{i+3} & 1 \end{bmatrix} \begin{Bmatrix} c_3 \\ c_2 \\ c_1 \\ c_0 \end{Bmatrix} = \begin{Bmatrix} f(\omega_i) \\ f(\omega_{i+1}) \\ f(\omega_{i+2}) \\ f(\omega_{i+3}) \end{Bmatrix} \tag{4.36}$$

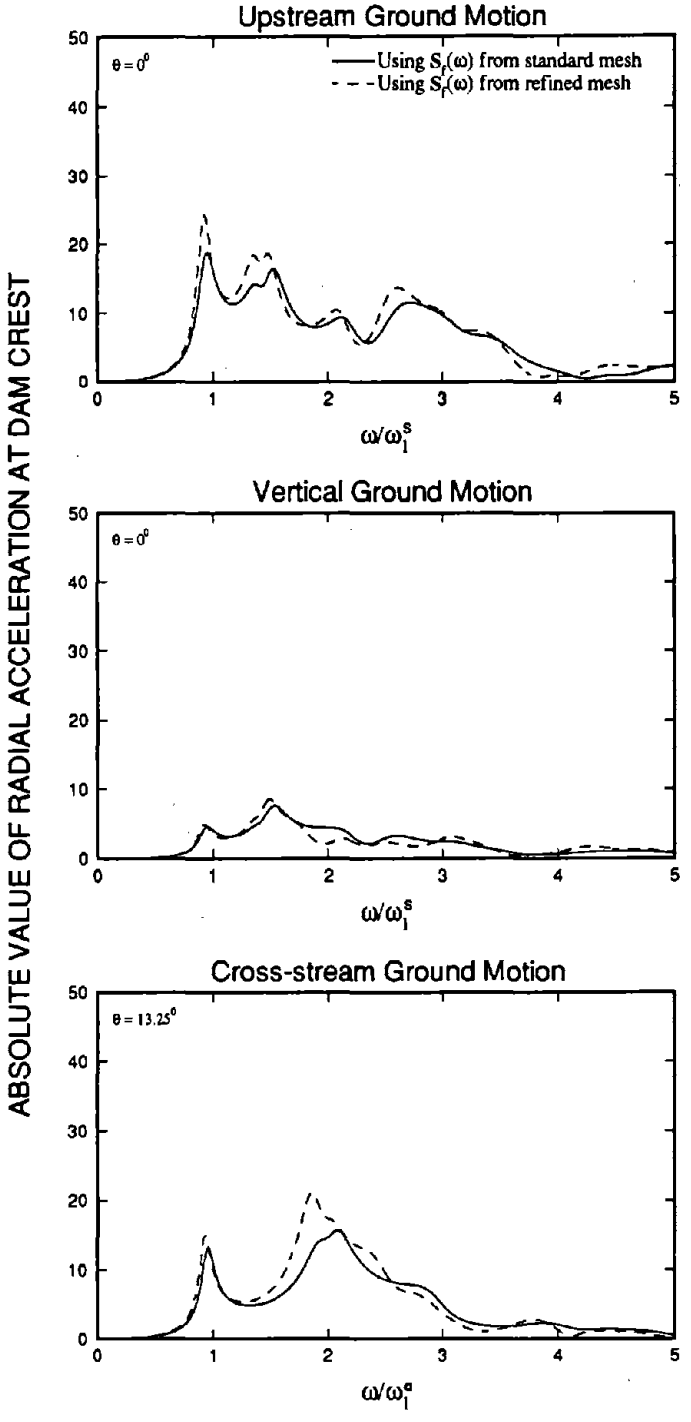

Figure 4.11 Comparison of frequency response functions for Morrow Point Dam obtained using $\mathbf{S}_f(\omega)$ from two different boundary element meshes for the foundation rock; $E_f/E_s = 1$.

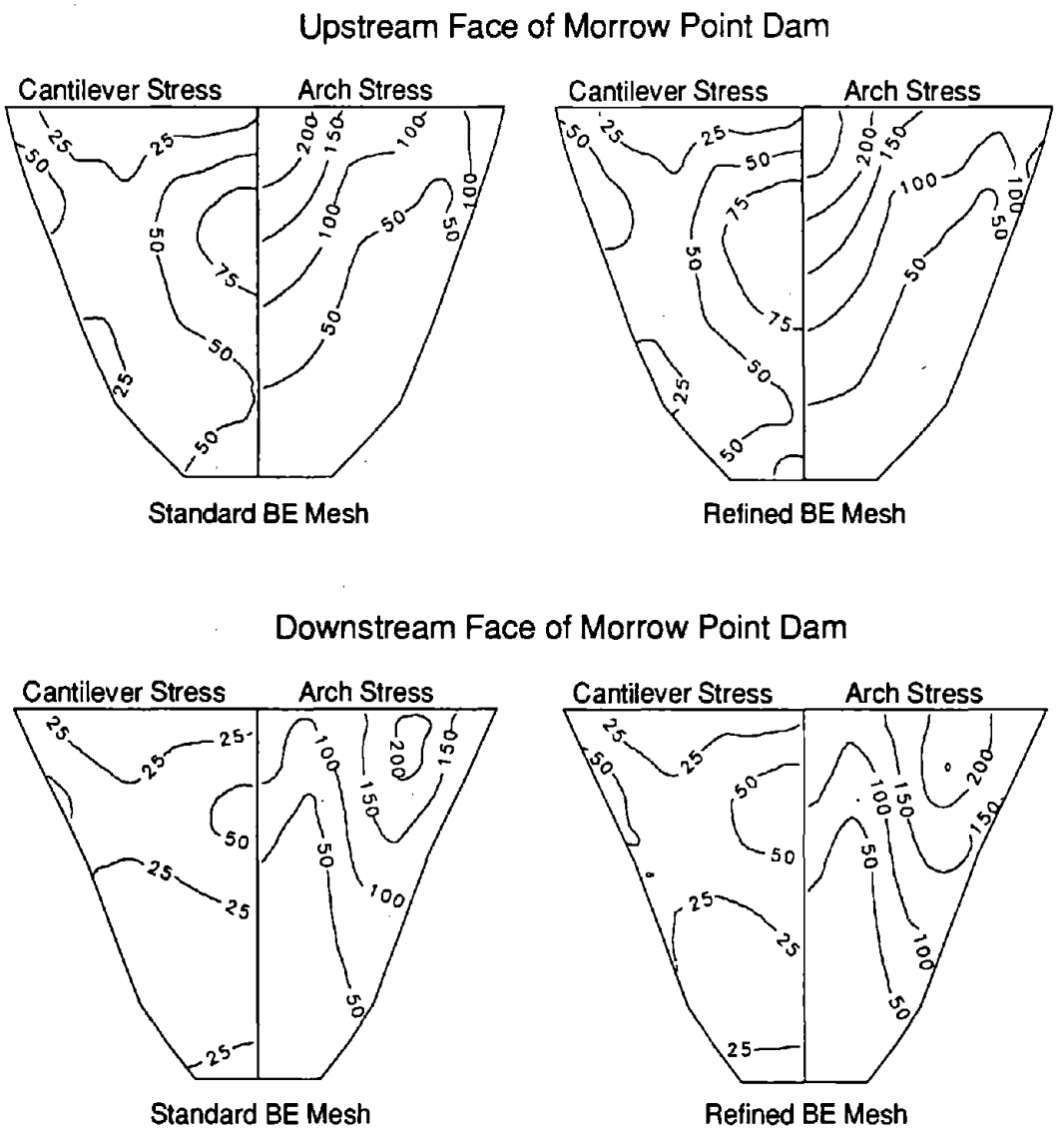

Figure 4.12 Comparison of envelope values of maximum arch and cantilever stresses (in psi) on the upstream and downstream faces of Morrow Point Dam due to the upstream component of Taft ground motion obtained using $\mathbf{S}_f(\omega)$ from two different boundary element meshes for the foundation rock; $E_f/E_s = 1$.

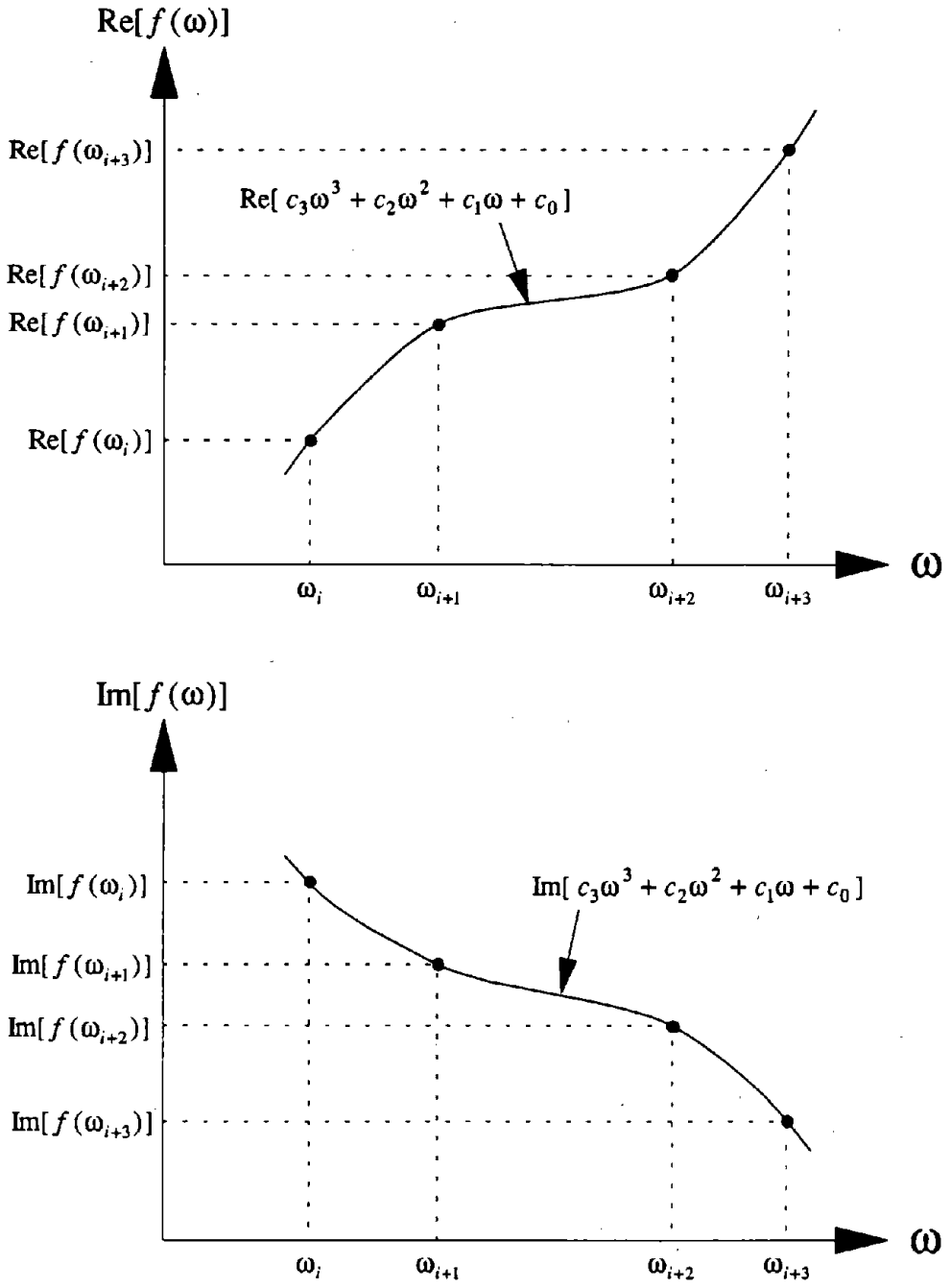

Figure 4.13 Approximate representation of complex-valued function $f(\omega)$ by a cubic polynomial with complex-valued coefficients c_0, c_1, c_2, and c_3.

Because the elements of the 4×4 matrix in Equation (4.36) are all real-valued, the real and imaginary parts of c_0, c_1, c_2, and c_3 can be determined separately with a real-valued linear equation solver. With the coefficients c_i known, Equation (4.36) provides interpolated values for $f(\omega)$.

The above-described interpolation scheme would require that, for each frequency segment, Equation (4.36) be solved $N_b(N_b+1)/2$ times, the number of independent elements in the symmetric matrix $\mathbf{S}_f(\omega)$ of order N_b, the number of DOFs on the dam-foundation rock interface. For Morrow Point Dam subjected to symmetric excitation, $N_b=76$, and 2926 solutions of Equation (4.36) are required. The required computational effort can be reduced considerably by interpolating instead each element of the matrix that appears in Equation (4.24):

$$g_{nj}(\omega)=(\psi_n^b)^T\left[\mathbf{S}_f(\omega)-(1+i\eta_s)\mathbf{S}_f(0)\right]\psi_j^b \tag{4.37}$$

This symmetric matrix is of order J, the number of generalized coordinates included in the analysis. For Morrow Point Dam $J=20$ and Equation (4.36) needs to be solved only 210 times. These computational savings would be especially significant if N_b, is large, because the choice of J is essentially unaffected by N_b.

The preceding interpolation procedure was used in computing the frequency response functions of Figure 4.11 and the stress responses of Figure 4.12. By the boundary element procedure $\mathbf{S}_f(\omega)$ was computed for the standard mesh at 13 values of ω, and for the refined mesh at 8 values of ω; at intermediate ω values $\mathbf{S}_f(\omega)$ was obtained by interpolation. The similarity between the frequency response functions and between the stress responses suggests that the interpolation procedure is satisfactory.

4.4.3 Utilizing Existing Impedance Matrix

The impedance coefficient s_{ij} for foundation rock with Young's modulus E_f is related to that for a foundation rock with a different Young's modulus, say E_{f_0}, provided the mass density, Poisson's ratio and hysteretic damping factor of the foundation rock are identical. As seen in Equation (4.33),

the impedance coefficients are proportional to the shear modulus μ_s, and hence to the Young's modulus E_f if the Poisson's ratio is unchanged. In fact, the impedance matrix can be written in a different format as

$$\mathbf{S}_f\left(\sqrt{\frac{E_{f_0}}{E_f}}\, a_0\right) = \frac{E_f}{E_{f_0}} \mathbf{S}_{f_0}(a_0) \tag{4.38}$$

where $\mathbf{S}_{f_0}(a_0)$ is the "base" impedance matrix for foundation rock with modulus E_{f_0} as a function of the non-dimensional normalized frequency a_0 [Equation (4.34) with $C_s = C_{s_0}$]. Therefore the impedance matrix for modulus E_f does not need to be computed but can be obtained directly from the impedance matrix for E_{f_0}. However, because the factor $\sqrt{E_{f_0}/E_f}$ enters in the frequency range, it is better to compute $\mathbf{S}_{f_0}(a_0)$ for foundation rock with the smallest modulus of interest E_{f_0} so that the impedance matrices for other values of $E_f > E_{f_0}$ can be readily computed.

4.5 Computer Program

The EACD-3D program originally developed in 1985 [6] is modified and extended to implement the response analysis procedure described in the preceding sections. In addition to the various effects that had been included in the old EACD-3D program: foundation rock flexibility, dam-water interaction, water compressibility and reservoir absorption, the extended program also includes the effects of material damping and inertia of the foundation rock, and the radiation damping due to dam-foundation rock interaction. In other words, the full effects of dam-foundation rock interaction are included in the EACD-3D-95 computer program. The dam and fluid domain substructures are still modeled by three-dimensional finite elements as in the old program; however, the foundation rock region is modeled by boundary elements on the surface of the canyon and half space. These two-dimensional boundary elements are much easier to generate than the three-dimensional finite elements for the foundation rock region required in the old program.

The EACD-3D-95 computer program retains the many advantageous features of the old program such as efficient evaluation of the hydrodynamic terms, interpolation of the frequency response functions of the dam, and efficient evaluation of the Fourier integrals by the special FFT algorithm [21]. The program can still be run in several stages; the output from one stage is stored and can subsequently be used as input to the other stages. Output from a static run of the program consists of static displacements and stresses of the dam due to the gravity loads of the dam and the hydrostatic pressure. In the dynamic run, the output consists of the complex-valued frequency response functions for the generalized coordinates and the complete time-history of displacements and stresses at specified locations within the dam as well as the extreme values of stresses at all stress points. The static responses can be evaluated in a separate run of the program and later combined with the earthquake responses, if desired.

5 FREQUENCY RESPONSE FUNCTIONS

5.1 Introduction

The dynamic response of concrete arch dams to harmonic ground motion has been shown to be affected by interaction between the dam and foundation rock [10], interaction between the dam and impounded water, and the absorption of hydrodynamic waves in the alluvium and sediments at the reservoir boundary [5,7,11]. Utilizing the newly developed analytical procedure presented in Chapter 4, the response of a selected arch dam to harmonic ground motion in the upstream, vertical, and cross-stream directions is determined and presented in the form of complex-valued frequency response functions for a wide range of the important parameters characterizing the properties of the dam, foundation rock, impounded water and reservoir boundary materials. Based on these frequency response functions, the influence of damping — material and radiation — and the inertia of the foundation rock besides its flexibility on the response of the dam is studied. We then identify the significance of dam-foundation rock interaction effects ignored in standard analyses [3,6] that consider flexibility of the foundation rock but not its inertia or damping — material and radiation — effects. Finally, the effects of dam-foundation rock interaction in the presence of dam-water interaction and reservoir boundary absorption on the response of the dam are also investigated, leading to better understanding of these effects. This investigation emphasizes the effects of dam-foundation rock interaction compared to dam-water interaction which have already been studied extensively [7,8,9].

5.2 System, Ground Motion, Cases Analyzed, and Response Results

5.2.1 Dam-Water-Foundation Rock System

The dam selected for this study is Morrow Point Dam. The finite element idealization selected for the dam body, the combined finite element and continuum idealization of the impounded water,

and the boundary element idealization for the foundation rock region are presented in Chapter 3. The refined boundary element mesh [Figure 4.4(b)] is chosen for the foundation rock region to compute accurately the foundation impedance matrix (see Section 4.4). The reservoir is considered either empty or full, i.e., H/H_s = 0 or 1, where H is the depth of water and H_s is the dam height, except that additional partially-full reservoir cases (H/H_s = 0.4, 0.6, 0.7, 0.8 and 0.9) are considered for studying the influence of reservoir level on the fundamental resonant period of the system.

The material properties of the dam-water-foundation rock system for this study are as follows. For the mass concrete of the dam, Young's modulus E_s = 4 million psi, unit weight w_s = 155 pcf, Poisson's ratio ν_s = 0.2, and the constant hysteretic damping factor η_s = 0.1. This corresponds to a viscous damping ratio of 0.05 in all natural vibration modes of the dam supported on rigid foundation rock with empty reservoir. For the foundation rock, Young's modulus E_f is varied so that $E_f/E_s = \infty$, 2, 1, 1/2 or 1/4, unit weight w_f = 165 pcf, Poisson's ratio ν_f = 0.2, and constant hysteretic damping factor η_f = 0.1. The unit weight of water w_w= 62.4 pcf and the velocity of pressure waves in water C = 4720 ft/sec. The wave reflection coefficient α of the reservoir boundary materials is varied over a wide range: α = 1.0 (non-absorptive reservoir boundary), 0.95, 0.90, 0.75, 0.50, and 0.

5.2.2 Ground Motion

The excitation for the dam-water-foundation rock system is defined by three components of free-field ground acceleration: the upstream (x) component $a_g^x(t)$, the vertical (y) component $a_g^y(t)$, and the cross-stream (z) component $a_g^z(t)$. Each component of ground acceleration is assumed to be harmonic, i.e., $a_g(t) = e^{i\omega t}$, with the excitation frequency ω to be varied over a wide range.

5.2.3 Cases Analyzed

The frequency response functions are presented for several dam-water-foundation rock systems, defined by the chosen values for the important system parameters, E_s, E_f/E_s, H/H_s, and α (Table 5.1). The response results for various systems are organized to facilitate interpretation of the effects

Table 5.1 Cases of Dam-Water-Foundation Rock System Analyzed

Case	E_s	Foundation Rock		Impounded Water		Reservoir Boundary	
	(million psi)	Condition	E_f/E_s	Condition	H/H_s	Condition	α
1	any*	rigid	∞	empty	0	-	-
2	4	flexible	2	empty	0	-	-
3	4	flexible	1	empty	0	-	-
4	4	flexible	1/2	empty	0	-	-
5	4	flexible	1/4	empty	0	-	-
6	any*	rigid	∞	full	1	non-absorptive	1
7	any*	rigid	∞	full	1	absorptive	0.95
8	any*	rigid	∞	full	1	absorptive	0.90
9	any*	rigid	∞	full	1	absorptive	0.75
10	any*	rigid	∞	full	1	absorptive	0.5
11	any*	rigid	∞	full	1	absorptive	0
12	4	flexible	2	full	1	non-absorptive	1
13	4	flexible	2	full	1	absorptive	0.5
14	4	flexible	1	full	1	non-absorptive	1
15	4	flexible	1	full	1	absorptive	0.95
16	4	flexible	1	full	1	absorptive	0.90
17	4	flexible	1	full	1	absorptive	0.75
18	4	flexible	1	full	1	absorptive	0.5
19	4	flexible	1	full	1	absorptive	0
20	4	flexible	1/2	full	1	non-absorptive	1
21	4	flexible	1/2	full	1	absorptive	0.5
22	4	flexible	1/4	full	1	non-absorptive	1
23	4	flexible	1/4	full	1	absorptive	0.5

* Response results for these cases, when presented in normalized form, are valid for all E_s.

of dam-foundation rock interaction, dam-water interaction, and reservoir boundary absorption on the response of the dam. For some cases in Table 5.1, the frequency response functions computed from the "standard" procedure that considers only the foundation flexibility effects are also presented for reference and comparison. These results are obtained by replacing the frequency-dependent foundation impedance matrix $\mathbf{S}_f(\omega)$ in the analysis procedure with $\mathbf{S}_f(0)$, the foundation stiffness matrix (Section 4.1.6).

5.2.4 Response Quantities

The complex-valued frequency response functions presented are dimensionless response factors that represent the acceleration components in selected directions at a few locations in the dam due to unit harmonic, free-field ground acceleration. The frequency response function for radial acceleration at one location at the dam crest is presented; the location is defined by an angle value θ measured from the crown (plane of symmetry) along the dam crest, which is selected as: $\theta = 0^o$ (nodal point 60 in Figure 3.1) for upstream and vertical ground motions and $\theta = 13.25^o$ (nodal point 54 in Figure 3.1) for cross-stream ground motion. The frequency response functions are for acceleration relative to the free-field ground motion; they are not direct measures of deformation.

The frequency response functions were determined using the analytical procedure described in Chapter 4 with the excitation frequency ω varied over a relevant range of interest. For all cases in Table 5.1, the first 20 generalized coordinates were included in computing the response, although the number can be reduced for cases with larger E_f/E_s ratio. The results should be accurate for excitation frequencies up to approximately four times the fundamental natural frequency ω_1 of the dam supported on rigid foundation rock with empty reservoir.

For each case in Table 5.1 the absolute value of the complex-valued frequency response function for acceleration is plotted against the normalized excitation frequency parameter ω/ω_1, where $\omega_1 = \omega_1^s$ for symmetric (upstream and vertical) ground motions and $\omega_1 = \omega_1^a$ for antisymmetric

(cross-stream) ground motion (Chapter 3). If the reservoir is empty, these response results plotted in this manner are independent of E_s and α.

5.3 Dam-Foundation Rock Interaction Effects

The effects of dam-foundation rock interaction on the dam response to upstream, vertical, and cross-stream ground motions are studied first; the reservoir is assumed empty. The upstream and vertical ground motions excite only the symmetric modes of vibration of the dam whereas the cross-stream ground motion excites only the antisymmetric modes of vibration. The frequency response functions for the dam supported on foundation rock with varying modulus E_f are shown in Figure 5.1 (Cases 1 to 5 in Table 5.1). When presented in this form, these functions do not depend separately on E_s or E_f but only on the ratio E_f/E_s. Results are presented for five values of $E_f/E_s = \infty$, 2, 1, 1/2 and 1/4. The first represents rigid foundation rock whereas in the last case the elastic modulus of the foundation rock is one-fourth of the modulus for dam concrete, an assumption that may be appropriate if the foundation rock is severely fractured.

As the E_f/E_s ratio decreases, which for a fixed concrete modulus E_s implies decreasing foundation modulus E_f, the fundamental resonant frequency of the dam decreases because of increasing foundation flexibility (Figure 5.1). Furthermore, as the E_f/E_s ratio decreases, the response at the fundamental frequency decreases and the frequency bandwidth at resonance widens, implying an increase in the apparent damping of the structure, resulting from material damping in the foundation rock and the radiation damping associated with wave propagation away from the dam into the unbounded foundation rock region. The amplitude of resonant response to vertical and cross-stream ground motions shows somewhat different trends as the E_f/E_s ratio decreases. In the case of vertical ground motion, the fundamental resonant peak is essentially unaffected by E_f/E_s in the range $E_f/E_s = \infty$ to 2 [Figure 5.1(b)]. For cross-stream ground motion, the fundamental resonant response is essentially independent of E_f/E_s over the range $E_f/E_s = \infty$ to 1/2 [Figure 5.1(c)]. Dam-foundation rock interaction also reduces the higher resonant frequencies to a similar degree as the fundamental

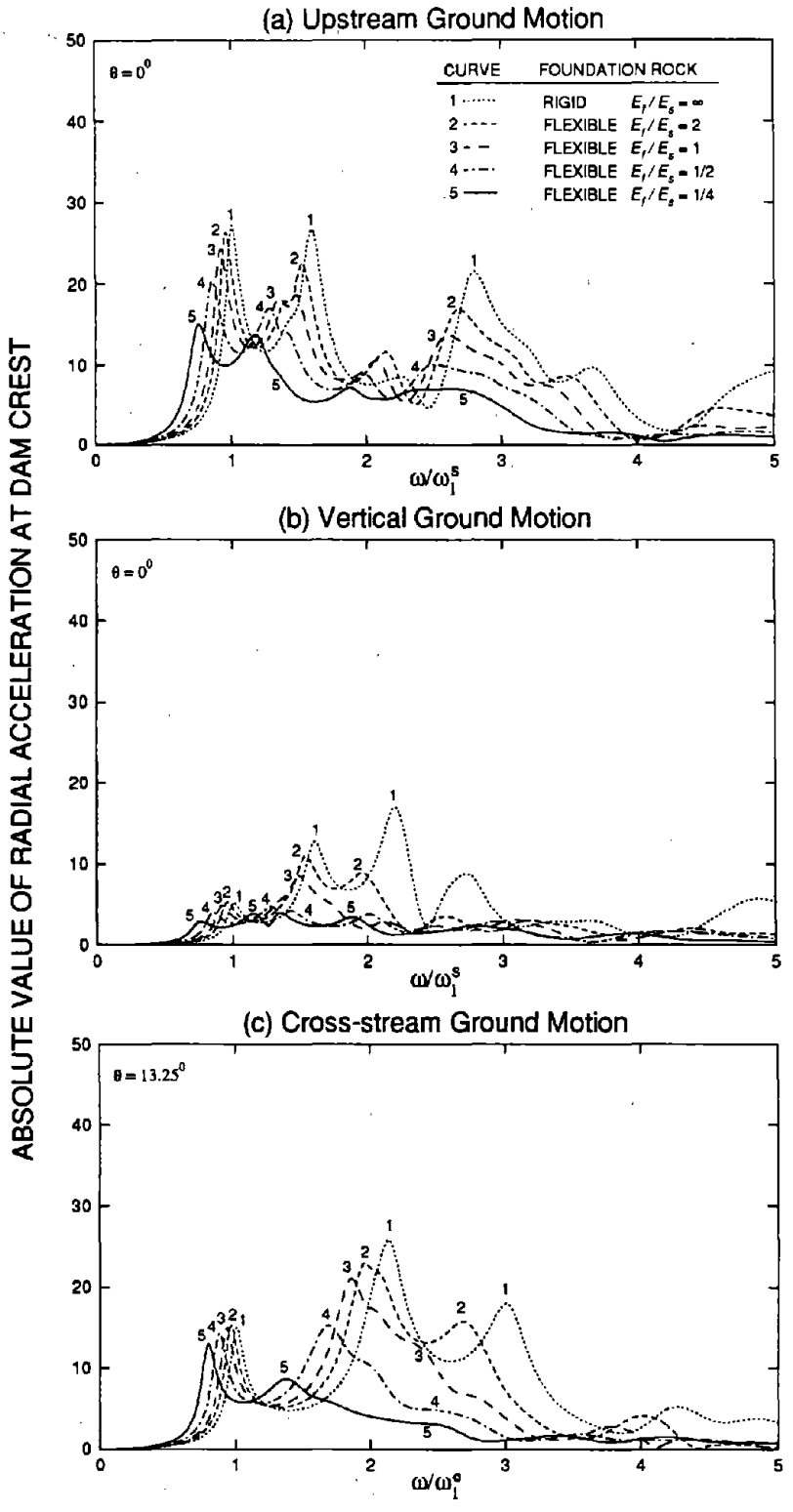

Figure 5.1 Influence of moduli ratio E_f/E_s on response of dams with empty reservoir to harmonic upstream, vertical and cross-stream ground motions (Cases 1 to 5 of Table 5.1).

resonant frequency. For all three components of ground motion, the amplitude of the second resonant peak decreases systematically as E_f/E_s decreases.

Table 5.2 shows that as the moduli ratio E_f/E_s decreases the fundamental resonant period of the symmetric as well as the antisymmetric mode of vibration lengthens. The ratio $\tilde{T}_f/T_1$ of the fundamental resonant period $\tilde{T}_f$ of the dam supported on flexible foundation rock to T_1 on rigid foundation rock is plotted in Figure 5.2 as a function of E_f/E_s. Presented in this form, these results are applicable to dams of any height with the specific geometry and chosen values for Poisson's ratio and density of concrete and rock. For a fixed E_f/E_s value, the period of the symmetric mode is lengthened more than that of the antisymmetric mode. In particular, for E_f/E_s = 1/4, the period is lengthened by 32% for the symmetric mode compared to 25% for the antisymmetric mode. Also presented in Figure 5.2 is the period ratio for a gravity dam [12], which indicates that the elongation of the vibration period of gravity dams due to dam-foundation rock interaction is two to three times greater than for arch dams. These interaction effects are more significant for gravity dams, in part, because they are massive compared to arch dams.

The effective damping ratio of the dam for Cases 1 to 5, estimated by the half-power bandwidth method applied to the frequency response function near the fundamental resonance, is presented in Table 5.2 and plotted in Figure 5.3. Dam-foundation rock interaction has the effect of increasing the effective damping ratio, assumed to be 5% for the dam on rigid foundation rock, as E_f/E_s decreases, suggesting that radiation damping associated with interaction increases as the foundation rock becomes more flexible since the selected foundation material damping is the same for all E_f/E_s values. For a fixed E_f/E_s value, the effective damping ratio of the symmetric mode is increased more than that of the antisymmetric mode. In particular, for E_f/E_s = 1/4, the effective damping ratio increases from 5% to 9.3-9.6% in the symmetric vibration mode; and from 5% to 6.3% in the antisymmetric vibration mode. Also presented in Figure 5.3 is the effective damping ratio for a gravity dam [12], which indicates that the increase of the damping of gravity dams due to dam-

Table 5.2 Fundamental Resonance Period (seconds) and Damping Ratio at Fundamental Resonance of Morrow Point Dam with Empty Reservoir

Case	Foundation Rock Condition	E_f/E_s	Resonant Period		Damping Ratio	
			Symmetric Mode	Antisymmetric Mode	Symmetric Mode	Antisymmetric Mode
1	rigid	∞	0.234	0.263	5.0	5.0
2	flexible	2	0.245	0.273	5.4-5.6†	5.1
3	flexible	1	0.255	0.284	6.0	5.4
4	flexible	1/2	0.277	0.302	7.2-7.4	5.8
5	flexible	1/4	0.315	0.332	9.3-9.6	6.3

† The two values are from frequency response curves associated with upstream and vertical ground motions, respectively.

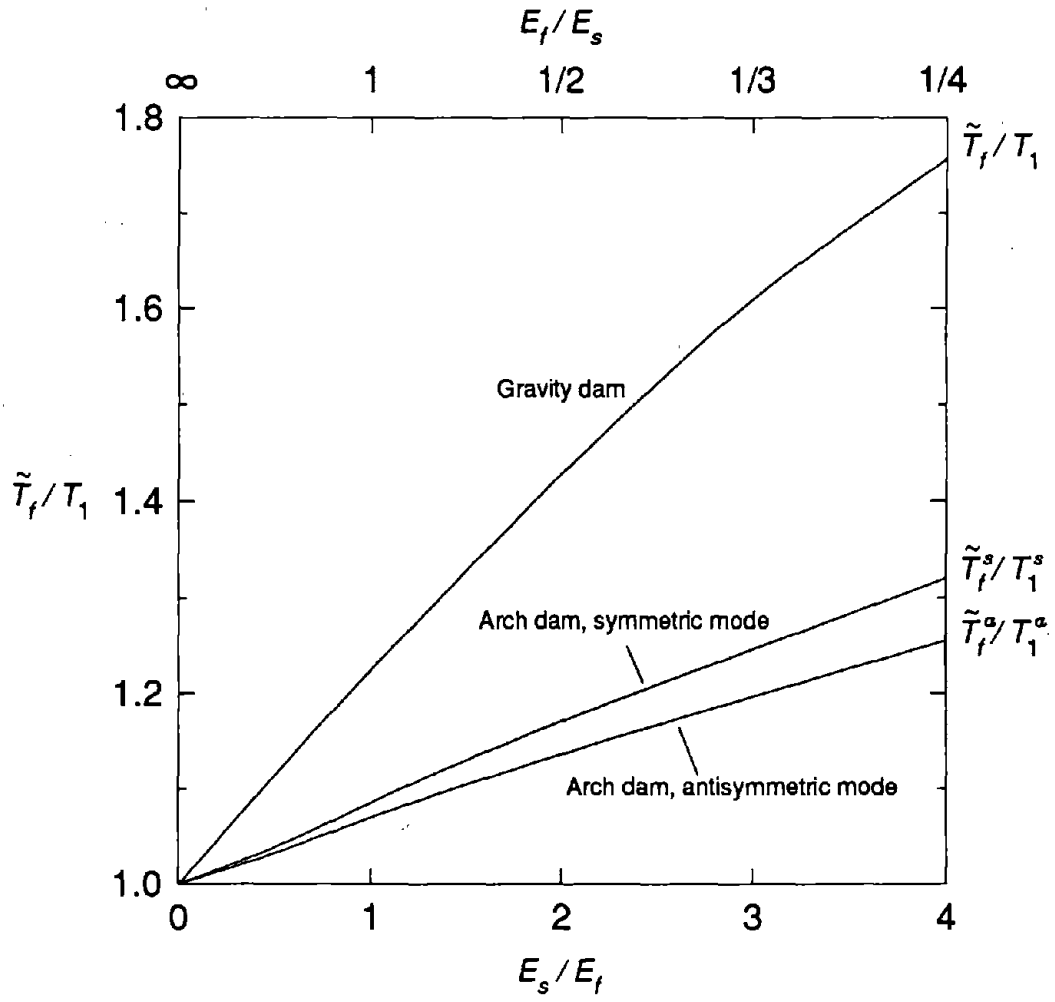

Figure 5.2 Variation of the fundamental period ratios, $\tilde{T}_f/T_1$, $\tilde{T}_f^s/T_1^s$ and $\tilde{T}_f^a/T_1^a$, with the moduli ratio E_f/E_s, for dam with an empty reservoir. Results for the gravity dam are from Fenves and Chopra [12].

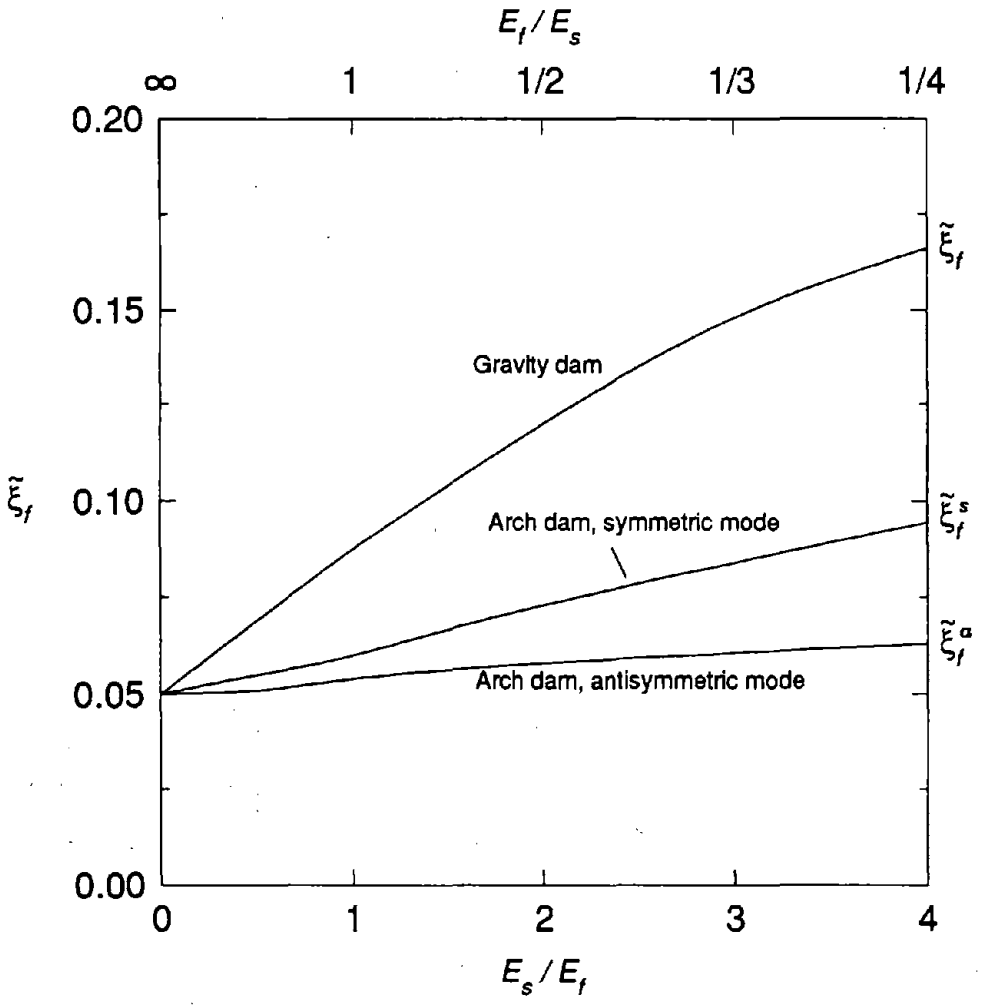

Figure 5.3 Variation of the effective damping ratios, $\tilde{\xi}_f$, $\tilde{\xi}_f^s$ and $\tilde{\xi}_f^a$, with the moduli ratio E_f/E_s, for dam with empty reservoir. Results for the gravity dam are from Fenves and Chopra [12].

foundation rock interaction is much larger than for arch dams, confirming that dam-foundation rock interaction effects are more significant for gravity dams.

The preceding results indicate that dam-foundation rock interaction affects the response of the dam in its symmetric vibration modes, excited by upstream and vertical ground motions, more than in its antisymmetric modes, excited by cross-stream ground motion.

5.4 Foundation Idealization

In this section we study how the response of the dam is affected if only the foundation flexibility is considered but the other effects of dam-foundation rock interaction are ignored. Figures 5.4, 5.5 and 5.6 show the frequency-response curves for the dam due to upstream, vertical and cross-stream ground motions, respectively, considering (1) foundation flexibility only and (2) all effects of dam-foundation rock interaction; also included for reference is the response of the dam on rigid foundation rock. It is clear that the fundamental resonant frequency is essentially the same for both idealizations of foundation rock, implying that the lowering of this frequency is almost entirely due to foundation flexibility with negligible influence of foundation mass, material damping, or radiation damping. However, the response amplitudes at the fundamental and higher resonant frequencies are too large when only foundation flexibility is considered because the reduction in response due to foundation material and radiation damping is ignored. For the smaller values of E_f/E_s, the overestimation of response by considering foundation flexibility only is especially large because the substantial damping due to dam-foundation rock interaction discussed in the previous section is ignored.

It is clear that the standard analysis commonly used in engineering practice, which considers only the flexibility of the foundation rock, ignores important effects of dam-foundation rock interaction. Therefore these effects are included in all subsequent response results presented in this chapter.

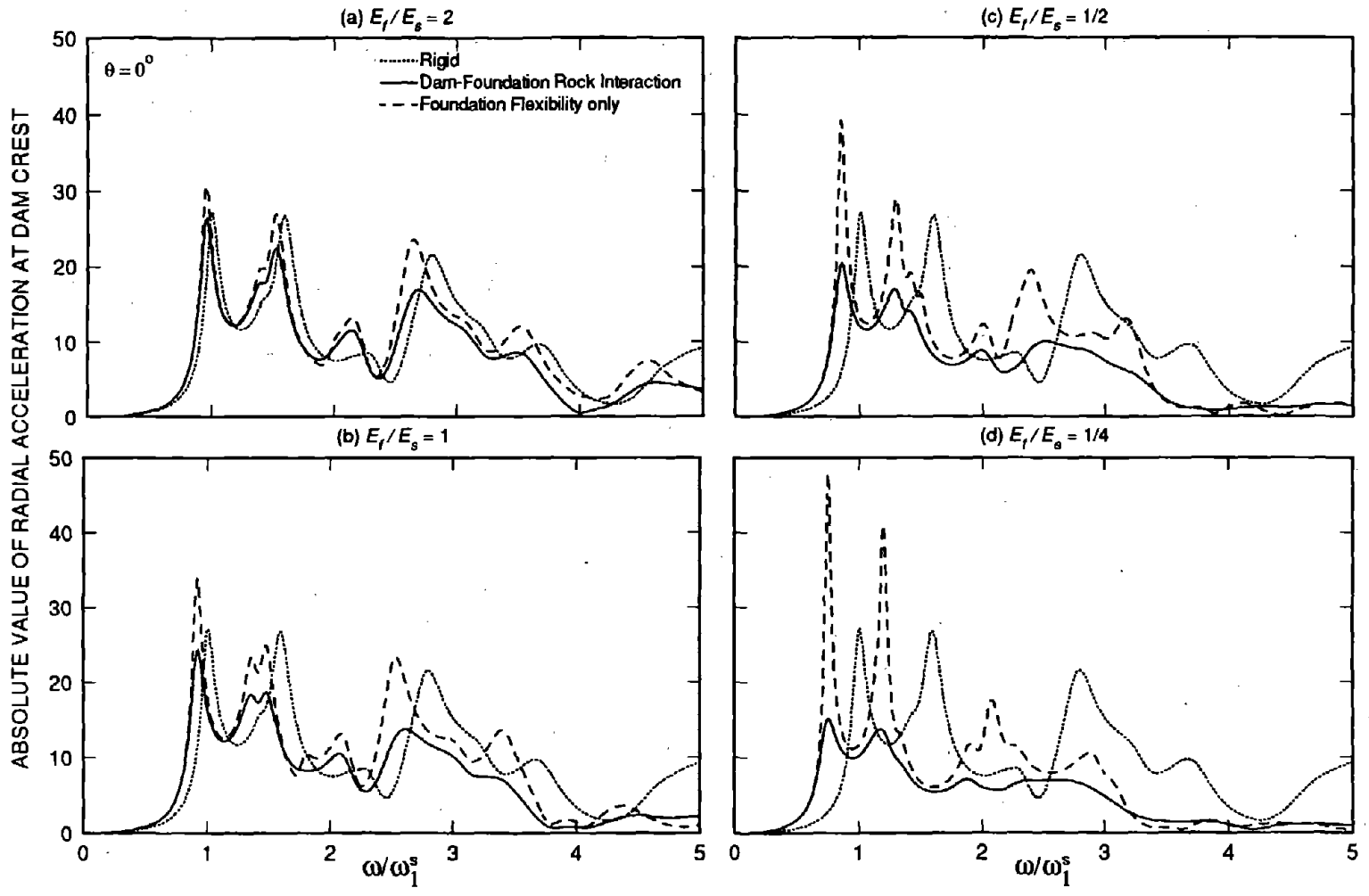

Figure 5.4 Influence of foundation rock idealization on the response of dams with empty reservoir to harmonic upstream ground motion (Cases 1 to 5 of Table 5.1).

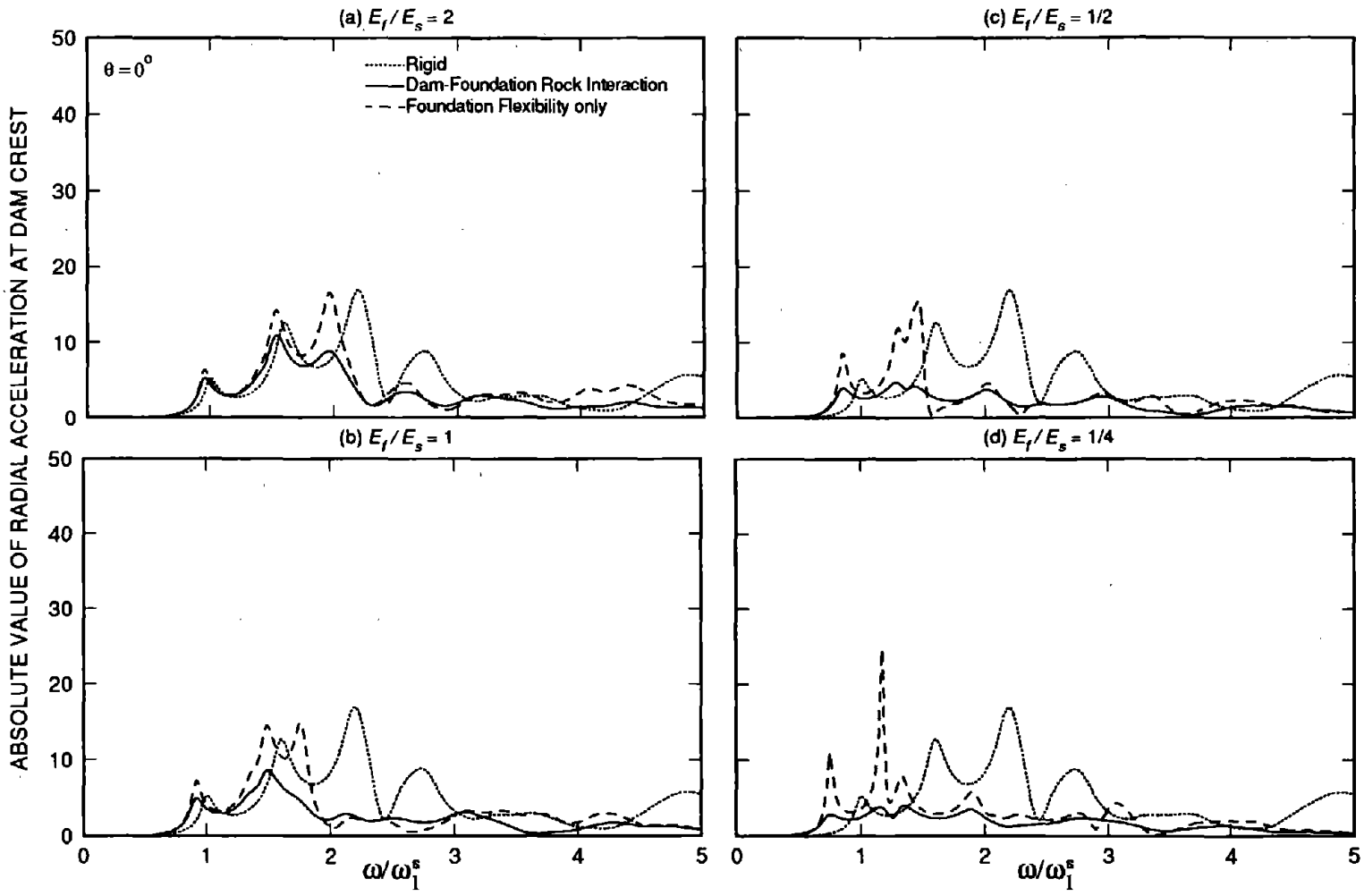

Figure 5.5 Influence of foundation rock idealization on the response of dams with empty reservoir to harmonic vertical ground motion (Cases 1 to 5 of Table 5.1).

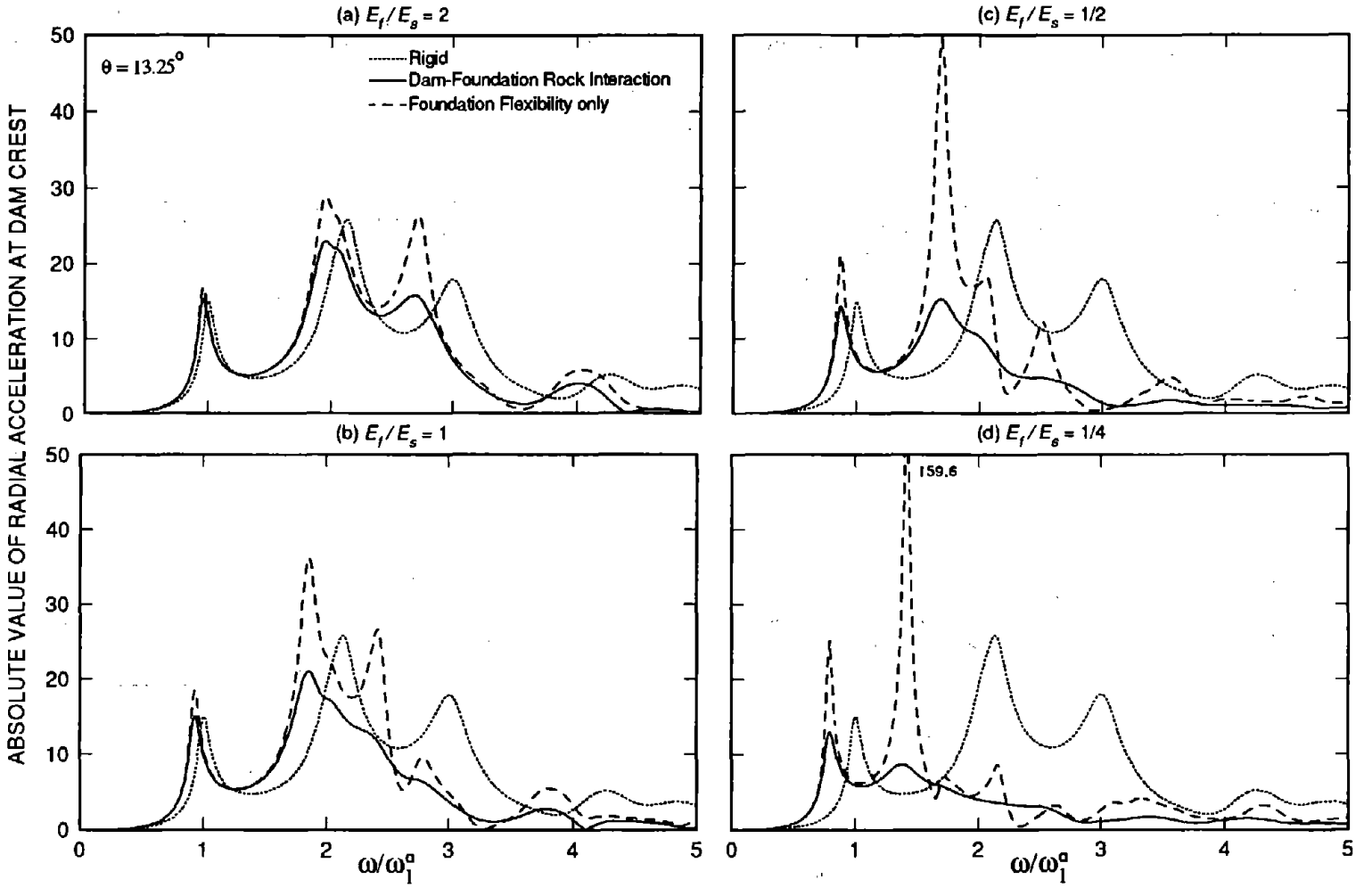

Figure 5.6 Influence of foundation rock idealization on the response of dams with empty reservoir to harmonic cross-stream ground motion (Cases 1 to 5 of Table 5.1).

5.5 Dam-Water-Foundation Rock Interaction Effects

The simultaneous effects of dam-foundation rock interaction and dam-water interaction on the response of the dam to upstream, vertical, and cross-stream ground motions are investigated in this section. Water compressibility is considered, allowing pressure waves to propagate in the upstream direction when the excitation frequency is greater than the fundamental natural frequency ω_1^i of the infinite uniform channel of water (Figure 3.2): ω_1^{is} for the symmetric mode and ω_1^{ia} for the antisymmetric mode [7]. Results are presented in Figures 5.7, 5.8 and 5.9 for four systems: dam on rigid foundation rock with empty reservoir (Case 1); dam on flexible foundation rock with empty reservoir (Case 3); dam on rigid foundation rock with full reservoir (Cases 6 and 10); and dam on flexible foundation rock with full reservoir (Cases 14 and 18).

Interaction between the dam and flexible foundation rock affects the response of the dam in a simpler manner than does dam-water interaction (compare curve 2 to 3 in each of Figures 5.7, 5.8 and 5.9), because the impedances of the semi-infinite foundation-rock region are slowly-varying, smooth functions of excitation frequency (see Section 4.4), whereas the added hydrodynamic forces, mass, and damping display sharp resonant peaks at ω_n^i [7]. In particular, these resonant peaks are unbounded for vertical and cross-stream ground excitations if the reservoir boundary is non-absorptive.

5.5.1 Hydrodynamic and Reservoir Boundary Absorption Effects

The effects of dam-water interaction on the dam response to each of the three ground motion components are qualitatively similar for rigid and flexible foundation rock (Figures 5.7, 5.8 and 5.9). The change in the amplitude of the fundamental resonant peak depends on the contribution of damping from dam-foundation rock interaction, dam-water interaction and reservoir boundary absorption, and on the added hydrodynamic forces. For the response of the dam with non-absorptive reservoir boundary to upstream ground motion [Figure 5.7(a)], dam-water interaction increases the added force and decreases the effective damping at the fundamental resonant frequency, resulting in

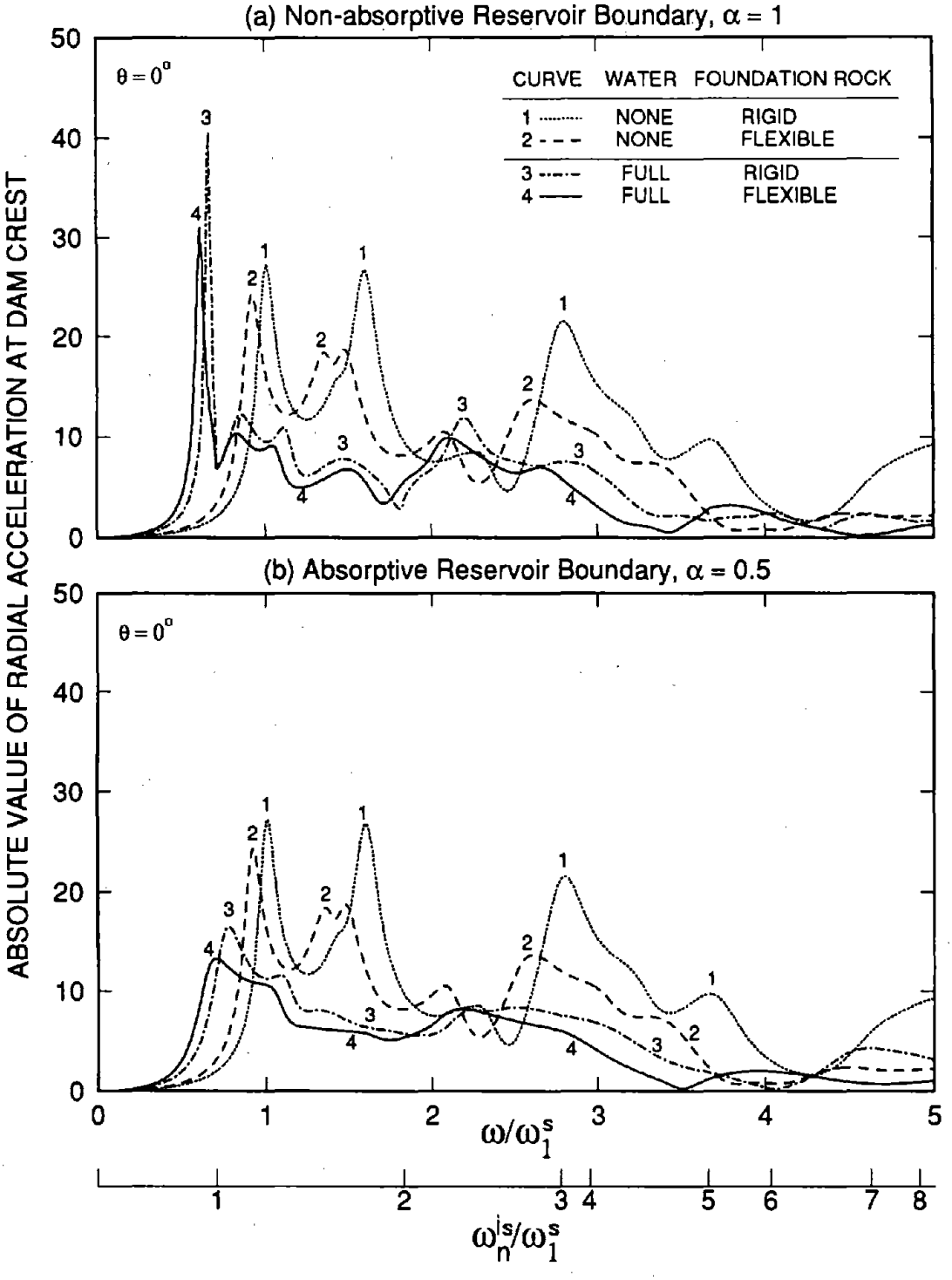

Figure 5.7 Response of dams to harmonic upstream ground motion for four conditions: dam on rigid foundation rock with no water (Case 1 of Table 5.1); dam on flexible foundation rock with no water (Case 3 of Table 5.1); dam on rigid foundation rock with full reservoir (Cases 6 and 10 of Table 5.1); and dam on flexible foundation rock with full reservoir (Cases 14 and 18 of Table 5.1).

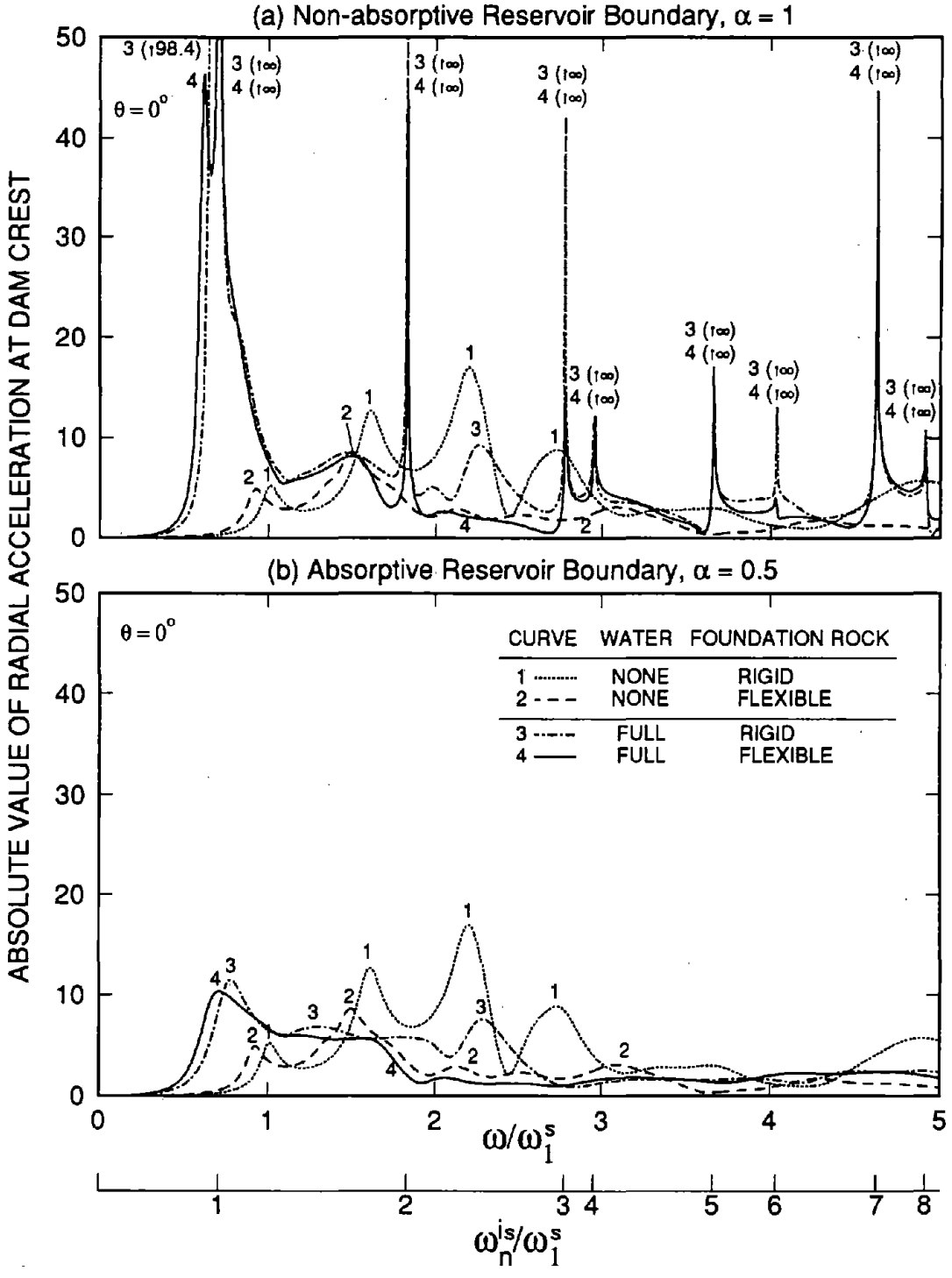

Figure 5.8 Response of dams to harmonic vertical ground motion for four conditions: dam on rigid foundation rock with no water (Case 1 of Table 5.1); dam on flexible foundation rock with no water (Case 3 of Table 5.1); dam on rigid foundation rock with full reservoir (Cases 6 and 10 of Table 5.1); and dam on flexible foundation rock with full reservoir (Cases 14 and 18 of Table 5.1).

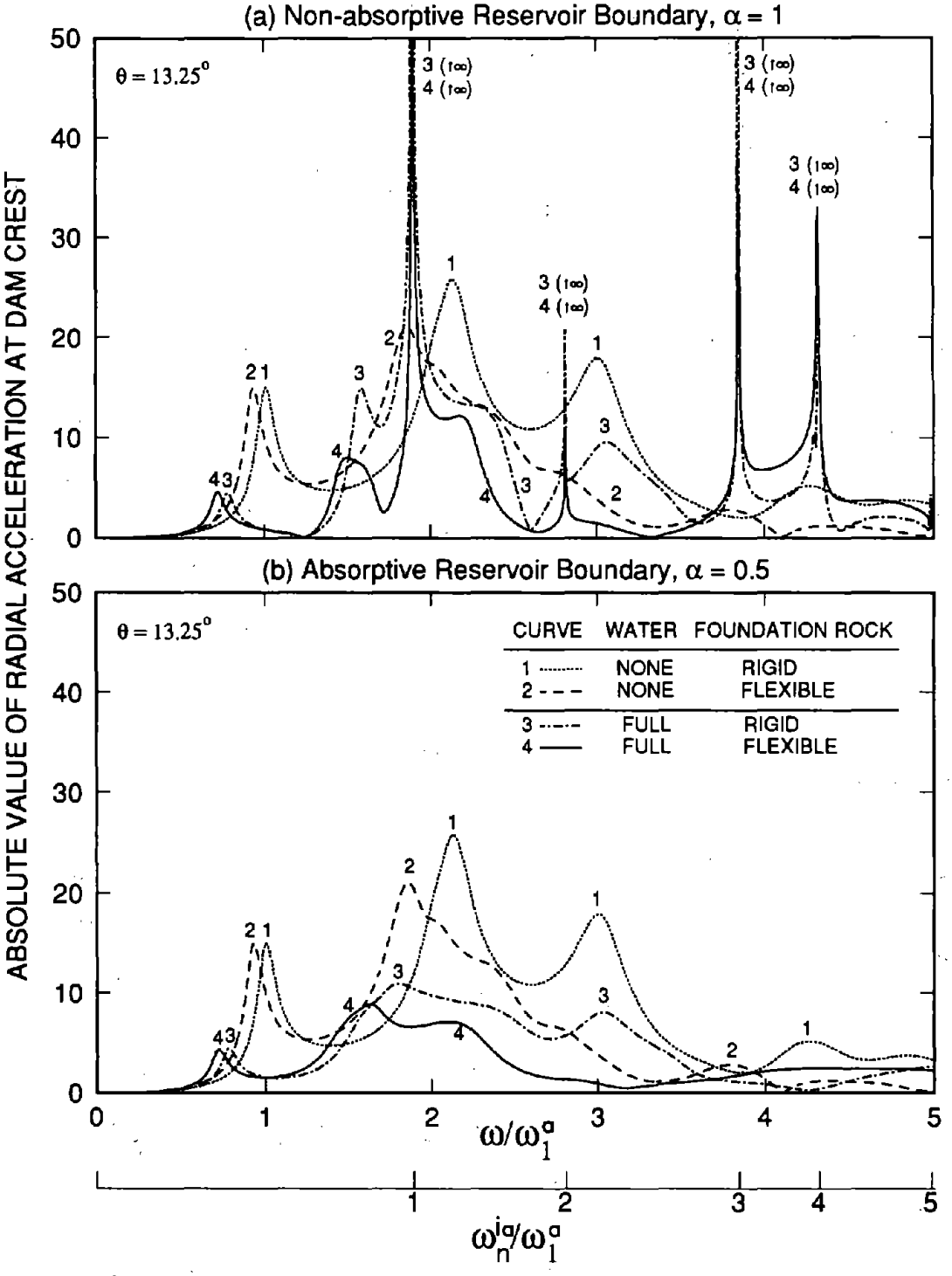

Figure 5.9 Response of dams to harmonic cross-stream ground motion for four conditions: dam on rigid foundation rock with no water (Case 1 of Table 5.1); dam on flexible foundation rock with no water (Case 3 of Table 5.1); dam on rigid foundation rock with full reservoir (Cases 6 and 10 of Table 5.1); and dam on flexible foundation rock with full reservoir (Cases 14 and 18 of Table 5.1).

increased fundamental resonant response, whether the foundation rock is rigid or flexible (compare curve 1 to 3 and curve 2 to 4). The added hydrodynamic forces have less influence on the dam response if the foundation rock is flexible than if it is rigid (compare the change from curve 2 to 4 with the change from curve 1 to 3) because of the material and radiation damping resulting from dam-foundation rock interaction. If the reservoir boundary is absorptive [Figure 5.7(b)], the trends are opposite: dam-water interaction increases the effective damping at the fundamental resonant frequency, resulting in reduced resonant response, whether the foundation rock is rigid or flexible (compare curve 1 to 3 and curve 2 to 4).

The amplitude of the fundamental resonant peak due to vertical ground motion (Figure 5.8) is affected more by the added hydrodynamic force and less by the previously discussed trends in added damping. However, the fundamental resonant response is much less affected by dam-water interaction if the foundation rock is flexible (compare the change from curve 2 to 4 with the change from curve 1 to 3). If the reservoir boundary is non-absorptive [Figure 5.8(a)], dam-water interaction greatly increases the added force and reduces the effective damping ratio at the fundamental resonant frequency, leading to much increased resonant response and a double resonant peak, of which the second peak is unbounded, whether the foundation rock is rigid or flexible (compare curve 1 to 3 and curve 2 to 4). If the reservoir boundary is absorptive [Figure 5.8(b)], dam-water interaction still increases the fundamental resonant response because of the added hydrodynamic force, whether the foundation rock is rigid or flexible (compare curve 1 to 3 and curve 2 to 4). The higher resonant peaks associated with ω_n^{is} are reduced to bounded values.

The amplitude of the fundamental resonant peak due to cross-stream ground motion (Figure 5.9) is also affected more by the added hydrodynamic force and less by the previously discussed trends in added damping. In this case the total earthquake force decreases at the fundamental resonant frequency because the hydrodynamic force is of opposite-phase relative to the inertia force of the dam [7], leading to reduced resonant response, whether the foundation rock is rigid or flexible (compare curve 1 to 3 and curve 2 to 4). The fundamental resonant response is essentially

unaffected by reservoir boundary absorption [compare parts (a) and (b) of Figure 5.9] and by dam-foundation rock interaction (compare curve 3 to 4). However, when the reservoir boundary is absorptive, the resonant peaks at ω_n^{ia} are reduced to bounded values.

The effects of reservoir boundary absorption on the response of the dam to upstream, vertical and cross-stream ground motions are shown in Figures 5.10 and 5.11 for $E_f/E_s = \infty$ and 1, respectively, For this purpose frequency response functions are presented for six values of the wave reflection coefficient α = 1 (non-absorptive reservoir boundary), 0.95, 0.9, 0.75, 0.5 and 0 (Cases 6 to 11 for $E_f/E_s = \infty$, and Cases 14 to 19 for E_f/E_s = 1). Comparison of Figures 5.10 and 5.11 indicates that the effects of reservoir boundary absorption on the dam response are similar whether the foundation rock is rigid or flexible. For upstream and vertical ground motions, reservoir boundary absorption mainly affects the fundamental resonant response, reducing its amplitude with little change in the resonant frequency, except when double peaks for lower α values merge into a single peak. Response at higher frequencies is less affected by reservoir boundary absorption except that the unbounded peaks at ω_n^{is} due to vertical ground motion are reduced to bounded values if the reservoir boundary is absorptive. For cross-stream ground motion, reservoir boundary absorption has little influence on the fundamental resonant response but reduces the unbounded peaks at ω_n^{ia} to bounded values. However, the second resonant peak (between the fundamental resonant peak and the resonant peak at ω_1^{ia}) decreases as α decreases from 1 to 0 if the foundation rock is rigid [Figure 5.10(c)], whereas it increases as α decreases from 1 to 0 if the foundation rock is flexible [Figure 5.11(c)].

The amplitude of the fundamental resonant peak of the response curves in Figures 5.10 and 5.11 is listed in Table 5.3. The data for upstream and vertical ground motions, indicates that the radiation damping due to reservoir boundary absorption is more effective in reducing the response of the dam if the foundation rock is rigid, and the damping — material and radiation — due to dam-foundation rock interaction is more effective in reducing the response of the dam if the reservoir boundary is less absorptive (some exceptions to this trend are seen in Table 5.3). This observation can be explained based on energy dissipation concepts. Damping due to dam-foundation rock

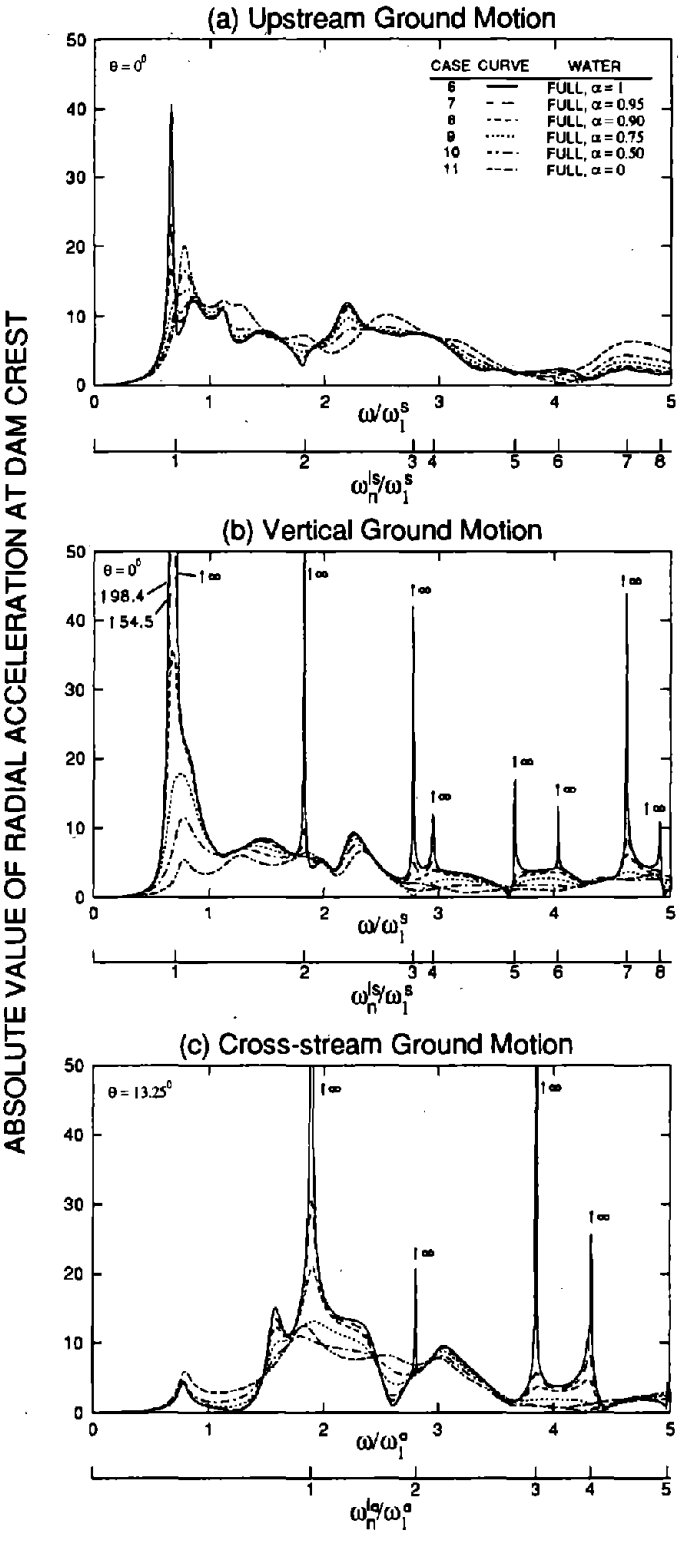

Figure 5.10 Influence of wave reflection coefficient α on the response of dams on rigid foundation rock with full reservoir to harmonic ground motion (Cases 6 to 11 of Table 5.1).

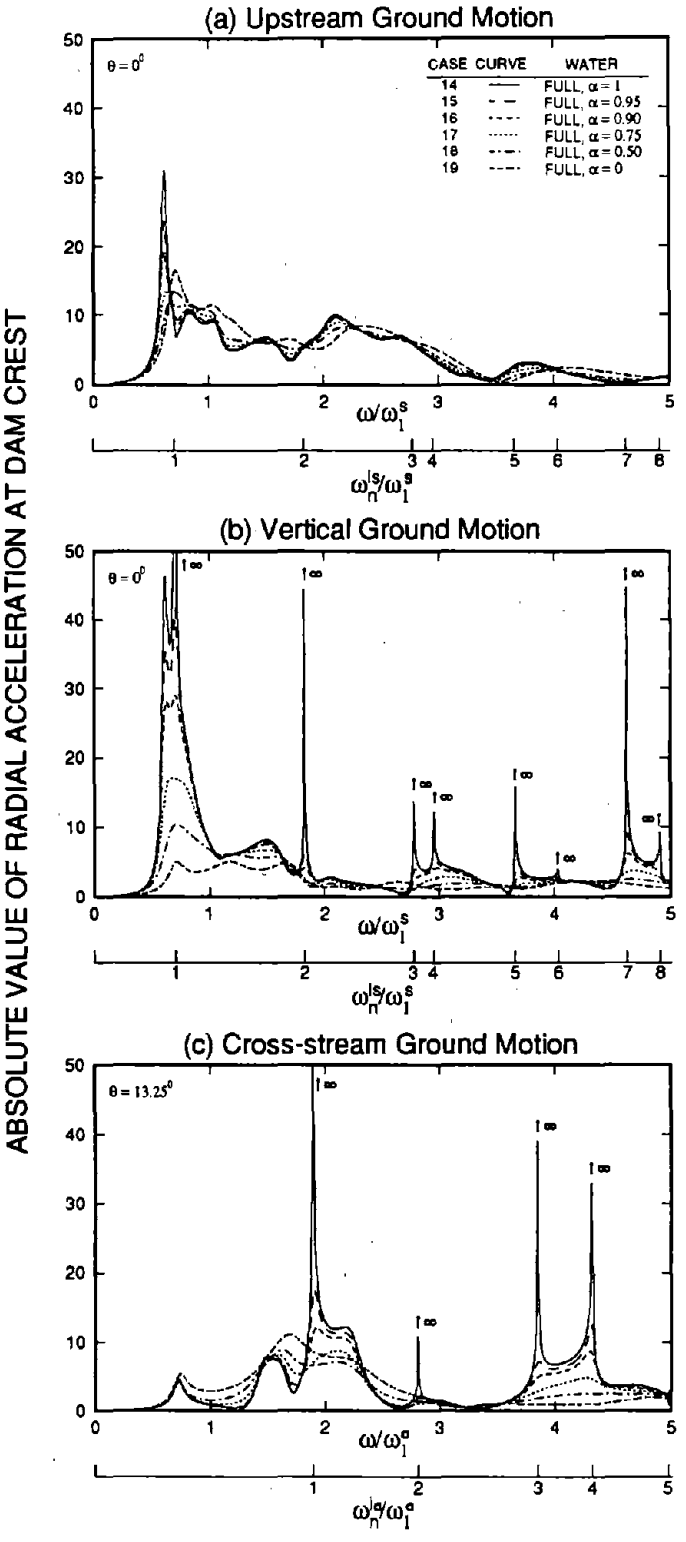

Figure 5.11 Influence of wave reflection coefficient α on the response of dams on flexible foundation rock with full reservoir to harmonic ground motion (Cases 14 to 19 of Table 5.1).

Table 5.3 Amplitude of the Fundamental Resonant Peak of Morrow Point Dam with Full Reservoir, due to Upstream, Vertical and Cross-stream Ground Motions

α	Rigid Foundation Rock ($E_f/E_s = \infty$)			Flexible Foundation Rock ($E_f/E_s = 1$)		
	Upstream	Vertical	Cross-stream	Upstream	Vertical	Cross-stream
1	40.5	98.4	4.51	31.0	46.7	4.64
0.95	23.2	54.5	4.46	23.6	35.4	4.57
0.9	16.9	35.7	4.41	19.1	28.1	4.51
0.75	13.9	17.8	4.33	13.3	17.0	4.38
0.5	16.5	11.6	4.50	13.3	10.4	4.38
0	20.2	5.46	5.93	16.5	4.98	5.43

interaction is more influential without hydrodynamic damping (non-absorptive reservoir boundary) but less effective when combined with hydrodynamic damping (arising from reservoir boundary absorption). Moreover, hydrodynamic damping is more influential without damping due to dam-foundation rock interaction (rigid foundation rock) but less effective when combined with damping due to dam-foundation rock interaction (arising from flexible foundation rock).

The fundamental resonant frequency ω_1 of the dam alone (without water, supported on rigid foundation rock) is reduced to $\tilde{\omega}_f$ due to dam-foundation rock interaction, to $\tilde{\omega}_r$ due to dam-water interaction, and to $\tilde{\omega}$ due to both effects simultaneously. The vibration periods corresponding to these frequencies are denoted as T_1, $\tilde{T}_f$, $\tilde{T}_r$, and $\tilde{T}$, respectively. The period ratio $\tilde{T}/\tilde{T}_f$ is plotted in Figure 5.12(a) against normalized water depth ratio H/H_s (where H is the water depth and H_s is the dam height) for three values of E_f/E_s. Dam-water interaction lengthens the fundamental resonant period rapidly for H/H_s greater than 0.5, especially for the symmetric vibration mode. To examine how the increase in period due to dam-water interaction is affected by dam-foundation rock interaction, the data of Figure 5.12(a) is replotted in Figure 5.12(b) where the period ratio is plotted against the E_f/E_s ratio for different values of H/H_s. For a fixed H/H_s, this plot would have been a horizontal line if the increase in period due to dam-water interaction was completely independent of E_f/E_s. It is apparent that the effects of dam-foundation rock interaction, characterized by E_f/E_s, on the period ratio are small if the reservoir is close to full. This implies that the fundamental resonant period satisfies the approximate equation suggested earlier [7,12]:

$$\frac{\tilde{T}}{T_1} \approx \frac{\tilde{T}_r}{T_1}\frac{\tilde{T}_f}{T_1}$$

This approximate relationship, valid for arch dams with non-absorptive reservoir boundary (Figure 5.12) as well as absorptive reservoir boundary (figures not presented), implies that the increase in period due to dam-water interaction is essentially unaffected by dam-foundation rock interaction.

Also presented in Figure 5.12 are the period ratio $\tilde{T}/\tilde{T}_f$ curves for a gravity dam [12]. Dam-water interaction lengthens the vibration period of the symmetric mode of arch dams more than that of

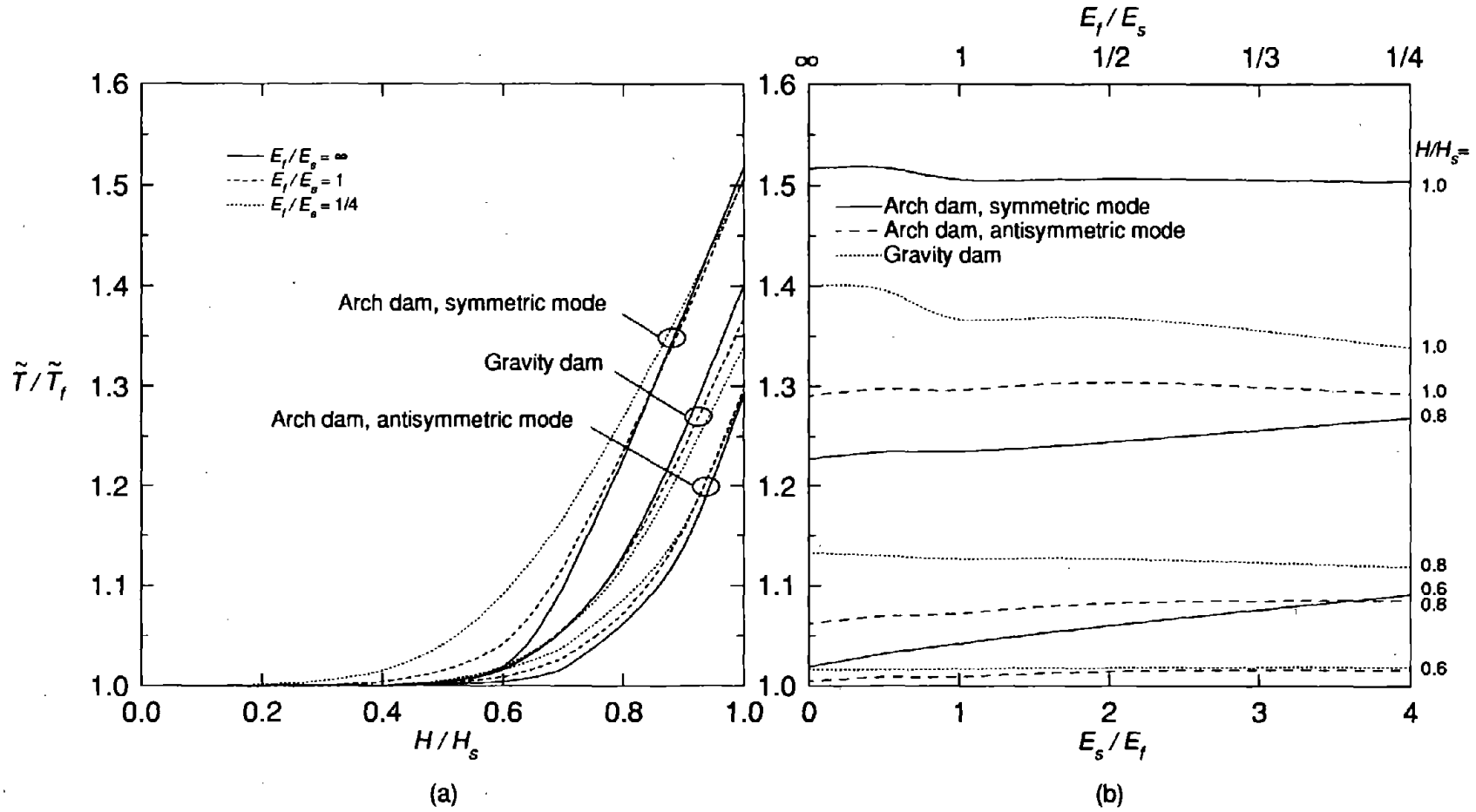

Figure 5.12 Hydrodynamic and dam-foundation rock interaction effects on the fundamental resonant period of the dam: (a) variation of the fundamental resonant period ratios, $\tilde{T}^s/\tilde{T}_f^s$ and $\tilde{T}^a/\tilde{T}_f^a$, with the water depth ratio H/H_s for different moduli ratio E_f/E_s, and (b) variation of the fundamental resonant period ratios, $\tilde{T}^s/\tilde{T}_f^s$ and $\tilde{T}^a/\tilde{T}_f^a$, with the moduli ratio E_f/E_s for different water depth ratio H/H_s.

gravity dams for all values of the moduli ratio E_f/E_s because the added hydrodynamic mass has more effect on the mass of a slender arch dam than of a massive gravity dam. Dam-water interaction lengthens the vibration period of the antisymmetric mode of an arch dam to a lesser degree than the period of its symmetric vibration mode or the vibration period of a gravity dam.

5.5.2 Influence of Moduli Ratio E_f/E_s

To understand how the effects of reservoir boundary absorption are influenced by dam-foundation rock interaction, the response of the dam with full reservoir to upstream, vertical, and cross-stream ground motions is presented in Figures 5.13, 5.14 and 5.15, respectively, for five values of $E_f/E_s = \infty$, 2, 1, 1/2 and 1/4. Response results are included for dam on rigid foundation rock with non-absorptive reservoir boundary (α = 1, Case 6); dam on rigid foundation rock with absorptive reservoir boundary (α = 0.5, Case 10); dam on flexible foundation rock with non-absorptive reservoir boundary (α = 1; Cases 12, 14, 20 and 22); and dam on flexible foundation rock with absorptive reservoir boundary (α = 0.5; Cases 13, 18, 21 and 23). The response functions for the first two systems (Cases 6 and 10) are repeated in parts (a), (b) (c) and (d) of Figures 5.13, 5.14 and 5.15; they show the effects of reservoir boundary absorption on the response of the dam supported on rigid foundation rock which were discussed in the previous section. The remaining curves in Figure 5.13 show that, as the moduli ratio E_f/E_s decreases, which for a fixed E_s means increasingly flexible foundation rock, reservoir boundary absorption has less effect on the response of the dam to upstream ground motion, especially at higher excitation frequencies. The effects of reservoir boundary absorption are small at excitation frequencies greater than the fundamental resonant frequency, even if the foundation rock is stiff with E_f/E_s = 2. However, the effects of reservoir boundary absorption are significant near the fundamental resonant frequency even if the foundation rock is very flexible, e.g. E_f/E_s = 1/4. Similarly, as E_f/E_s decreases, reservoir boundary absorption has less effect on the response of the dam to vertical and cross-stream ground motions, except at excitation frequencies near the natural vibration frequencies ω_n^i of the infinite water channel (Figures 5.14 and 5.15). Furthermore, in the case of cross-stream ground motion, reservoir boundary absorption effects are

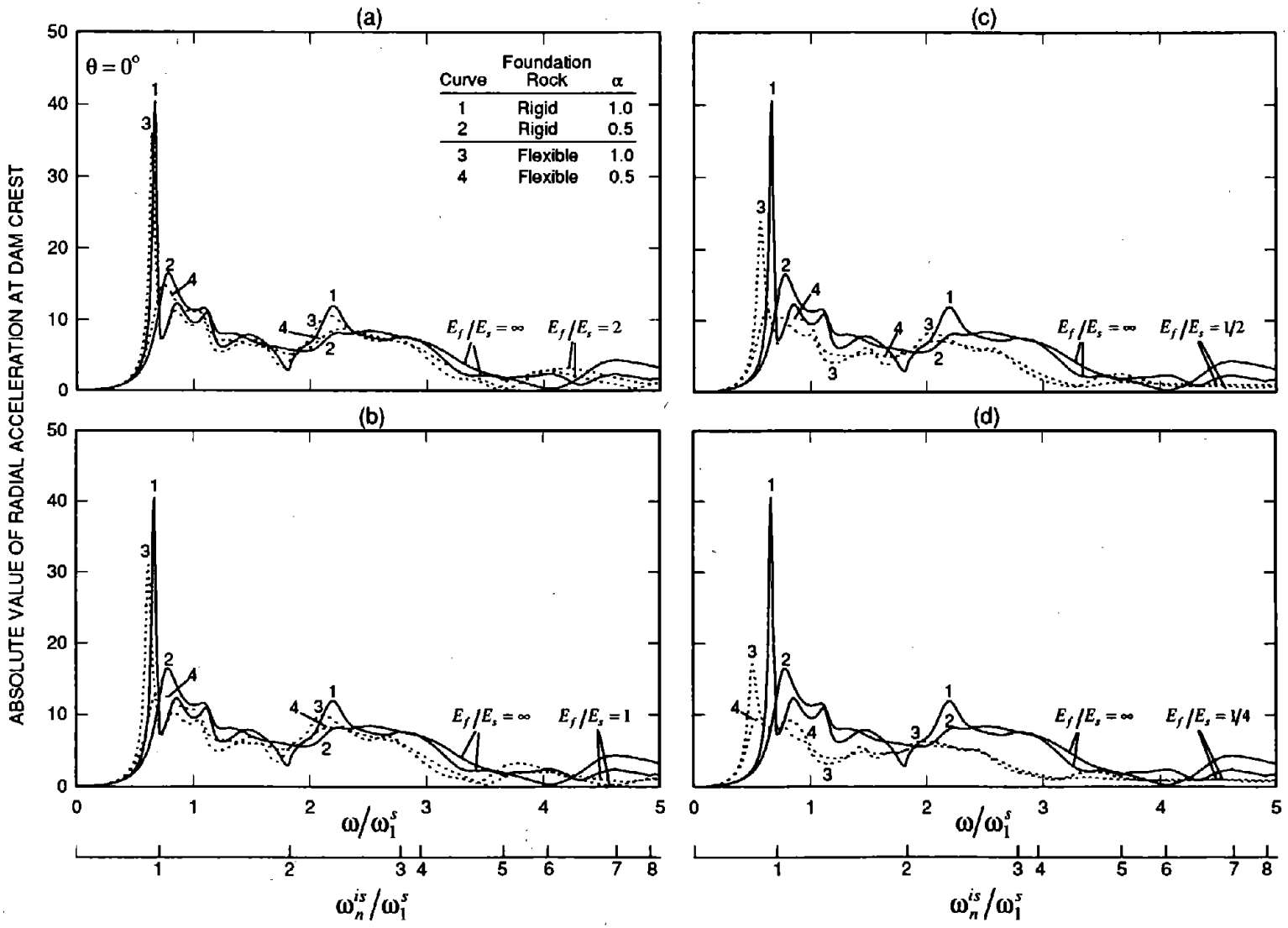

Figure 5.13 Effects of reservoir boundary absorption on response of dams with full reservoir due to harmonic upstream ground motion for various values of the moduli ratios E_f/E_s (Cases 6, 10, 12-14, 18 and 20-23 of Table 5.1).

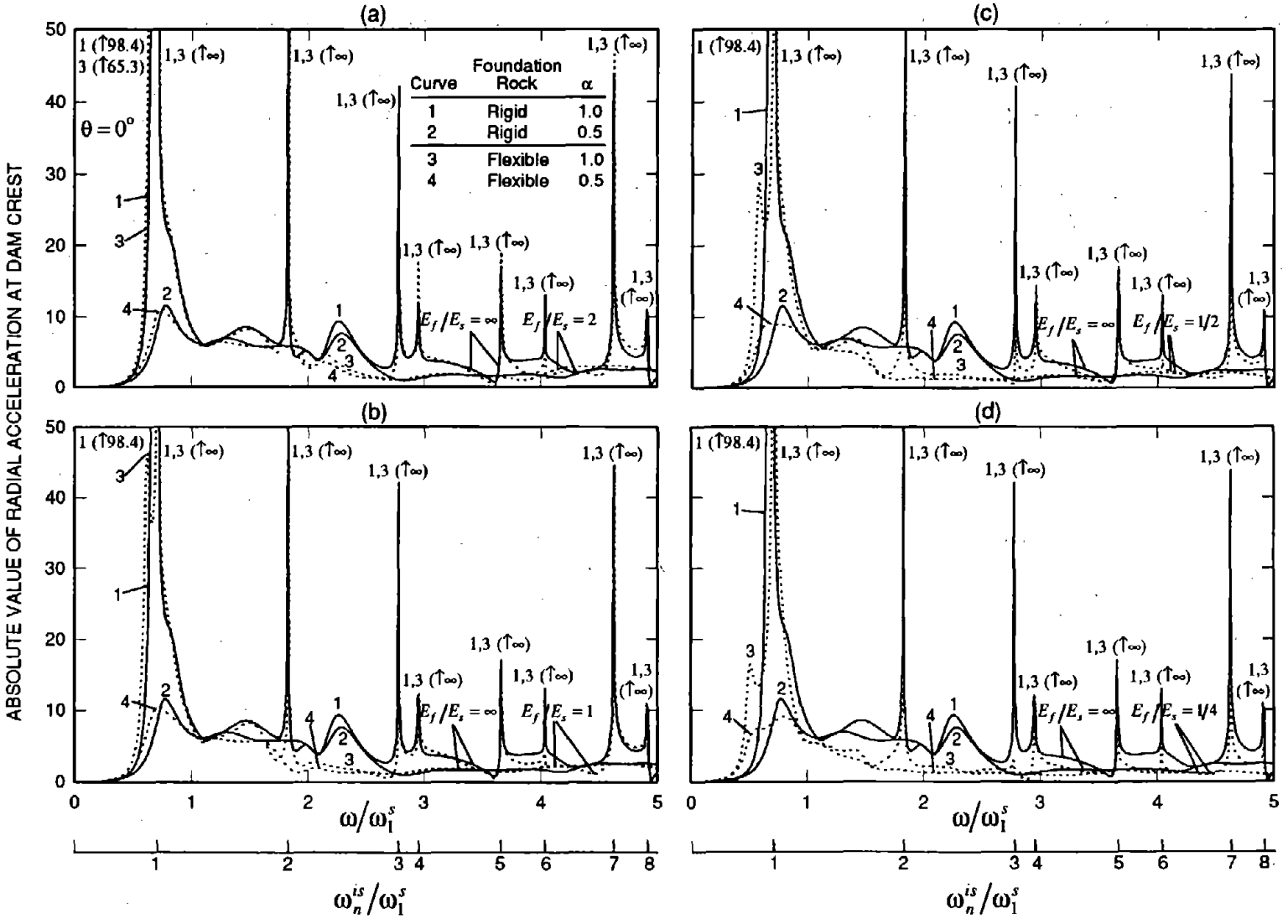

Figure 5.14 Effects of reservoir boundary absorption on response of dams with full reservoir due to harmonic vertical ground motion for various values of the moduli ratios E_f/E_s (Cases 6, 10, 12-14, 18 and 20-23 of Table 5.1).

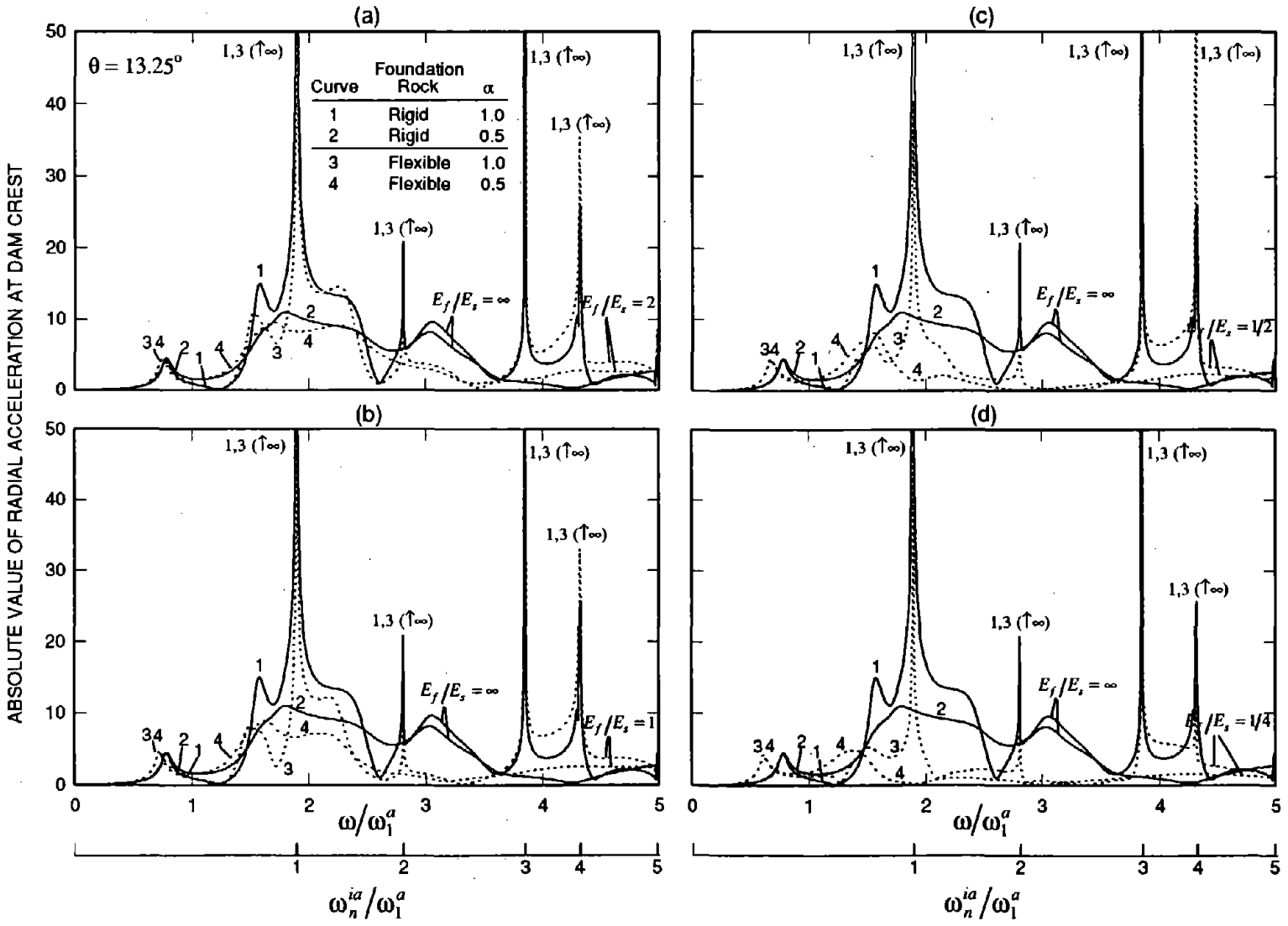

Figure 5.15 Effects of reservoir boundary absorption on response of dams with full reservoir due to harmonic cross-stream ground motion for various values of the moduli ratios E_f/E_s (Cases 6, 10, 12-14, 18 and 20-23 of Table 5.1).

negligible near the fundamental resonant frequency whether the foundation rock is rigid or flexible.

The reduced importance of reservoir boundary absorption as E_f/E_s decreases was explained in the previous section by considering the contribution of damping from dam-foundation rock interaction, dam-water interaction and reservoir boundary absorption. In particular, the effects of reservoir boundary absorption are most significant if the foundation rock is rigid because, except for material damping in the dam, there is no other damping mechanism at the fundamental resonant frequency of the dam-water system. As the foundation rock becomes more flexible, more energy radiates into the semi-infinite foundation rock region because of dam-foundation rock interaction, so that the additional damping due to reservoir boundary absorption is not as effective in further reducing the response.

The frequency response curves of Figures 5.13, 5.14 and 5.15 are reorganized in Figures 5.16, 5.17 and 5.18 to show further the influence of the moduli ratio E_f/E_s on the response of the dam. As E_f/E_s decreases, which for a fixed E_s means an increasingly flexible foundation rock, the fundamental resonant frequency decreases; the dam response to upstream and vertical ground motions at this frequency decreases and the frequency bandwidth widens irrespective of whether the reservoir boundary is non-absorptive [Figures 5.16(a) and 5.17(a)] or absorptive [Figures 5.16(b) and 5.17(b)]. It is apparent from Figures 5.16 and 5.17 that the effects of decreasing moduli ratio E_f/E_s on the fundamental resonant response of the dam are qualitatively similar for upstream and vertical excitations, whether the reservoir boundary is non-absorptive or absorptive; but quantitatively, the relative decrease in amplitude of the fundamental resonant peak depends on the wave reflection coefficient α, being less pronounced for an absorptive reservoir boundary. However as E_f/E_s decreases, the dam fundamental resonant response due to cross-stream ground motion increases slightly and then decreases; and the frequency bandwidth widens only slightly whether the reservoir boundary is non-absorptive [Figure 5.18(a)] or absorptive [Figure 5.18(b)].

As the moduli ratio E_f/E_s decreases, the response amplitudes at the higher resonant frequencies of the dam also decrease, except that the response to vertical and cross-stream ground

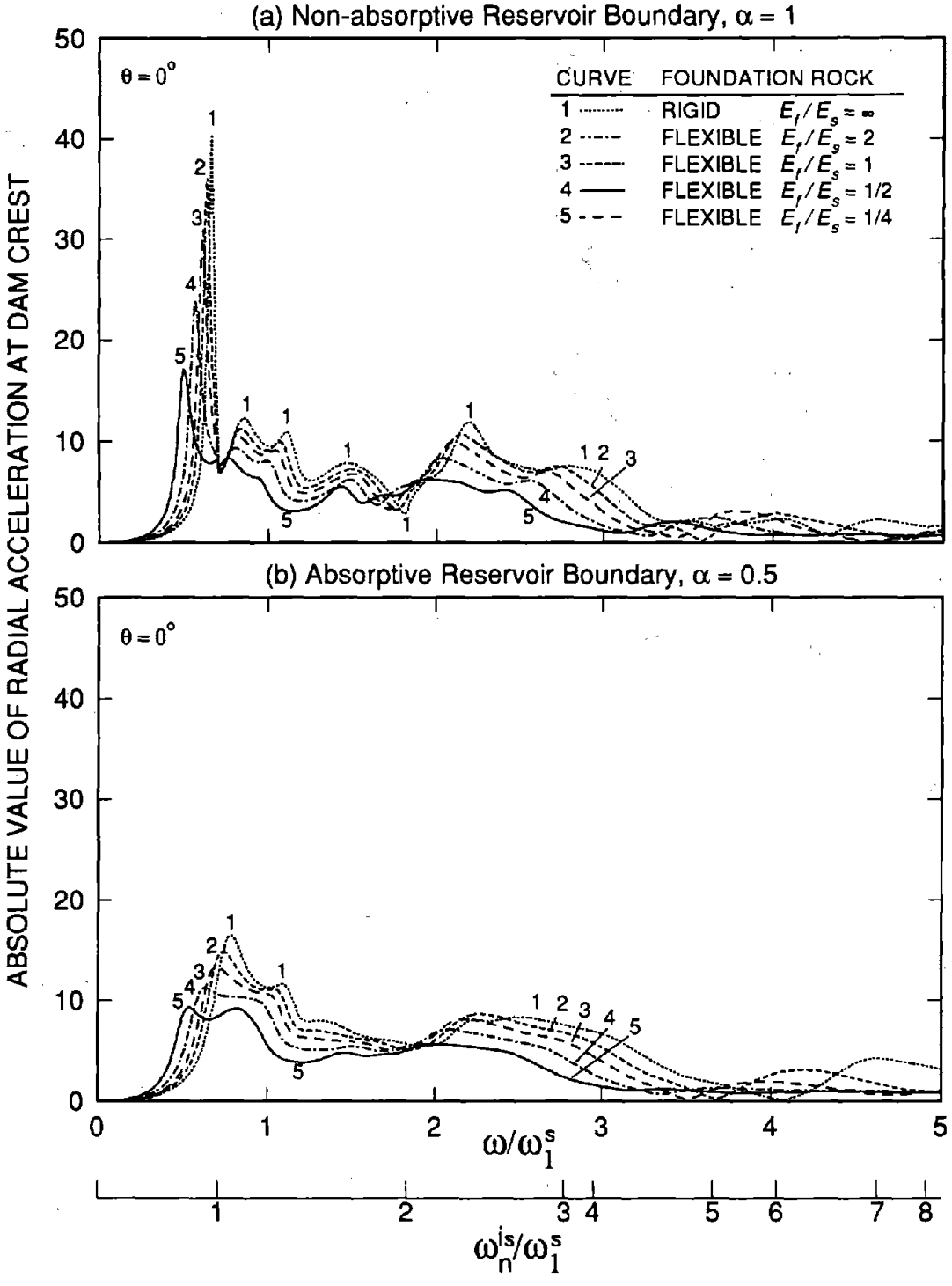

Figure 5.16 Influence of moduli ratio E_f/E_s on response of dams with full reservoir to harmonic upstream ground motion (Cases 6, 12, 14, 20 and 22 of Table 5.1 for non-absorptive reservoir boundary; Cases 10, 13, 18, 21 and 23 for absorptive reservoir boundary).

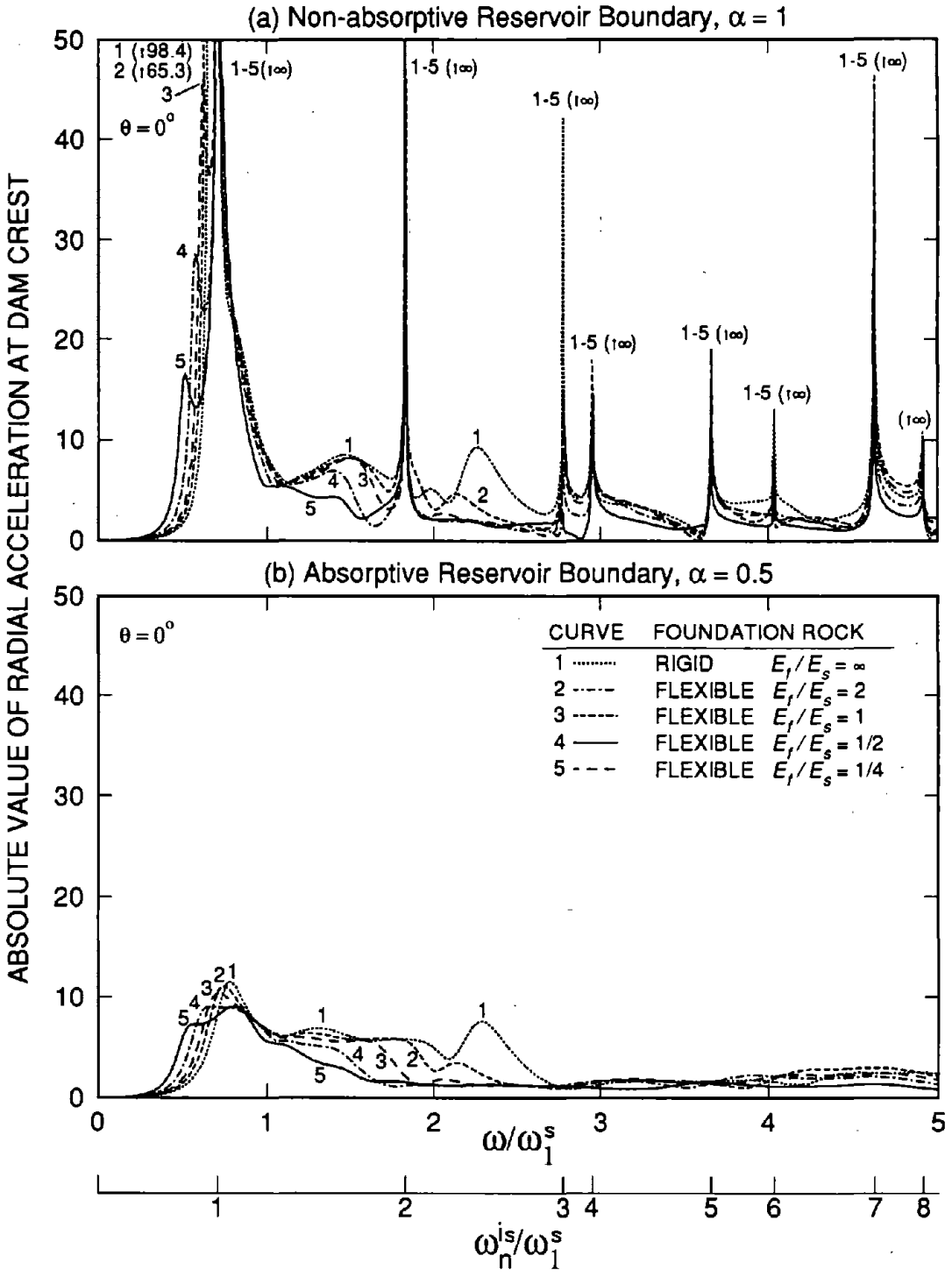

Figure 5.17 Influence of moduli ratio E_f/E_s on response of dams with full reservoir to harmonic vertical ground motion (Cases 6, 12, 14, 20 and 22 of Table 5.1 for non-absorptive reservoir boundary; Cases 10, 13, 18, 21 and 23 for absorptive reservoir boundary).

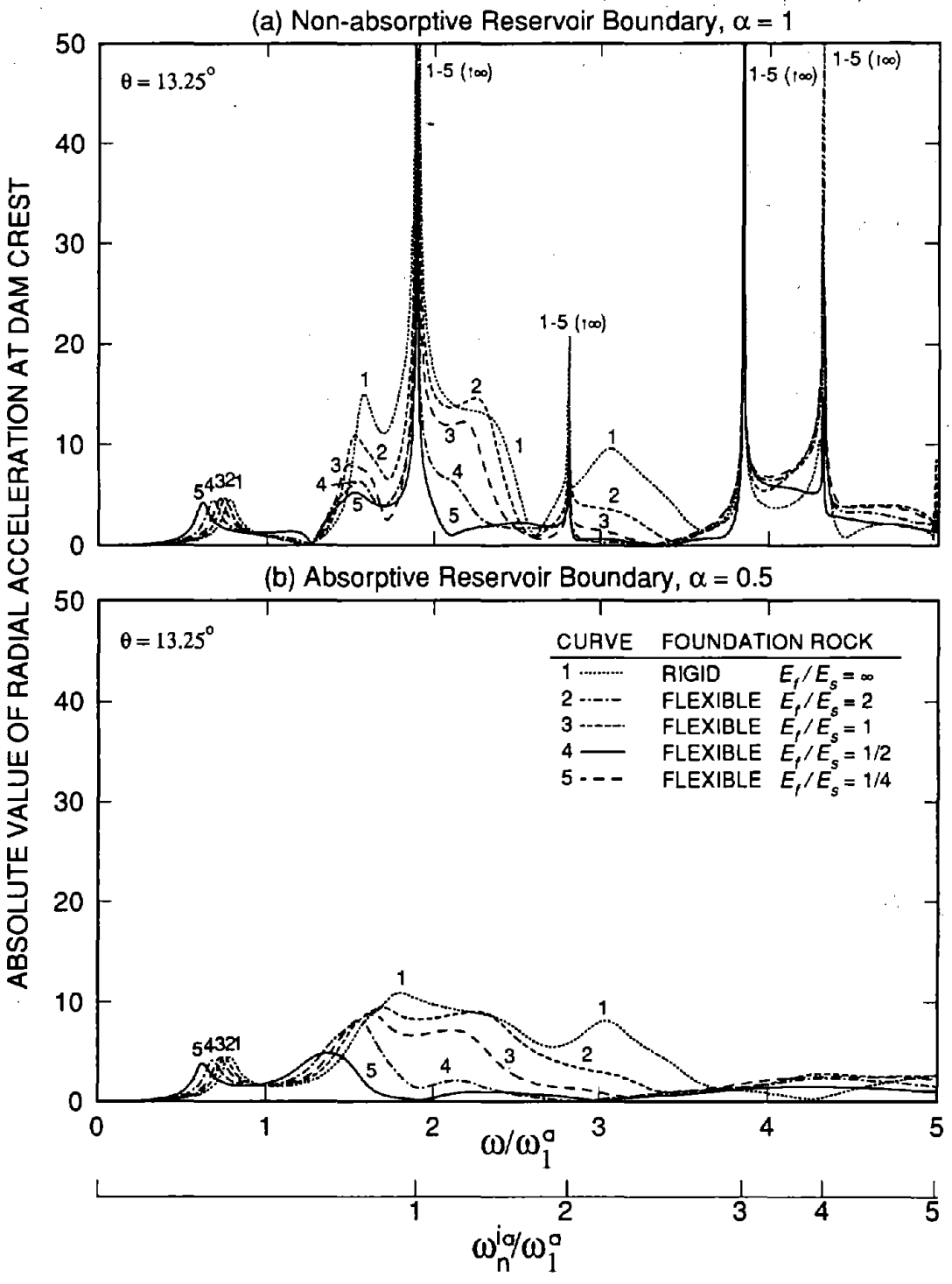

Figure 5.18 Influence of moduli ratio E_f/E_s on response of dams with full reservoir to harmonic cross-stream ground motion (Cases 6, 12, 14, 20 and 22 of Table 5.1 for non-absorptive reservoir boundary; Cases 10, 13, 18, 21 and 23 for absorptive reservoir boundary).

motions remains unbounded at the natural frequencies ω_n^i of the infinite water channel if the reservoir boundary is non-absorptive. As E_f/E_s decreases, dam-foundation rock interaction introduces increased radiation damping at the higher resonant frequencies, in addition to the damping from hydrodynamic effects, thus reducing the amplitude of the higher resonant peaks. This reduction is small for upstream or vertical ground motion (Figures 5.16 and 5.17), but is significant for cross-stream ground motion (Figure 5.18), whether the reservoir boundary is non-absorptive or absorptive. When the foundation rock is very flexible and the reservoir boundary is absorptive, some higher resonant peaks are completely suppressed by the large damping in the system.

6 EARTHQUAKE RESPONSE OF MORROW POINT DAM

6.1 Introduction

Previous investigations have shown that the earthquake response of concrete arch dams is affected by the interaction between the dam and impounded water, by water compressibility, and by the absorption of hydrodynamic pressure waves at the reservoir boundary [4,8,9]. Presented in this chapter is the earthquake response of Morrow Point Dam to Taft ground motion, determined for a wide range of parameters characterizing the properties of the dam, foundation rock, impounded water and reservoir boundary materials, using the new analytical procedure developed in Chapter 4. The response results presented are the time variations of radial displacements at the dam crest and the envelope values of the maximum tensile stresses at the upstream and downstream faces of the dam. Based on these response results, the effects of dam-foundation rock interaction with empty reservoir are studied first. The significance of these interaction effects ignored in standard analyses that consider flexibility of the foundation rock but not its inertia or damping — material and radiation — effects are then identified. The combined effects of dam-foundation rock interaction, dam-water interaction, and reservoir boundary absorption are studied next. The relative significance of the response to the three components of ground motion are also investigated. Finally, the results of a practical earthquake analysis of the arch dam are presented to demonstrate the effectiveness of the analytical procedure. This study emphasizes the effects of dam-foundation rock interaction compared to those of dam-water interaction which have been studied extensively [8].

6.2 System and Ground Motion

6.2.1 Dam-Water-Foundation Rock System

The finite element idealization selected for Morrow Point Dam, the combined finite element and continuum idealization of the impounded water, and the boundary element idealization for the

foundation rock region are presented in Figures 3.1, 3.2 and 3.3. For the mass concrete of the dam, Young's modulus E_s = 4 million psi, unit weight w_s = 155 pcf, Poisson's ratio ν_s = 0.2, and the constant hysteretic damping factor η_s = 0.1. This corresponds to a viscous damping ratio of 0.05 in all natural vibration modes of the dam supported on rigid foundation rock with empty reservoir. For the foundation rock, Young's modulus E_f is varied so that $E_f/E_s = \infty$, 2, 1, 1/2 or 1/4, unit weight w_f = 165 pcf; Poisson's ratio ν_f = 0.2, and constant hysteretic damping factor η_f = 0.1. The unit weight of water w_w = 62.4 pcf and the velocity of pressure waves in water C = 4720 ft/sec. For the reservoir boundary materials, the wave reflection coefficient α varies over a wide range; the values considered are: α = 1 (non-absorptive reservoir boundary), 0.95, 0.5 and 0.

6.2.2 Ground Motion

The ground motion recorded at Taft Lincoln School Tunnel during the Kern County, California, earthquake of 21 July 1952 is selected as the free-field ground acceleration for the analysis of Morrow Point Dam. The ground motion acting in the upstream (x), vertical (y), and cross-stream (z) directions is defined as the S69E, vertical, and S21W components of the recorded ground motion, respectively. The time variation of these three components of ground acceleration and their peak accelerations are shown in Figure 6.1.

6.3 Response Results

The response of Morrow Point Dam was analyzed for a total of 13 sets of assumptions and conditions listed in Table 6.1 for the dam, foundation rock, impounded water, and reservoir boundary materials. For each of these 13 cases, the response of the dam was computed for four excitations: upstream ground motion, only; vertical ground motion, only; cross-stream ground motion, only; and all three ground motion components, simultaneously, of Taft ground motion; the effects of static loads were excluded.

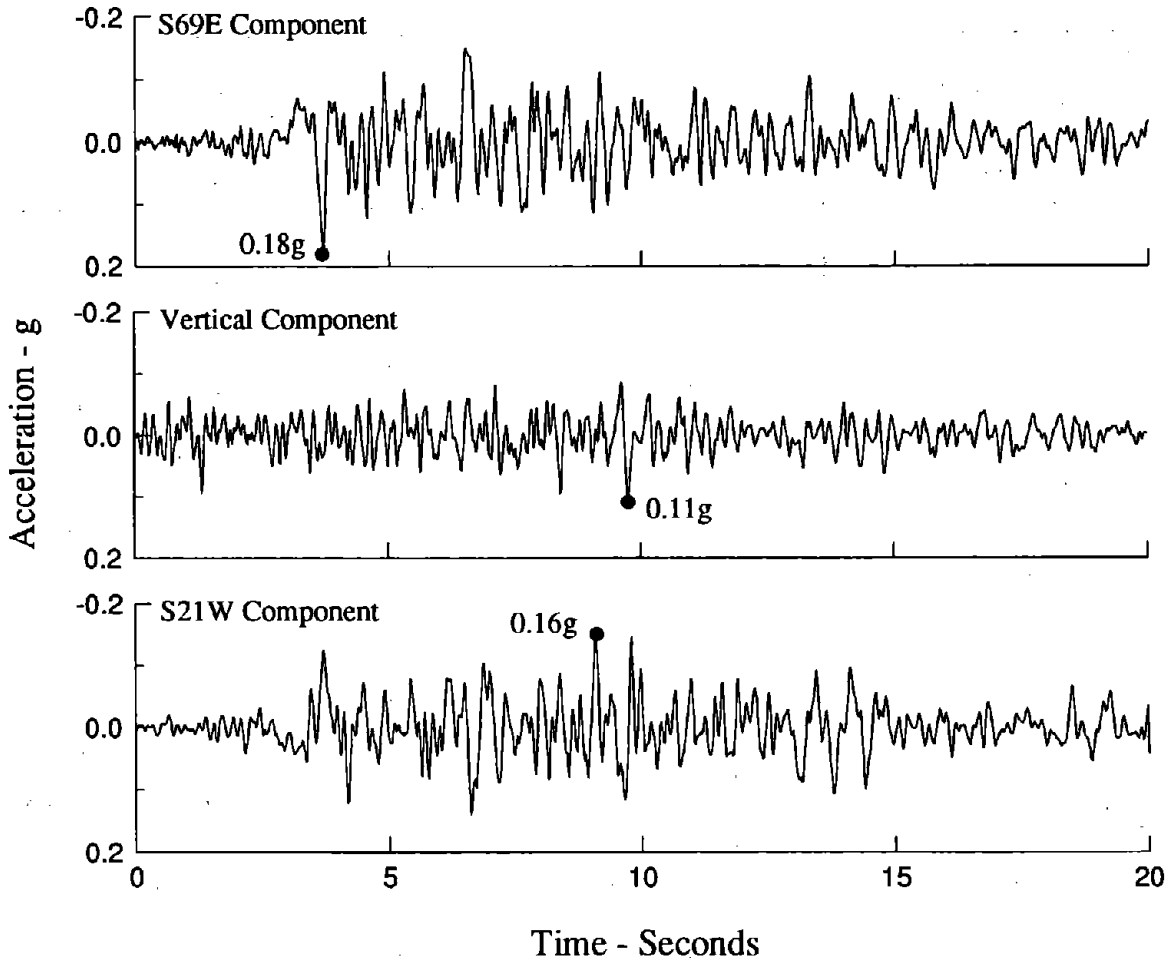

Figure 6.1 Ground motion at Taft Lincoln School Tunnel, Kern County, California, Earthquake, 21 July, 1952.

Table 6.1 Cases of Morrow Point Dam Analyzed, Fundamental Resonant Periods of Vibration, Damping Ratios, and Response Spectrum Ordinates for the Three Components of Taft Ground Motion

Case	Foundation Rock		Water	α	Fundamental Mode Properties								
					Upstream Ground Motion			Vertical Ground Motion			Cross-stream Ground Motion		
	E_f/E_s	Condition			Resonant Period T_1^x (sec)	Damping Ratio ξ_1^x (%)	$S_a(T_1^x,\xi_1^x)$ (g)	Resonant Period T_1^y (sec)	Damping Ratio ξ_1^y (%)	$S_a(T_1^y,\xi_1^y)$ (g)	Resonant Period T_1^z (sec)	Damping Ratio ξ_1^z (%)	$S_a(T_1^z,\xi_1^z)$ (g)
1	∞	Rigid	Empty	-	0.234	5.0	0.433	0.234	5.0	0.299	0.263	5.0	0.370
2	2	Interaction	Empty	-	0.245	5.4	0.376	0.245	5.6	0.249	0.273	5.1	0.373
3	1	Interaction	Empty	-	0.255	6.0	0.351	0.255	6.0	0.223	0.284	5.4	0.334
4	1/2	Interaction	Empty	-	0.277	7.2	0.319	0.277	7.4	0.203	0.302	5.8	0.362
5	1/4	Interaction	Empty	-	0.315	9.3	0.343	0.315	9.6	0.244	0.332	6.3	0.417
6	∞	Rigid	Full	1	0.355	2.2	0.661	0.353	4.4	0.366	0.340	4.9	0.526
7	∞	Rigid	Full	0.95	0.355	3.8	0.498	0.349	4.9	0.364	0.340	5.0	0.522
8	∞	Rigid	Full	0.5	0.310	11.8	0.316	0.310	11.3	0.225	0.338	5.9	0.467
9	∞	Rigid	Full	0	0.305	7.6	0.364	0.304	7.7	0.226	0.334	7.2	0.399
10	1	Flexible	Full	1	0.385	3.7	0.356	0.383	4.5	0.229	0.367	5.2	0.524
11	1	Flexible	Full	0.95	0.385	4.8	0.338	0.381	10.5	0.208	0.367	5.2	0.519
12	1	Flexible	Full	0.5	0.353	14.9	0.267	0.349	14.3	0.220	0.367	6.3	0.465
13	1	Flexible	Full	0	0.336	9.7	0.312	0.334	9.8	0.273	0.361	8.0	0.426

The earthquake response of the dam was computed under the assumption of linear behavior of the dam-water-foundation rock system, using the analytical procedure developed in Chapter 4, where the displacement-time history was obtained by Fourier synthesis of the complex-valued frequency response functions for the generalized coordinates. These response functions were computed for the excitation frequency range 0 to 25 Hz, which has been tested to be adequate for the selected dam and the Taft ground motion. The first 20 generalized coordinates were included in the analyses for all cases.

The fundamental resonant period and effective damping ratio at that period, determined by the half-power bandwidth method from the frequency response function for the crest displacement due to each of the three ground motion components, are presented in Table 6.1. Strictly speaking, the half-power bandwidth method does not apply to dams because hydrodynamic and foundation interaction introduces frequency-dependent added mass, damping and force. However, the method is employed here to obtain a rough measure of damping to assist in interpretation of response results. As seen in Table 6.1, the fundamental resonant periods T_1^x and T_1^y obtained from the response to upstream (x) or vertical (y) ground motion are the same; it is the period of the fundamental, symmetric mode of vibration, modified by the added mass from dam-water interaction and the flexibility of the foundation rock. The frequency-dependent hydrodynamic force which is not the same for the two ground motions influences the resonant period slightly. If the reservoir is empty, the damping ratios ξ_1^x and ξ_1^y corresponding to the upstream and vertical ground motions, respectively, have the same value if the foundation rock is rigid; however, they are slightly different if the foundation rock is flexible because dam-foundation rock interaction effects are not identical for the two excitations. When the reservoir is full, the damping ratios ξ_1^x and ξ_1^y are different because the frequency-dependent added hydrodynamic force is not the same for the two ground motions. The fundamental resonant period T_1^z and damping ratio ξ_1^z, obtained from the response to cross-stream ground motion, are the period and damping ratio of the fundamental, antisymmetric mode of vibration, modified by dam-water interaction and dam-foundation rock interaction. For each of the 13 cases, the pseudo-acceleration S_a corresponding to the

fundamental vibration period and damping ratio, determined from the response to each ground motion component, is obtained from the response spectrum for that particular ground motion and is listed in Table 6.1.

The response results selected to illustrate the different effects consist of displacement-time histories and contours of envelope values of maximum tensile stresses. The radial component of the displacement at the dam crest nodal point defined by $\theta = 13.25^{o}$ (nodal point 54 in Figure 3.1), where θ is the angle measured from the x-y plane along the dam crest arch, is presented. The distributions of envelope values of the maximum tensile stresses in the arch and cantilever directions are presented for both the upstream and downstream faces of the dam. The maximum radial displacement at the dam crest nodal point 54 ($\theta = 13.25^{o}$, Figure 3.1), and the maximum tensile values of arch and cantilever stresses over the upstream and downstream dam faces, are also summarized and grouped into Tables 6.2, 6.4, 6.6 and 6.7 in the following sections for convenient comparison of the results.

A point worth mentioning concerns the stress contour presentation in this chapter. The envelope values of maximum tensile stresses are shown for the right half of the dam when looking from the downstream side in the upstream direction. Because the Morrow Point Dam system is assumed to be symmetric about the x-y plane, the maximum tensile stresses are symmetric about this plane for the dam subjected to upstream or vertical component of ground motion; and, as explained in Reference [8], they are approximately symmetric about the x-y plane for the dam subjected to the cross-stream component of ground motion. However, the maximum tensile stresses due to all three components of ground motion acting simultaneously are shown for the whole dam since they are not symmetric about the x-y plane.

The displacement and stresses due to static loads such as the dead weight of the dam and the hydrostatic pressure on the upstream face of the dam are not included in most of the results presented here to study the effects of dam-foundation rock interaction, dam-water interaction, and reservoir boundary absorption on dynamic response. The static loads should be included, however, for practical earthquake analyses of the dam; an example is given at the end of this chapter.

6.4 Dam-Foundation Rock Interaction Effects

Dam-foundation rock interaction effects in the earthquake response of Morrow Point Dam are studied first; the reservoir is assumed empty. These effects can be visualized as arising partly from the change in the complex-valued frequency response functions of the dam (Chapter 5), and partly from the change in the response spectrum ordinate corresponding to each resonant peak, especially the fundamental resonant peak, corresponding to the changes in resonant period and damping. As the moduli ratio E_f/E_s decreases, which for a fixed concrete modulus E_s means increasingly flexible foundation rock, the period and the effective damping ratio at the fundamental resonance of the symmetric and antisymmetric modes of vibration increases. For example, as E_f/E_s decreases from ∞ to 1/4, the fundamental resonant period of Morrow Point Dam lengthens from 0.234 sec to 0.315 sec for the symmetric vibration mode and from 0.263 sec to 0.332 sec for the antisymmetric vibration mode; and the effective damping at the fundamental resonant period increases from 5% to 9.3%, 9.6% or 6.3% due to upstream, vertical or cross-stream ground motion, respectively (Table 6.1). As discussed in Chapter 5, the fundamental resonant period is affected almost entirely by the flexibility of foundation rock; whereas the effective damping ratio at the fundamental resonance is affected primarily by material and radiation damping resulting from dam-foundation rock interaction. As the moduli ratio E_f/E_s decreases, the radiation damping from dam-foundation rock interaction increases, resulting in larger effective damping ratio (Table 6.1). The combined change in the vibration period and damping ratio results in a change in the pseudo-acceleration response spectrum ordinate for each of the three components of Taft ground motion. For the selected dam and excitation, as the moduli ratio E_f/E_s changes from ∞ to 1/4, $S_a(T_1^x,\xi_1^x)$ changes from 0.433g to 0.343g; $S_a(T_1^y,\xi_1^y)$ changes from 0.299g to 0.244g; and $S_a(T_1^z,\xi_1^z)$ changes from 0.370g to 0.417g (Table 6.1).

The effects of dam-foundation rock interaction on the response of the dam with an empty reservoir are identified by examining the results presented for the various E_f/E_s values (Table 6.2 and Figures 6.2-6.8). The displacement histories in Figure 2 indicate that, as E_f/E_s decreases, the fundamental resonant period is lengthened and the contributions of the higher vibration modes of the

Table 6.2 Summary of Responses* of Morrow Point Dam with Empty Reservoir, Including Dam-Foundation Rock Interaction, to Taft Ground Motion

Case	Foundation Rock		Maximum Radial Crest Displacement (inches)	Maximum Tensile Stress (psi)			
				Upstream Face		Downstream Face	
	E_f/E_s	Condition		Arch Stress	Cantilever Stress	Arch Stress	Cantilever Stress
(a) Response to Upstream (S69E Component of Taft) Ground Motion							
1	∞	Rigid	0.382	268	100	244	65
2	2	Interaction	0.396	262	104	239	67
3	1	Interaction	0.438	271	100	251	62
4	1/2	Interaction	0.451	289	102	274	71
5	1/4	Interaction	0.635	293	96	301	62
(b) Response to Vertical Component of Taft Ground Motion							
1	∞	Rigid	0.068	55	48	43	41
2	2	Interaction	0.069	57	54	44	44
3	1	Interaction	0.075	63	66	45	38
4	1/2	Interaction	0.072	70	81	51	35
5	1/4	Interaction	0.095	70	86	75	36
(c) Response to Cross-stream (S21W Component of Taft) Ground Motion							
1	∞	Rigid	0.368	153	100	209	90
2	2	Interaction	0.453	169	107	181	77
3	1	Interaction	0.438	173	96	185	76
4	1/2	Interaction	0.544	184	113	231	96
5	1/4	Interaction	0.726	260	157	316	157
(d) Response to Upstream, Vertical, and Cross-stream Components, Simultaneously, of Taft Ground Motion							
1	∞	Rigid	0.486	336	118	307	137
2	2	Flexible	0.615	301	119	337	140
3	1	Flexible	0.658	313	125	292	128
4	1/2	Flexible	0.645	304	115	295	121
5	1/4	Flexible	0.950	407	191	414	178

* Effects of static loads are excluded.

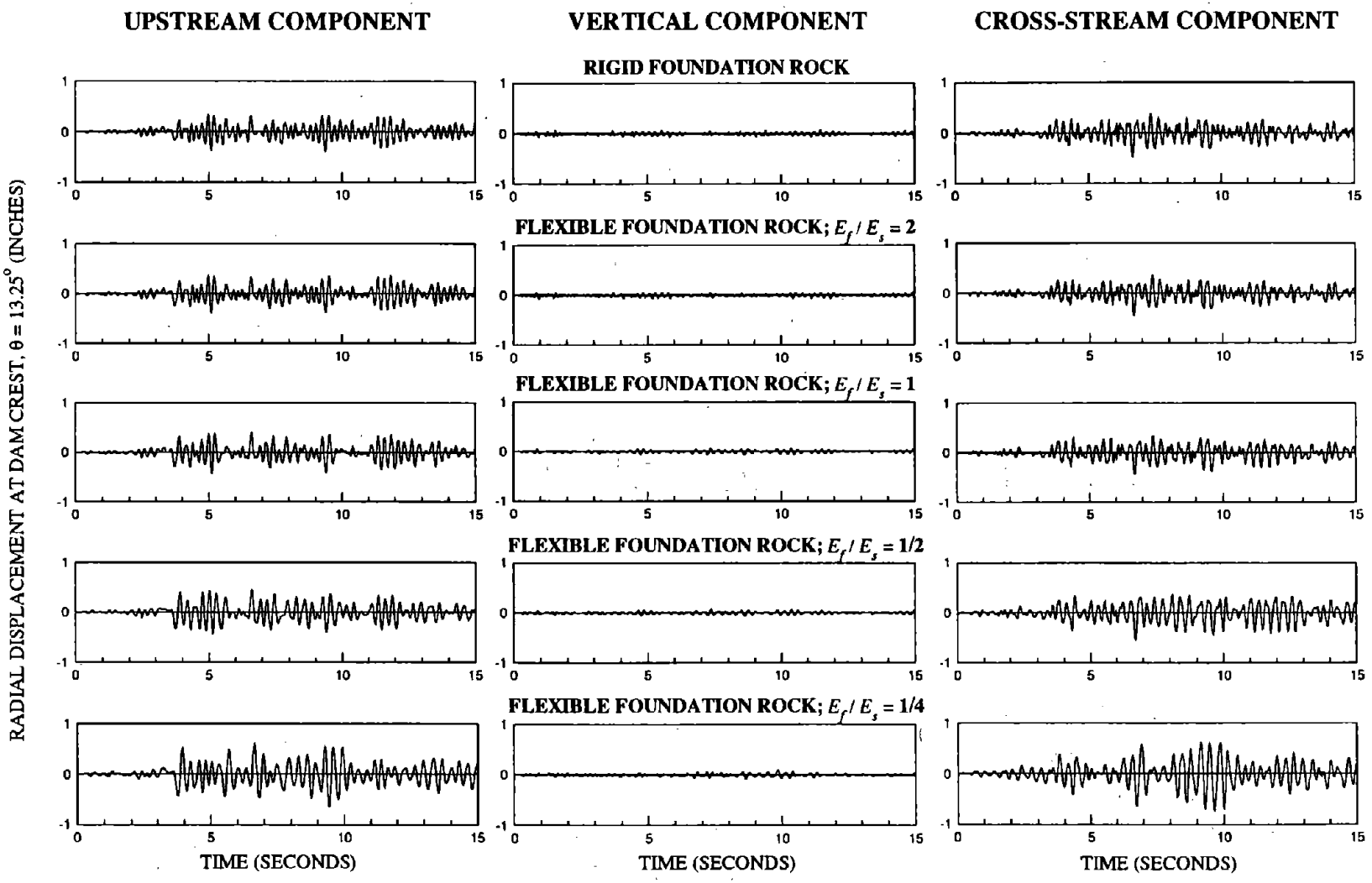

Figure 6.2 Displacement response of Morrow Point Dam on rigid and flexible foundation rock with empty reservoir due to upstream, vertical and cross-stream components, separately, of Taft ground motion.

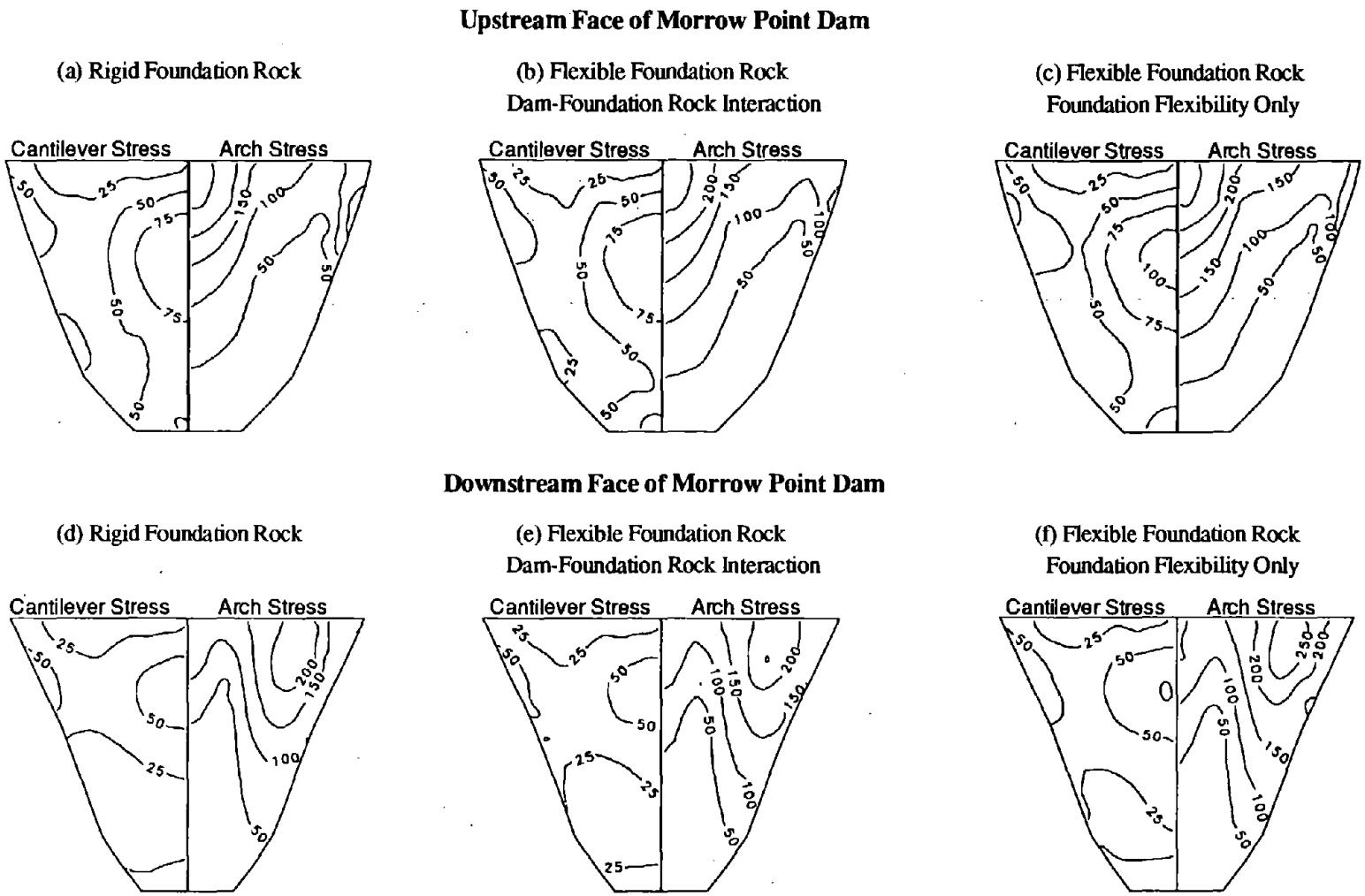

Figure 6.3 Envelope values of maximum tensile stress (in psi) on faces of Morrow Point Dam with empty reservoir, supported on rigid or flexible foundation rock with $E_f/E_s = 1$, due to upstream component, only, of Taft ground motion. Initial static stresses are excluded.

Upstream Face of Morrow Point Dam

(a) Rigid Foundation Rock

(b) Flexible Foundation Rock
Dam-Foundation Rock Interaction

(c) Flexible Foundation Rock
Foundation Flexibility Only

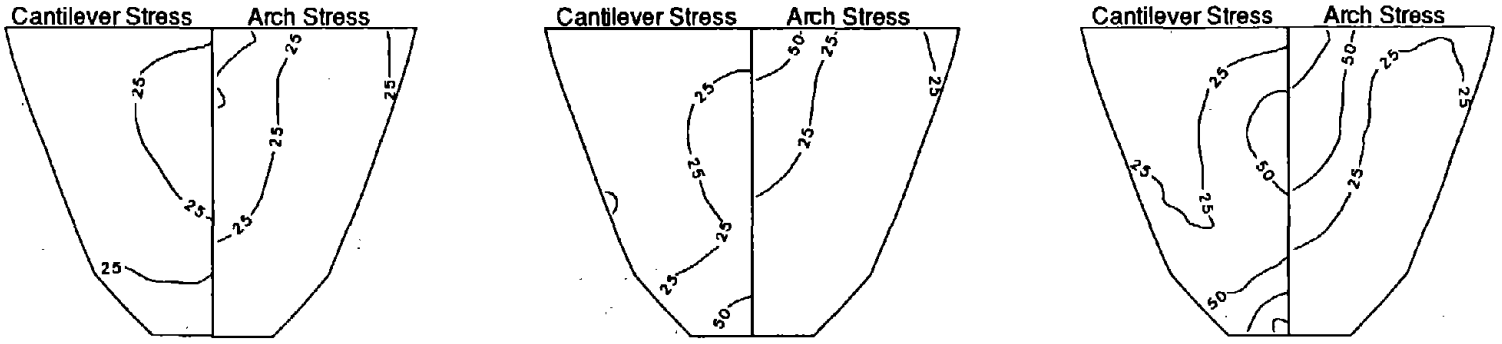

Downstream Face of Morrow Point Dam

(d) Rigid Foundation Rock

(e) Flexible Foundation Rock
Dam-Foundation Rock Interaction

(f) Flexible Foundation Rock
Foundation Flexibility Only

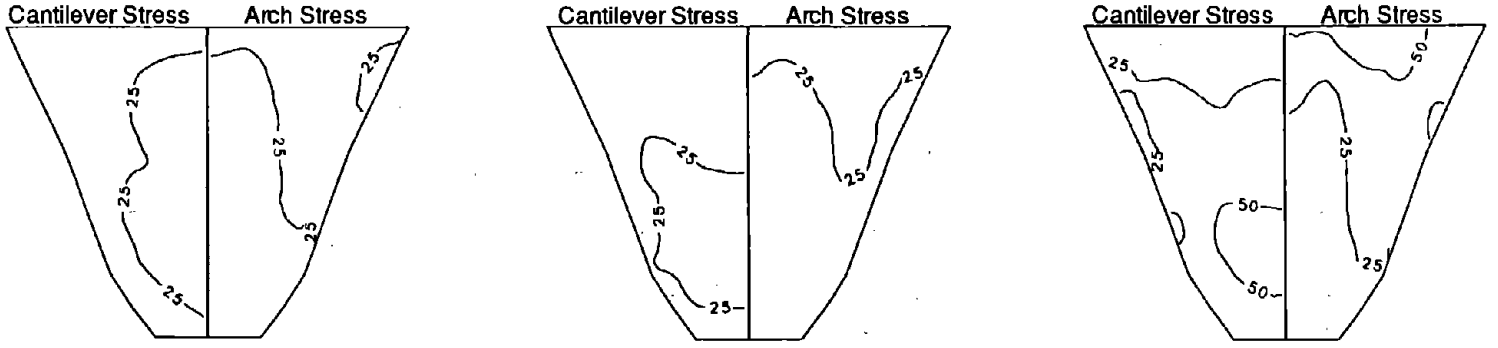

Figure 6.4 Envelope values of maximum tensile stress (in psi) on faces of Morrow Point Dam with empty reservoir, supported on rigid or flexible foundation rock with $E_f/E_s = 1$, due to vertical component, only, of Taft ground motion. Initial static stresses are excluded.

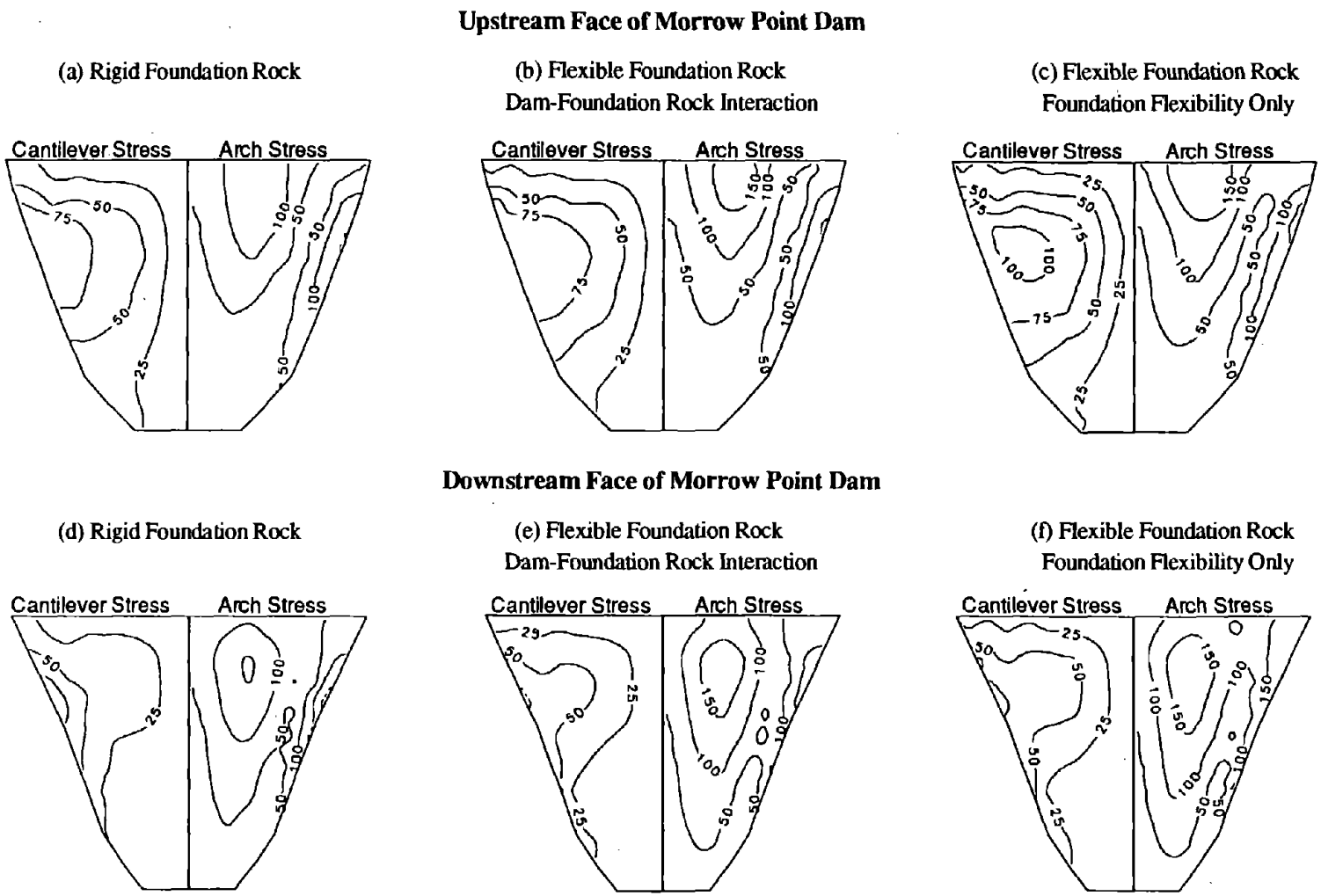

Figure 6.5 Envelope values of maximum tensile stress (in psi) on faces of Morrow Point Dam with empty reservoir, supported on rigid or flexible foundation rock with $E_f/E_s = 1$, due to cross-stream component, only, of Taft ground motion. Initial static stresses are excluded.

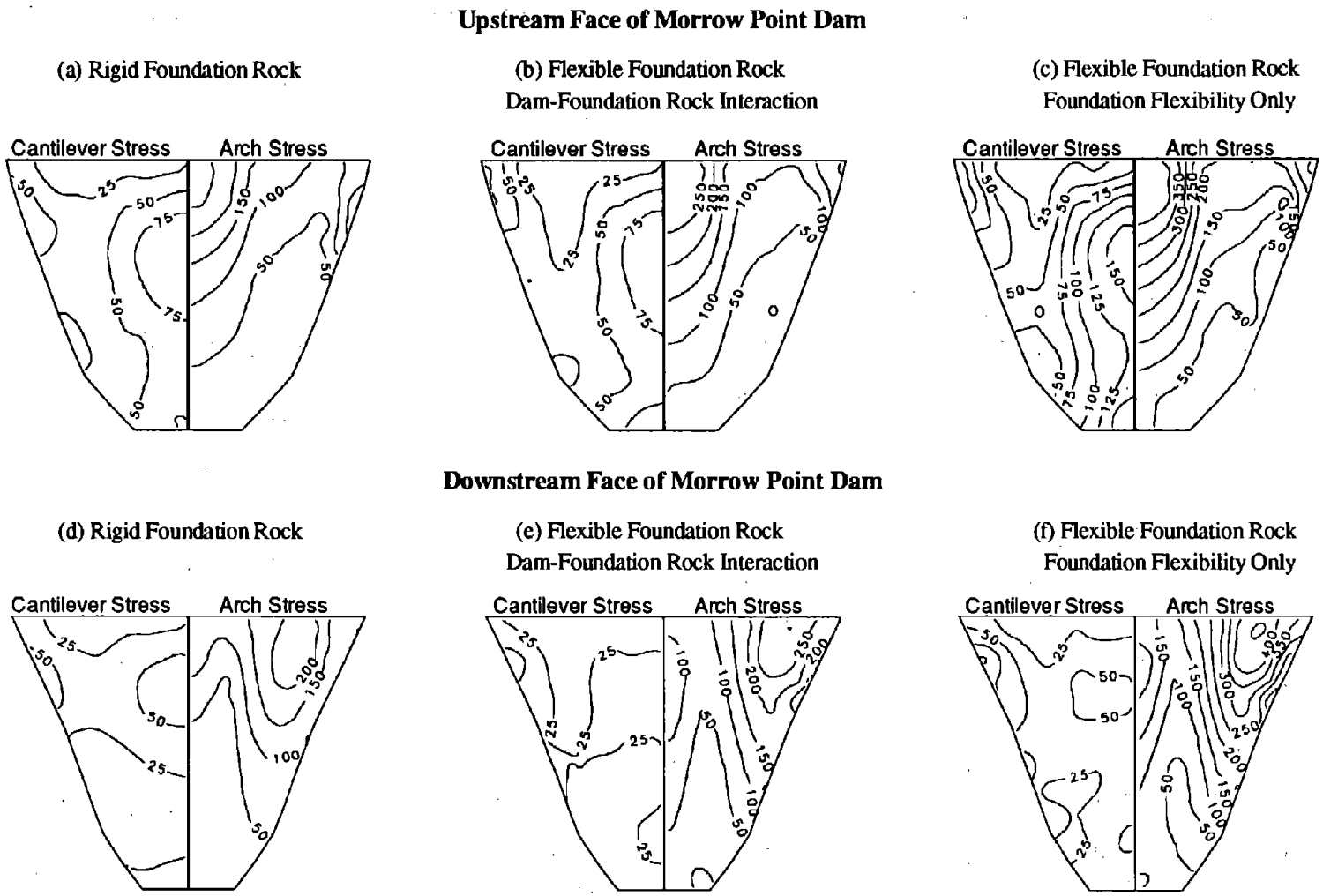

Figure 6.6 Envelope values of maximum tensile stress (in psi) on faces of Morrow Point Dam with empty reservoir, supported on rigid or flexible foundation rock with $E_f/E_s = 1/4$, due to upstream component, only, of Taft ground motion. Initial static stresses are excluded.

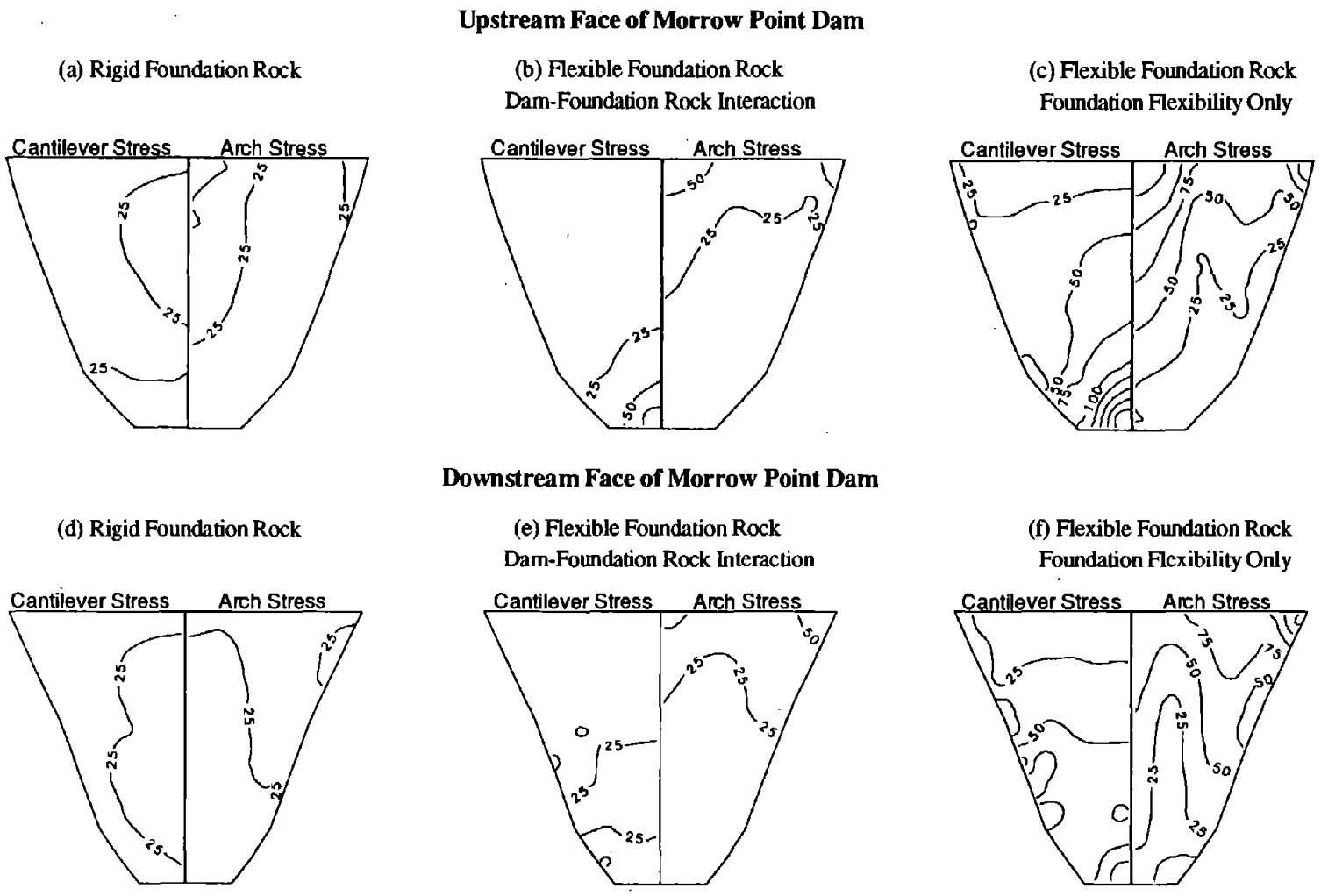

Figure 6.7 Envelope values of maximum tensile stress (in psi) on faces of Morrow Point Dam with empty reservoir, supported on rigid or flexible foundation rock with $E_f/E_s = 1/4$, due to vertical component, only, of Taft ground motion. Initial static stresses are excluded.

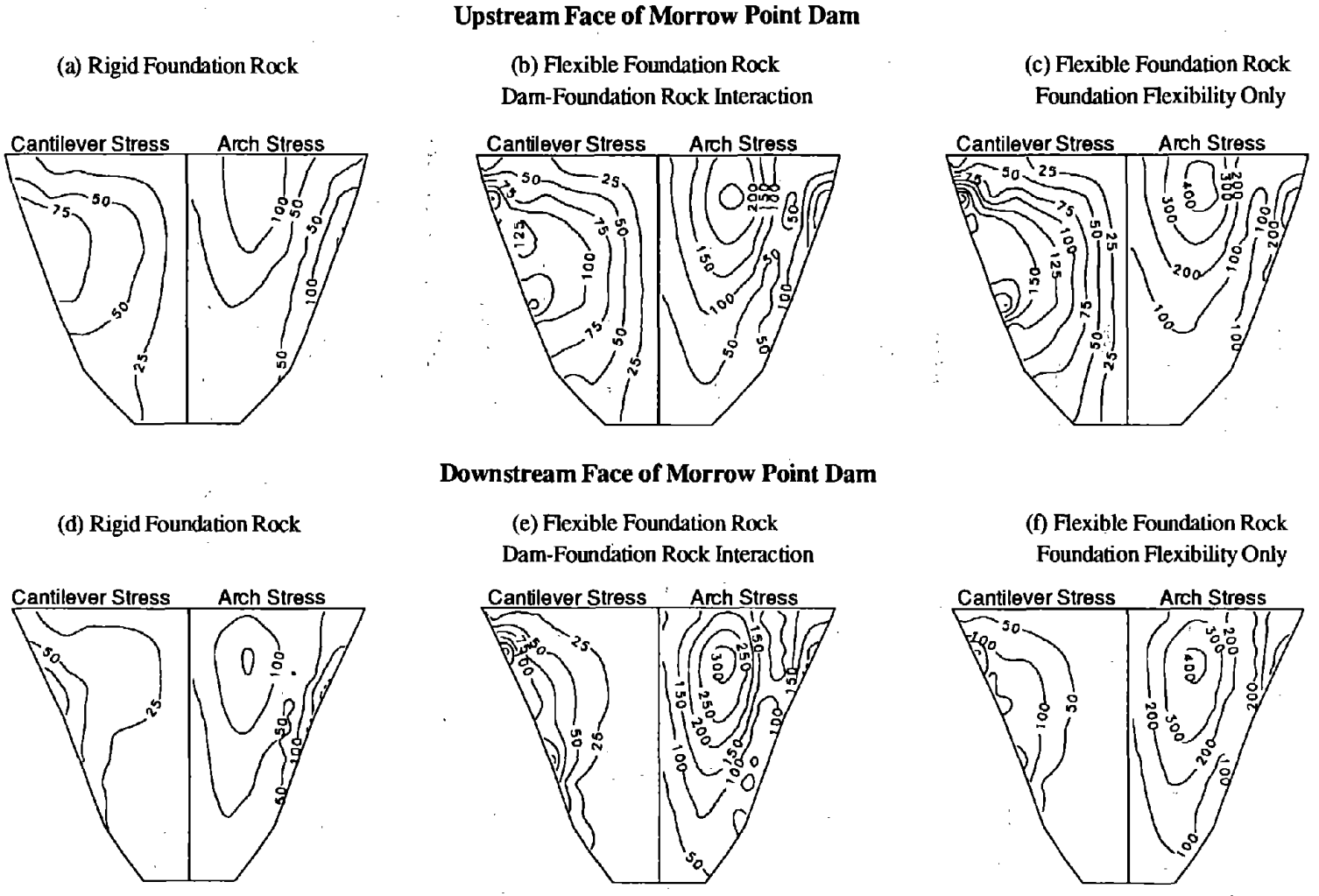

Figure 6.8 Envelope values of maximum tensile stress (in psi) on faces of Morrow Point Dam with empty reservoir, supported on rigid or flexible foundation rock with $E_f/E_s = 1/4$, due to cross-stream component, only, of Taft ground motion. Initial static stresses are excluded.

dam decrease; the latter happens because the material and radiation damping arising from interaction effects reduces the resonant amplitudes, especially at the higher resonant peaks (Section 5.3). As E_f/E_s decreases, the displacements increase in spite of the reduced values of S_a primarily because of the increase in the effective earthquake forces in individual vibration modes arising from modification in the mode shapes due to foundation flexibility. For example, as E_f/E_s decreases from ∞ to 1/4, the maximum crest displacement of the dam increases from 0.382 in. to 0.635 in. due to upstream ground motion; from 0.068 in. to 0.095 in. due to vertical ground motion; and from 0.368 in. to 0.726 in. due to cross-stream ground motion (Table 6.2). As a result of these trends dam-foundation rock interaction generally increases by a small amount the maximum principal stresses throughout the dam [compare part (b) to (a) and part (e) to (d) of Figures 6.3-6.8 and compare Cases 2-5 to Case 1 of Table 6.2]. For example, as E_f/E_s decreases from ∞ to 1/4, the maximum arch stress increases from 268 psi to 293 psi at the upstream face and from 244 psi to 301 psi at the downstream face due to upstream ground motion, although the maximum cantilever stress remains practically unchanged at both upstream and downstream faces [Cases 1 and 5 of Table 6.2(a)]. However, dam-foundation rock interaction does not significantly alter the general distribution of maximum tensile stresses on the dam faces [compare part (b) to (a) and part (e) to (d) of Figures 6.3-6.8]. Furthermore, the arch stresses are generally greater than the cantilever stresses over both faces of the dam, and the response to vertical ground motion is much smaller than the response to horizontal (upstream and cross-stream) ground motions, both phenomena seem little affected by dam-foundation rock interaction.

The small increase in the stress response of arch dams due to dam-foundation rock interaction is in contrast to gravity dams whose response is reduced significantly by interaction [12] because of the significant increase in damping resulting from interaction of the massive gravity dam with its foundation rock (Section 5.3).

6.5 Foundation Idealization

In this section we study how the earthquake response of the dam is affected if only the foundation flexibility is considered but its inertia and damping effects are ignored. The fundamental mode properties of the dam and the corresponding ordinates of the response spectrum for the three components of Taft ground motion considering (1) foundation flexibility only and (2) all effects of dam-foundation rock interaction are summarized in Table 6.3. The fundamental resonant period is essentially the same for both idealizations of the foundation rock but the effective damping ratio is larger if full effects of dam-foundation rock interaction are considered. For example, for E_f/E_s = 1/4, the fundamental resonant period of Morrow Point Dam is 0.311 sec and 0.332 sec for symmetric and antisymmetric modes of vibration, respectively, if only foundation rock flexibility effects are considered, and they are 0.315 sec and 0.332 sec if all dam-foundation rock interaction effects are considered (Case 5 of Table 6.3). However, for E_f/E_s = 1/4, ξ_1^x = 2.8%, ξ_1^y = 2.7%, and ξ_1^z = 3.3% if only foundation rock flexibility effects are considered; whereas ξ_1^x = 9.3%, ξ_1^y = 9.6%, and ξ_1^z = 6.3% if all dam-foundation rock interaction effects are considered (Case 5 of Table 6.3). Therefore, the spectral ordinates are always larger if only foundation rock flexibility is considered but other effects of dam-foundation rock interaction are ignored (Table 6.3). For example, for E_f/E_s = 1/4, $S_a(T_1^x,\xi_1^x)$ = 0.511g, $S_a(T_1^y,\xi_1^y)$ = 0.308g, and $S_a(T_1^z,\xi_1^z)$ = 0.572g if only foundation rock flexibility effects are considered are larger than $S_a(T_1^x,\xi_1^x)$ = 0.343g, $S_a(T_1^y,\xi_1^y)$ = 0.244g, and $S_a(T_1^z,\xi_1^z)$ = 0.417g if all dam-foundation rock interaction effects are considered (Case 5 of Table 6.3).

Consequently, the earthquake response of the dam is overestimated when only foundation flexibility is considered but damping — material and radiation — arising from dam-foundation rock interaction is excluded [see Table 6.4 and compare part (c) to (b) and part (f) to (e) of Figures 6.3-6.8]. For example, for E_f/E_s = 1/4, the maximum crest displacements are 0.921 in., 0.168 in., and 0.982 in. due to upstream, vertical and cross-stream components of Taft ground motion, respectively, if only foundation flexibility is considered; whereas they are 0.635 in., 0.095 in., and 0.726 in. if all

Table 6.3 Influence of Foundation Rock Idealization on Fundamental Resonant Periods of Vibration, Damping Ratios, and Taft Response Spectrum Ordinates for Morrow Point Dam with Empty Reservoir

Case	Foundation Rock		Fundamental Mode Properties								
			Upstream Ground Motion			Vertical Ground Motion			Cross-stream Ground Motion		
	E_f/E_s	Idealization*	Resonant Period T (sec)	Damping Ratio ξ_1^x (%)	$S_a(T,\xi_1^x)$ (g)	Resonant Period T (sec)	Damping Ratio ξ_1^y (%)	$S_a(T,\xi_1^y)$ (g)	Resonant Period T (sec)	Damping Ratio ξ_1^z (%)	$S_a(T,\xi_1^z)$ (g)
2	2	Flexibility	0.245	4.6	0.385	0.245	4.7	0.270	0.273	4.6	0.385
		Interaction	0.245	5.4	0.376	0.245	5.6	0.249	0.273	5.1	0.373
3	1	Flexibility	0.255	4.2	0.373	0.255	4.2	0.254	0.283	4.3	0.343
		Interaction	0.255	6.0	0.351	0.255	6.0	0.223	0.284	5.4	0.334
4	1/2	Flexibility	0.276	3.6	0.434	0.276	3.7	0.294	0.301	3.9	0.390
		Interaction	0.277	7.2	0.319	0.277	7.4	0.203	0.302	5.8	0.362
5	1/4	Flexibility	0.311	2.8	0.511	0.311	2.7	0.308	0.332	3.3	0.572
		Interaction	0.315	9.3	0.343	0.315	9.6	0.244	0.332	6.3	0.417

* "Flexibility" implies that only foundation flexibility effects are considered. "Interaction" indicates that dam-foundation rock interaction effects are included.

Table 6.4 Influence of Foundation Rock Idealization on Responses* of Morrow Point Dam with Empty Reservoir to Taft Ground Motion

Case	Foundation Rock		Maximum Radial Crest Displacement (inches)	Maximum Tensile Stress (psi)			
				Upstream Face		Downstream Face	
	E_f/E_s	Idealization†		Arch Stress	Cantilever Stress	Arch Stress	Cantilever Stress
(a) Response to Upstream (S69E Component of Taft) Ground Motion							
2	2	Flexibility	0.421	277	113	253	75
		Interaction	0.396	262	104	239	67
3	1	Flexibility	0.494	317	113	288	76
		Interaction	0.438	271	100	251	62
4	1/2	Flexibility	0.627	418	137	374	98
		Interaction	0.451	289	102	274	71
5	1/4	Flexibility	0.921	445	174	461	103
		Interaction	0.635	293	96	301	62
(b) Response to Vertical Component of Taft Ground Motion							
2	2	Flexibility	0.086	66	69	56	57
		Interaction	0.069	57	54	44	44
3	1	Flexibility	0.096	85	104	61	62
		Interaction	0.075	63	66	45	38
4	1/2	Flexibility	0.121	132	155	83	68
		Interaction	0.072	70	81	51	35
5	1/4	Flexibility	0.168	139	223	154	94
		Interaction	0.095	70	86	75	36
(c) Response to Cross-stream (S21W Component of Taft) Ground Motion							
2	2	Flexibility	0.478	178	114	192	79
		Interaction	0.453	169	107	181	77
3	1	Flexibility	0.487	199	108	195	80
		Interaction	0.438	173	96	185	76
4	1/2	Flexibility	0.624	249	144	266	114
		Interaction	0.544	184	113	231	96
5	1/4	Flexibility	0.982	438	226	443	207
		Interaction	0.726	260	157	316	157

* Effects of static loads are excluded.

† "Flexibility" implies that foundation flexibility effects are considered. "Interaction" indicates that dam-foundation rock interaction effects are included.

effects of dam-foundation rock interaction are considered (Table 6.4). Similarly, the maximum arch stresses are 461 psi, 154 psi, and 443 psi due to upstream, vertical and cross-stream Taft ground motions, respectively, if only foundation flexibility is considered; whereas they are only 301 psi, 75 psi, and 316 psi if all effects of dam-foundation rock interaction are considered (Table 6.4). Such overestimation of the response is especially significant for smaller values of E_f/E_s because larger radiation damping resulting from dam-foundation rock interaction is ignored (Table 6.5). For example, for E_f/E_s = 1/4, the maximum response to upstream, vertical and cross-stream ground motions is overestimated by 45%, 77% and 35%, respectively, for the crest displacement; 53%, 105% and 69% for the arch stress; and 81%, 161% and 44% for the cantilever stress (Table 6.5). The overestimation is especially large for the response to vertical ground motion. However, the distributions of maximum tensile stresses on the dam faces are similar for the two idealizations of the foundation rock [compare part (c) to (b) and (f) to (e) of Figures 6.3-6.8].

Based on the preceding results, it is clear that the standard procedure commonly used in engineering practice, which considers only the flexibility of the foundation rock but ignores other effects of dam-foundation rock interaction, significantly overestimates the earthquake response of arch dams. Therefore, dam-foundation rock effects are included in all subsequent results presented in this chapter.

6.6 Dam-Water-Foundation Rock Interaction Effects

6.6.1 Hydrodynamic Effects

As discussed in Section 5.5.1, hydrodynamic effects (the effects of dam-water interaction with non-absorptive reservoir boundary; α = 1) on the response of the dam to the harmonic ground motion in the upstream, vertical or cross-stream direction are qualitatively similar whether the effects of dam-foundation rock interaction are included or not. In particular, the percentage increase in the fundamental resonant period due to hydrodynamic effects is approximately the same, as demonstrated by comparing the periods for Cases 1 and 6 to those for Cases 3 and 10 of Table 6.1. The increase is

Table 6.5 Overestimation of Responses (in %) by Ignoring Foundation Inertia and Damping Effects

Case	E_f/E_s	Maximum Radial Crest Displacement	Maximum Tensile Stress			
			Upstream Face		Downstream Face	
			Arch Stress	Cantilever Stress	Arch Stress	Cantilever Stress
(a) Response to Upstream (S69E Component of Taft) Ground Motion						
2	2	6%	6%	9%	6%	12%
3	1	13%	17%	13%	15%	23%
4	1/2	39%	45%	34%	36%	38%
5	1/4	45%	52%	81%	53%	66%
(b) Response to Vertical Component of Taft Ground Motion						
2	2	25%	16%	28%	27%	30%
3	1	28%	35%	58%	36%	63%
4	1/2	68%	89%	91%	63%	94%
5	1/4	77%	99%	159%	105%	161%
(c) Response to Cross-stream (S21W Component of Taft) Ground Motion						
2	2	6%	5%	7%	6%	3%
3	1	11%	15%	13%	5%	5%
4	1/2	15%	35%	27%	15%	19%
5	1/4	35%	68%	44%	40%	32%

about 50% for the symmetric vibration mode and about 30% for the antisymmetric vibration mode, regardless of the foundation rock condition [see also Figure 5.12(a) at $H/H_s = 1$].

Hydrodynamic effects increase the displacement and stress responses of the dam on rigid foundation rock due to upstream ground motion [compare Case 1 to 6 of Table 6.6(a)]. The increase in the dam response is caused by the increase of the fundamental resonant peak in the frequency response function [Figure 5.7(a)] and by the increase in the pseudo-acceleration $S_a(T_1^x, \xi_1^x)$ from 0.433g to 0.661g because hydrodynamic effects lengthen the fundamental resonant period from 0.234 sec to 0.355 sec and decrease the effective damping ratio from 5% to 2.2% (Table 6.1). For example, the maximum crest displacement increases from 0.382 in. to 0.806 in.; the maximum arch stress increases from 268 psi to 686 psi at the upstream face and from 244 psi to 616 psi at the downstream face; and the maximum cantilever stress increases from 100 psi to 286 psi at the upstream face and from 65 psi to 218 psi at the downstream face [Cases 1 and 6 of Table 6.6(a)]. The lengthening of the fundamental resonant period can also be observed from the displacement histories [compare the responses to upstream ground motion in Figures 6.9(a) and 6.9(b)]. When dam-foundation rock interaction is considered, the hydrodynamic effects are smaller [compare the change from Case 3 to 10 in Table 6.7(a) with the change from Case 1 to 6 in Table 6.6(a)] because of the material and radiation damping effects arising from the interaction (Section 5.5.1). Hydrodynamic effects change little the distribution pattern of the arch stresses; however, these effects increase the cantilever stresses at the base of the dam along the abutment, with these areas becoming the most-stressed area instead of the upper, central portion of the dam, regardless of the foundation rock condition [compare part (a) to (b) of Figures 6.10-6.11 and 6.17-6.18]. The arch stresses are generally much larger than the cantilever stresses over both faces of the dam, an observation that is unaffected by the hydrodynamic effects [Cases 1 and 6 of Table 6.6(a) and Cases 3 and 10 of Table 6.7(a)].

Similar to the case of upstream ground motion, hydrodynamic effects increase the displacement and stress responses of the dam on rigid foundation rock due to vertical ground motion [compare

Table 6.6 Summary of Responses* of Morrow Point Dam on Rigid Foundation Rock to Taft Ground Motion

Case	Water	α	Maximum Radial Crest Displacement (inches)	Maximum Tensile Stress (psi)			
				Upstream Face		Downstream Face	
				Arch Stress	Cantilever Stress	Arch Stress	Cantilever Stress
(a) Response to Upstream (S69E Component of Taft) Ground Motion							
1	None	-	0.382	268	100	244	65
6	Full	1.0	0.806	686	286	616	218
7	Full	0.95	0.674	574	231	513	174
8	Full	0.5	0.622	487	166	422	122
9	Full	0	0.622	482	147	411	111
(b) Response to Vertical Component of Taft Ground Motion							
1	None	-	0.068	55	48	43	41
6	Full	1.0	1.704	1348	524	1214	328
7	Full	0.95	1.243	998	398	898	231
8	Full	0.5	0.270	216	115	183	54
9	Full	0	0.107	89	55	69	39
(c) Response to Cross-stream (S21W Component of Taft) Ground Motion							
1	None	-	0.368	153	100	209	90
6	Full	1.0	0.359	198	121	173	88
7	Full	0.95	0.331	177	102	177	84
8	Full	0.5	0.313	160	72	183	83
9	Full	0	0.365	172	93	216	99
(d) Response to Upstream, Vertical, and Cross-stream Components, Simultaneously, of Taft Ground Motion							
1	None	-	0.486	336	118	307	137
6	Full	1.0	2.202	1784	734	1591	550
7	Full	0.95	1.546	1223	531	1093	403
8	Full	0.5	0.624	490	182	444	169
9	Full	0	0.678	491	166	441	168

* Effects of static loads are excluded.

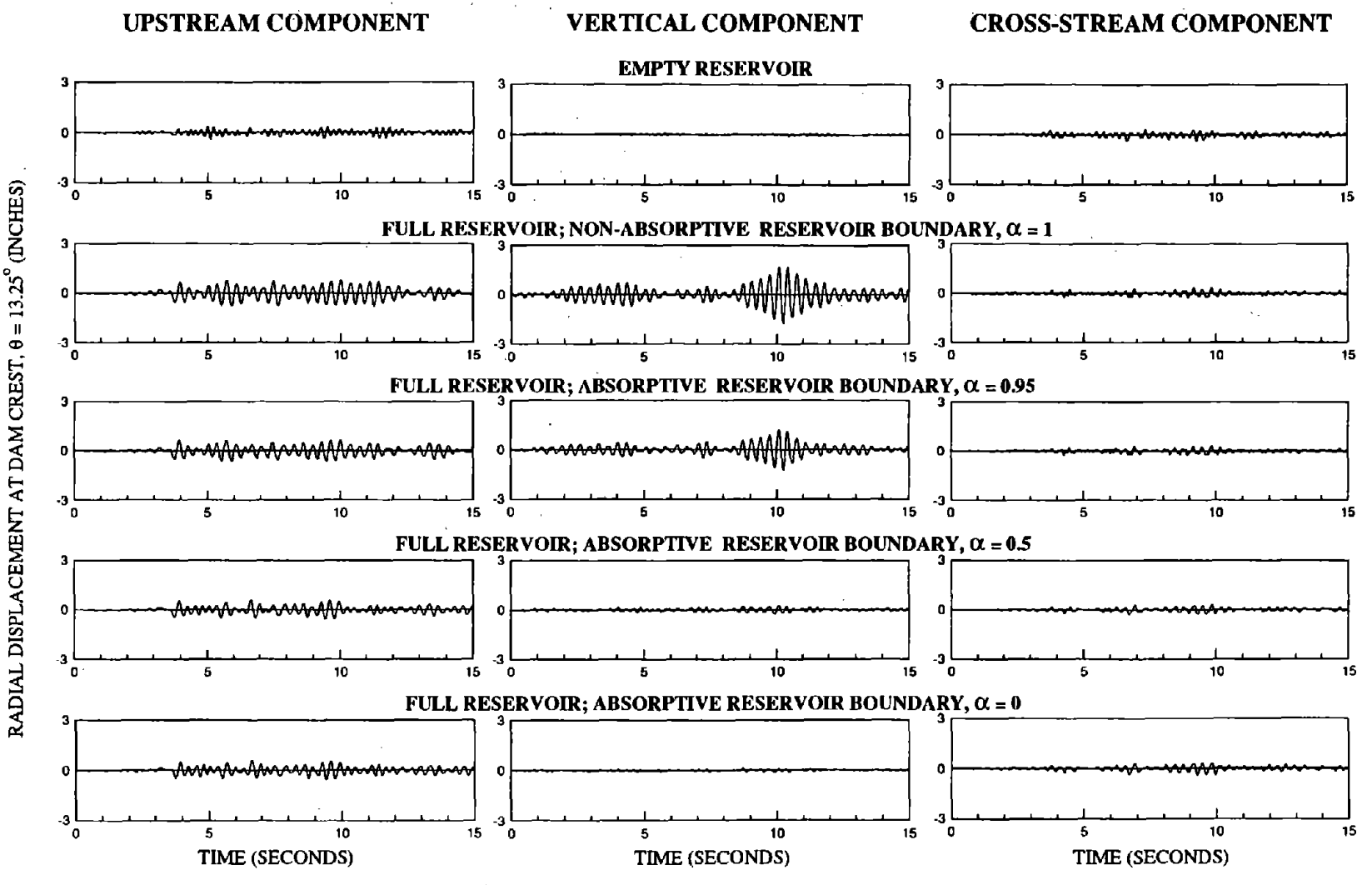

Figure 6.9 Displacement response of Morrow Point Dam on rigid foundation rock due to upstream, vertical and cross-stream components, separately, of Taft ground motion.

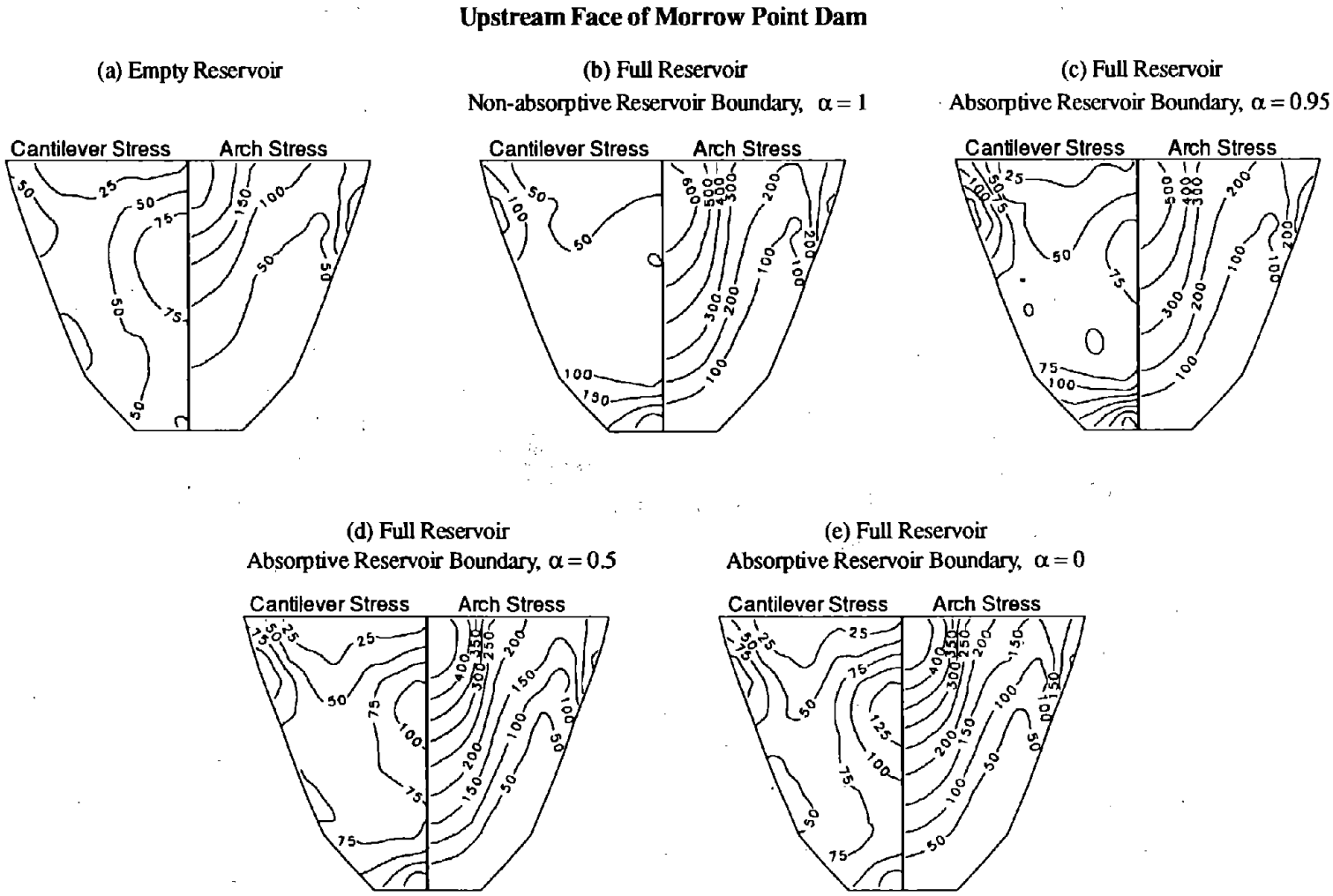

Figure 6.10 Envelope values of maximum tensile stress (in psi) on the upstream face of Morrow Point Dam with empty or full reservoir, supported on rigid foundation rock, due to upstream component, only, of Taft ground motion. Initial static stresses are excluded.

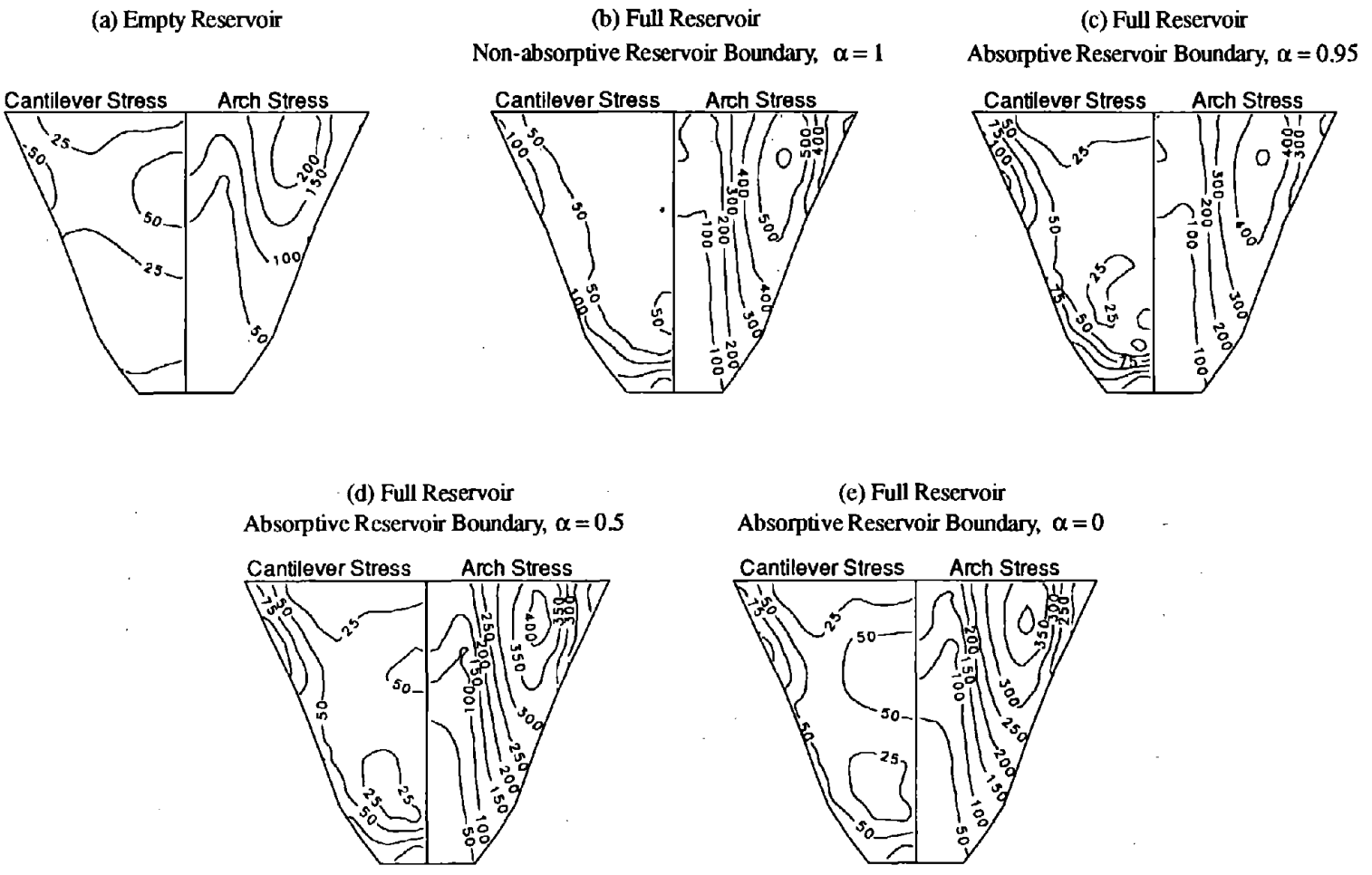

Figure 6.11 Envelope values of maximum tensile stress (in psi) on the downstream face of Morrow Point Dam with empty or full reservoir, supported on rigid foundation rock, due to upstream component, only, of Taft ground motion. Initial static stresses are excluded.

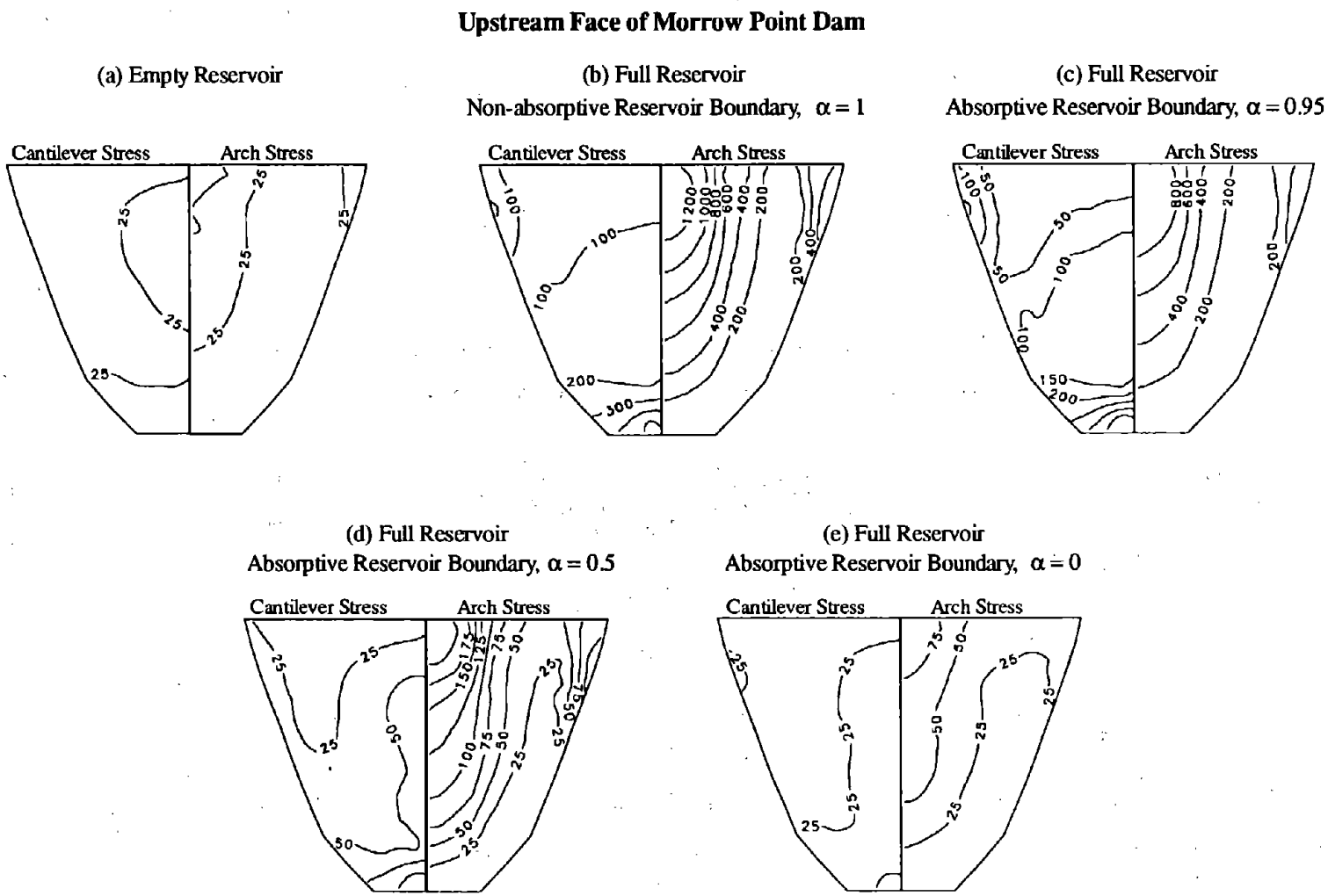

Figure 6.12 Envelope values of maximum tensile stress (in psi) on the upstream face of Morrow Point Dam with empty or full reservoir, supported on rigid foundation rock, due to vertical component, only, of Taft ground motion. Initial static stresses are excluded.

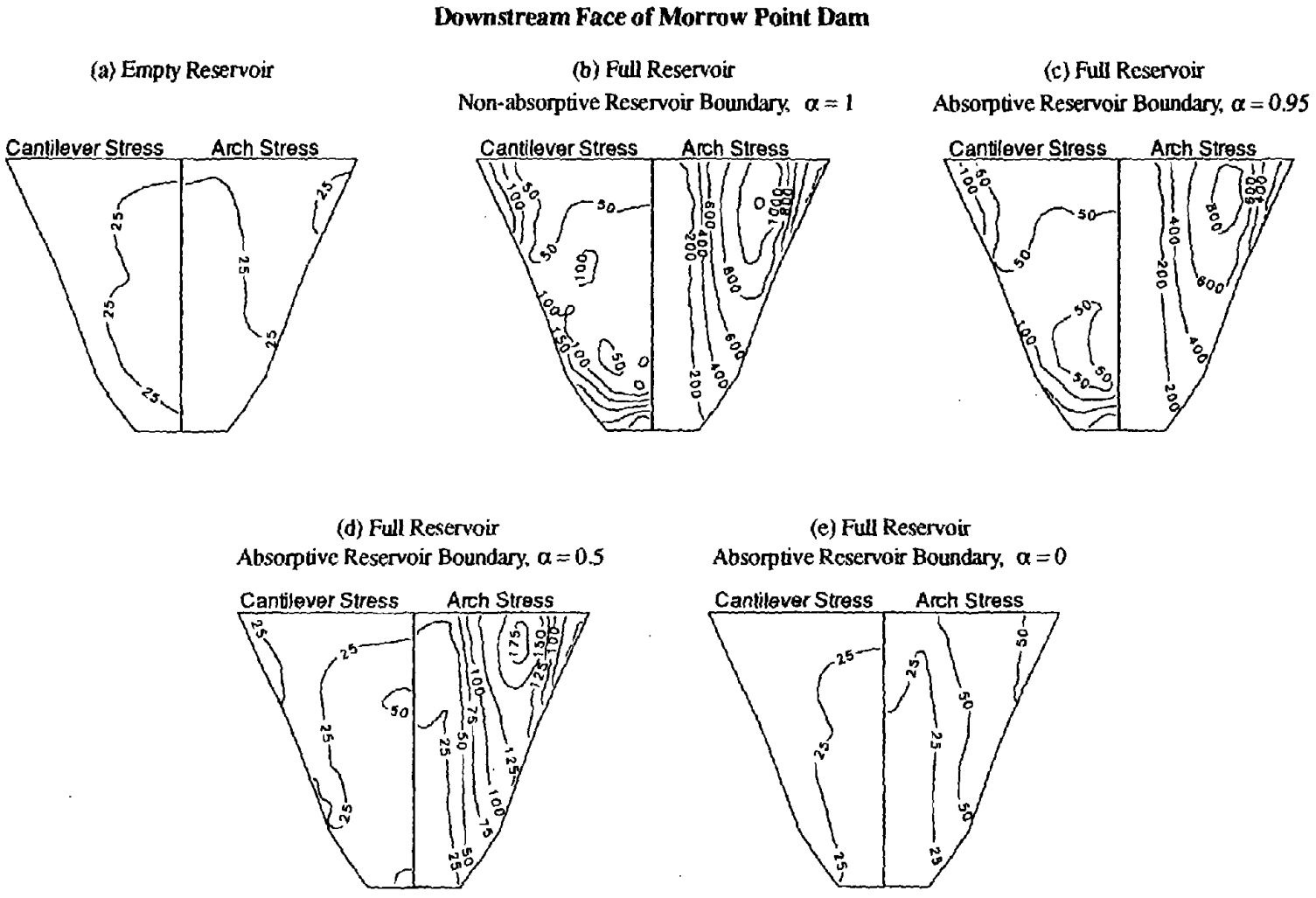

Figure 6.13 Envelope values of maximum tensile stress (in psi) on the downstream face of Morrow Point Dam with empty or full reservoir, supported on rigid foundation rock, due to vertical component, only, of Taft ground motion. Initial static stresses are

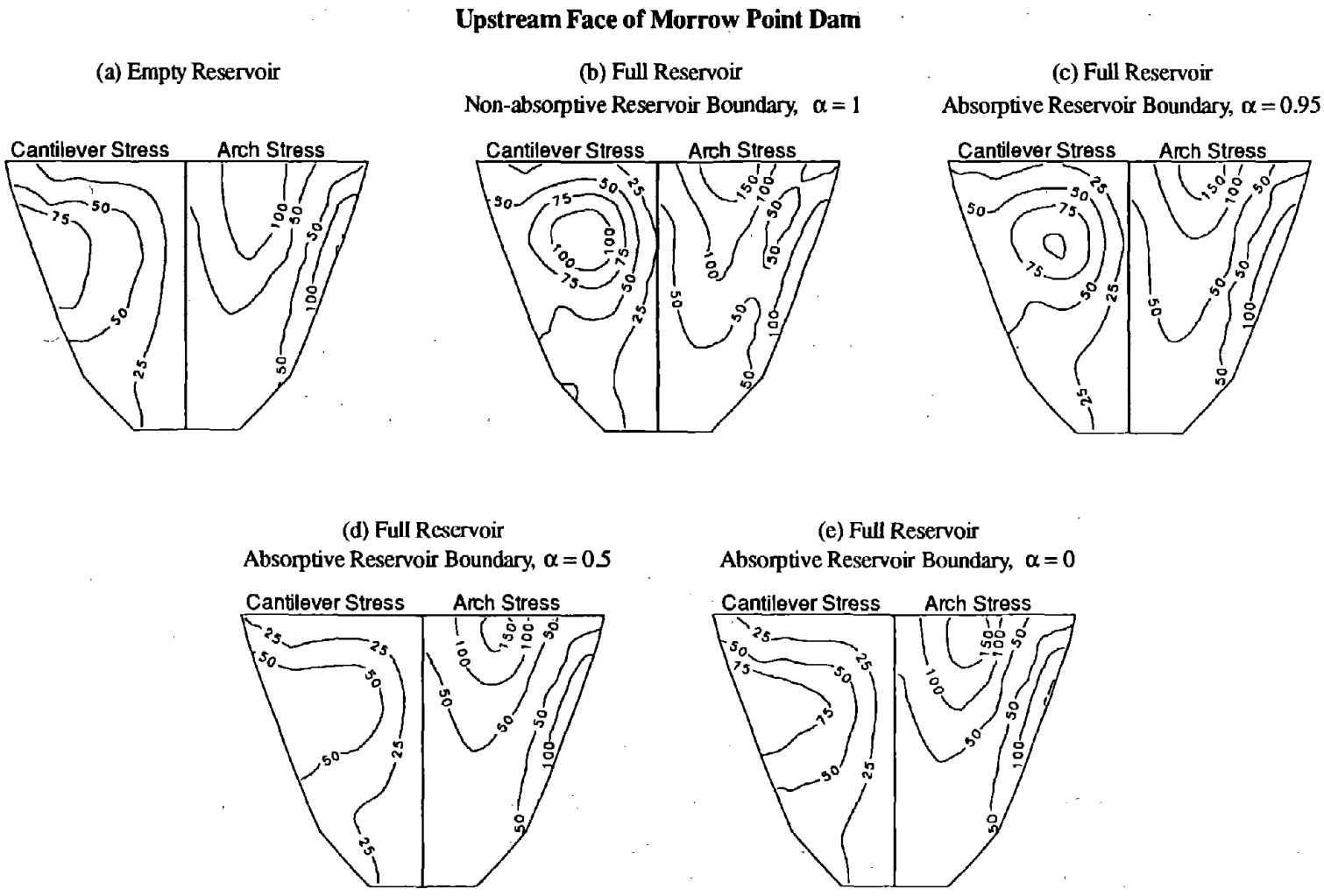

Figure 6.14 Envelope values of maximum tensile stress (in psi) on the upstream face of Morrow Point Dam with empty or full reservoir, supported on rigid foundation rock, due to cross-stream component, only, of Taft ground motion. Initial static stresses are excluded.

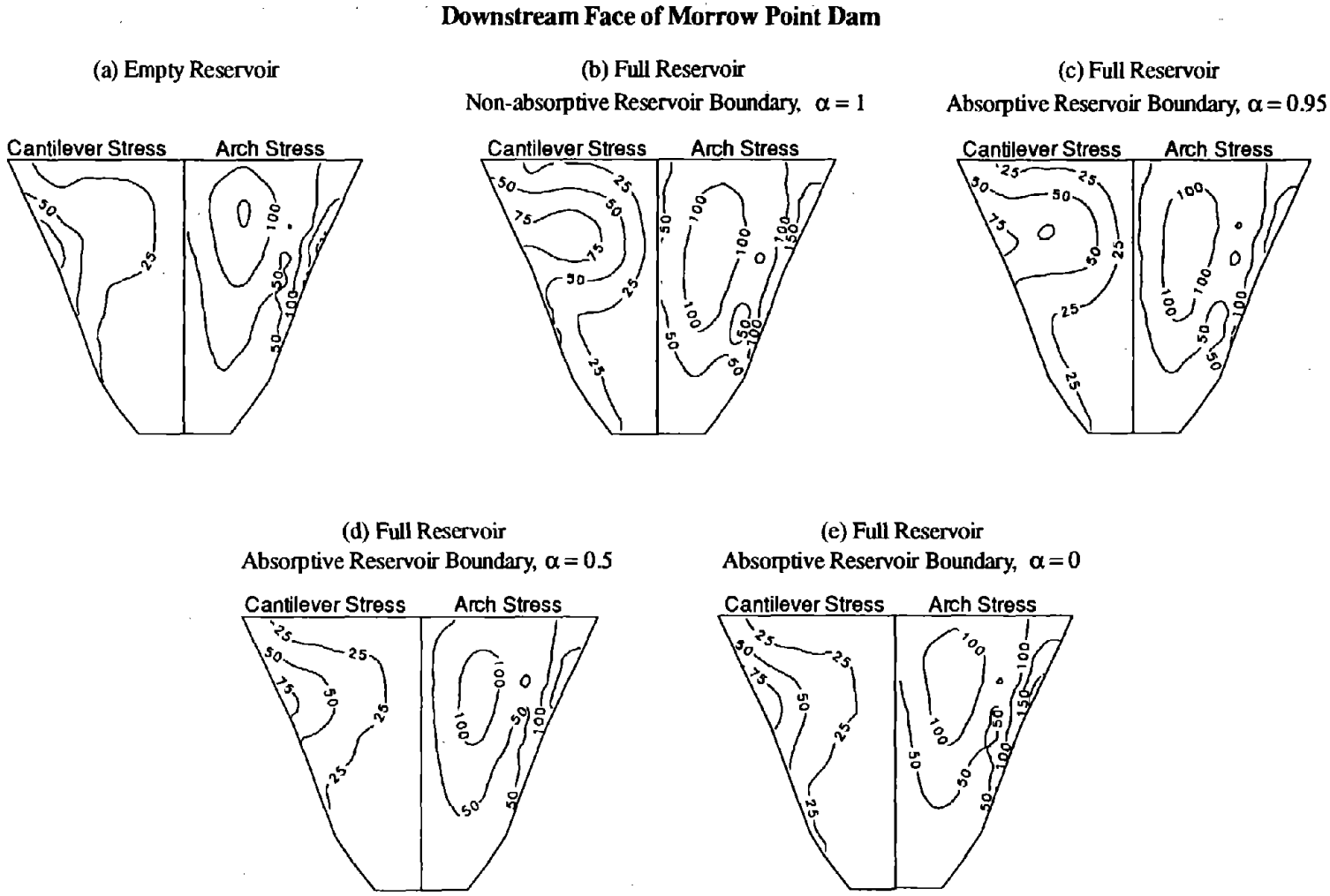

Figure 6.15 Envelope values of maximum tensile stress (in psi) on the downstream face of Morrow Point Dam with empty or full reservoir, supported on rigid foundation rock, due to cross-stream component, only, of Taft ground motion. Initial static stresses are excluded.

Case 1 to 6 of Table 6.6(b)]. However, the increase in the dam response is caused less by the increase in the pseudo-acceleration $S_a(T_1^y,\xi_1^y)$ from 0.299g to 0.366g — due to the lengthening of the vibration period and the reduction of the effective damping ratio from 5% to 4.4% (Table 6.1) — but more by the greatly amplified fundamental resonant peak and unbounded peaks at ω_n^s in the frequency response function due to hydrodynamic effects [Figure 5.8(a)]. Consequently, the increase in the dam response to vertical ground motion is much larger than that due to upstream ground motion. For example, the maximum crest displacement of the dam due to vertical ground motion increases from 0.068 in. to 1.704 in.; the maximum arch stress increases from 55 psi to 1348 psi at the upstream face and from 43 psi to 1214 psi at the downstream face; and the maximum cantilever stress increases from 48 psi to 524 psi at the upstream face and from 41 psi to 328 psi at the downstream face [Cases 1 and 6 of Table 6.6(b)]. Dam-foundation rock interaction moderately reduces the hydrodynamic effects on the dam response [compare the change from Case 3 to 10 in Table 6.7(b) with the change from Case 1 to 6 in Table 6.6(b)] because foundation damping arising from the interaction reduces the fundamental resonant response without eliminating the unbounded peaks at ω_n^s (Section 5.5.1). Similar to the case of upstream ground motion, hydrodynamic effects change little the distribution pattern of the arch stresses due to vertical ground motion, except greatly increasing the cantilever stresses at the base of the dam along the abutment, with these areas becoming the most-stressed area instead of the upper, central portion of the dam, regardless of the foundation rock condition [compare part (a) to (b) of Figures 6.12-6.13 and 6.19-6.20]. The arch stresses over both faces of the dam, which are about the same as the cantilever stresses when the reservoir is empty [Case 1 of Table 6.6(b) and Case 3 of Table 6.7(b)], become much larger than the cantilever stresses when the reservoir is full [Case 6 of Table 6.6(b) and Case 10 of Table 6.7(b)].

On the contrary, the response of the dam on rigid foundation rock due to cross-stream ground motion is influenced by hydrodynamic effects to a much less degree than is the response due to the upstream and vertical components of ground motion [compare Cases 1 and 6 of Table 6.6(c) to those of Table 6.6(a)-(b)], even though the pseudo-acceleration $S_a(T_1^z,\xi_1^z)$ increases from 0.370g to 0.526g

Table 6.7 Summary of Responses* of Morrow Point Dam, Considering Dam-Foundation Rock Interaction, to Taft Ground Motion; $E_f/E_s = 1$

Case	Water	α	Maximum Radial Crest Displacement (inches)	Maximum Tensile Stress (psi)			
				Upstream Face		Downstream Face	
				Arch Stress	Cantilever Stress	Arch Stress	Cantilever Stress
(a) Response to Upstream (S69E Component of Taft) Ground Motion							
3	None	-	0.451	271	100	251	62
10	Full	1.0	0.835	589	212	556	124
11	Full	0.95	0.802	566	203	533	115
12	Full	0.5	0.703	497	150	457	111
13	Full	0	0.708	510	134	454	113
(b) Response to Vertical Component of Taft Ground Motion							
3	None	-	0.072	63	66	45	38
10	Full	1.0	1.559	1082	292	979	148
11	Full	0.95	1.201	835	224	753	114
12	Full	0.5	0.414	268	107	230	63
13	Full	0	0.194	118	89	92	53
(c) Response to Cross-stream (S21W Component of Taft) Ground Motion							
3	None	-	0.544	173	96	185	76
10	Full	1.0	0.342	187	92	213	80
11	Full	0.95	0.347	189	88	205	79
12	Full	0.5	0.423	218	80	212	79
13	Full	0	0.537	274	96	274	104
(d) Response to Upstream, Vertical, and Cross-stream Components, Simultaneously, of Taft Ground Motion							
3	None	-	0.658	313	125	292	128
10	Full	1.0	1.605	1261	386	1115	250
11	Full	0.95	1.285	973	322	898	214
12	Full	0.5	0.682	540	187	474	149
13	Full	0	0.708	565	190	464	168

* Effects of static loads are excluded.

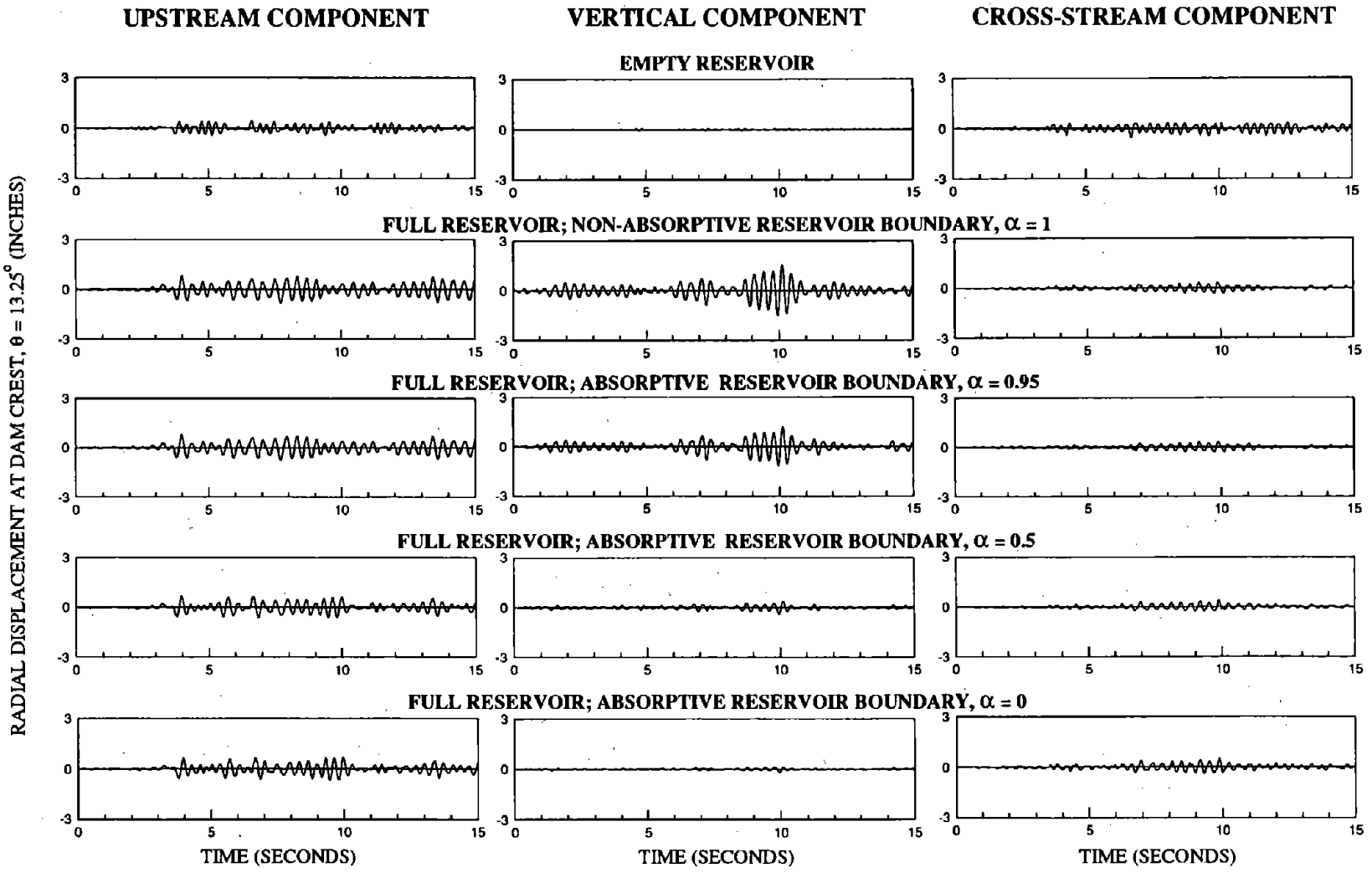

Figure 6.16 Displacement response of Morrow Point Dam on flexible foundation rock with $E_f / E_s = 1$, considering dam-foundation rock interaction effects , due to upstream, vertical, and cross-stream components, separately, of Taft ground motion.

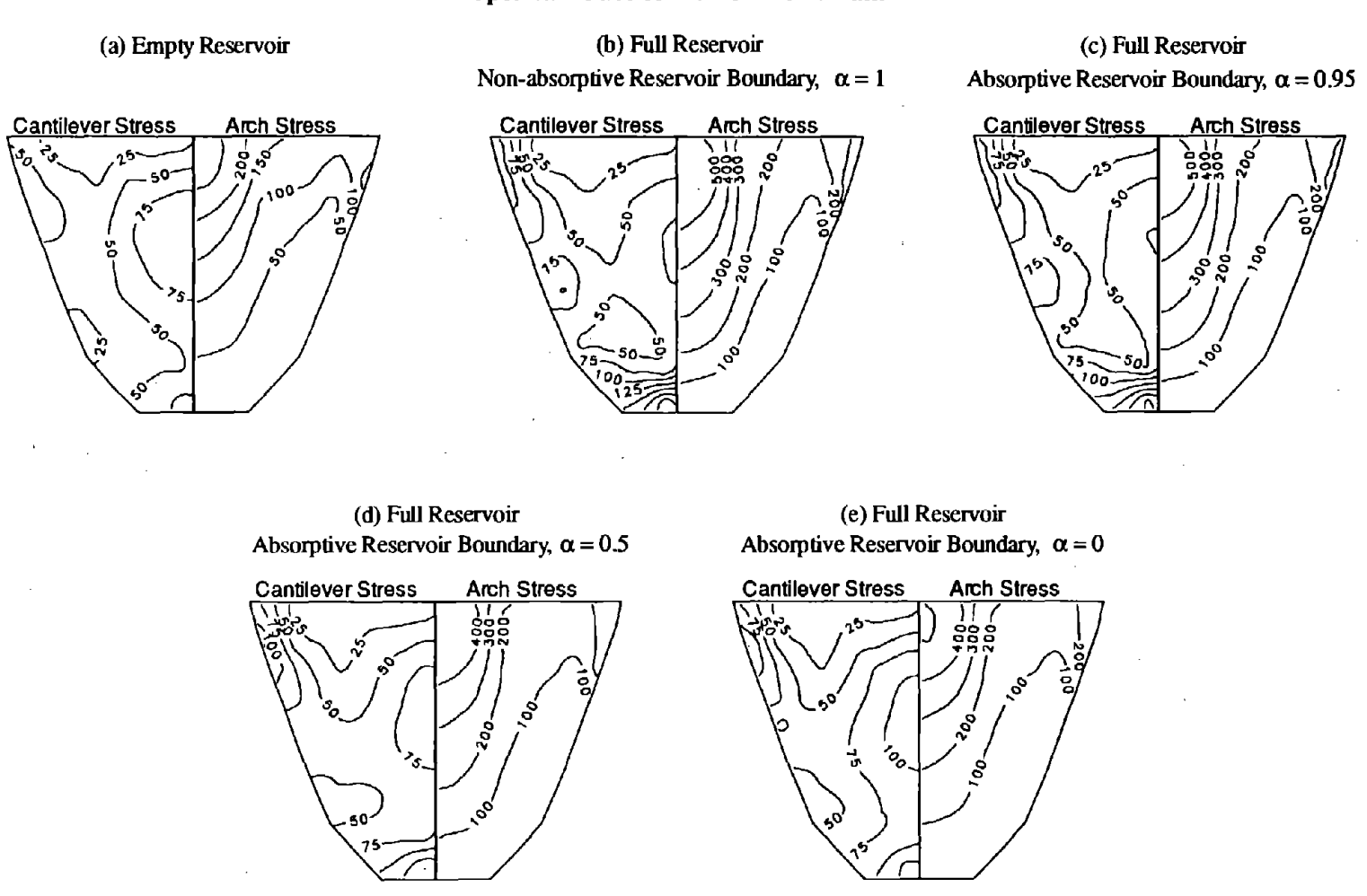

Figure 6.17 Envelope values of maximum tensile stress (in psi) on the upstream face of Morrow Point Dam with empty or full reservoir, supported on flexible foundation rock with $E_f/E_s = 1$, due to upstream component, only, of Taft ground motion. Initial static stresses are excluded..

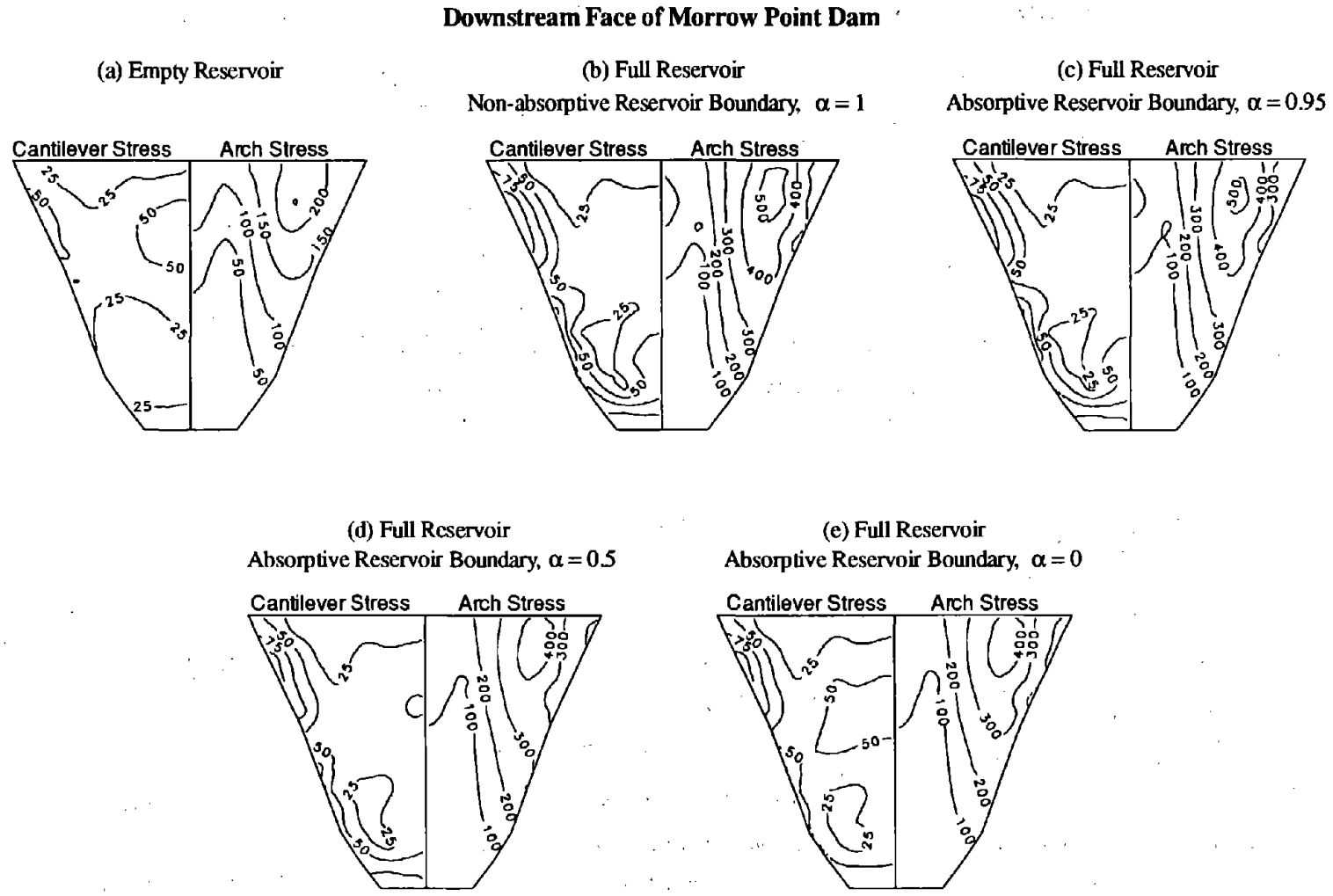

Figure 6.18 Envelope values of maximum tensile stress (in psi) on the downstream face of Morrow Point Dam with empty or full reservoir, supported on flexible foundation rock with $E_f/E_s = 1$, due to upstream component, only, of Taft ground motion. Initial static stresses are excluded..

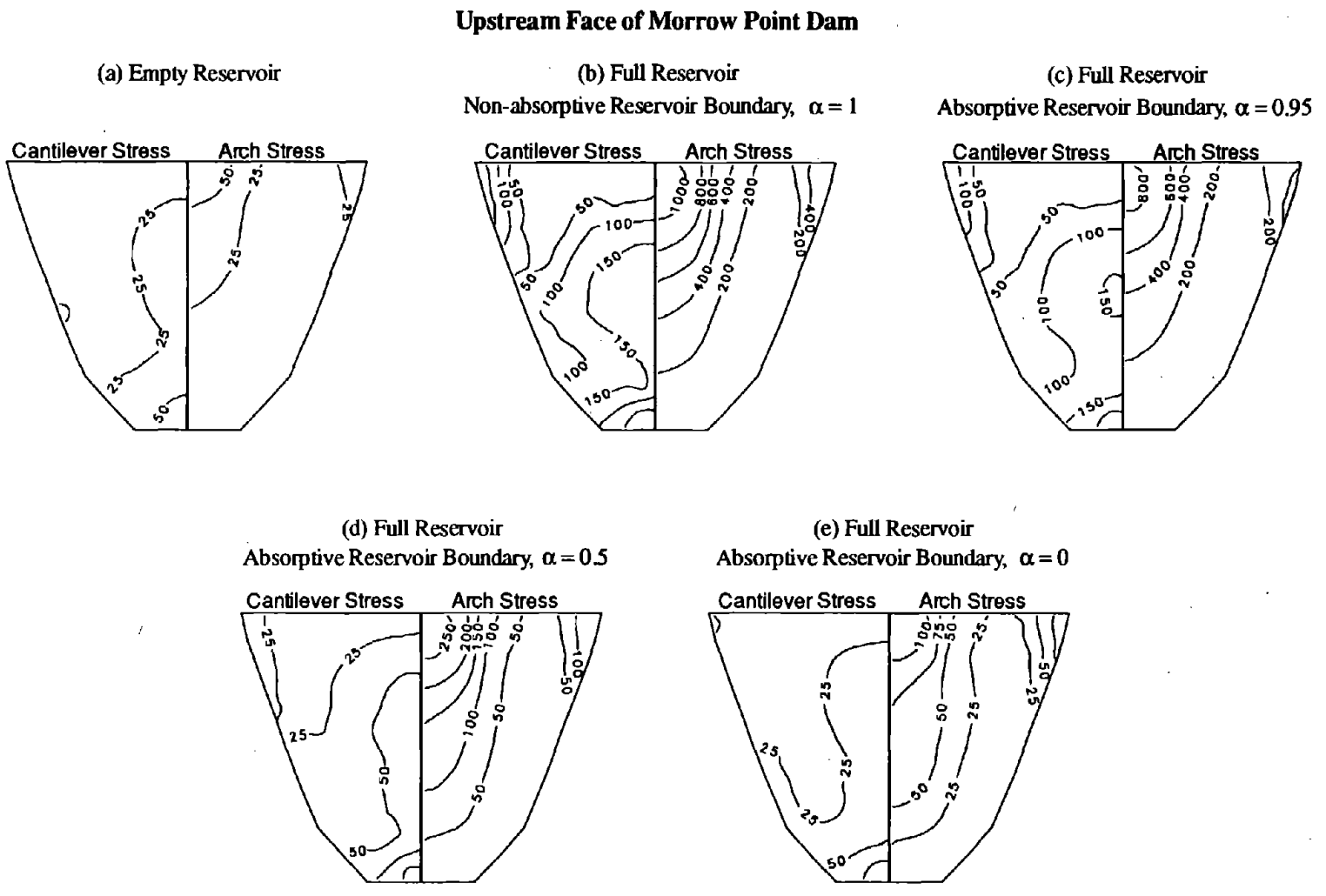

Figure 6.19 Envelope values of maximum tensile stress (in psi) on the upstream face of Morrow Point Dam with empty or full reservoir, supported on flexible foundation rock with $E_f/E_s = 1$, due to vertical component, only, of Taft ground motion. Initial static stresses are excluded..

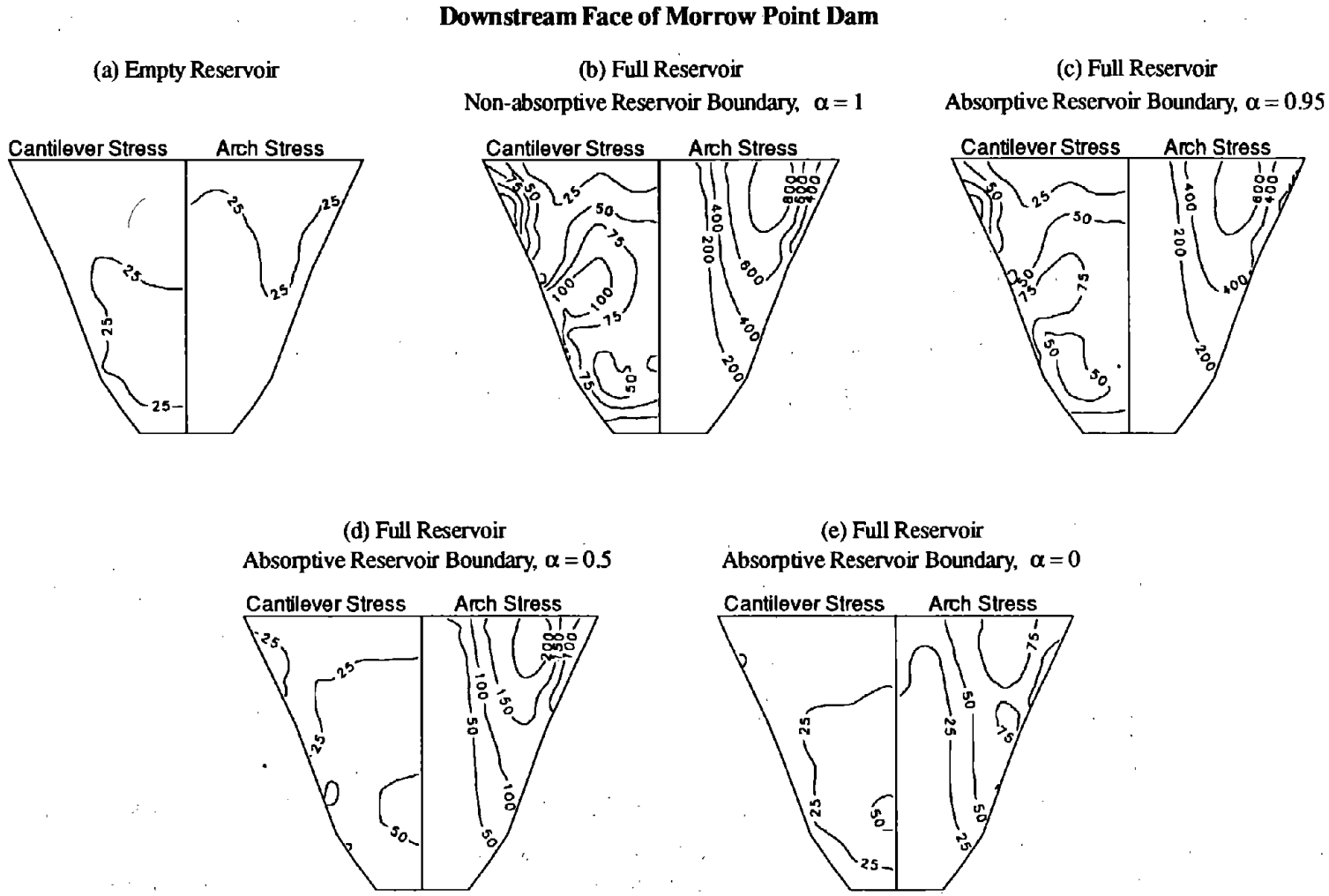

Figure 6.20 Envelope values of maximum tensile stress (in psi) on the downstream face of Morrow Point Dam with empty or full reservoir, supported on flexible foundation rock with $E_f/E_s = 1$, due to vertical component, only, of Taft ground motion. Initial static stresses are excluded..

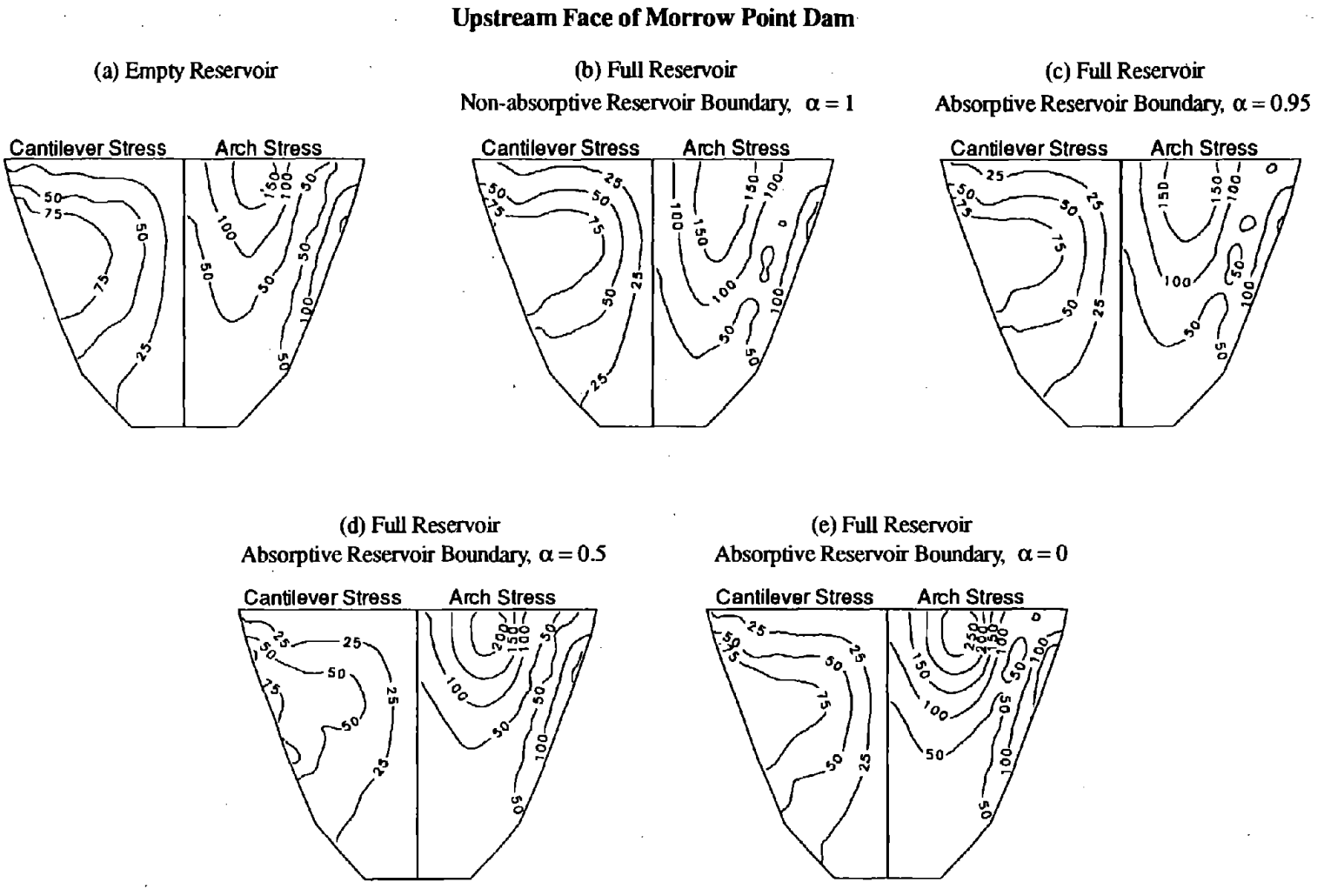

Figure 6.21 Envelope values of maximum tensile stress (in psi) on the upstream face of Morrow Point Dam with empty or full reservoir, supported on flexible foundation rock with $E_f/E_s = 1$, due to cross-stream component, only, of Taft ground motion. Initial static stresses are excluded..

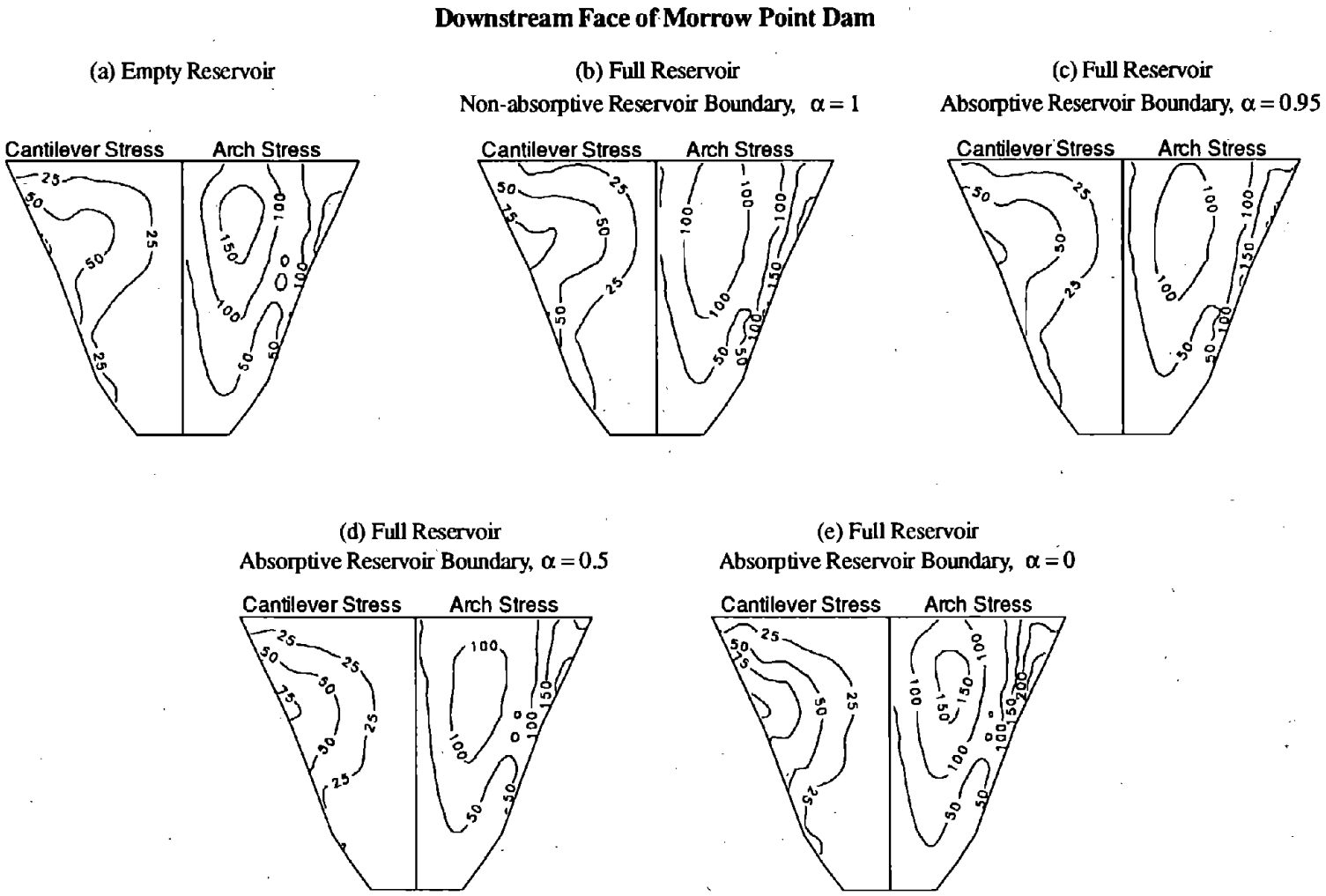

Figure 6.22 Envelope values of maximum tensile stress (in psi) on the downstream face of Morrow Point Dam with empty or full reservoir, supported on flexible foundation rock with $E_f/E_s = 1$, due to cross-stream component, only, of Taft ground motion. Initial static stresses are excluded..

due to the lengthening of the fundamental resonant period from 0.263 sec to 0.340 sec and the small decrease in the effective damping ratio from 5% to 4.9% (Table 6.1). For example, the crest displacement of the dam decreases slightly from 0.368 in. to 0.359 in.; the change in stress is also small: the arch stress increases from 153 psi to 198 psi at the upstream face, but decreases from 209 psi to 173 psi at the downstream face; the cantilever stress increases from 100 psi to 121 psi at the upstream face, but decreases from 90 psi to 88 psi at the downstream face [Cases 1 and 6 of Table 6.6(c)]. If dam-foundation rock interaction effects are included, the displacements decrease by a greater degree (from 0.544 in. to 0.342 in.) but the stresses change very little [Cases 3 and 10 of Table 6.7(c)]. The displacements decrease mainly because the fundamental resonant peak in the frequency response function is reduced since the "added" hydrodynamic force is of opposite-phase compared to the effective earthquake force associated with the mass of the dam [Figure 5.9(a)]. The added hydrodynamic force is unbounded at the natural frequencies ω_n^{ia} of the infinite water channel (Figure 3.2), causing unbounded response peaks at these frequencies which remain unbounded when dam-foundation rock interaction effects are included [Figure 5.9(a)]. Because of the large decrease in the fundamental resonant peak and of the unbounded peaks at ω_n^{ia}, both due to hydrodynamic effects, the contribution of higher modes to the earthquake response greatly increases; this is evident from observing the displacement-time histories [compare the cross-stream responses in parts (a) and (b) of Figures 6.9 and 6.16] from the fact that the displacement decreases because of hydrodynamic effects but the stresses increase [Tables 6.6(c) and 6.7(c)]. Hydrodynamic effects do not alter much the distribution pattern of the maximum tensile arch and cantilever stresses of the dam due to cross-stream ground motion. Similar to the response to upstream ground motion, the arch stresses due to cross-stream ground motion are generally much larger than the cantilever stresses over both faces of the dam, irrespective of the foundation rock condition [Cases 1 and 6 of Table 6.6(c) and Cases 3 and 10 of Table 6.7(c)].

These earthquake response results are consistent generally but not always with the conclusion of Chapter 5 based on frequency response functions that dam-foundation rock interaction does not

have significant influence on the hydrodynamic effects in the dam response. However, when the excitation is arbitrary ground motion, there are significant differences, as noted in this section, because of the complexity of the earthquake excitation and response [compare Cases 1 and 6 of Table 6.6 to Cases 3 and 10 of Table 6.7, and compare parts (a) and (b) of Figures 6.9-6.15, to parts (a) and (b) of Figures 6.16-6.22].

Hydrodynamic effects are more significant in the earthquake response of arch dams than that of gravity dams [12], regardless of the foundation rock condition. For example, if the foundation rock is rigid, hydrodynamic effects increase the maximum crest displacement of the arch dam by 110% (from 0.382 in. to 0.806 in.) due to upstream ground motion and by 2406% (from 0.068 in. to 1.704 in.) due to vertical ground motion (Table 6.6); whereas the displacement of a gravity dam is increased only by 37% due to upstream ground motion and 525% due to vertical ground motion [12]. If the foundation rock is flexible with $E_f/E_s = 1$, hydrodynamic effects increase the maximum crest displacement of the arch dam by 85% (from 0.451 in. to 0.835 in.) due to upstream ground motion and by 2065% (from 0.072 in. to 1.559 in.) due to vertical ground motion (Table 6.7); whereas the displacement of a gravity dam is increased only by 69% due to upstream ground motion and 500% due to vertical ground motion [12]. Hydrodynamic effects are more significant in the response of arch dams because the added hydrodynamic mass, damping and force have more influence on the vibration properties of a slender arch dam than on a massive gravity dam.

6.6.2 Reservoir Boundary Absorption Effects

The main effect of reservoir boundary absorption is to reduce the larger displacement peaks due to upstream ground motion without significantly altering the frequency content of the response [upstream ground motion responses in parts (b)-(e) of Figures 6.9 and 6.16]. The response of the dam decreases as the reservoir boundary becomes more absorptive [Tables 6.6(a) and 6.7(a)]. The only exception is when α decreases from 0.5 to 0 and dam-foundation rock interaction effects are included [compare Case 12 to 13 of Table 6.7(a)]. This is because the added damping decreases, contrary to

intuition, with increasing reservoir boundary absorption at the fundamental resonant frequency due to the merging of double peaks into a single peak (Section 5.5.1), resulting in a decrease in the effective damping ratio and a corresponding increase in $S_a(T_1^x,\xi_1^x)$ (Table 6.1), and thus the slight increase in some of the responses. However, reservoir boundary absorption has less influence on the dam response when dam-foundation rock interaction effects are included [compare Table 6.7(a) to 6.6(a)]. The relatively large reduction of the displacement and stress response as α decreases from 1 to 0.95 but smaller change in response as α decreases from 0.95 to 0 [Table 6.6(a)] indicates that the initial absorptiveness of the reservoir boundary materials is most effective in reducing the response of the dam to upstream ground motion if the foundation rock is rigid. However, reservoir boundary absorption is less effective if the foundation rock is flexible and dam-foundation rock interaction effects are included [compare the change from Case 10 to 11 of Table 6.7(a) to the change from Case 6 to 7 of Table 6.6(a)]. Reservoir boundary absorption does not alter much the general pattern of the maximum stresses, particularly the pattern of maximum arch stresses [parts (b)-(e) of Figures 6.10-6.11 and 6.17-6.18]. As the reservoir boundary becomes absorptive, the distribution pattern and the magnitude of the maximum cantilever stresses approach those of the dam with empty reservoir [compare, for example, part (a) to (e) in each of Figures 6.10-6.11 and 6.17-6.18], indicating that reservoir boundary absorption not only reduces the maximum stresses over both faces of the dam but also tends to eliminate the redistribution of cantilever stresses due to hydrodynamic effects mentioned in Section 6.6.1.

Reservoir boundary absorption has significant influence on reducing the response of the dam to vertical ground motion because it greatly reduces the fundamental resonant peak in the dam response, and eliminates the unbounded peaks in the dam response, at excitation frequencies equal to the natural vibration frequencies ω_n^{is} of the infinite water channel [Figures 5.10(b) and 5.11(b)]. Contrary to the case of upstream ground motion, increasing absorptiveness of the reservoir boundary is always effective in further reducing the response [compare part (b) to (a) of Tables 6.6 and 6.7]. This is because, although the effective damping ratio does not increase monotonically and the pseudo-

acceleration $S_a(T_1^y,\xi_1^y)$ does not decrease monotonically as α decreases (Table 6.1), the added hydrodynamic force and the fundamental resonant response of the dam continue to decrease due to increasing reservoir boundary absorption as α decreases [Figures 5.10(b) and 5.11(b)]. The above-mentioned reservoir boundary absorption effects on the dam response are qualitatively similar irrespective of the foundation rock condition. However, reservoir boundary absorption is less effective in reducing the response when the foundation rock is flexible [compare Cases 10-13 of Table 6.7(b) to Cases 6-9 of Table 6.6(b)] due to the existence of material and radiation damping resulting from dam-foundation rock interaction (Section 5.5.1). Similar to the case of upstream ground motion, reservoir boundary absorption does not substantially alter the frequency content of the displacement-time histories or the general distribution pattern of the maximum stresses, whether dam-foundation rock interaction effects are included or not [vertical ground motion responses in part (b)-(e) of Figures 6.9 and 6.16; and parts (b)-(e) of Figures 6.12-6.13 and 6.19-6.20]. It also tends to eliminate the redistribution of cantilever stresses caused by the hydrodynamic effects [compare parts (a) and (e) of Figures 6.12-6.13 and 6.19-6.20].

Reservoir boundary absorption generally has less influence on the response of the dam to cross-stream ground motion than to upstream ground motion, whether the foundation rock is rigid [Tables 6.6(c) and 6.6(a)] or flexible [Tables 6.7(c) and 6.7(a)]. If the dam is excited by cross-stream ground motion, the fundamental resonant response is essentially unaffected by reservoir boundary absorption and the higher modes that are most affected have smaller contribution to the dam response [Figures 5.10(c) and 5.11(c)]. As α decreases from 1.0 to 0, the pseudo-acceleration $S_a(T_1^z,\xi_1^z)$ decreases monotonically, irrespective of the foundation rock condition (Table 6.1). However, reservoir boundary absorption affects the dam response differently when dam-foundation rock interaction effects are included: the response increases as α decreases from 1.0 to 0, contrary to the case of rigid foundation rock in which the response decreases as α decreases from 1.0 to 0.5 but increases as α decreases from 0.5 to 0 [compare Table 6.7(c) to Table 6.6(c)]. The response increases partly because the magnitude of the fundamental resonant response increases as α decreases from 0.5 to 0,

and partly because as α decreases from 1 to 0, the second resonant peak decreases if the foundation rock is rigid [Figure 5.10(c)] but increases if the foundation rock is flexible [Figure 5.11(c)]. Furthermore, dam-foundation rock interaction greatly reduces the frequency response at frequencies beyond the second resonant frequency, making the fundamental and second resonant responses more significant [compare Figure 5.11(c) to Figure 5.10(c)]. Reservoir boundary absorption affects the displacement history and stress distribution pattern of the dam on rigid and flexible foundation rock in a similar manner [compare parts (b)-(e) of Figures 6.9 and 6.14-6.15 to those of Figures 6.16 and 6.21-6.22], except that reservoir boundary absorption has less influence on the distribution pattern of the cantilever stresses if the foundation rock is flexible [compare the cantilever stress portion of parts (b)-(e) of Figures 6.21-6.22 to those of Figures 6.14-6.15]. As in the case of upstream and vertical ground motions, reservoir boundary absorption also eliminates the changes due to hydrodynamic effects in the distribution pattern of arch and cantilever stresses over the dam faces [compare part (a) to (e) of Figures 6.14-6.15 and 6.21-6.22].

It is apparent from the preceding discussion that, regardless of the foundation rock condition, the effects of reservoir boundary absorption are most pronounced in the dam response to vertical ground motion and generally least pronounced in the response to cross-stream ground motion. In general, assuming a non-absorptive reservoir boundary leads to unrealistically large response for dams with impounded water, particularly due to vertical ground motion.

The effects of reservoir boundary absorption on the earthquake response of arch dams identified in the preceding discussion are generally similar to those presented earlier for gravity dams [12]. However, dam-foundation rock interaction has less influence on the reservoir boundary absorption effects in the earthquake response of arch dams than for gravity dams. Such is the case primarily because the hydrodynamic terms affected by reservoir boundary absorption are relatively more important for arch dams, and because dam-foundation rock interaction effects are relatively less significant for arch dams. For both types of dams, the response to vertical ground motion is

significantly affected by reservoir boundary absorption; whereas the response to upstream ground motion is only moderately affected.

6.7 Relative Significance of Response to Ground Motion Components

As seen in Section 6.6, the earthquake response of the dam with full reservoir is increased by dam-water interaction if the reservoir boundary is non-absorptive and generally decreased by reservoir boundary absorption, with the magnitude of these effects depending on the condition of the foundation rock, rigid or flexible, and on the component of ground motion. In particular, both dam-water interaction and reservoir boundary absorption profoundly affect the response of the dam to the vertical component of ground motion irrespective of the foundation rock condition, but have relatively less — although significant — effect on the response of the dam to the horizontal (upstream and cross-stream) components of ground motion. Stated differently, the response of the dam with an empty reservoir due to vertical ground motion, expressed as a percentage of the response to one of the horizontal ground motion components, is small; the percentage greatly increases because of dam-water interaction with a non-absorptive reservoir boundary; and from this increased value it decreases significantly because of reservoir boundary absorption.

The earthquake response of the dam with full reservoir to the three components, separately and simultaneously, of Taft ground motion is presented in Figures 6.23 to 6.36, with the maximum response values summarized in Tables 6.6 and 6.7. All the conclusions stated in the preceding paragraph would be fully applicable to the total response if the individual responses to the three components of ground motion were exactly in phase and the maximum responses were directly additive. But this is not the case as is apparent from the displacement-time history at the dam crest in Figure 6.23 for rigid foundation rock and Figure 6.30 for flexible foundation rock (E_f/E_s = 1). If the reservoir is empty, the contribution of the response to the vertical component is very small whether the foundation rock is rigid [Figure 6.23(a) for displacements and Figures 6.24-6.25 for stresses] or flexible [Figure 6.30(a) for displacements and Figures 6.31-6.32 for stresses]; and the contribution of

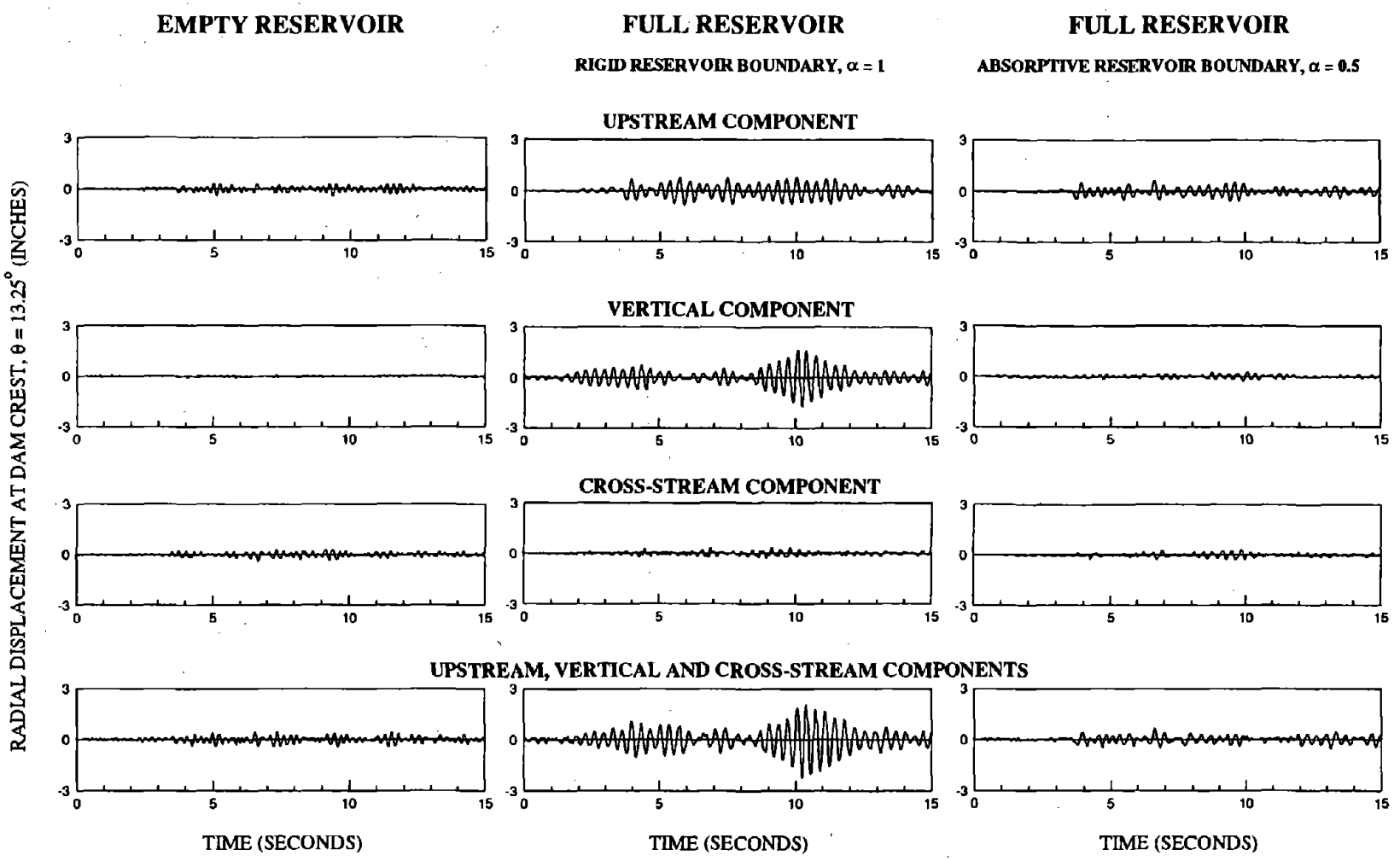

Figure 6.23 Displacement response of Morrow Point Dam on rigid foundation rock due to upstream, vertical and cross-stream components, separately and simultaneously, of Taft ground motion: (i) empty reservoir, (ii) full reservoir with non-absorptive reservoir boundary ($\alpha = 1$), and (iii) full reservoir with absorptive reservoir boundary ($\alpha = 0.5$).

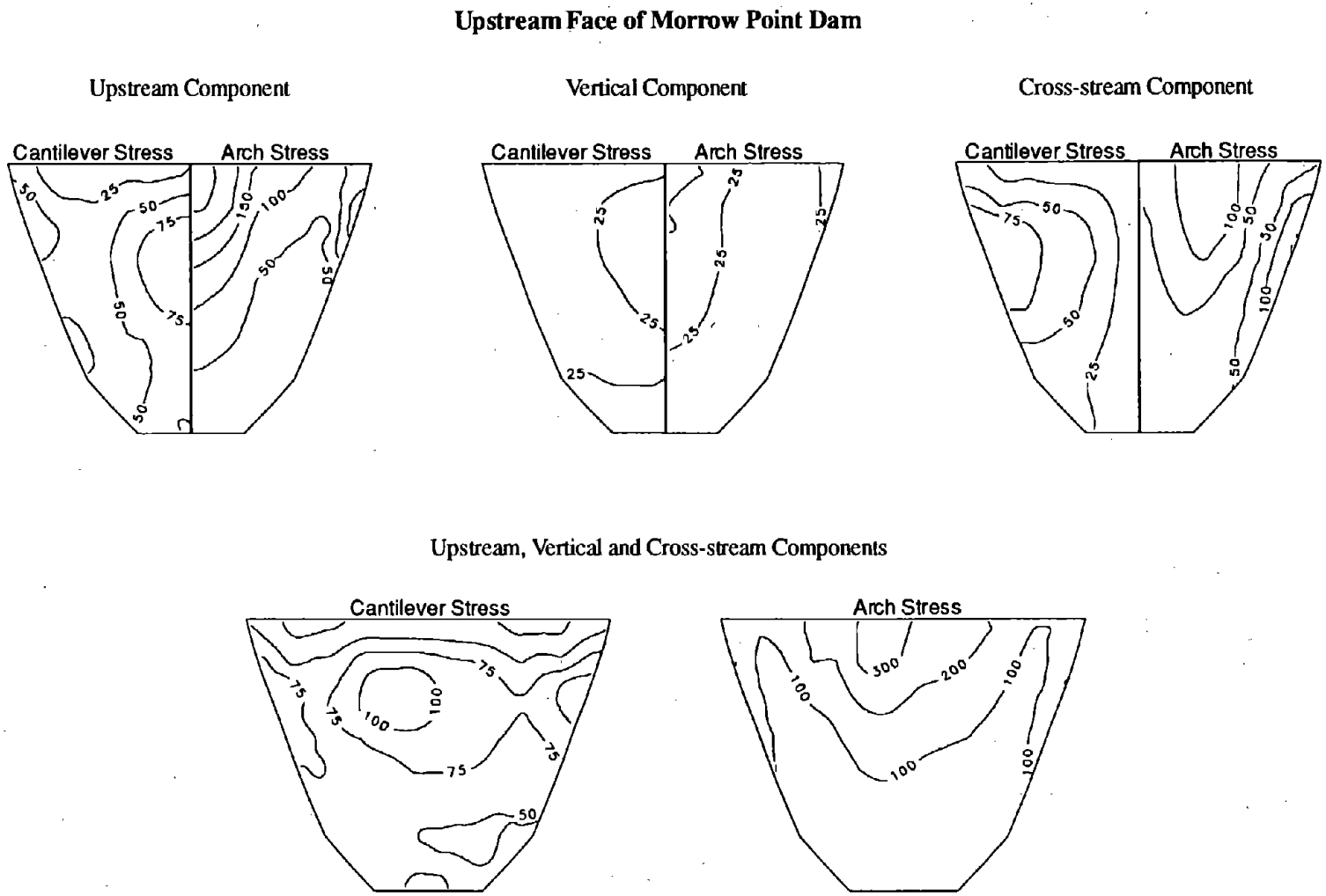

Figure 6.24 Envelope values of maximum tensile stress (in psi) on the upstream face of Morrow Point Dam with empty reservoir, supported on rigid foundation rock, due to upstream, vertical and cross-stream components, separately and simultaneously, of Taft ground motion. Initial static stresses are excluded.

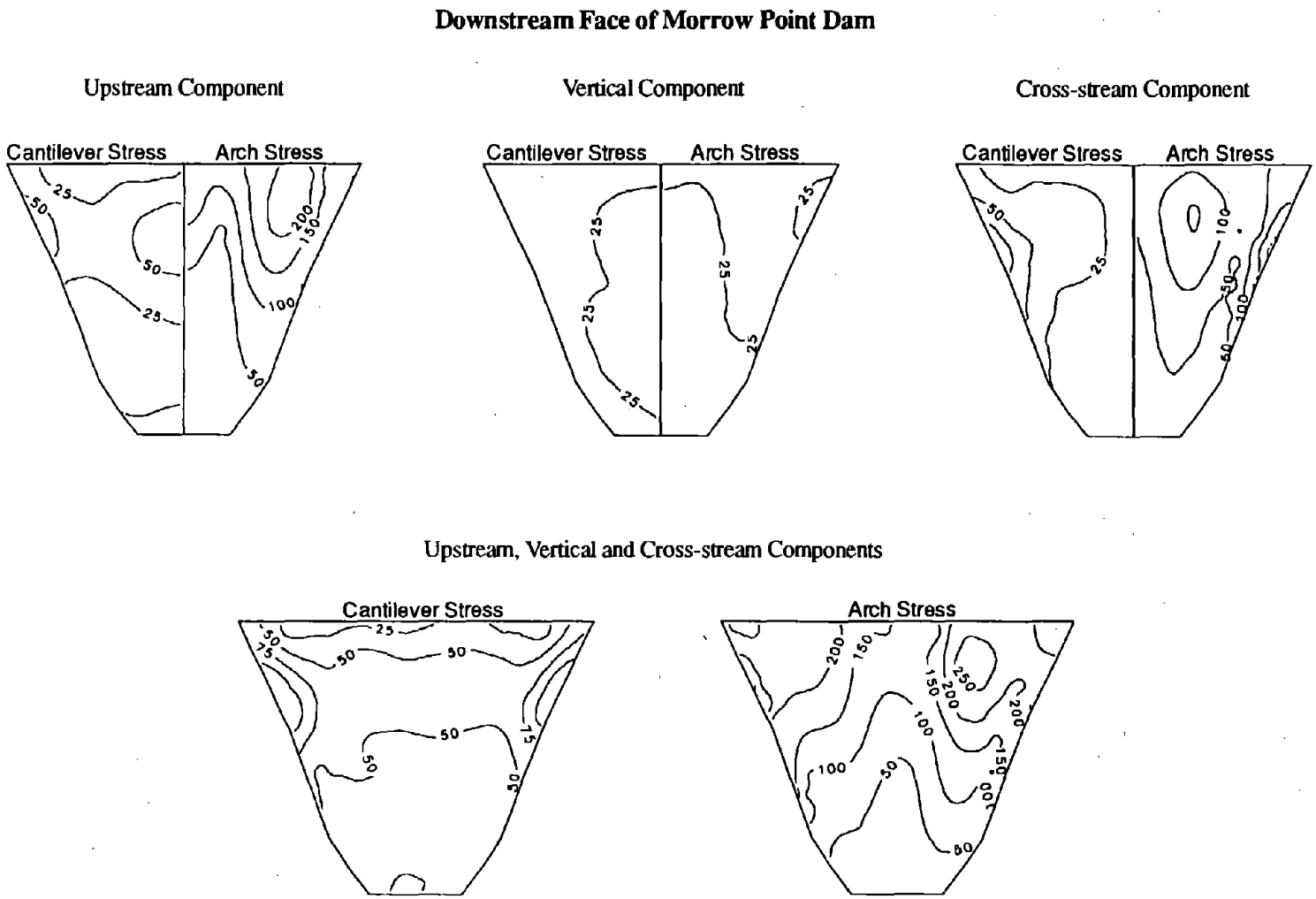

Figure 6.25 Envelope values of maximum tensile stress (in psi) on the downstream face of Morrow Point Dam with empty reservoir, supported on rigid foundation rock, due to upstream, vertical and cross-stream components, separately and simultaneously, of Taft ground motion. Initial static stresses are excluded.

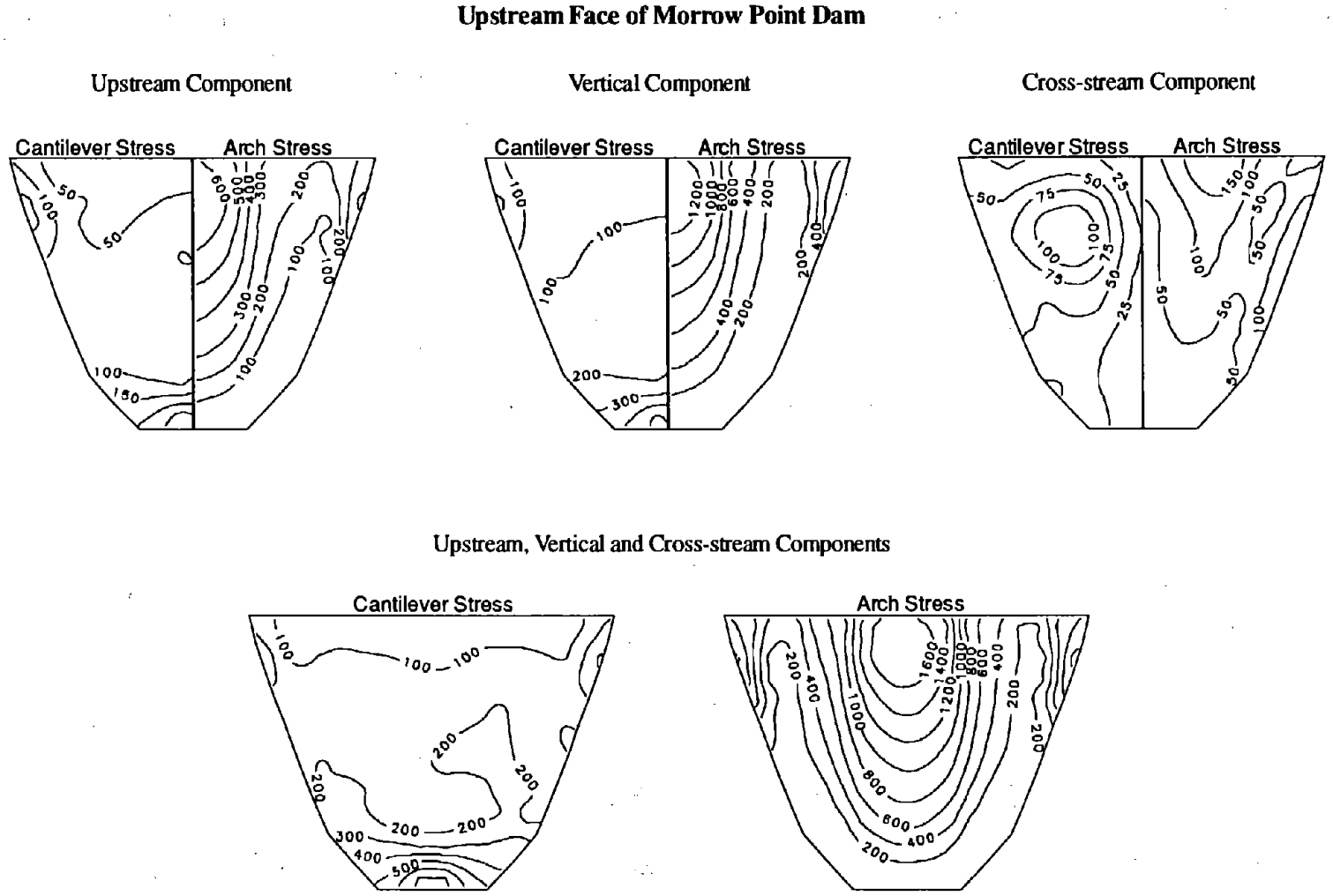

Figure 6.26 Envelope values of maximum tensile stress (in psi) on the upstream face of Morrow Point Dam with full reservoir and non-absorptive reservoir boundary ($\alpha = 1$), supported on rigid foundation rock, due to upstream, vertical and cross-stream components, separately and simultaneously, of Taft ground motion. Initial static stresses are excluded.

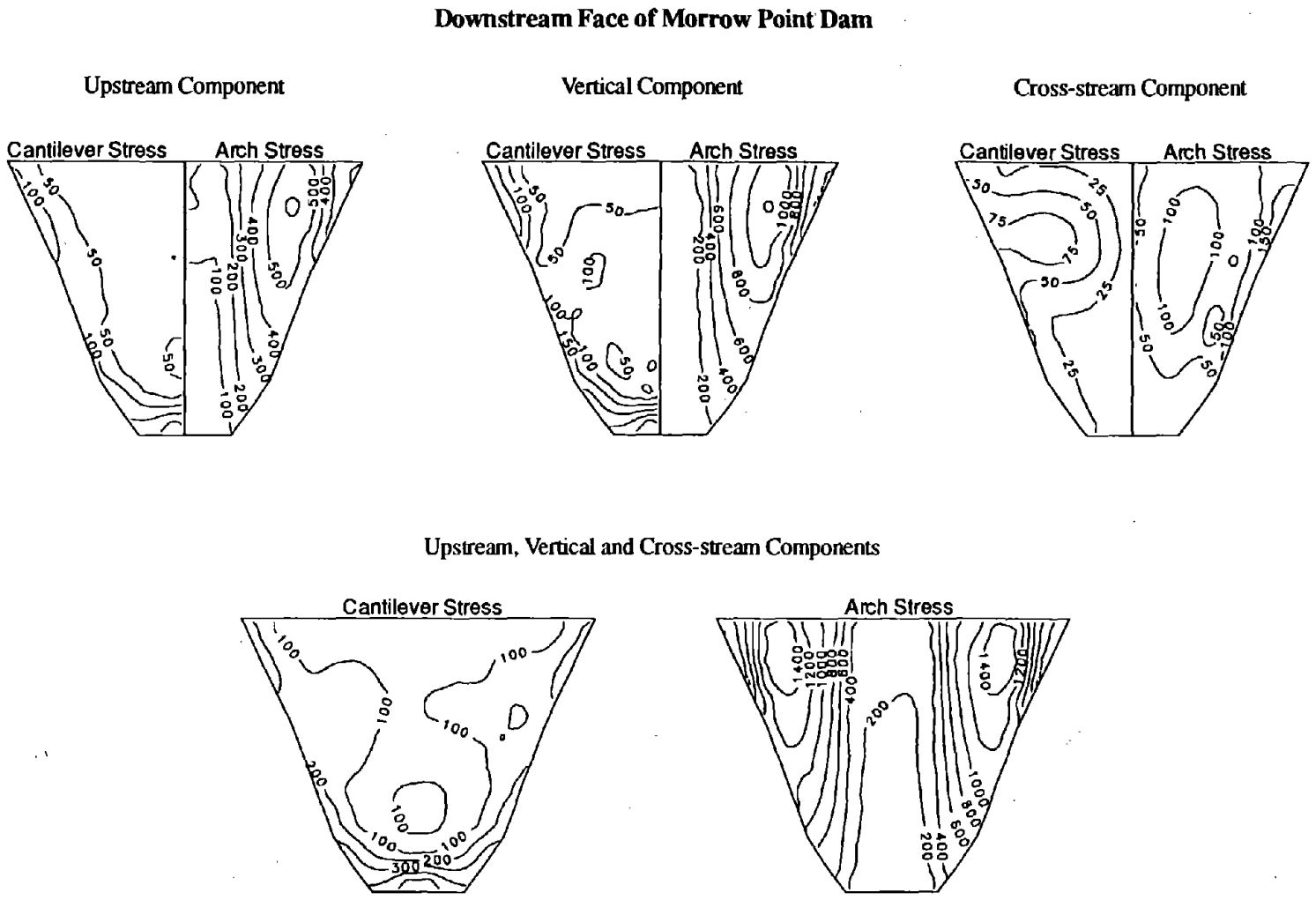

Figure 6.27 Envelope values of maximum tensile stress (in psi) on the downstream face of Morrow Point Dam with full reservoir and non-absorptive reservoir boundary ($\alpha = 1$), supported on rigid foundation rock, due to upstream, vertical and cross-stream components, separately and simultaneously, of Taft ground motion. Initial static stresses are excluded.

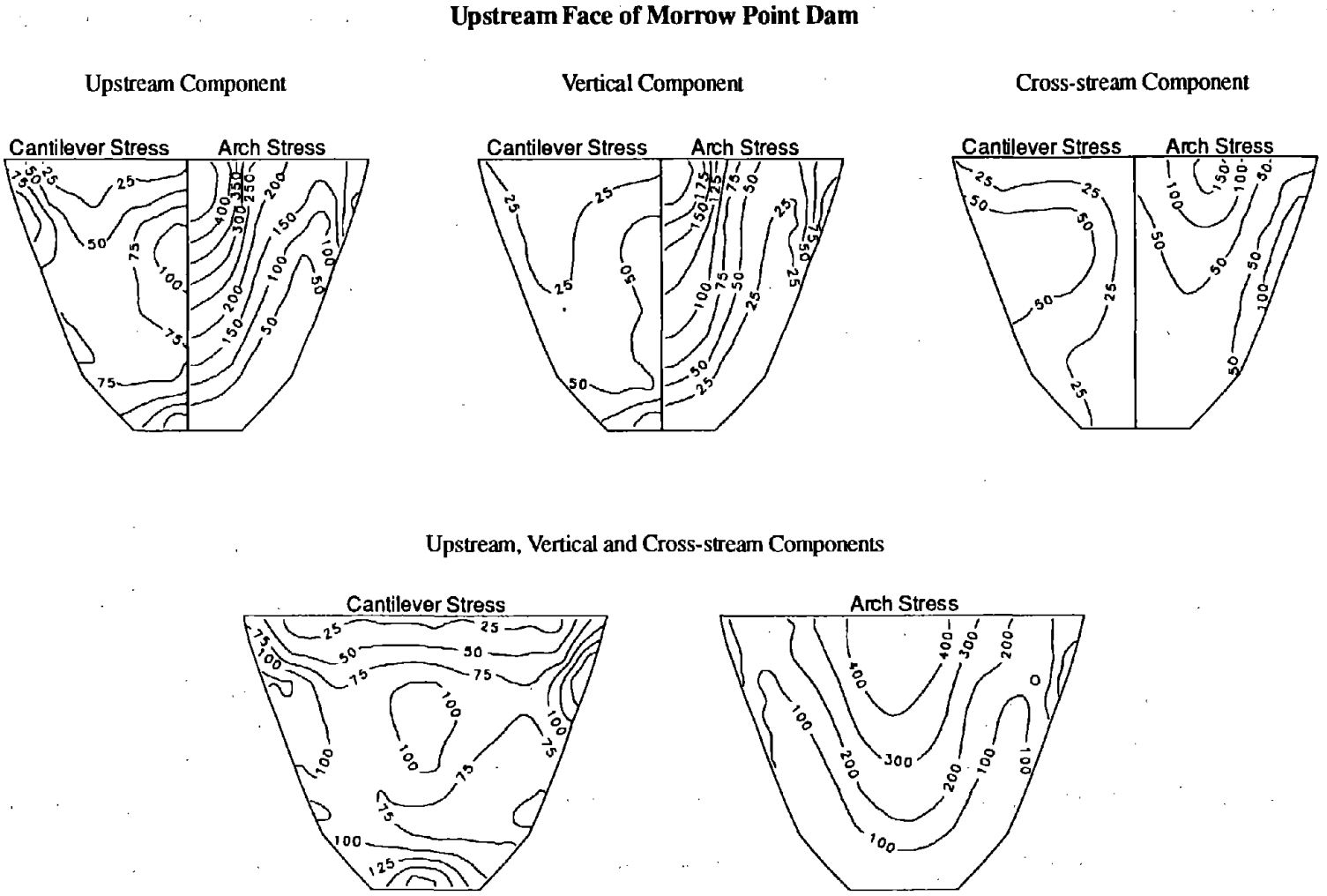

Figure 6.28 Envelope values of maximum tensile stress (in psi) on the upstream face of Morrow Point Dam with full reservoir and absorptive reservoir boundary ($\alpha = 0.5$), supported on rigid foundation rock, due to upstream, vertical and cross-stream components, separately and simultaneously, of Taft ground motion. Initial static stresses are excluded.

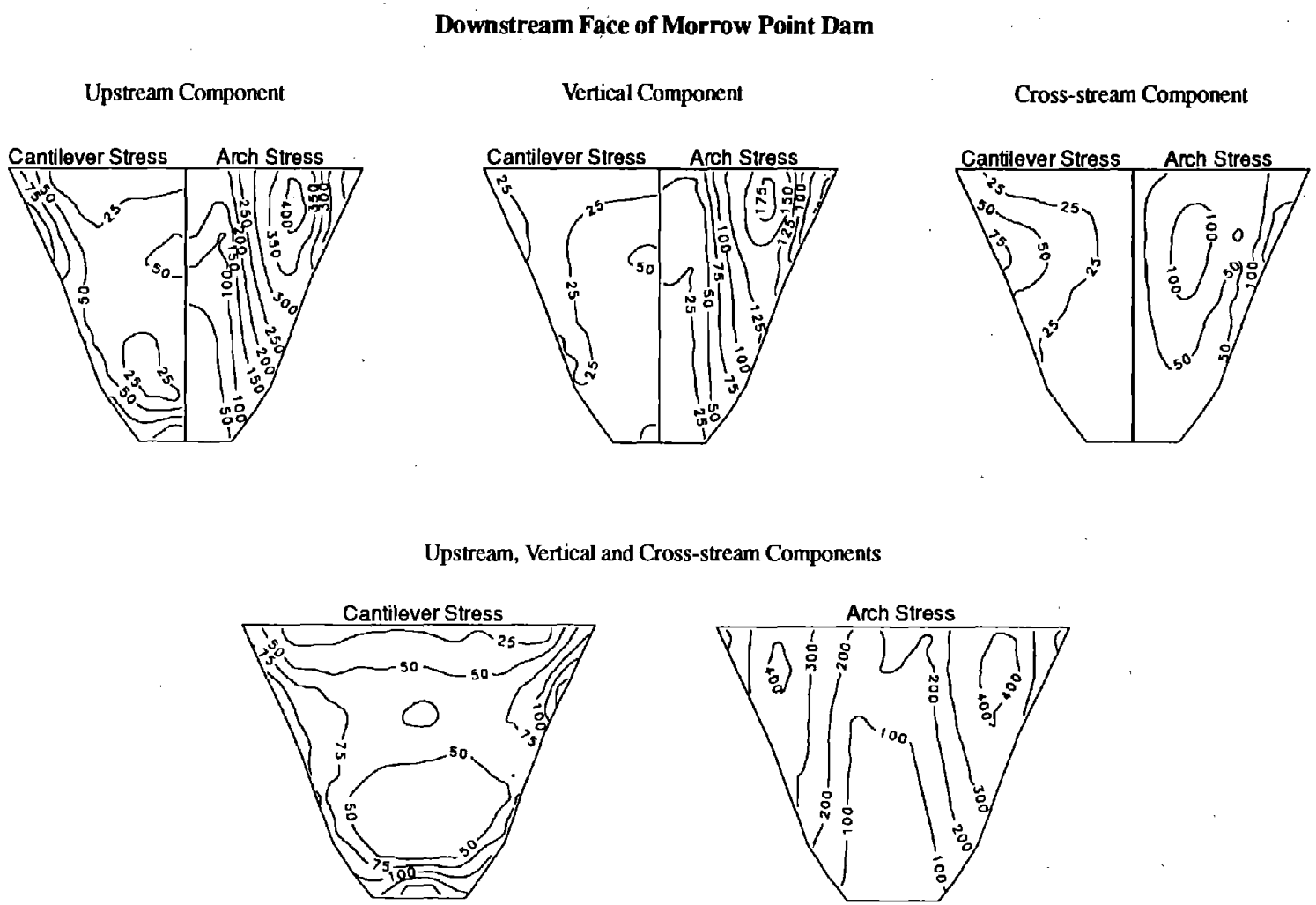

Figure 6.29 Envelope values of maximum tensile stress (in psi) on the downstream face of Morrow Point Dam with full reservoir and absorptive reservoir boundary ($\alpha = 0.5$), supported on rigid foundation rock, due to upstream, vertical and cross-stream components, separately and simultaneously, of Taft ground motion. Initial static stresses are excluded.

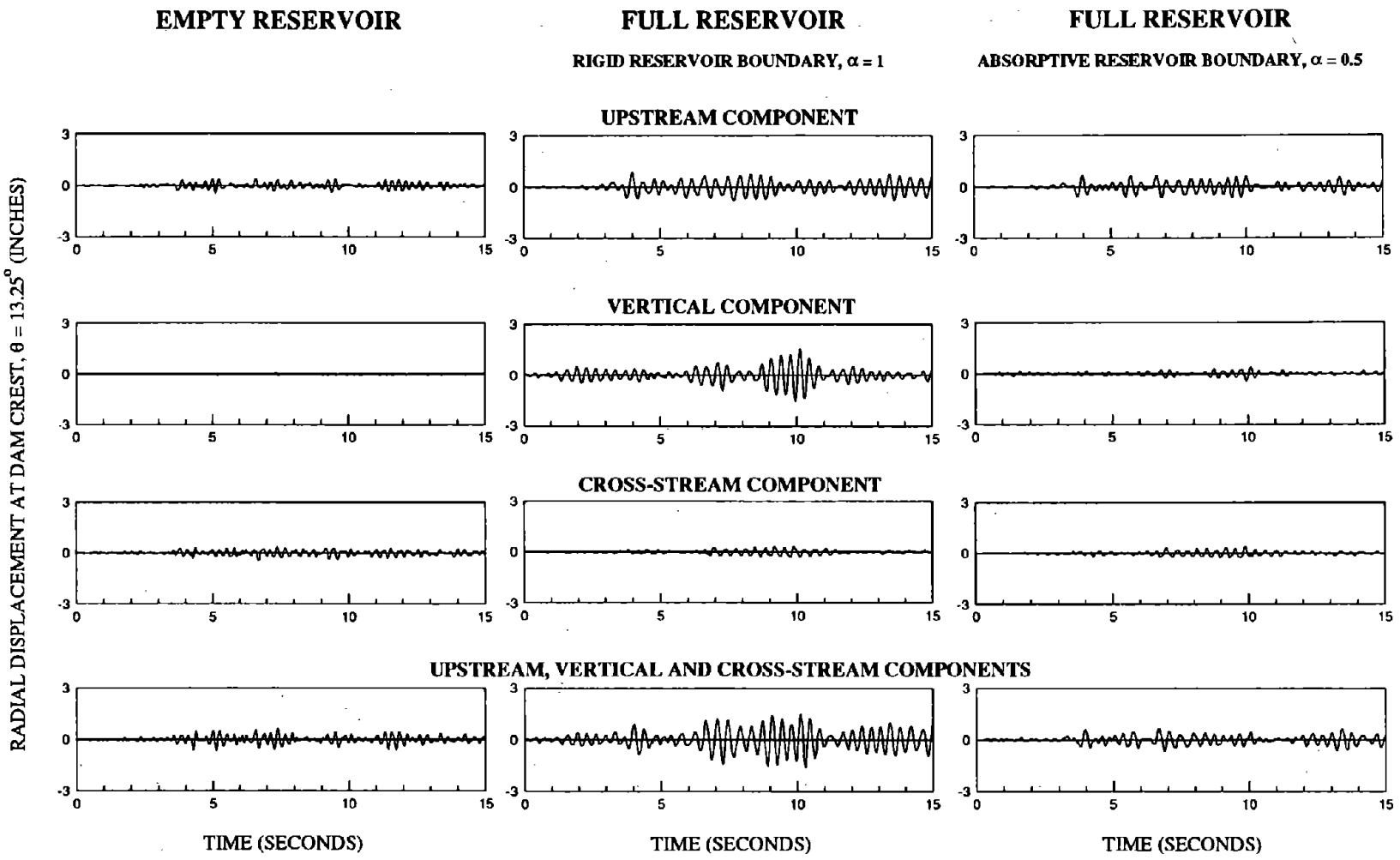

Figure 6.30 Displacement response of Morrow Point Dam on flexible foundation rock with $E_f / E_s = 1$ due to upstream, vertical and cross-stream components, separately and simultaneously, of Taft ground motion: (i) empty reservoir, (ii) full reservoir with non-absorptive reservoir boundary ($\alpha = 1$), and (iii) full reservoir with absorptive reservoir boundary ($\alpha = 0.5$).

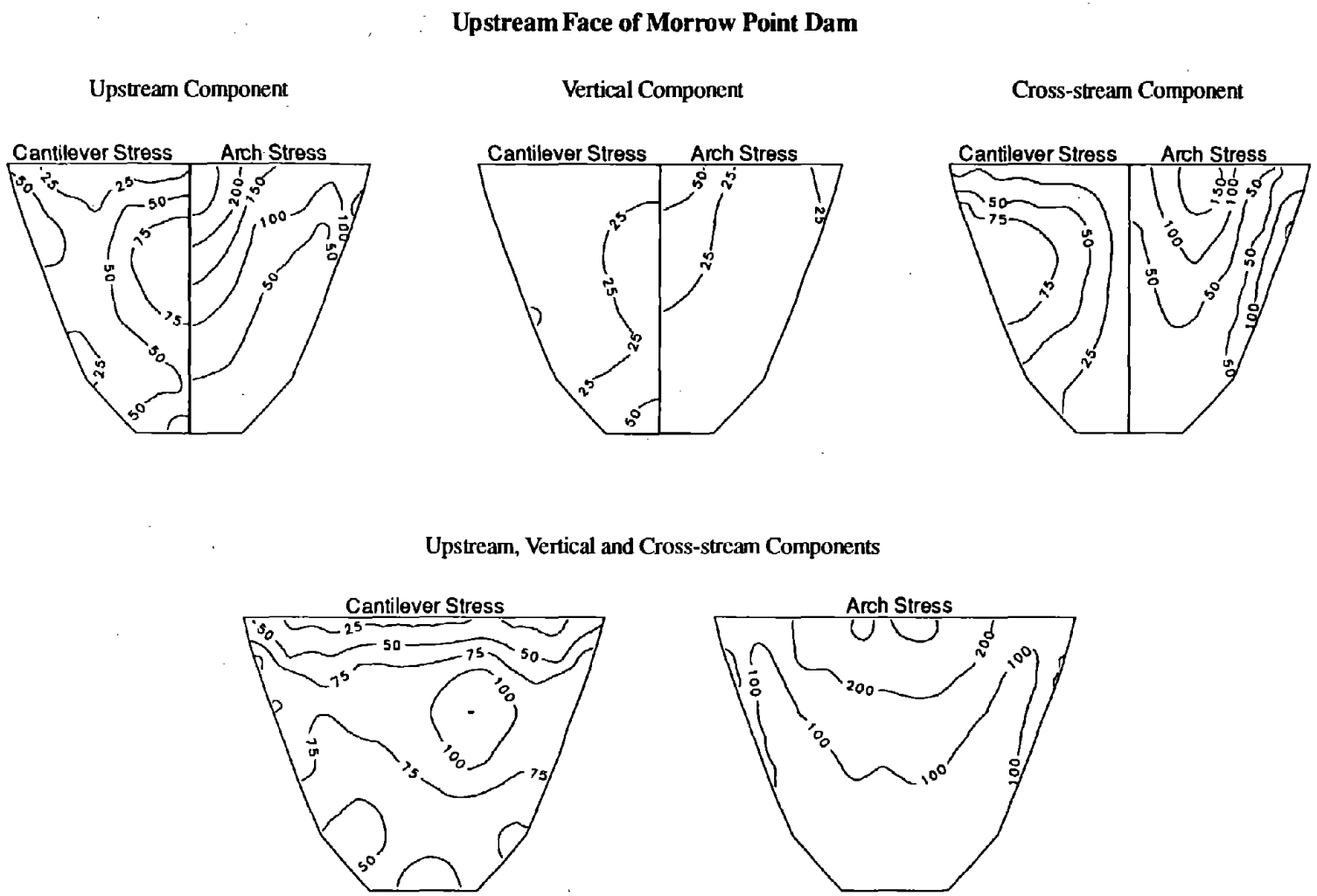

Figure 6.31 Envelope values of maximum tensile stress (in psi) on the upstream face of Morrow Point Dam with empty reservoir, supported on flexible foundation rock with $E_f/E_s = 1$, due to upstream, vertical and cross-stream components, separately and simultaneously, of Taft ground motion. Initial static stresses are excluded.

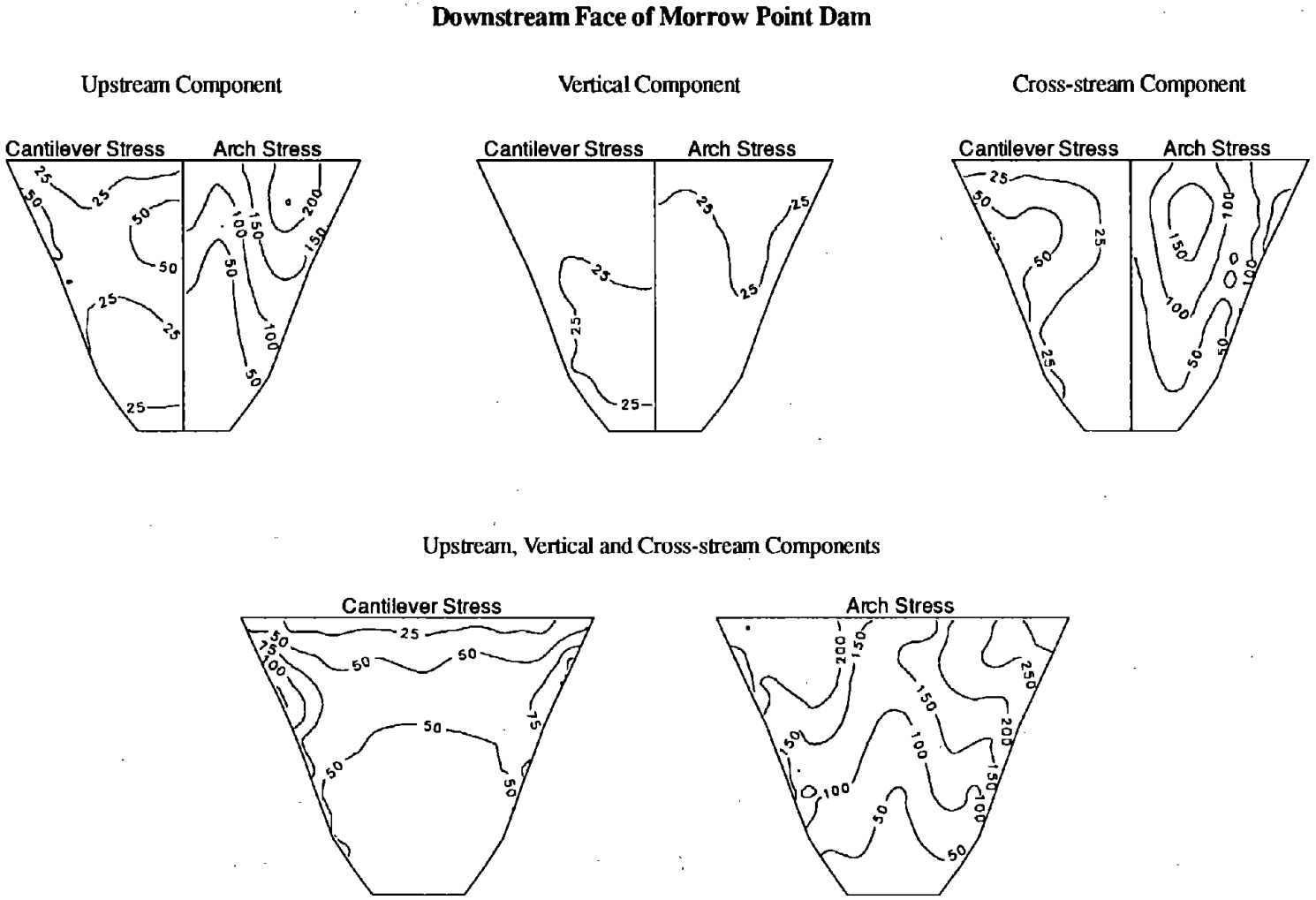

Figure 6.32 Envelope values of maximum tensile stress (in psi) on the downstream face of Morrow Point Dam with empty reservoir, supported on flexible foundation rock with $E_f/E_s = 1$, due to upstream, vertical and cross-stream components, separately and simultaneously, of Taft ground motion. Initial static stresses are excluded.

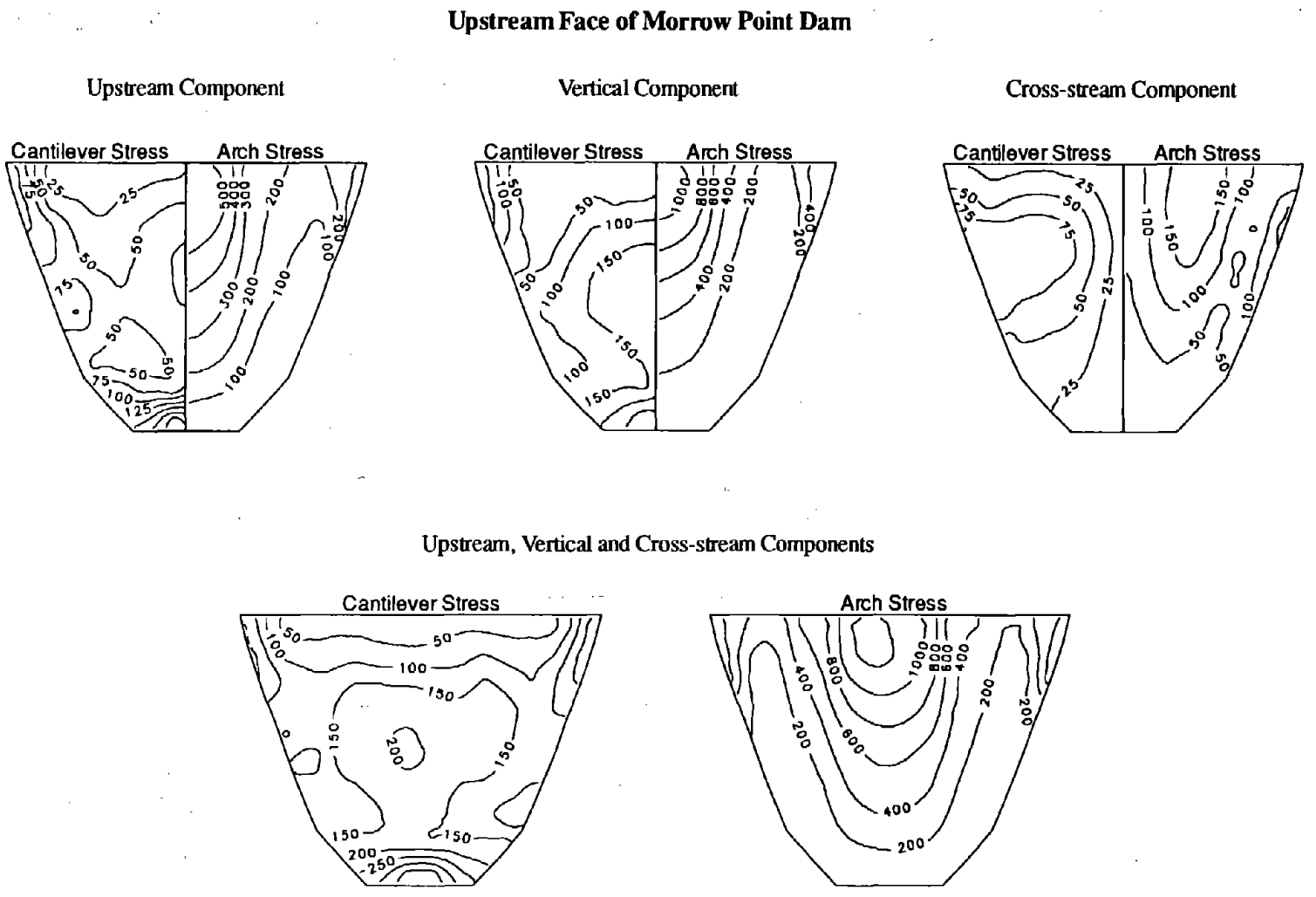

Figure 6.33 Envelope values of maximum tensile stress (in psi) on the upstream face of Morrow Point Dam with full reservoir and non-absorptive reservoir boundary ($\alpha = 1$), supported on flexible foundation rock with $E_f/E_s = 1$, due to upstream, vertical and cross-stream components, separately and simultaneously, of Taft ground motion. Initial static stresses are excluded.

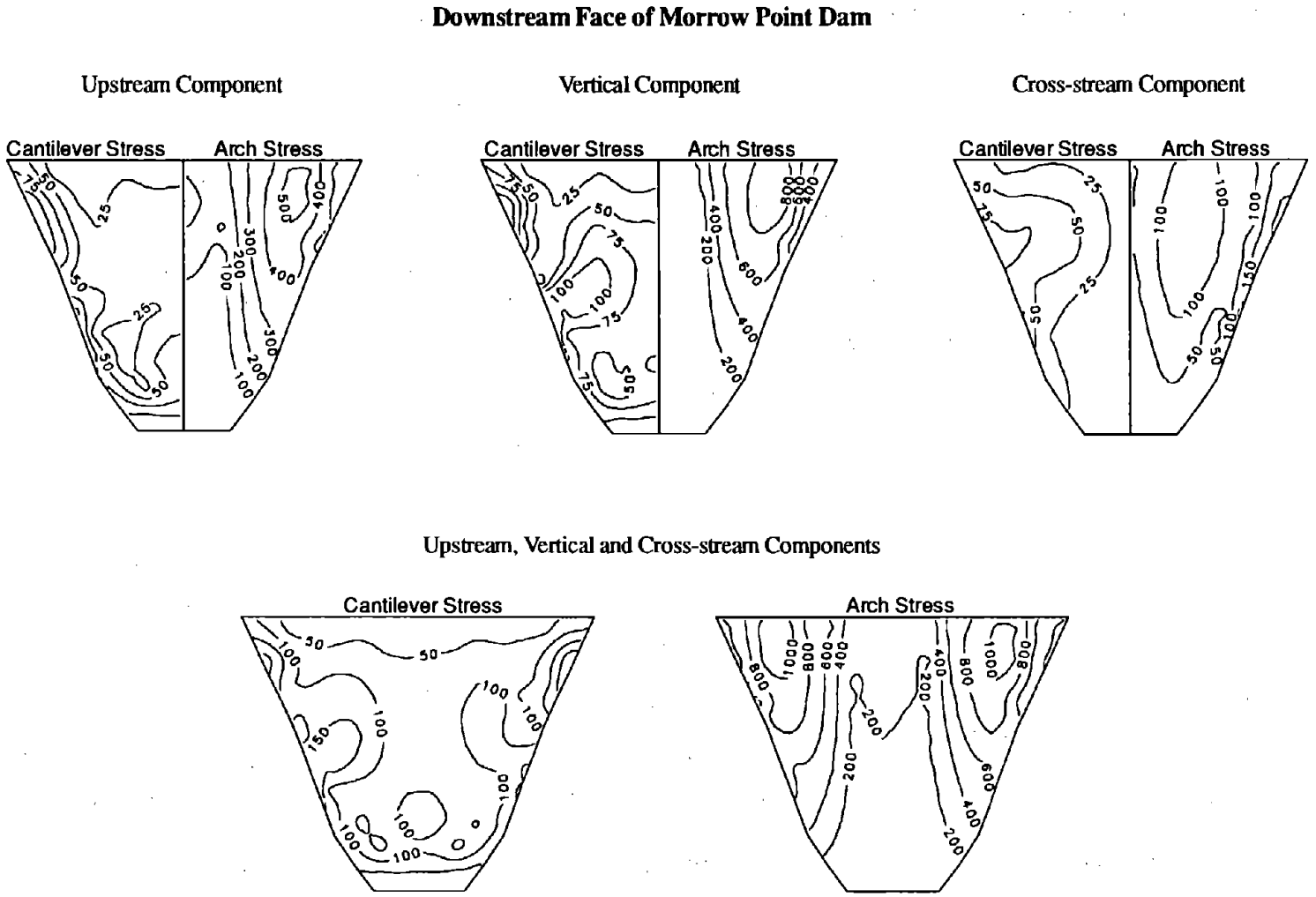

Figure 6.34 Envelope values of maximum tensile stress (in psi) on the downstream face of Morrow Point Dam with full reservoir and non-absorptive reservoir boundary ($\alpha = 1$), supported on flexible foundation rock with $E_f/E_s = 1$, due to upstream, vertical and cross-stream components, separately and simultaneously, of Taft ground motion. Initial static stresses are excluded.

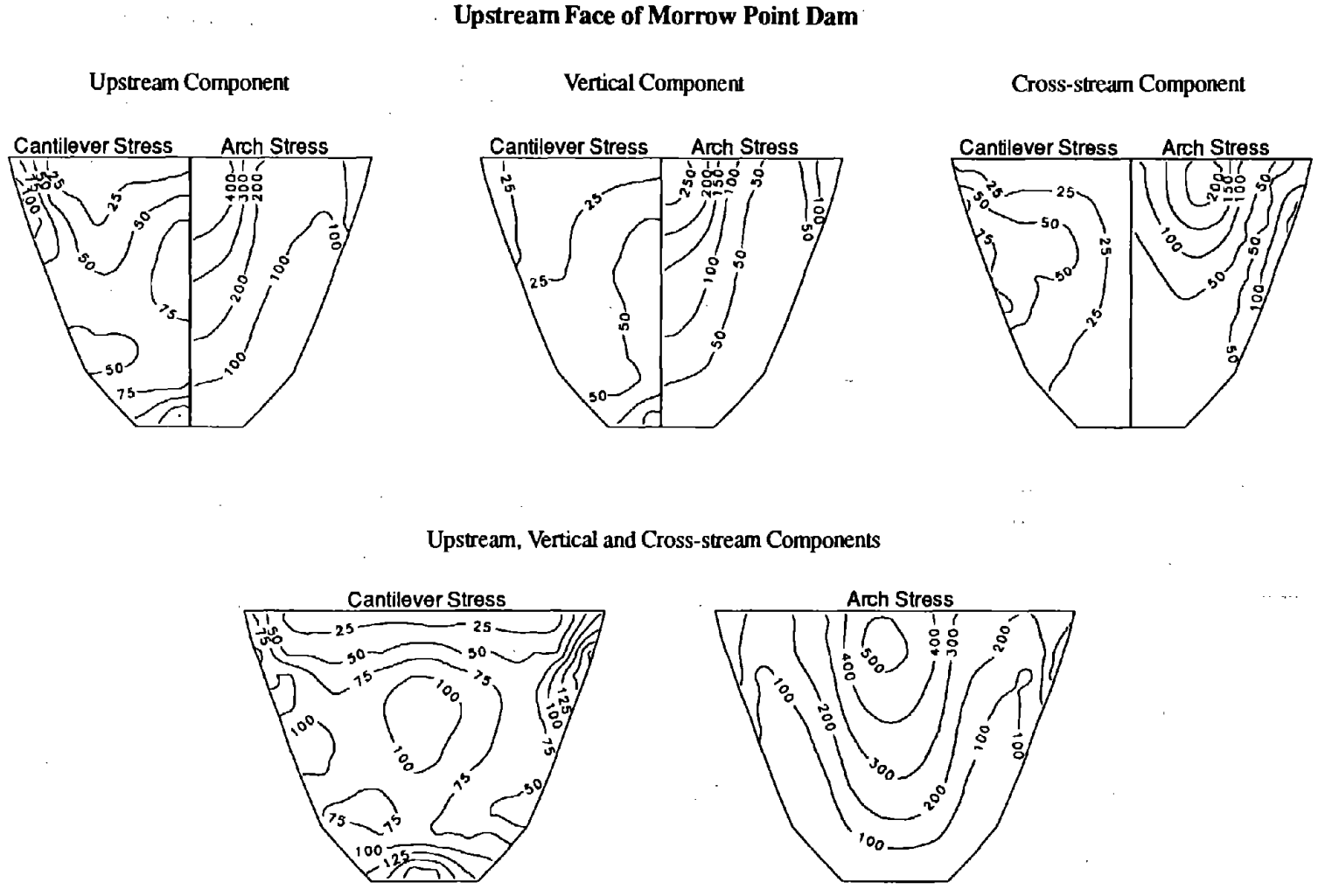

Figure 6.35 Envelope values of maximum tensile stress (in psi) on the upstream face of Morrow Point Dam with full reservoir and absorptive reservoir boundary ($\alpha = 0.5$), supported on flexible foundation rock with $E_f/E_s = 1$, due to upstream, vertical and cross-stream components, separately and simultaneously, of Taft ground motion. Initial static stresses are excluded.

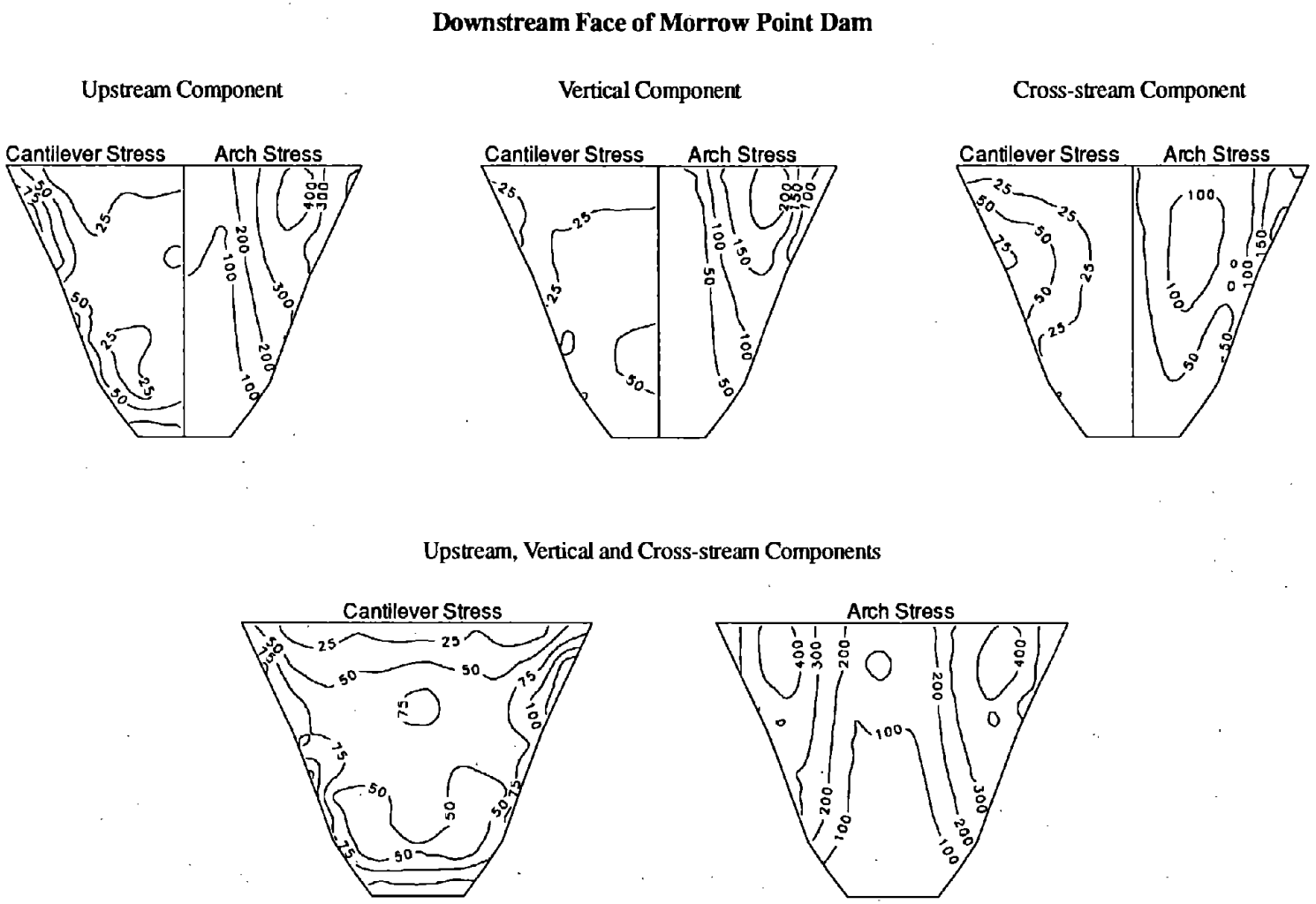

Figure 6.36 Envelope values of maximum tensile stress (in psi) on the downstream face of Morrow Point Dam with full reservoir and absorptive reservoir boundary ($\alpha = 0.5$), supported on flexible foundation rock with $E_f/E_s = 1$, due to upstream, vertical and cross-stream components, separately and simultaneously, of Taft ground motion. Initial static stresses are excluded.

the response to cross-stream component is generally smaller than that due to upstream ground motion whether the foundation rock is rigid [Figure 6.23(a) for displacements and Figures 6.24-6.25 for stresses] or flexible [Figure 6.30(a) for displacements and Figures 6.31-6.32 for stresses].

For the dam with impounded water and non-absorptive reservoir boundary, the response to the vertical component of ground motion is so large that it dominates the total response irrespective of the phase differences among responses to the individual ground motion components [Figures 6.23(b) and 6.26-6.27 for rigid foundation rock; Figures 6.30(b) and 6.33-6.34 for flexible foundation rock]. However, this dominance drastically decreases as the reservoir boundary becomes more absorptive [Figures 6.23(c) and 6.28-6.29 for rigid foundation rock; Figures 6.30(c) and 6.35-6.36 for flexible foundation rock]. In particular, for $\alpha = 0.5$ the total response becomes dominated by the response to upstream ground motion with increasing influence from the response to cross-stream ground motion [Figures 6.23(c), 6.28-6.29, 6.30(c), and 6.35-6.36].

The most important implication of these response results and their interpretation is that the assumption of a non-absorptive reservoir boundary overestimates the significance of the response of the dam, particularly due to vertical ground motion, whether the foundation rock is rigid or flexible. The large amplification of the response to vertical ground motion at excitation frequencies corresponding to the natural vibration frequencies of the infinite uniform channel of the reservoir, predicted by the assumption of a non-absorptive reservoir boundary, is unlikely because of the alluvium and sediments invariably present at the reservoir boundary. An absorptive reservoir boundary that models the alluvium and sediments gives a more realistic estimate of the earthquake response of concrete arch dams, especially of the response to vertical ground motion and its contribution to the total dynamic response.

6.8 Practical Earthquake Analysis of Arch Dams

The analytical procedure and EACD-3D-95 computer program (Chapter 4) is efficient in obtaining the earthquake response results in the preceding sections. Therefore, it is the most advanced

tool for calculating, under the assumption of linear behavior, the earthquake response of existing arch dams or of designs proposed for new dams. However, in such practical application, the effects of the static loads should be combined with the earthquake response of the dam to the three components of ground motion considering dam-water-foundation rock interaction.

A complete analysis of the response of Morrow Point Dam due to its weight, the hydrostatic pressure and the simultaneous action of the S69E, vertical, and S21W components of Taft ground motion was performed. The material properties of the dam body, the foundation rock region and the impounded reservoir were the same as described in Chapter 3. The moduli ratio E_f/E_s was chosen to be 1 ($E_f = E_s = 4.0$ million psi); the reservoir was assumed to be full and the wave reflection coefficient α at the reservoir boundary was selected as 0.5. Although the accuracy of the static analysis of arch dams is not much affected by water-foundation rock interaction due to hydrostatic pressure acting on the canyon boundary upstream of the dam (Appendix B), a length of the canyon boundary about 1.5 times of the full canyon width (Figure B.1) was included in the static analysis.

Some typical response results are shown in Figures 6.37 to 6.39. Figure 6.37 shows the time history of the radial, vertical, and tangential displacements at nodal points 44 and 60 located at the dam crest, and at nodal points 1 and 13 located at the dam-foundation rock interface (Figure 3.1). Figure 6.38 shows the time history of the arch and cantilever stresses on the upstream face at stress points 4 and 19 and on the downstream face at stress points 22 and 61 (Figure 3.1). Figure 6.39 shows the distribution of the envelope values of the maximum tensile arch and cantilever stresses on the upstream and downstream faces of the dam. Such stress results, which include the stresses due to the static loads, aid in identifying areas in the dam that may crack during an earthquake.

The total CPU time needed for earthquake analysis of this selected dam including 20 generalized coordinates is about 2 minutes on a CRAY X-MP EA/1 supercomputer or 10 minutes on a DECstation 5000/240 machine if the frequency-dependent foundation impedance matrix is already available. However, calculation of this impedance matrix at 13 frequency values requires 20 minutes on the CRAY computer for the standard boundary element mesh in this example analysis.

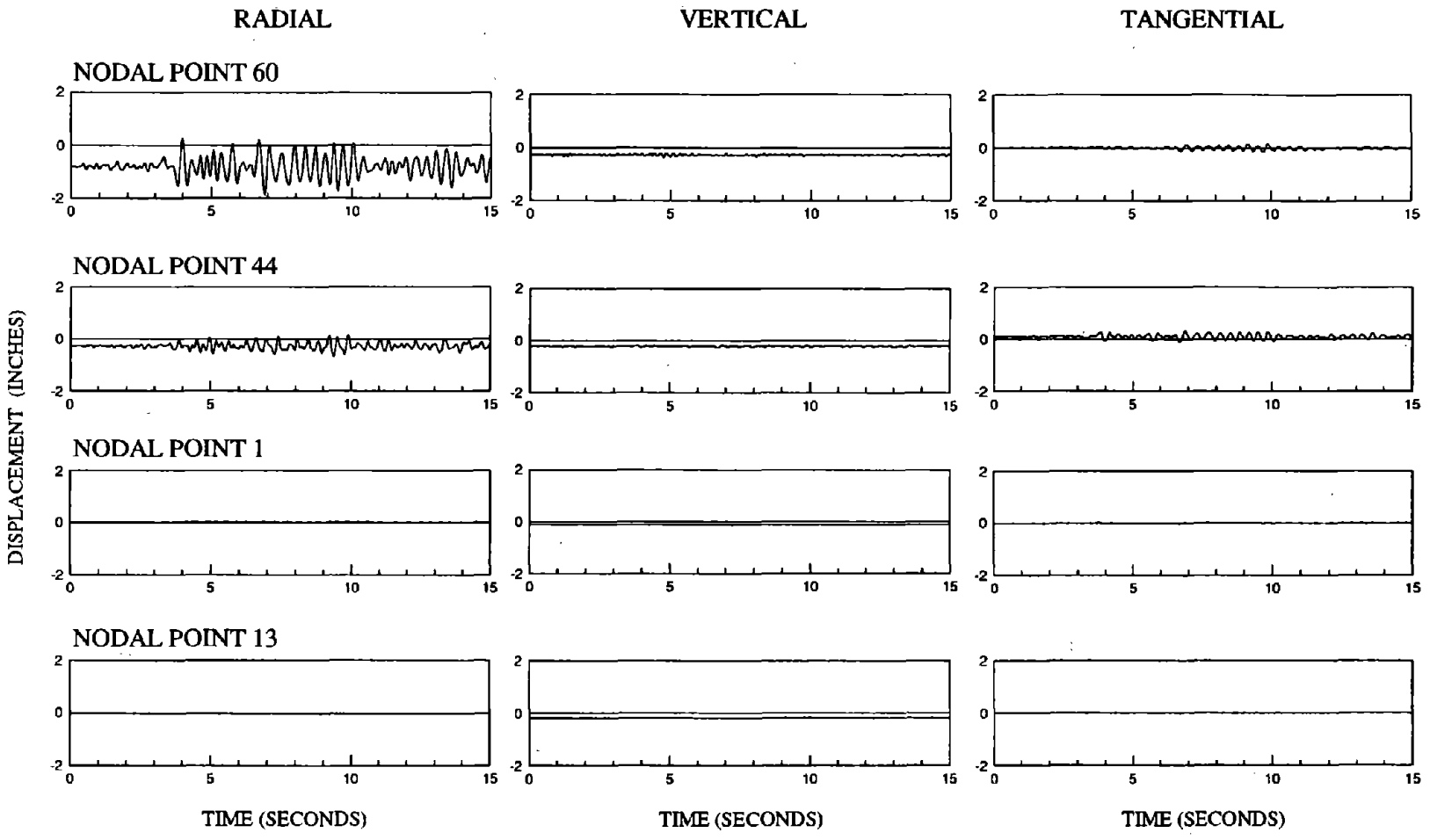

Figure 6.37 Displacement response of Morrow Point Dam with full reservoir and absorptive reservoir boundary ($\alpha = 0.5$), supported on flexible foundation rock with $E_f/E_s = 1$, due to upstream, vertical, and cross-stream components, simultaneously, of Taft ground motion.

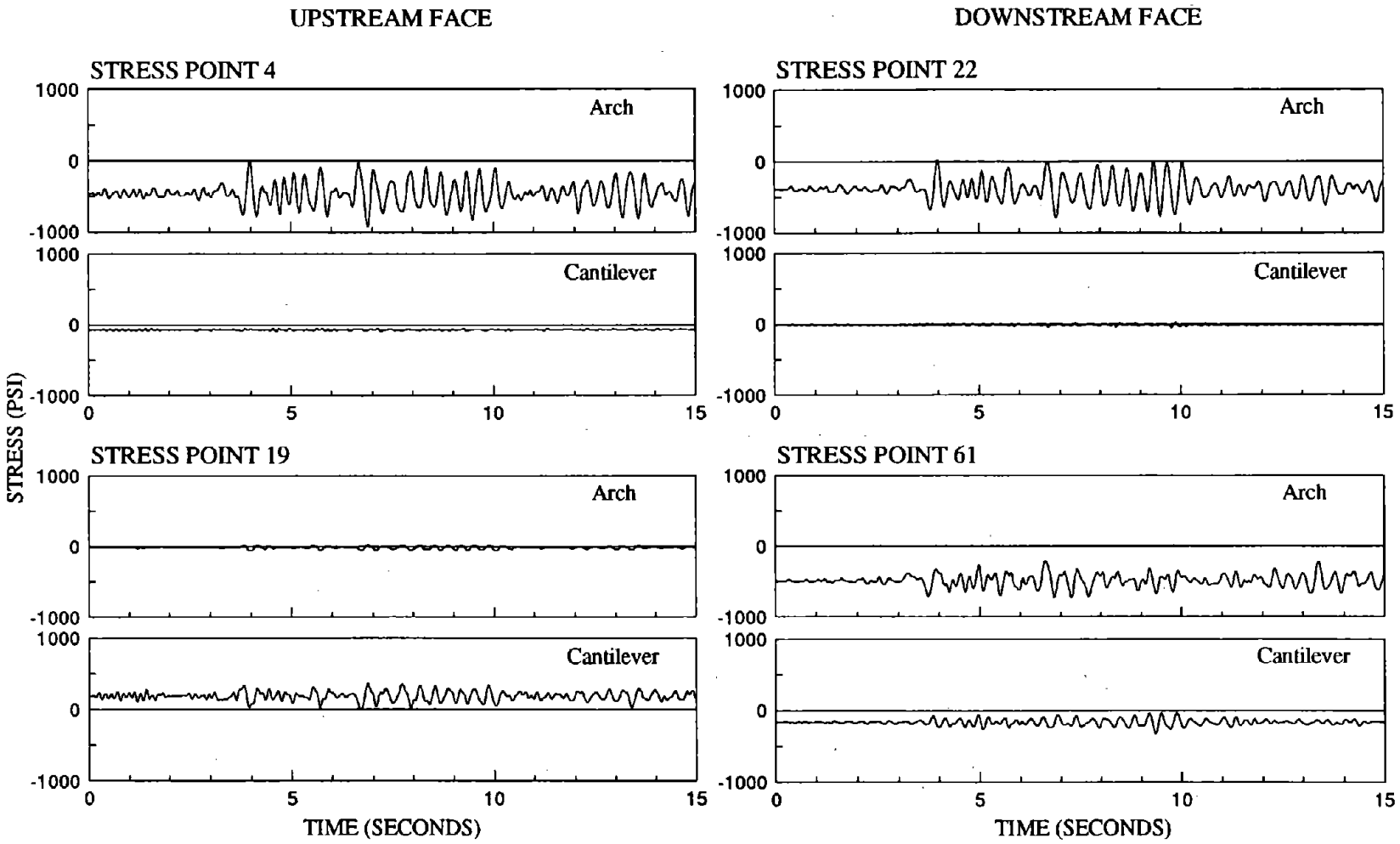

Figure 6.38 Stress response of Morrow Point Dam with full reservoir and absorptive reservoir boundary ($\alpha = 0.5$), supported on flexible foundation rock with $E_f/E_s = 1$, due to upstream, vertical, and cross-stream components, simultaneously, of Taft ground motion.

Upstream Face of Morrow Point Dam

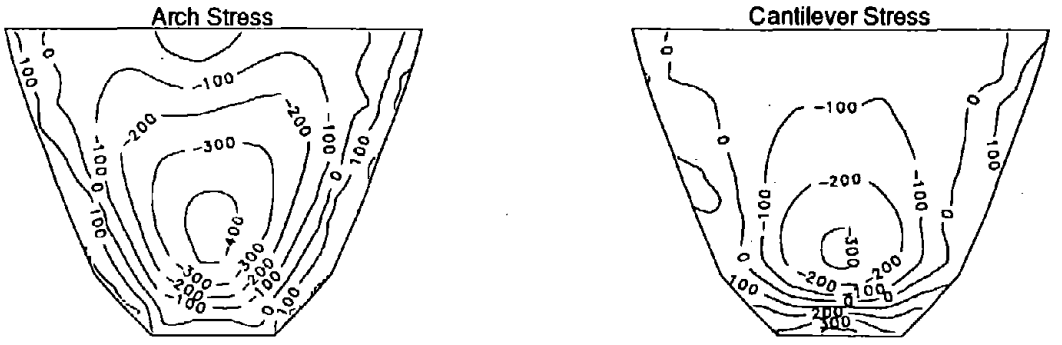

Downstream Face of Morrow Point Dam

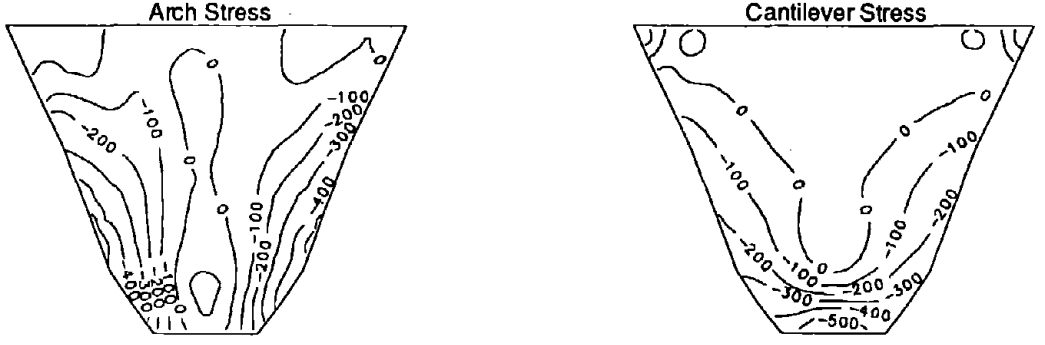

Figure 6.39 Envelope values of maximum arch and cantilever stress (in psi) on the faces of Morrow Point Dam with full reservoir and absorptive reservoir boundary ($\alpha = 0.5$), supported on flexible foundation rock with $E_f/E_s = 1$, due to upstream, vertical and cross-stream components, simultaneously, of Taft ground motion. Initial static stresses are included.

7 CONCLUSIONS

The earlier analytical procedure [5] to evaluate the earthquake response of arch dams considering the various effects of dam-water interaction has been extended to include the effects of dam-foundation rock interaction with inertia and damping of the foundation rock considered. In this extended procedure, the foundation impedance matrix is computed by a direct boundary element method [13]. Since only the surface of the uniform canyon is discretized in the boundary element approach, preparation of the foundation mesh is much easier than for a three-dimensional finite element idealization of the foundation. Because computation of the foundation impedance coefficients is extremely time-consuming and they are smooth functions of the excitation frequency, these coefficients are calculated only at a few selected frequencies and determined at other frequencies by a cubic interpolation scheme. The resulting computational procedure described in this report represents the most advanced tool for calculating, under the assumption of linear behavior, the earthquake response of existing arch dams or of designs proposed for new dams.

Utilizing this analytical procedure presented in Chapter 4, the effects of dam-foundation rock interaction, dam-water interaction, and reservoir boundary absorption on the response of Morrow Point Dam to harmonic ground motion have been studied. The frequency-response functions presented for a wide range of system parameters lead to the following conclusions:

1. Dam-foundation rock interaction reduces the fundamental resonant frequency of the dam primarily because of foundation flexibility, and widens the frequency bandwidth at the fundamental resonance because of material damping in the foundation rock and radiation damping associated with wave propagation away from the dam into the unbounded foundation rock region; as a result, the fundamental resonant response of the dam is generally reduced. These effects of dam-foundation rock interaction increase as E_f/E_s decreases.

2. Dam-foundation rock interaction also reduces the amplitude of higher resonant peaks and their resonant frequencies. It is more effective in reducing the fundamental resonant peak due to upstream and vertical ground motions than due to cross-stream ground motion, and in reducing the higher resonant peaks than the fundamental resonant peak due to cross-stream ground motion.

3. Dam-foundation rock interaction affects the response of the dam in its symmetric vibration modes, excited by upstream and vertical ground motions, more than its antisymmetric vibration modes, excited by cross-stream ground motion. These interaction effects for slender arch dams are less significant compared to gravity dams which are more massive.

4. The commonly used "standard" analysis, which considers only the flexibility of the foundation rock, ignores important effects of dam-foundation rock interaction. This procedure predicts the fundamental and higher resonant periods fairly accurately but overestimates the response amplitudes at these periods.

5. The fundamental resonant period T_1 of the dam alone (without water, and supported on rigid foundation rock) is lengthened to $\tilde{T}_r$ due to dam-water interaction, to $\tilde{T}_f$ due to dam-foundation rock interaction, and to $\tilde{T}$ due to both interaction effects simultaneously. Dam-water interaction effect is very small when the reservoir is less than half full, but increases rapidly with water depth thereafter. Dam-foundation rock interaction has little effect on the percentage increase in the resonant period due to dam-water interaction, especially if the reservoir is close to full.

6. The radiation damping due to reservoir boundary absorption is more effective in reducing the response of the dam if the foundation rock is rigid, and the damping — material and radiation — due to dam-foundation rock interaction is more effective in reducing the response of the dam if the reservoir boundary is less absorptive.

Utilizing the new analytical procedure presented in Chapter 4, the effects of dam-foundation rock interaction, dam-water interaction, and reservoir boundary absorption on the earthquake-induced

displacements and stresses of Morrow Point Dam due to Taft ground motion have also been studied for a wide range of system parameters. These results lead to the following conclusions:

1. The "standard" procedure commonly used in engineering practice, which considers only the flexibility of the foundation rock but ignores other effects of dam-foundation rock interaction, significantly overestimates the earthquake-induced stresses in arch dams. This discrepancy is especially significant in evaluating the seismic safety of existing dams because the standard procedure may lead to the erroneous conclusion that a dam is unsafe.

2. Dam-foundation rock interaction generally increases by a small amount the maximum tensile stresses computed for the dam on rigid foundation rock, but does not significantly alter the distribution of stresses over the dam faces.

3. The water impounded behind the dam increases the displacement and stress responses of the dam on rigid foundation rock to upstream and vertical ground motions, with the increase being much larger if the excitation is vertical ground motion. These hydrodynamic effects are smaller if dam-foundation rock interaction is considered. The response of the dam on rigid foundation rock to cross-stream ground motion is influenced by hydrodynamic effects to a much less degree than is the response to upstream and vertical ground motions. Hydrodynamic effects decrease the displacement response but increase some stress responses due to cross-stream ground motion. The displacement response decreases further but the stress responses change very little due to dam-foundation rock interaction effects.

4. The earthquake response of the dam on rigid foundation rock to upstream and vertical ground motions is generally decreased due to reservoir boundary absorption; this reduction of response is especially significant in the case of vertical excitation. However, reservoir boundary absorption is less effective in reducing the dam response if dam-foundation rock interaction effects are included. Reservoir boundary absorption has less influence on the response of the dam to cross-

stream ground motion than to upstream ground motion, whether the foundation rock is rigid or flexible.

5. The relative significance of the response of arch dams to the three components of ground motion depends on the assumptions implied in the response analysis. For the dam with impounded water and non-absorptive reservoir boundary, the response to the vertical component of ground motion is so large that it dominates the total response. However, this dominance drastically decreases as the reservoir boundary becomes more absorptive.

6. The small increase in stresses in an arch dam due to dam-foundation rock interaction is in contrast to gravity dams whose response is reduced significantly by interaction. However, dam-water interaction and reservoir boundary absorption effects have more significant influence on the earthquake response of arch dams than on the response of gravity dams.

The above conclusions deduced from the dynamic responses of the selected arch dam to harmonic ground motion and to earthquake-induced Taft ground motion may not apply to all arch dams and ground motions because the effects of dam-foundation rock interaction, dam-water interaction, and reservoir boundary absorption depend, in part, on the particular dam and earthquake ground motion. Although the detailed observations may be problem-dependent, the broad conclusions should apply to many cases.

The results presented demonstrate that foundation-rock inertia and damping, dam-water interaction, and reservoir boundary absorption may significantly affect the earthquake response of arch dams. Similarly, water compressibility may be an important factor [9]. Therefore, these effects should be included in the design of new arch dams and in the seismic safety evaluation of existing dams. Such analyses of arch dams can be effectively accomplished by the analytical procedure and the EACD-3D-95 computer program described in Chapter 4.

REFERENCES

1. R. W. Clough, J. M. Raphael, and S. Mojtahedi, "ADAP – A Computer Program for Static and Dynamic Analysis of Arch Dams," *Report No. UCB/EERC-73/14*, Earthquake Engineering research Center, University of California, Berkeley, California, 1973.

2. J. S.-H. Kuo, "Fluid-Structure Interactions: Added Mass Computations for Incompressible Fluid," *Report No. UCB/EERC-82/09*, Earthquake Engineering research Center, University of California, Berkeley, California, 1982.

3. Y. Ghanaat and R. W. Clough, "EADAP Enhanced Arch Dam Analysis Program, User's Manual," *Report No. UCB/EERC-89/07*, Earthquake Engineering Research Center, University of California, Berkeley, California, 1989.

4. J. F. Hall and A. K. Chopra, "Dynamic Analysis of Arch Dams Including Hydrodynamic Effects," *Journal of Engineering Mechanics, ASCE*, **109**, 149-167 (1983).

5. K.-L. Fok and A. K. Chopra, "Earthquake Analysis of Arch Dams Including Dam-Water Interaction, Reservoir Boundary Absorption and Foundation Flexibility," *Earthquake Engineering and Structural Dynamics*, **14**, 155-184 (1986).

6. K-L. Fok, J. F. Hall, and A. K. Chopra, "EACD-3D: A Computer Program for Three-Dimensional Earthquake Analysis of Concrete Dams," *Report No. UCB/EERC-86/09*, Earthquake Engineering Research Center, University of California, Berkeley, California, 1986.

7. K.-L. Fok and A. K. Chopra, "Frequency Response Functions for Arch Dams: Hydrodynamic and Foundation Flexibility Effects," *Earthquake Engineering and Structural Dynamics*, **14**, 769-795 (1986).

8. K.-L. Fok and A. K. Chopra, "Hydrodynamic and Foundation Flexibility Effects in Earthquake Response of Arch Dams," *Journal of Structural Engineering, ASCE*, **112**, 1810-1828 (1986).

9. K.-L. Fok and A. K. Chopra, "Water Compressibility in Earthquake Response of Arch Dams," *Journal of Structural Engineering, ASCE*, **113**, 958-975 (1987).

10. O. Maeso, and J. Domínguez, "Earthquake Analysis of Arch Dams. I: Dam-Foundation Interaction," *Journal of Engineering Mechanics, ASCE*, **119**, 496-512 (1993).

11. J. Domínguez, and O. Maeso, "Earthquake Analysis of Arch Dams. II: Dam-Water-Foundation Interaction," *Journal of Engineering Mechanics, ASCE*, **119**, 513-530 (1993).

12. G. Fenves and A. K. Chopra, "Earthquake Analysis of Concrete Gravity Dams Including Reservoir Bottom Absorption and Dam-Water-Foundation Rock Interaction," *Earthquake Engineering and Structural Dynamics*, **12**, 663-680 (1984).

13. L.-P. Zhang and A. K. Chopra, "Impedance Functions for Three-Dimensional Foundations Supported on an Infinitely Long Canyon of Uniform Cross-Section in a Homogeneous Half-Space," *Earthquake Engineering and Structural Dynamics*, **20**, 1011-1028 (1991).

14. E. Rosenblueth, "Presion Hidrodinamica en Presas Debida a la Aceleracion Vertical con Refraccion en el Fondo," *Proceedings*, Second Congreso Nacional de Ingenieria Sismica, held at Veracruz, Mexico, 1968.

15. M. Nose, "Observation and Measurement of Dynamic Behavior of the Kurobe Dam," *Proceedings*, Tenth International Congress on Large Dams, Communication, Montreal, 1970.

16. CSMIP, "Strong Motion Records from the Northridge, California Earthquake of January 17, 1994," *Report No. OSMS 94-07*, California Department of Conservation, Strong Motion Instrumentation Program, 1994.

17. T. Fujii, K. Egawa and I. Katayama, "Dynamic Behavior of Nagawado Arch Dam in the Event of 1984 Naganoken Seibu Earthquake," *Earthquake Spectra*, **3**, Earthquake Engineering Research Institute, 347-364 (1987).

18. U.S. Department of the Interior, Bureau of Reclamation, *Design of Arch Dams*, U.S. Government Printing Office, Denver, Colorado, 1977.

19. S. F. Pawsey, "The Analysis of Moderately Thick to Thin Shells by the Finite Element Method," *Report No. UC SESM 70-12*, Structural Engineering Laboratory, University of California, Berkeley, California, 1970.

20. A. K. Chopra and P. Chakrabarti, "Earthquake Analysis of Concrete Gravity Dams Including Dam-Water-Foundation Rock Interaction," *Earthquake Engineering and Structural Dynamics*, **9**, 363-383 (1981).

21. J. F. Hall, "An FFT Algorithm for Structural Dynamics," *Earthquake Engineering and Structural Dynamics*, **10**, 797-811 (1982).

22. G. Fenves and A. K. Chopra, "EAGD-84: A Computer Program for Earthquake Analysis of Concrete Gravity Dams," *Report No. UCB/EERC-84/11*, Earthquake Engineering Research Center, University of California, Berkeley, California, 1984.

APPENDIX A: NOTATIONS

a_0	non-dimensional frequency defined in Equation (4.34)
$a_g^l(t)$	l-component free-field ground acceleration; $l = x, y, z$
$A_g^l(\omega)$	Fourier transform of $a_g^l(t)$
c_0, c_1, c_2, c_3	complex-valued coefficients c_0, c_1, c_2, and c_3 for the complex-valued cubic function $f(\omega)$ defined as $f(\omega) = c_3\omega^3 + c_2\omega^2 + c_1\omega + c_0$
$\mathbf{c}_c$	damping matrix of the finite element idealization of the dam
C	velocity of pressure wave in water
C_r	velocity of compression wave in the materials at reservoir boundary; defined as $C_r = \sqrt{E_r/\rho_r}$
C_s	velocity of shear wave in foundation rock computed as $C_s = (g\mu_f/w_f)^{1/2}$
C_{s_0}	velocity of shear wave in foundation rock with Young's modulus E_{f_0}
d	duration of the free-field ground motion
E_f	Young's moduli of the foundation rock
E_{f_0}	Young's moduli of the foundation rock for computing the "base" foundation impedance matrix $\mathbf{S}_{f_0}(a_0)$
E_r	Young's modulus of the reservoir boundary materials
E_s	Young's modulus of the dam
f	cyclic frequency
$f(\omega)$	complex-valued function of circular frequency ω
g	the acceleration due to gravity
$g_{nj}(\omega)$	complex-valued cubic function of circular frequency ω defined in Equation (4.37)
H	y-coordinate of the free surface of water measured from the base of the dam
H_s	height of the dam
i	$=\sqrt{-1}$

J	number of generalized coordinates
$\mathbf{k}$, $\mathbf{k}_b$, $\mathbf{k}_{bb}$	submatrices of $\mathbf{k}_c$
$\mathbf{k}_c$	stiffness matrix of the finite element idealization of the dam
l	direction of the free-field ground motion; l = x, y, z
L	reference length taken as the half width of the canyon
$\mathbf{L}^l(\omega)$	forcing vector of the dam-water-foundation rock system containing terms $L_n^l(\omega)$ defined in Equation (4.16)
$\mathbf{m}$, $\mathbf{m}_b$	submatrices of $\mathbf{m}_c$
$\mathbf{m}_c$	mass matrix of the finite element idealization of the dam
n	inward normal direction at the free surface, upstream dam face or reservoir boundary as illustrated in Figure 4.3
N	number of nodal points of the dam not at the abutment
N_b	number of nodal points at the abutment of the dam
$p(x,y,z,t)$	hydrodynamic pressure in the impounded water; $p^l(x,y,z,t)$ denotes the pressure due to the l^{th} component of ground acceleration
$\overline{p}(x,y,z,\omega)$	frequency response function for $p(x,y,z,t)$
$\overline{p}^l(x,y,z,\omega)$	frequency response function for $p^l(x,y,z,t)$ due to the l^{th} component of ground acceleration
$\overline{p}_0^l(x,y,z,\omega)$	frequency response function for hydrodynamic pressure due to the l^{th} component of unit harmonic acceleration with a rigid dam and reservoir boundary
$\overline{p}_0^l(s,r,\omega)$	$\overline{p}_0^l(x,y,z,\omega)$ at the upstream face of the dam due to boundary condition of Equation (4.20)
$\overline{p}_j^f(x,y,z,\omega)$	frequency response function for hydrodynamic pressure due to normal harmonic acceleration of dam in the j^{th} natural vibration mode corresponding to the j^{th} generalized coordinate, without any reservoir boundary motion
$\overline{p}_j^f(s,r,\omega)$	$\overline{p}_j^f(x,y,z,\omega)$ at the upstream face of the dam due to boundary condition of Equation (4.21)
q	admittance or damping coefficient of the reservoir boundary materials; defined as $q = \rho/\rho_r C_r$

$\mathbf{r}(t)$	vector of displacements in time domain at the dam-foundation rock interface
$\bar{\mathbf{r}}^l(\omega)$	subvector of $\bar{\mathbf{r}}_c^l(\omega)$ corresponding to nodal points other than on the abutment of the dam
$\bar{\mathbf{r}}_b^l(\omega)$	subvector of $\bar{\mathbf{r}}_c^l(\omega)$ corresponding to nodal points on the abutment of the dam
$\mathbf{r}_c$	vector of nodal point displacements relative to the free-field ground displacement; $\mathbf{r}_c^l(t)$ denotes the vector due to the l-component of ground motion
$\bar{\mathbf{r}}_c^l(\omega)$	vector of frequency response functions for $\mathbf{r}_c^l(t)$ due to the l-component of ground motion
$\bar{\mathbf{r}}_f^l(\omega)$	vector of frequency response functions for displacements of nodal points of foundation rock at the dam-foundation rock interface due to the l-component of ground motion
$\mathbf{r}_p(t)$	nodal relative displacement vector for finite element p of the dam
$\bar{\mathbf{r}}_{rigid}(\omega)$	vector of 6 frequency response functions for displacements at the dam-foundation rock interface moved as a rigid body; defined in Equation (4.30)
R_f	radius parameter describing the size of the foundation rock for finite element modeling shown in Figure 3.5
$\mathbf{R}(t)$	vector of interaction forces in time domain at the dam-foundation rock interface
$\bar{\mathbf{R}}_0^l(\omega)$	vector of nodal forces statically equivalent to the pressure function $-\bar{p}_0^l(x,y,z,\omega)$
$\mathbf{R}_b(t)$	force vector at the abutment of the dam due to dam-foundation rock interaction; $\mathbf{R}_b^l(t)$ denotes the vector due to the l-component of ground motion
$\bar{\mathbf{R}}_b^l(\omega)$	vector of frequency response functions for $\mathbf{R}_b^l(t)$
$\bar{\mathbf{R}}_f^l(\omega)$	vector of frequency response functions for forces of nodal points of foundation rock at the dam-foundation rock interface due to the l-component of ground motion
$\mathbf{R}_h(t)$	hydrodynamic force vector at the upstream face of the dam; $\mathbf{R}_h^l(t)$ denotes the vector due to the l-component of ground motion
$\bar{\mathbf{R}}_h^l(\omega)$	vector of frequency response functions for $\mathbf{R}_h^l(t)$
$\bar{\mathbf{R}}_j^f(\omega)$	vector of nodal forces statically equivalent to the pressure function $-\bar{p}_j^f(x,y,z,\omega)$
$\bar{\mathbf{R}}_{rigid}(\omega)$	vector of 6 frequency response functions for forces at the dam-foundation rock interface moved as a rigid body; defined in Equation (4.31)

s, r	spatial coordinates on the upstream dam face boundary of the fluid as illustrated in Figure 4.3
s', r'	spatial coordinates on the reservoir boundary as illustrated in Figure 4.3
s_{ij}	non-dimensional frequency-dependent coefficients of the 6×6 impedance matrix $\mathbf{S}_{f_{rigid}}(\omega)$; $i, j = x, y, z, r, t, m$
$S_a(T_1,\xi_1)$	pseudo-acceleration value of a component of ground motion at period T_1 and damping ratio ξ_1; T_1 is the fundamental vibration period, associated with the symmetric mode for the x- or y-component of ground motion, or associated with the antisymmetric mode for the z-component of ground motion; $\xi_1 = \xi_1^x$, ξ_1^y, or ξ_1^z respectively for the x-, y-, or z-component of ground motion
$\mathbf{S}(\omega)$	matrix of the dam-water-foundation rock system containing elements $S_{nj}(\omega)$ defined in Equation (4.16)
$\mathbf{S}_f(\omega)$	frequency-dependent impedance matrix for the foundation rock region
$\mathbf{S}_{f_0}(a_0)$	"base" foundation impedance matrix corresponding to the foundation rock with Young's modulus E_{f_0} as a function of dimensionless frequency a_0
$\mathbf{S}_{f_{rigid}}(\omega)$	6×6 frequency-dependent impedance matrix of the dam-foundation rock interface moved as a rigid body; defined in Equation (4.32)
$\tilde{\mathbf{S}}_f(\omega)$	expanded foundation impedance matrix that includes all degrees of freedom of nodal points on the dam defined in Equation (4.14)
t	time
T_1	fundamental vibration period of the dam on rigid foundation rock with no water; T_1^s and T_1^a denote periods associated with symmetric and antisymmetric modes, respectively
$\tilde{T}$	fundamental vibration period of the dam on flexible foundation rock including dam-water interaction; $\tilde{T}^s$ and $\tilde{T}^a$ denote periods associated with symmetric and antisymmetric modes, respectively
$\tilde{T}_f$	fundamental vibration period of the dam supported on flexible foundation rock with no water; T_f^s and T_f^a denote periods associated with symmetric and antisymmetric modes, respectively
$\tilde{T}_r$	fundamental vibration period of the dam on rigid foundation rock including dam-water interaction; $\tilde{T}_r^s$ and $\tilde{T}_r^a$ denote periods associated with symmetric and antisymmetric modes, respectively
$\mathbf{T}_p$	stress-displacement transformation matrix for finite element p of the dam

w_f	unit weight of the foundation rock
w_s	unit weight of the concrete
w_w	unit weight of water
$Z_j(t)$	generalized coordinate corresponding to the j^{th} Ritz vector
$Z_j^l(t)$	generalized coordinate corresponding to the j^{th} Ritz vector due to the l-component of ground motion
$\overline{Z}_j^l(\omega)$	frequency response function for $Z_j^l(t)$
$\overline{\mathbf{Z}}^l(\omega)$	vector of frequency response of generalized coordinates $\overline{Z}_j^l(\omega)$ of the dam-water-foundation rock system
α	wave reflection coefficient of the reservoir boundary materials as computed in Equation (2.2)
δ_{nj}	Kroneker delta function
$\epsilon^l(s,r)$	function illustrated in Figure 4.3; when represented by $\epsilon^l(s',r')$, it refers to s', r' coordinates
Γ_i	dam-foundation rock interface
η_f	constant hysteretic damping factor of the foundation rock
η_s	constant hysteretic damping factor of the dam
λ_j	j^{th} eigenvalue from the eigenvalue problem defined in Equation (4.13)
μ_f	shear modules of the foundation rock computed as $\mu_f = E_f/2(1+\nu_f)$
ν_f	Poisson's ratio for the foundation rock
ν_s	Poisson's ratio for the dam
θ	angle describing the position along the dam crest measured from the x-y plane
ρ	unit mass of water
ρ_r	unit mass of the materials at reservoir boundary
$\sigma_p(t)$	stress vector for finite element p of the dam
ω	circular or radial frequency

ω_1 fundamental natural frequency of the dam supported on rigid foundation rock with an empty reservoir; ω_1^s and ω_1^a denote natural frequencies associated with symmetric and antisymmetric modes, respectively

$\omega_i, \cdots, \omega_{i+3}$ four different circular frequencies in ascending order to obtain values of $f(\omega)$

ω_n^i n^{th} natural frequency of the infinite fluid channel; ω_n^{is} and ω_n^{ia} denote frequencies associated with symmetric and antisymmetric eigenfunctions, respectively

$\tilde{\omega}$ fundamental natural frequency of the dam on flexible foundation rock including dam-water interaction

$\tilde{\omega}_f$ fundamental natural frequency of the dam on flexible foundation rock with no water

$\tilde{\omega}_r$ fundamental natural frequency of the dam on rigid foundation rock including dam-water interaction

ξ_1 damping ratio at the fundamental period estimated using the half-power bandwidth method; ξ_1^x, ξ_1^y, and ξ_1^z denote the fundamental damping ratio associated with the x-, y-, and z-components of ground motion, respectively

$\psi_j^f(s,r)$ function representing the normal component of the j^{th} natural vibration mode shape on the dam-water interface

$\boldsymbol{\psi}_j$ j^{th} Ritz vector of the associated dam-foundation rock system

$\boldsymbol{\psi}_n^b$ subvector of $\boldsymbol{\psi}_n$ that contains only the elements corresponding to the nodal points at the dam-foundation rock interface

$\boldsymbol{\psi}_n^f$ subvector of $\boldsymbol{\psi}_n$ that contains only the elements corresponding to the nodal points at the dam-water interface

$\mathbf{1}^l$ subvector of $\mathbf{1}_c^l$ corresponding to nodal points other than on the abutment of the dam

$\mathbf{1}_b^l$ subvector of $\mathbf{1}_c^l$ corresponding to nodal points on the abutment of the dam

$\mathbf{1}_c^l$ vector contains ones in positions corresponding to the l translational degrees of freedom of the dam, and zeros elsewhere; $l = x, y, z$

APPENDIX B: INFLUENCE OF WATER-FOUNDATION ROCK INTERACTION ON THE STATIC RESPONSE OF ARCH DAMS

Water-foundation rock interaction effects have been ignored in the dynamic analysis of arch dams and gravity dams because in the mathematical formulation the terms relating to water-foundation rock interaction are relatively small compared to the terms relating to dam-foundation rock interaction and dam-water interaction [5,12]; therefore, these effects are ignored in the new analytical procedure presented in Chapter 4. For the static analysis, the water-foundation rock interaction effects are excluded in the EAGD-84 computer program for gravity dams [22], but are included as an option in the EACD-3D program for arch dams [6]. This is easily done by retaining some DOFs on the water-foundation rock interface during the condensation of the DOFs not on the dam-foundation rock interface to obtain the static foundation impedance matrix because the foundation rock region is discretized as finite elements in the EACD-3D program. However, it is much more complicated in processing and time-consuming in computing to have such an option in the EACD-3D-95 program wherein the foundation rock region is modeled by boundary elements. An extended boundary element mesh containing the dam-foundation rock interface and portion of the water-foundation rock interface must be used to compute the static impedance matrix (at $\omega = 0$). Therefore, it is important as well as interesting to see how water-foundation rock interaction affects the static response of arch dams and if it can also be ignored.

The water-foundation rock interaction effects are included in the static analysis of Morrow Point Dam with an extended boundary element mesh shown in Figure B.1; whereas these effects are ignored if only the "standard" boundary mesh [Figure 4.4(a)] is used. The extended mesh consists of six boundary elements along the dam-foundation rock interface (which is identical to the "standard" mesh) and additional thirty elements along the water-foundation rock interface extending approximately 1000 ft (about 3 times of the half canyon width) in the upstream direction from the upstream face of the dam. Material properties for the dam, foundation rock and impounded water are

the same as described in Chapter 3. The Young's moduli of the dam and foundation rock are $E_s = E_f$ = 4 million psi, and the reservoir is assumed full. Figure B.2 shows the static displacements along the crown cantilever and the arch stresses adjacent to the crown cantilever section due to hydrostatic pressure. The displacements are apparently little affected by water-foundation rock interaction; the arch stresses are more affected by the interaction especially at the lower portion of the dam over the downstream dam face. However, because the arch stresses over the downstream face are much smaller in scale than those over the upstream face of the dam, the overall water-foundation rock interaction effects on the static response of the dam are quite small and can be ignored. Consequently, water-foundation rock interaction is not considered in the EACD-3D-95 program. This finding also partially justifies the exclusion of these interaction effects in the dynamic analysis of arch dams.

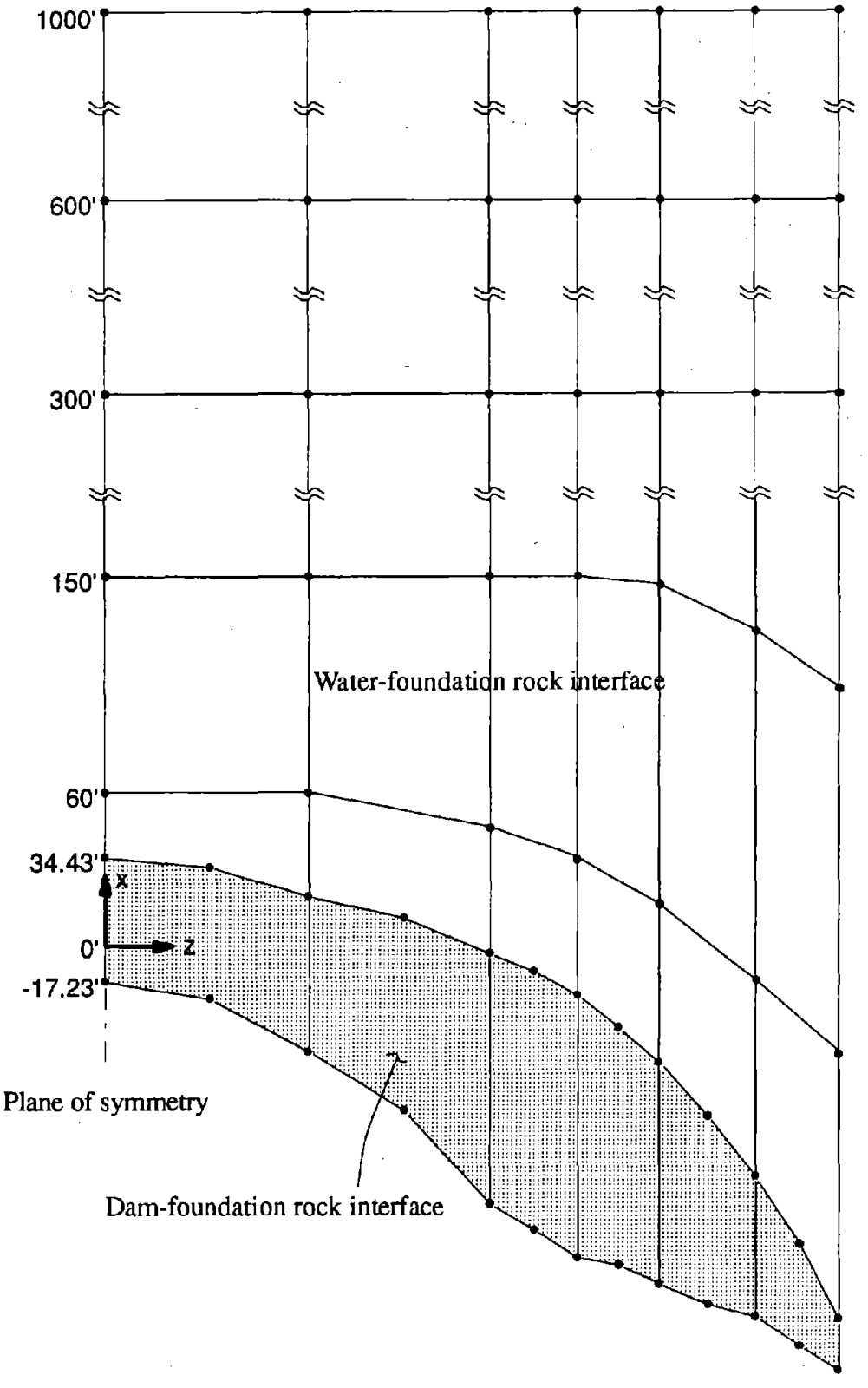

Figure B.1 Plan view of boundary element mesh of one-half of the dam-foundation rock interface and water-foundation rock interface of Morrow Point Dam on an infinitely-long uniform canyon.

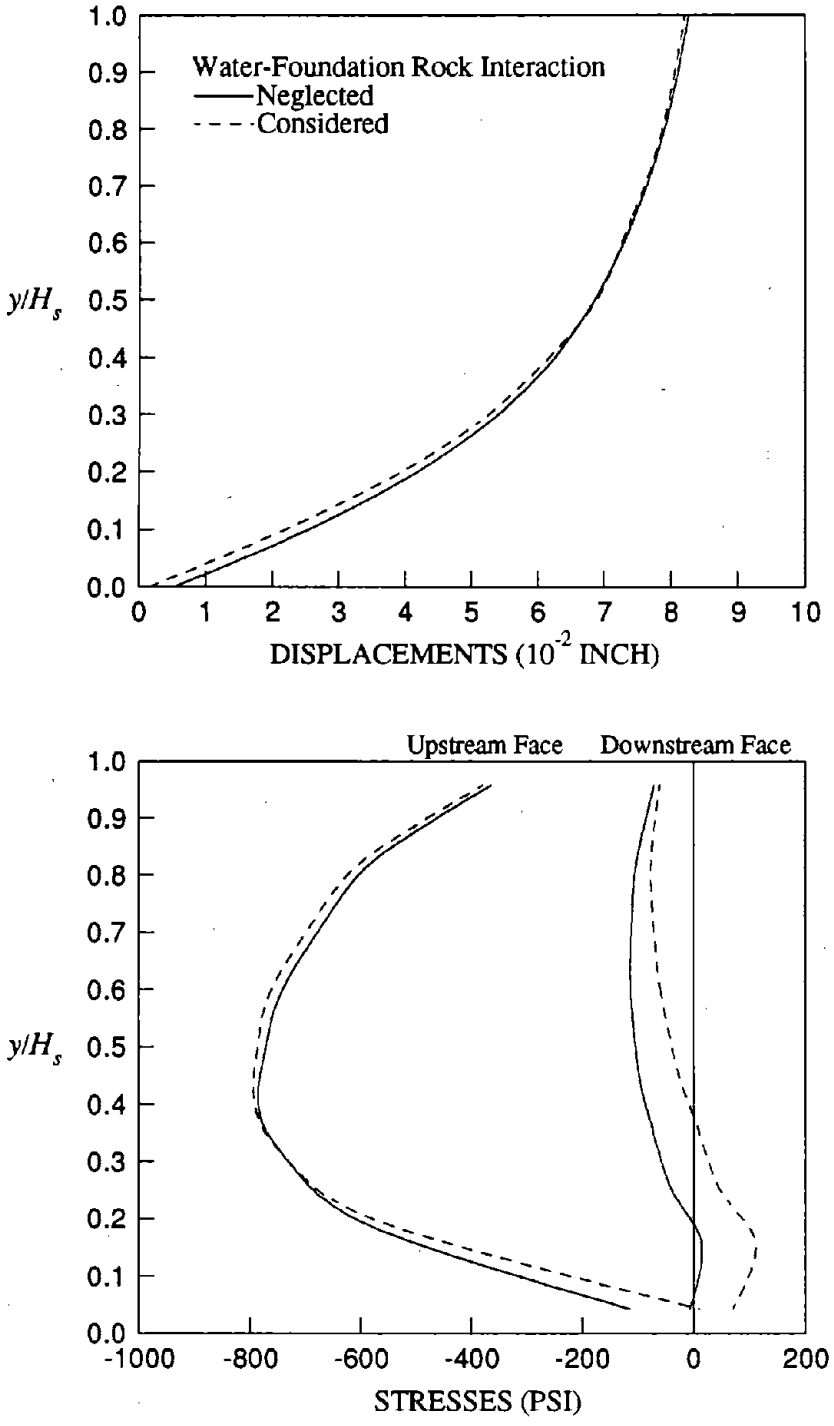

Figure B.2 Variation of static responses of Morrow Point Dam due to hydrostatic pressure only; H_s = 465 ft and E_f / E_s = 1. Results presented are for static displacements at crown cantilever and arch stresses near the crown cantilever ($\theta = 0^{\circ}$).

EARTHQUAKE ENGINEERING RESEARCH CENTER REPORT SERIES

EERC reports are available from the National Information Service for Earthquake Engineering (NISEE) and from the National Technical Information Service (NTIS). Numbers in parentheses are Accession Numbers assigned by the National Technical Information Service; these are followed by a price code. Contact NTIS, 5285 Port Royal Road, Springfield Virginia, 22161 for more information. Reports without Accession Numbers were not available from NTIS at the time of printing. For a current complete list of EERC reports (from EERC 67-1) and availablity information, please contact University of California, EERC, NISEE, 1301 South 46th Street, Richmond, California 94804-4698.

UCB/EERC-84/01 "Pseudodynamic Test Method for Seismic Performance Evaluation: Theory and Implementation," by Shing, P.-S.B. and Mahin, S.A., January 1984, (PB84 190 644)A08.

UCB/EERC-84/02 "Dynamic Response Behavior of Kiang Hong Dian Dam," by Clough, R.W., Chang, K.-T., Chen, H.-Q. and Stephen, R.M., April 1984, (PB84 209 402)A08.

UCB/EERC-84/03 "Refined Modelling of Reinforced Concrete Columns for Seismic Analysis," by Kaba, S.A. and Mahin, S.A., April 1984, (PB84 234 384)A06.

UCB/EERC-84/04 "A New Floor Response Spectrum Method for Seismic Analysis of Multiply Supported Secondary Systems," by Asfura, A. and Der Kiureghian, A., June 1984, (PB84 239 417)A06.

UCB/EERC-84/05 "Earthquake Simulation Tests and Associated Studies of a 1/5th-scale Model of a 7-Story R/C Frame-Wall Test Structure," by Bertero, V.V., Aktan, A.E., Charney, F.A. and Sause, R., June 1984, (PB84 239 409)A09.

UCB/EERC-84/06 "Unassigned," by Unassigned, 1984.

UCB/EERC-84/07 "Behavior of Interior and Exterior Flat-Plate Connections Subjected to Inelastic Load Reversals," by Zee, H.L. and Moehle, J.P., August 1984, (PB86 117 629/AS)A07.

UCB/EERC-84/08 "Experimental Study of the Seismic Behavior of a Two-Story Flat-Plate Structure," by Moehle, J.P. and Diebold, J.W., August 1984, (PB86 122 553/AS)A12.

UCB/EERC-84/09 "Phenomenological Modeling of Steel Braces under Cyclic Loading," by Ikeda, K., Mahin, S.A. and Dermitzakis, S.N., May 1984, (PB86 132 198/AS)A08.

UCB/EERC-84/10 "Earthquake Analysis and Response of Concrete Gravity Dams," by Fenves, G.L. and Chopra, A.K., August 1984, (PB85 193 902/AS)A11.

UCB/EERC-84/11 "EAGD-84: A Computer Program for Earthquake Analysis of Concrete Gravity Dams," by Fenves, G.L. and Chopra, A.K., August 1984, (PB85 193 613/AS)A05.

UCB/EERC-84/12 "A Refined Physical Theory Model for Predicting the Seismic Behavior of Braced Steel Frames," by Ikeda, K. and Mahin, S.A., July 1984, (PB85 191 450/AS)A09.

UCB/EERC-84/13 "Earthquake Engineering Research at Berkeley - 1984," by EERC, August 1984, (PB85 197 341/AS)A10.

UCB/EERC-84/14 "Moduli and Damping Factors for Dynamic Analyses of Cohesionless Soils," by Seed, H.B., Wong, R.T., Idriss, I.M. and Tokimatsu, K., September 1984, (PB85 191 468/AS)A04.

UCB/EERC-84/15 "The Influence of SPT Procedures in Soil Liquefaction Resistance Evaluations," by Seed, H.B., Tokimatsu, K., Harder, L.F. and Chung, R.M., October 1984, (PB85 191 732/AS)A04.

UCB/EERC-84/16 "Simplified Procedures for the Evaluation of Settlements in Sands Due to Earthquake Shaking," by Tokimatsu, K. and Seed, H.B., October 1984, (PB85 197 887/AS)A03.

UCB/EERC-84/17 "Evaluation of Energy Absorption Characteristics of Highway Bridges Under Seismic Conditions - Volume I (PB90 262 627)A16 and Volume II (Appendices) (PB90 262 635)A13," by Imbsen, R.A. and Penzien, J., September 1986.

UCB/EERC-84/18 "Structure-Foundation Interactions under Dynamic Loads," by Liu, W.D. and Penzien, J., November 1984, (PB87 124 889/AS)A11.

UCB/EERC-84/19 "Seismic Modelling of Deep Foundations," by Chen, C.-H. and Penzien, J., November 1984, (PB87 124 798/AS)A07.

UCB/EERC-84/20 "Dynamic Response Behavior of Quan Shui Dam," by Clough, R.W., Chang, K.-T., Chen, H.-Q., Stephen, R.M., Ghanaat, Y. and Qi, J.-H., November 1984, (PB86 115177/AS)A07.

UCB/EERC-85/01 "Simplified Methods of Analysis for Earthquake Resistant Design of Buildings," by Cruz, E.F. and Chopra, A.K., February 1985, (PB86 112299/AS)A12.

UCB/EERC-85/02 "Estimation of Seismic Wave Coherency and Rupture Velocity using the SMART 1 Strong-Motion Array Recordings," by Abrahamson, N.A., March 1985, (PB86 214 343)A07.

UCB/EERC-85/03 "Dynamic Properties of a Thirty Story Condominium Tower Building," by Stephen, R.M., Wilson, E.L. and Stander, N., April 1985, (PB86 118965/AS)A06.

UCB/EERC-85/04 "Development of Substructuring Techniques for On-Line Computer Controlled Seismic Performance Testing," by Dermitzakis, S. and Mahin, S., February 1985, (PB86 132941/AS)A08.

UCB/EERC-85/05 "A Simple Model for Reinforcing Bar Anchorages under Cyclic Excitations," by Filippou, F.C., March 1985, (PB86 112 919/AS)A05.

UCB/EERC-85/06 "Racking Behavior of Wood-framed Gypsum Panels under Dynamic Load," by Oliva, M.G., June 1985, (PB90 262 643)A04.

UCB/EERC-85/07 "Earthquake Analysis and Response of Concrete Arch Dams," by Fok, K.-L. and Chopra, A.K., June 1985, (PB86 139672/AS)A10.

UCB/EERC-85/08 "Effect of Inelastic Behavior on the Analysis and Design of Earthquake Resistant Structures," by Lin, J.P. and Mahin, S.A., June 1985, (PB86 135340/AS)A08.

UCB/EERC-85/09 "Earthquake Simulator Testing of a Base-Isolated Bridge Deck," by Kelly, J.M., Buckle, I.G. and Tsai, H.-C., January 1986, (PB87 124 152/AS)A06.

UCB/EERC-85/10 "Simplified Analysis for Earthquake Resistant Design of Concrete Gravity Dams," by Fenves, G.L. and Chopra, A.K., June 1986, (PB87 124 160/AS)A08.

UCB/EERC-85/11 "Dynamic Interaction Effects in Arch Dams," by Clough, R.W., Chang, K.-T., Chen, H.-Q. and Ghanaat, Y., October 1985, (PB86 135027/AS)A05.

UCB/EERC-85/12 "Dynamic Response of Long Valley Dam in the Mammoth Lake Earthquake Series of May 25-27, 1980," by Lai, S. and Seed, H.B., November 1985, (PB86 142304/AS)A05.

UCB/EERC-85/13 "A Methodology for Computer-Aided Design of Earthquake-Resistant Steel Structures," by Austin, M.A., Pister, K.S. and Mahin, S.A., December 1985, (PB86 159480/AS)A10 .

UCB/EERC-85/14 "Response of Tension-Leg Platforms to Vertical Seismic Excitations," by Liou, G.-S., Penzien, J. and Yeung, R.W., December 1985, (PB87 124 871/AS)A08.

UCB/EERC-85/15 "Cyclic Loading Tests of Masonry Single Piers: Volume 4 - Additional Tests with Height to Width Ratio of 1," by Sveinsson, B., McNiven, H.D. and Sucuoglu, H., December 1985, (PB87 165031/AS)A08.

UCB/EERC-85/16 "An Experimental Program for Studying the Dynamic Response of a Steel Frame with a Variety of Infill Partitions," by Yanev, B. and McNiven, H.D., December 1985, (PB90 262 676)A05.

UCB/EERC-86/01 "A Study of Seismically Resistant Eccentrically Braced Steel Frame Systems," by Kasai, K. and Popov, E.P., January 1986, (PB87 124 178/AS)A14.

UCB/EERC-86/02 "Design Problems in Soil Liquefaction," by Seed, H.B., February 1986, (PB87 124 186/AS)A03.

UCB/EERC-86/03 "Implications of Recent Earthquakes and Research on Earthquake-Resistant Design and Construction of Buildings," by Bertero, V.V., March 1986, (PB87 124 194/AS)A05.

UCB/EERC-86/04 "The Use of Load Dependent Vectors for Dynamic and Earthquake Analyses," by Leger, P., Wilson, E.L. and Clough, R.W., March 1986, (PB87 124 202/AS)A12.

UCB/EERC-86/05 "Two Beam-To-Column Web Connections," by Tsai, K.-C. and Popov, E.P., April 1986, (PB87 124 301/AS)A04.

UCB/EERC-86/06 "Determination of Penetration Resistance for Coarse-Grained Soils using the Becker Hammer Drill," by Harder, L.F. and Seed, H.B., May 1986, (PB87 124 210/AS)A07.

UCB/EERC-86/07 "A Mathematical Model for Predicting the Nonlinear Response of Unreinforced Masonry Walls to In-Plane Earthquake Excitations," by Mengi, Y. and McNiven, H.D., May 1986, (PB87 124 780/AS)A06.

UCB/EERC-86/08 "The 19 September 1985 Mexico Earthquake: Building Behavior," by Bertero, V.V., July 1986.

UCB/EERC-86/09 "EACD-3D: A Computer Program for Three-Dimensional Earthquake Analysis of Concrete Dams," by Fok, K.-L., Hall, J.F. and Chopra, A.K., July 1986, (PB87 124 228/AS)A08.

UCB/EERC-86/10 "Earthquake Simulation Tests and Associated Studies of a 0.3-Scale Model of a Six-Story Concentrically Braced Steel Structure," by Uang, C.-M. and Bertero, V.V., December 1986, (PB87 163 564/AS)A17.

UCB/EERC-86/11 "Mechanical Characteristics of Base Isolation Bearings for a Bridge Deck Model Test," by Kelly, J.M., Buckle, I.G. and Koh, C.-G., November 1987, (PB90 262 668)A04.

UCB/EERC-86/12 "Effects of Axial Load on Elastomeric Isolation Bearings," by Koh, C.-G. and Kelly, J.M., November 1987, PB88-179015(A06).

UCB/EERC-87/01 "The FPS Earthquake Resisting System: Experimental Report," by Zayas, V.A., Low, S.S. and Mahin, S.A., June 1987, (PB88 170 287)A06.

UCB/EERC-87/02 "Earthquake Simulator Tests and Associated Studies of a 0.3-Scale Model of a Six-Story Eccentrically Braced Steel Structure," by Whittaker, A., Uang, C.-M. and Bertero, V.V., July 1987, (PB88 166 707/AS)A18.

UCB/EERC-87/03 "A Displacement Control and Uplift Restraint Device for Base-Isolated Structures," by Kelly, J.M., Griffith, M.C. and Aiken, I.D., April 1987, (PB88 169 933)A04.

UCB/EERC-87/04 "Earthquake Simulator Testing of a Combined Sliding Bearing and Rubber Bearing Isolation System," by Kelly, J.M. and Chalhoub, M.S., December 1990, PB92-192962(A09).

UCB/EERC-87/05 "Three-Dimensional Inelastic Analysis of Reinforced Concrete Frame-Wall Structures," by Moazzami, S. and Bertero, V.V., May 1987, (PB88 169 586/AS)A08.

UCB/EERC-87/06 "Experiments on Eccentrically Braced Frames with Composite Floors," by Ricles, J. and Popov, E., June 1987, (PB88 173 067/AS)A14.

UCB/EERC-87/07 "Dynamic Analysis of Seismically Resistant Eccentrically Braced Frames," by Ricles, J. and Popov, E., June 1987, (PB88 173 075/AS)A16.

UCB/EERC-87/08 "Undrained Cyclic Triaxial Testing of Gravels-The Effect of Membrane Compliance," by Evans, M.D. and Seed, H.B., July 1987, (PB88 173 257)A19.

UCB/EERC-87/09 "Hybrid Solution Techniques for Generalized Pseudo-Dynamic Testing," by Thewalt, C. and Mahin, S.A., July 1987, (PB 88 179 007)A07.

UCB/EERC-87/10 "Ultimate Behavior of Butt Welded Splices in Heavy Rolled Steel Sections," by Bruneau, M., Mahin, S.A. and Popov, E.P., September 1987, (PB90 254 285)A07.

UCB/EERC-87/11 "Residual Strength of Sand from Dam Failures in the Chilean Earthquake of March 3, 1985," by De Alba, P., Seed, H.B., Retamal, E. and Seed, R.B., September 1987, (PB88 174 321/AS)A03.

UCB/EERC-87/12 "Inelastic Seismic Response of Structures with Mass or Stiffness Eccentricities in Plan," by Bruneau, M. and Mahin, S.A., September 1987, (PB90 262 650/AS)A14.

UCB/EERC-87/13 "CSTRUCT: An Interactive Computer Environment for the Design and Analysis of Earthquake Resistant Steel Structures," by Austin, M.A., Mahin, S.A. and Pister, K.S., September 1987, (PB88 173 339/AS)A06.

UCB/EERC-87/14 "Experimental Study of Reinforced Concrete Columns Subjected to Multi-Axial Loading," by Low, S.S. and Moehle, J.P., September 1987, (PB88 174 347/AS)A07.

UCB/EERC-87/15 "Relationships between Soil Conditions and Earthquake Ground Motions in Mexico City in the Earthquake of Sept. 19, 1985," by Seed, H.B., Romo, M.P., Sun, J., Jaime, A. and Lysmer, J., October 1987, (PB88 178 991)A06.

UCB/EERC-87/16 "Experimental Study of Seismic Response of R. C. Setback Buildings," by Shahrooz, B.M. and Moehle, J.P., October 1987, (PB88 176 359)A16.

UCB/EERC-87/17 "The Effect of Slabs on the Flexural Behavior of Beams," by Pantazopoulou, S.J. and Moehle, J.P., October 1987, (PB90 262 700)A07.

UCB/EERC-87/18 "Design Procedure for R-FBI Bearings," by Mostaghel, N. and Kelly, J.M., November 1987, (PB90 262 718)A04.

UCB/EERC-87/19 "Analytical Models for Predicting the Lateral Response of R C Shear Walls: Evaluation of their Reliability," by Vulcano, A. and Bertero, V.V., November 1987, (PB88 178 983)A05.

UCB/EERC-87/20 "Earthquake Response of Torsionally-Coupled Buildings," by Hejal, R. and Chopra, A.K., December 1987, PB90-208638(A15).

UCB/EERC-87/21 "Dynamic Reservoir Interaction with Monticello Dam," by Clough, R.W., Ghanaat, Y. and Qiu, X-F., December 1987, (PB88 179 023)A07.

UCB/EERC-87/22 "Strength Evaluation of Coarse-Grained Soils," by Siddiqi, F.H., Seed, R.B., Chan, C.K., Seed, H.B. and Pyke, R.M., December 1987, (PB88 179 031)A04.

UCB/EERC-88/01 "Seismic Behavior of Concentrically Braced Steel Frames," by Khatib, I., Mahin, S.A. and Pister, K.S., January 1988, (PB91 210 898/AS)A11.

UCB/EERC-88/02 "Experimental Evaluation of Seismic Isolation of Medium-Rise Structures Subject to Uplift," by Griffith, M.C., Kelly, J.M., Coveney, V.A. and Koh, C.G., January 1988, (PB91 217 950/AS)A09.

UCB/EERC-88/03 "Cyclic Behavior of Steel Double Angle Connections," by Astaneh-Asl, A. and Nader, M.N., January 1988, (PB91 210 872)A05.

UCB/EERC-88/04 "Re-evaluation of the Slide in the Lower San Fernando Dam in the Earthquake of Feb. 9, 1971," by Seed, H.B., Seed, R.B., Harder, L.F. and Jong, H.-L., April 1988, (PB91 212 456/AS)A07.

UCB/EERC-88/05 "Experimental Evaluation of Seismic Isolation of a Nine-Story Braced Steel Frame Subject to Uplift," by Griffith, M.C., Kelly, J.M. and Aiken, I.D., May 1988, (PB91 217 968/AS)A07.

UCB/EERC-88/06 "DRAIN-2DX User Guide.," by Allahabadi, R. and Powell, G.H., March 1988, (PB91 212 530)A12.

UCB/EERC-88/07 "Theoretical and Experimental Studies of Cylindrical Water Tanks in Base-Isolated Structures," by Chalhoub, M.S. and Kelly, J.M., April 1988, (PB91 217 976/AS)A05.

UCB/EERC-88/08 "Analysis of Near-Source Waves: Separation of Wave Types Using Strong Motion Array Recording," by Darragh, R.B., June 1988, (PB91 212 621)A08.

UCB/EERC-88/09 "Alternatives to Standard Mode Superposition for Analysis of Non-Classically Damped Systems," by Kusainov, A.A. and Clough, R.W., June 1988, (PB91 217 992/AS)A04.

UCB/EERC-88/10 "The Landslide at the Port of Nice on October 16, 1979," by Seed, H.B., Seed, R.B., Schlosser, F., Blondeau, F. and Juran, I., June 1988, (PB91 210 914)A05.

UCB/EERC-88/11 "Liquefaction Potential of Sand Deposits Under Low Levels of Excitation," by Carter, D.P. and Seed, H.B., August 1988, (PB91 210 880)A15.

UCB/EERC-88/12 "Nonlinear Analysis of Reinforced Concrete Frames Under Cyclic Load Reversals," by Filippou, F.C. and Issa, A., September 1988, (PB91 212 589)A07.

UCB/EERC-88/13 "Implications of Recorded Earthquake Ground Motions on Seismic Design of Building Structures," by Uang, C.-M. and Bertero, V.V., November 1988, (PB91 212 548)A06.

UCB/EERC-88/14 "An Experimental Study of the Behavior of Dual Steel Systems," by Whittaker, A.S. , Uang, C.-M. and Bertero, V.V., September 1988, (PB91 212 712)A16.

UCB/EERC-88/15 "Dynamic Moduli and Damping Ratios for Cohesive Soils," by Sun, J.I., Golesorkhi, R. and Seed, H.B., August 1988, (PB91 210 922)A04.

UCB/EERC-88/16 "Reinforced Concrete Flat Plates Under Lateral Load: An Experimental Study Including Biaxial Effects," by Pan, A. and Moehle, J.P., October 1988, (PB91 210 856)A13.

UCB/EERC-88/17 "Earthquake Engineering Research at Berkeley - 1988," by EERC, November 1988, (PB91 210 864)A10.

UCB/EERC-88/18 "Use of Energy as a Design Criterion in Earthquake-Resistant Design," by Uang, C.-M. and Bertero, V.V., November 1988, (PB91 210 906/AS)A04.

UCB/EERC-88/19 "Steel Beam-Column Joints in Seismic Moment Resisting Frames," by Tsai, K.-C. and Popov, E.P., November 1988, (PB91 217 984/AS)A20.

UCB/EERC-88/20 "Base Isolation in Japan, 1988," by Kelly, J.M., December 1988, (PB91 212 449)A05.

UCB/EERC-89/01 "Behavior of Long Links in Eccentrically Braced Frames," by Engelhardt, M.D. and Popov, E.P., January 1989, (PB92 143 056)A18.

UCB/EERC-89/02 "Earthquake Simulator Testing of Steel Plate Added Damping and Stiffness Elements," by Whittaker, A., Bertero, V.V., Alonso, J. and Thompson, C., January 1989, (PB91 229 252/AS)A10.

UCB/EERC-89/03 "Implications of Site Effects in the Mexico City Earthquake of Sept. 19, 1985 for Earthquake-Resistant Design Criteria in the San Francisco Bay Area of California," by Seed, H.B. and Sun, J.I., March 1989, (PB91 229 369/AS)A07.

UCB/EERC-89/04 "Earthquake Analysis and Response of Intake-Outlet Towers," by Goyal, A. and Chopra, A.K., July 1989, (PB91 229 286/AS)A19.

UCB/EERC-89/05 "The 1985 Chile Earthquake: An Evaluation of Structural Requirements for Bearing Wall Buildings," by Wallace, J.W. and Moehle, J.P., July 1989, (PB91 218 008/AS)A13.

UCB/EERC-89/06 "Effects of Spatial Variation of Ground Motions on Large Multiply-Supported Structures," by Hao, H., July 1989, (PB91 229 161/AS)A08.

UCB/EERC-89/07 "EADAP - Enhanced Arch Dam Analysis Program: Users's Manual," by Ghanaat, Y. and Clough, R.W., August 1989, (PB91 212 522)A06.

UCB/EERC-89/08 "Seismic Performance of Steel Moment Frames Plastically Designed by Least Squares Stress Fields," by Ohi, K. and Mahin, S.A., August 1989, (PB91 212 597)A05.

UCB/EERC-89/09 "Feasibility and Performance Studies on Improving the Earthquake Resistance of New and Existing Buildings Using the Friction Pendulum System," by Zayas, V., Low, S., Mahin, S.A. and Bozzo, L., July 1989, (PB92 143 064)A14.

UCB/EERC-89/10 "Measurement and Elimination of Membrane Compliance Effects in Undrained Triaxial Testing," by Nicholson, P.G., Seed, R.B. and Anwar, H., September 1989, (PB92 139 641/AS)A13.

UCB/EERC-89/11 "Static Tilt Behavior of Unanchored Cylindrical Tanks," by Lau, D.T. and Clough, R.W., September 1989, (PB92 143 049)A10.

UCB/EERC-89/12 "ADAP-88: A Computer Program for Nonlinear Earthquake Analysis of Concrete Arch Dams," by Fenves, G.L., Mojtahedi, S. and Reimer, R.B., September 1989, (PB92 139 674/AS)A07.

UCB/EERC-89/13 "Mechanics of Low Shape Factor Elastomeric Seismic Isolation Bearings," by Aiken, I.D., Kelly, J.M. and Tajirian, F.F., November 1989, (PB92 139 732/AS)A09.

UCB/EERC-89/14 "Preliminary Report on the Seismological and Engineering Aspects of the October 17, 1989 Santa Cruz (Loma Prieta) Earthquake," by EERC, October 1989, (PB92 139 682/AS)A04.

UCB/EERC-89/15 "Experimental Studies of a Single Story Steel Structure Tested with Fixed, Semi-Rigid and Flexible Connections," by Nader, M.N. and Astaneh-Asl, A., August 1989, (PB91 229 211/AS)A10.

UCB/EERC-89/16 "Collapse of the Cypress Street Viaduct as a Result of the Loma Prieta Earthquake," by Nims, D.K., Miranda, E., Aiken, I.D., Whittaker, A.S. and Bertero, V.V., November 1989, (PB91 217 935/AS)A05.

UCB/EERC-90/01 "Mechanics of High-Shape Factor Elastomeric Seismic Isolation Bearings," by Kelly, J.M., Aiken, I.D. and Tajirian, F.F., March 1990.

UCB/EERC-90/02 "Javid's Paradox: The Influence of Preform on the Modes of Vibrating Beams," by Kelly, J.M., Sackman, J.L. and Javid, A., May 1990, (PB91 217 943/AS)A03.

UCB/EERC-90/03 "Earthquake Simulator Testing and Analytical Studies of Two Energy-Absorbing Systems for Multistory Structures," by Aiken, I.D. and Kelly, J.M., October 1990, (PB92 192 988)A13.

UCB/EERC-90/04 "Unassigned," by Unassigned, 1990.

UCB/EERC-90/05 "Preliminary Report on the Principal Geotechnical Aspects of the October 17, 1989 Loma Prieta Earthquake," by Seed, R.B., Dickenson, S.E., Riemer, M.F., Bray, J.D., Sitar, N., Mitchell, J.K., Idriss, I.M., Kayen, R.E., Kropp, A., Harder, L.F., Jr. and Power, M.S., April 1990, (PB 192 970)A08.

UCB/EERC-90/06 "Models of Critical Regions in Reinforced Concrete Frames Under Seismic Excitations," by Zulfiqar, N. and Filippou, F.C., May 1990.

UCB/EERC-90/07 "A Unified Earthquake-Resistant Design Method for Steel Frames Using ARMA Models," by Takewaki, I., Conte, J.P., Mahin, S.A. and Pister, K.S., June 1990, PB92-192947(A06).

UCB/EERC-90/08 "Soil Conditions and Earthquake Hazard Mitigation in the Marina District of San Francisco," by Mitchell, J.K., Masood, T., Kayen, R.E. and Seed, R.B., May 1990, (PB 193 267/AS)A04.

UCB/EERC-90/09 "Influence of the Earthquake Ground Motion Process and Structural Properties on Response Characteristics of Simple Structures," by Conte, J.P., Pister, K.S. and Mahin, S.A., July 1990, (PB92 143 064)A15.

UCB/EERC-90/10 "Experimental Testing of the Resilient-Friction Base Isolation System," by Clark, P.W. and Kelly, J.M., July 1990, (PB92 143 072)A08.

UCB/EERC-90/11 "Seismic Hazard Analysis: Improved Models, Uncertainties and Sensitivities," by Araya, R. and Der Kiureghian, A., March 1988, PB92-193010(A08).

UCB/EERC-90/12 "Effects of Torsion on the Linear and Nonlinear Seismic Response of Structures," by Sedarat, H. and Bertero, V.V., September 1989, (PB92 193 002/AS)A15.

UCB/EERC-90/13 "The Effects of Tectonic Movements on Stresses and Deformations in Earth Embankments," by Bray, J. D., Seed, R. B. and Seed, H. B., September 1989, PB92-192996(A18).

UCB/EERC-90/14 "Inelastic Seismic Response of One-Story, Asymmetric-Plan Systems," by Goel, R.K. and Chopra, A.K., October 1990, (PB93 114 767)A11.

UCB/EERC-90/15 "Dynamic Crack Propagation: A Model for Near-Field Ground Motion.," by Seyyedian, H. and Kelly, J.M., 1990.

UCB/EERC-90/16 "Sensitivity of Long-Period Response Spectra to System Initial Conditions," by Blasquez, R., Ventura, C. and Kelly, J.M., 1990.

UCB/EERC-90/17 "Behavior of Peak Values and Spectral Ordinates of Near-Source Strong Ground-Motion over a Dense Array," by Niazi, M., June 1990, (PB93 114 833)A07.

UCB/EERC-90/18 "Material Characterization of Elastomers used in Earthquake Base Isolation," by Papoulia, K.D. and Kelly, J.M., 1990, PB94-190063(A08).

UCB/EERC-90/19 "Cyclic Behavior of Steel Top-and-Bottom Plate Moment Connections," by Harriott, J.D. and Astaneh-Asl, A., August 1990, (PB91 229 260/AS)A05.

UCB/EERC-90/20 "Seismic Response Evaluation of an Instrumented Six Story Steel Building," by Shen, J.-H. and Astaneh-Asl, A., December 1990, (PB91 229 294/AS)A04.

UCB/EERC-90/21 "Observations and Implications of Tests on the Cypress Street Viaduct Test Structure," by Bollo, M., Mahin, S.A., Moehle, J.P., Stephen, R.M. and Qi, X., December 1990, (PB93 114 775)A13.

UCB/EERC-91/01 "Experimental Evaluation of Nitinol for Energy Dissipation in Structures," by Nims, D.K., Sasaki, K.K. and Kelly, J.M., 1991.

UCB/EERC-91/02 "Displacement Design Approach for Reinforced Concrete Structures Subjected to Earthquakes," by Qi, X. and Moehle, J.P., January 1991, (PB93 114 569/AS)A09.

UCB/EERC-91/03 "A Long-Period Isolation System Using Low-Modulus High-Damping Isolators for Nuclear Facilities at Soft-Soil Sites," by Kelly, J.M., March 1991, (PB93 114 577/AS)A10.

UCB/EERC-91/04 "Dynamic and Failure Characteristics of Bridgestone Isolation Bearings," by Kelly, J.M., April 1991, (PB93 114 528)A05.

UCB/EERC-91/05 "Base Sliding Response of Concrete Gravity Dams to Earthquakes," by Chopra, A.K. and Zhang, L., May 1991, (PB93 114 544/AS)A05.

UCB/EERC-91/06 "Computation of Spatially Varying Ground Motion and Foundation-Rock Impedance Matrices for Seismic Analysis of Arch Dams," by Zhang, L. and Chopra, A.K., May 1991, (PB93 114 825)A07.

UCB/EERC-91/07 "Estimation of Seismic Source Processes Using Strong Motion Array Data," by Chiou, S.-J., July 1991, (PB93 114 551/AS)A08.

UCB/EERC-91/08 "A Response Spectrum Method for Multiple-Support Seismic Excitations," by Der Kiureghian, A. and Neuenhofer, A., August 1991, (PB93 114 536)A04.

UCB/EERC-91/09 "A Preliminary Study on Energy Dissipating Cladding-to-Frame Connection," by Cohen, J.M. and Powell, G.H., September 1991, (PB93 114 510)A05.

UCB/EERC-91/10 "Evaluation of Seismic Performance of a Ten-Story RC Building During the Whittier Narrows Earthquake," by Miranda, E. and Bertero, V.V., October 1991, (PB93 114 783)A06.

UCB/EERC-91/11 "Seismic Performance of an Instrumented Six-Story Steel Building," by Anderson, J.C. and Bertero, V.V., November 1991, (PB93 114 809)A07.

UCB/EERC-91/12 "Performance of Improved Ground During the Loma Prieta Earthquake," by Mitchell, J.K. and Wentz, Jr., F.J., October 1991, (PB93 114 791)A06.

UCB/EERC-91/13 "Shaking Table - Structure Interaction," by Rinawi, A.M. and Clough, R.W., October 1991, (PB93 114 917)A13.

UCB/EERC-91/14 "Cyclic Response of RC Beam-Column Knee Joints: Test and Retrofit," by Mazzoni, S., Moehle, J.P. and Thewalt, C.R., October 1991, (PB93 120 277)A03.

UCB/EERC-91/15 "Design Guidelines for Ductility and Drift Limits: Review of State-of-the-Practice and State-of-the-Art in Ductility and Drift-Based Earthquake-Resistant Design of Buildings," by Bertero, V.V., Anderson, J.C., Krawinkler, H., Miranda, E. and The CUREe and The Kajima Research Teams, July 1991, (PB93 120 269)A08.

UCB/EERC-91/16 "Evaluation of the Seismic Performance of a Thirty-Story RC Building," by Anderson, J.C., Miranda, E., Bertero, V.V. and The Kajima Project Research Team, July 1991, (PB93 114 841)A12.

UCB/EERC-91/17 "A Fiber Beam-Column Element for Seismic Response Analysis of Reinforced Concrete Structures," by Taucer, F., Spacone, E. and Filippou, F.C., December 1991, (PB94 117 629AS)A07.

UCB/EERC-91/18 "Investigation of the Seismic Response of a Lightly-Damped Torsionally-Coupled Building," by Boroschek, R. and Mahin, S.A., December 1991, (PB93 120 335)A13.

UCB/EERC-92/01 "Studies of a 49-Story Instrumented Steel Structure Shaken During the Loma Prieta Earthquake," by Chen, C.-C., Bonowitz, D. and Astaneh-Asl, A., February 1992, (PB93 221 778)A08.

UCB/EERC-92/02 "Response of the Dumbarton Bridge in the Loma Prieta Earthquake," by Fenves, G.L., Filippou, F.C. and Sze, D.T., January 1992, (PB93 120 319)A09.

UCB/EERC-92/03 "Models for Nonlinear Earthquake Analysis of Brick Masonry Buildings," by Mengi, Y., McNiven, H.D. and Tanrikulu, A.K., March 1992, (PB93 120 293)A08.

UCB/EERC-92/04 "Shear Strength and Deformability of RC Bridge Columns Subjected to Inelastic Cyclic Displacements," by Aschheim, M. and Moehle, J.P., March 1992, (PB93 120 327)A06.

UCB/EERC-92/05 "Parameter Study of Joint Opening Effects on Earthquake Response of Arch Dams," by Fenves, G.L., Mojtahedi, S. and Reimer, R.B., April 1992, (PB93 120 301)A04.

UCB/EERC-92/06 "Seismic Behavior and Design of Semi-Rigid Steel Frames," by Nader, M.N. and Astaneh-Asl, A., May 1992, PB93-221760(A17).

UCB/EERC-92/07 "A Beam Element for Seismic Damage Analysis," by Spacone, E., Ciampi, V. and Filippou, F.C., August 1992, (PB95-192126)A06.

UCB/EERC-92/08 "Nonlinear Static and Dynamic Analysis of Reinforced Concrete Subassemblages," by Filippou, F.C., D'Ambrisi, A. and Issa, A., August 1992, PB95-192175(A09).

UCB/EERC-92/09 "Evaluation of Code Accidental-Torsion Provisions Using Earthquake Records from Three Nominally Symmetric-Plan Buildings," by De la Llera, J.C. and Chopra, A.K., September 1992, (PB94 117 611)A08.

UCB/EERC-92/10 "Slotted Bolted Connection Energy Dissipators," by Grigorian, C.E., Yang, T.-S. and Popov, E.P., July 1992, (PB92 120 285)A03.

UCB/EERC-92/11 "Mechanical Characteristics of Neoprene Isolation Bearings," by Kelly, J.M. and Quiroz, E., August 1992, (PB93 221 729)A07.

UCB/EERC-92/12 "Application of a Mass Damping System to Bridge Structures," by Hasegawa, K. and Kelly, J.M., August 1992, (PB93 221 786)A06.

UCB/EERC-92/13 "Earthquake Engineering Research at Berkeley - 1992," by EERC, October 1992, PB93-223709(A10).

UCB/EERC-92/14 "Earthquake Risk and Insurance," by Brillinger, D.R., October 1992, (PB93 223 352)A03.

UCB/EERC-92/15 "A Friction Mass Damper for Vibration Control," by Inaudi, J.A. and Kelly, J.M., October 1992, (PB93 221 745)A04.

UCB/EERC-92/16 "Tall Reinforced Concrete Buildings: Conceptual Earthquake-Resistant Design Methology," by Bertero, R.D. and Bertero, V.V., December 1992, (PB93 221 695)A12.

UCB/EERC-92/17 "Performance of Tall Buildings During the 1985 Mexico Earthquakes," by Terán-Gilmore, A. and Bertero, V.V., December 1992, (PB93 221 737)A11.

UCB/EERC-92/18 "Dynamic Analysis of Nonlinear Structures using State-Space Formulation and Partitioned Integration Schemes," by Inaudi, J.A. and De la Llera, J.C., December 1992, (PB94 117 702/AS/A05.

UCB/EERC-93/01 "Seismic Performance of an Instrumented Six-Story Reinforced-Concrete Building," by Anderson, J.C. and Bertero, V.V., 1993.

UCB/EERC-93/02 "Evaluation of an Active Variable-Damping-Structure," by Polak, E., Meeker, G., Yamada, K. and Kurata, N., 1993, (PB93 221 711)A05.

UCB/EERC-93/03 "An Experimental Study of Flat-Plate Structures under Vertical and Lateral Loads," by Hwang, S.-H. and Moehle, J.P., February 1993, (PB94 157 690/AS)A13.

UCB/EERC-93/04 "Seismic Performance of a 30-Story Building Located on Soft Soil and Designed According to UBC 1991," by Terán-Gilmore, A. and Bertero, V.V., 1993, (PB93 221 703)A17.

UCB/EERC-93/05 "Multiple-Support Response Spectrum Analysis of the Golden Gate Bridge," by Nakamura, Y., Der Kiureghian, A. and Liu, D., May 1993, (PB93 221 752)A05.

UCB/EERC-93/06 "On the Analysis of Structures with Viscoelastic Dampers," by Inaudi, J.A., Zambrano, A. and Kelly, J.M., August 1993, PB94-165867(A06).

UCB/EERC-93/07 "Earthquake Analysis and Response of Concrete Gravity Dams Including Base Sliding," by Chávez, J.W. and Fenves, G.L., December 1993, (PB94 157 658/AS)A10.

UCB/EERC-93/08 "Model for Anchored Reinforcing Bars under Seismic Excitations," by Monti, G., Spacone, E. and Filippou, F.C., December 1993, PB95-192183(A05).

UCB/EERC-93/09 "A Methodology for Design of Viscoelastic Dampers in Earthquake-Resistant Structures," by Abbas, H. and Kelly, J.M., November 1993, PB94-190071(A10).

UCB/EERC-93/10 "Tuned Mass Dampers Using Viscoelastic Dampers," by Inaudi, J.A., Lopez-Almansa, F. and Kelly, J.M., December 1993.

UCB/EERC-93/11 "Nonlinear Homogeneous Dynamical Systems," by Inaudi, J.A. and Kelly, J.M., December 1993.

UCB/EERC-93/12 "Synthesized Strong Ground Motions for the Seismic Condition Assessment of the Eastern Portion of the San Francisco Bay Bridge," by Bolt, B.A. and Gregor, N.J., December 1993, PB94-165842(A10).

UCB/EERC-93/13 "On the Analysis of Structures with Energy Dissipating Restraints," by Inaudi, J.A., Nims, D.K. and Kelly, J.M., December 1993, PB94-203619(A07).

UCB/EERC-94/01 "Preliminary Report on the Seismological and Engineering Aspects of the January 17, 1994 Northridge Earthquake," by EERC, January 1994, (PB94 157 666/AS)A05.

UCB/EERC-94/02 "Energy Dissipation with Slotted Bolted Connections," by Grigorian, C.E. and Popov, E.P., February 1994, PB94-164605.

UCB/EERC-94/03 "The Influence of Plate Flexibility on the Buckling Load of Elastomeric Isolators," by Kelly, J.M., March 1994, PB95-192134(A04).

UCB/EERC-94/04 "Insitu Test Results from Four Loma Prieta Earthquake Liquefaction Sites: SPT, CPT, DMT and Shear Wave Velocity," by Mitchell, J.K., Lodge, A.L., Coutinho, R.Q., Kayen, R.E., Seed, R.B., Nishio, S. and Stokoe II, K.H., April 1994, PB94-190089(A09).

UCB/EERC-94/05 "Seismic Response of Steep Natural Slopes," by Sitar, N. and Ashford, S.A., May 1994, PB94-203643(A10).

UCB/EERC-94/06 "Small-Scale Testing of a Self-Centering Friction Energy Dissipator for Structures," by Nims, D.K. and Kelly, J.M., August 1994.

UCB/EERC-94/07 "Accidental and Natural Torsion in Earthquake Response and Design of Buildings," by De la Llera, J.C. and Chopra, A.K., June 1994, PB94-203627(A14).

UCB/EERC-94/08 "Preliminary Report on the Principal Geotechnical Aspects of the January 17, 1994 Northridge Earthquake," by Stewart, J.P., Bray, J.D., Seed, R.B. and Sitar, N., June 1994, PB94203635(A12).

UCB/EERC-94/09 "Performance of Steel Building Structures During the Northridge Earthquake," by Bertero, V.V., Anderson, J.C. and Krawinkler, H., August 1994, PB95-112025(A10).

UCB/EERC-94/10 "Manual for Menshin Design of Highway Bridges: Ministry of Construction, Japan," by Sugita, H. and Mahin, S., August 1994, PB95-192100(A08).

UCB/EERC-94/11 "Earthquake Analysis and Response of Two-Level Viaducts," by Singh, S.P. and Fenves, G.L., October 1994, (A09).

UCB/EERC-94/12 "Response of the Northwest Connector in the Landers and Big Bear Earthquakes," by Fenves, G.L. and Desroches, R., December 1994, PB95-192001(A08).

UCB/EERC-95/01 "Geotechnical Reconnaissance of the Effects of the January 17, 1995, Hyogoken-Nanbu Earthquake, Japan," August 1995.

UCB/EERC-95/02 "The Attenuation of Strong Ground Motion Displacement," by Gregor, N.J., June 1995.

UCB/EERC-95/03 "Upgrading Bridge Outrigger Knee Joint Systems," by Stojadinovic, B. and Thewalt, C.R., June 1995.

UCB/EERC-95/04 "Earthquake Hazard Reduction in Historical Buildings Using Seismic Isolation," by Garevski, M., June 1995.

UCB/EERC-95/05 "Final Report on the International Workshop on the Use of Rubber-Based Bearings for the Earthquake Protection of Building," by Kelly, J.M., May 1995.

UCB/EERC-95/06 "Seismic Rehabilitation of Framed Buildings Infilled with Unreinforced Masonry Walls Using Post-Tensioned Steel Braces," by Terán-Gilmore, A., Bertero, V.V. and Youssef, N., June 1995.

UCB/EERC-95/07 "Earthquake Analysis and Resposne of Concrete Arch Dams," by Tan, H. and Chopra, A.K., August 1995.

REPORT DOCUMENTATION PAGE

Form Approved
OMB No 0704-0188

1

2. REPORT DATE: July 1995

3. REPORT TYPE AND DATES COVERED: Final

4. TITLE AND SUBTITLE
Earthquake Analysis and Response of Concrete Arch Dams

5. FUNDING NUMBERS
NSF Grant No.
BCS-9121943

6. AUTHOR(S)
Tan, Hanchen and
Chopra, Anil K.

7. PERFORMING ORGANIZATION NAME(S) AND ADDRESS(ES)
Earthquake Engineering Research Center
University of California at Berkeley
1301 S. 46th Street
Richmond, CA 94804

8. PERFORMING ORGANIZATION REPORT NUMBER
UCB/EERC-95/07

9. SPONSORING/MONITORING AGENCY NAME(S) AND ADDRESS(ES)
National Science Foundation
1800 G Street, N.W.
Washington, D.C. 20550

10. SPONSORING/MONITORING AGENCY REPORT NUMBER

11. SUPPLEMENTARY NOTES

12a. DISTRIBUTION/AVAILABILITY STATEMENT

12b. DISTRIBUTION CODE

13. ABSTRACT (Maximum 200 words)

Reliable analytical procedures to predict the earthquake response of arch dams are essential to design dams to be earthquake resistant or to evaluate the earthquake safety of existing dams. The objectives of this study are: (1) to develop an effective procedure for analyzing the response of concrete arch dams to earthquake ground motion, including the effects of dam-foundation rock interaction with inertia and damping of the foundation rock considered, dam-water interaction, and reservoir boundary absorption; (2) to identify the limitations of the "standard" analysis procedure which considers the flexibility of the foundation rock but ignores its inertia and damping --- material and radiation --- effects; and (3) to study the effects of dam-foundation rock interaction in the presence of dam-water interaction and reservoir boundary absorption on the response of the dam, leading to a better understanding of these effects. This investigation emphasizes the effects of dam-foundation rock interaction compared to dam-water interaction which have already been studied extensively.

14. SUBJECT TERMS

15. NUMBER OF PAGES
185

16. PRICE CODE

17. SECURITY CLASSIFICATION OF REPORT	18. SECURITY CLASSIFICATION OF THIS PAGE	19. SECURITY CLASSIFICATION OF ABSTRACT	20. LIMITATION OF ABSTRACT
unclassified	unclassified	unclassified	